Biocatalysis using lipase immobilised in organogels in supercritical carbon dioxide

Dissertation
zur Erlangung des Grades
Doktor der Naturwissenschaften
(Dr. rer. nat.)

der
Naturwissenschaftlichen Fakultät IV
Chemie und Pharmazie
der Universität Regensburg

von
Christian Blattner
Regensburg 2005

Promotionsgesuch eingereicht am:	14.12.2005
Tag des Kolloquiums:	27.01.2006
Die Arbeit wurde angeleitet von:	Prof. Dr. W. Kunz
Prüfungsausschuß:	Prof. Dr. H. Krienke, Vorsitzender
	Prof. Dr. W. Kunz
	Dr. A. Xenakis
	Prof. Dr. G. Schmeer

Meinen Eltern

Vorwort

Die vorliegende Arbeit entstand in der Zeit von Januar 2001 bis November 2005 am Lehrstuhl für Chemie VI – Physikalische Chemie – der naturwissenschaftlichen Fakultät IV – Chemie und Pharmazie – der Universität Regensburg.

Besonderer Dank gebührt meinem Doktorvater **Herrn Professor Dr. Werner Kunz** und **Herrn Professor Dr. Georg Schmeer** für die Erteilung des interessanten Themas, die wissenschaftliche Betreuung und ihr stetes Interesse am Fortgang der Arbeit. Ich bedanke mich bei beiden für die großzügige finanzielle Unterstützung und das Überlassen von Labor- und Arbeitsmitteln.

Herzlich danke ich auch Frau Maria Zoumpanioti und Herrn Dr. Aristotelis Xenakis vom Institute of Biological Research and Biotechnology der National Hellenic Research Foundation (Εθνικό Ίδρυμα Ερευνών) für die interessante Zusammenarbeit im Rahmen unseres gemeinsamen deutsch-griechischen IKYDA-Projekts und für ihre Gastfreundschaft während meiner beiden Athenaufenthalte. Mein Dank gilt hier auch dem Deutschen Akademischen Austauschdienst (DAAD) für die Förderung dieser Arbeit im Rahmen dieses Projekts.

Bei Herrn Dipl.-Ing. (FH) Franz Ziegler vom TÜV Süddeutschland bedanke ich mich für die freundliche und interessante Zusammenarbeit bei der technischen Abnahme der neu gebauten Hochdruckzelle.

Den Mitarbeitern der Feinmechanischen Werkstatt des Fachbereichs Chemie/Pharmazie gilt mein besonderer Dank für die zügige und gewissenhafte Erledigung zahlreicher Aufträge.

Des weiteren gilt mein Dank Herrn Dr. Jürgen Kröner für die Durchführung der kalorimetrischen Messungen an den Organogelen und für die interessanten Diskussionen bei der Interpretation der Ergebnisse.

Ferner danke ich Herrn Dr. Simon Schrödle, der durch seine Kenntnisse zur Vernickelung von Keramik die neuen Elektroden für Leitfähigkeitsmessungen möglich gemacht hat.

Bei Herrn Dr. Josef Duschl und den Studenten (J. Ehrl, J. Lodermeyer, F. Kraus) des Fortgeschrittenenpraktikums der Organischen Chemie im Wintersemester 2000/2001 bedanke ich mich für die Durchführung von organischen Synthesen.

Weiterer Dank gebührt Herrn Dipl-Chem. Fabian Glaab, der im Rahmen eines Schwerpunktpraktikums an Löslichkeitsversuchen und enzymkatalysierten Reaktionen in überkritischem Kohlendioxid mitgewirkt hat.

Danken möchte ich auch allen Mitarbeitern des Lehrstuhls, die durch ihre Hilfsbereitschaft und die gute Zusammenarbeit zu einem angenehmen Arbeitsklima beitrugen. Ich denke hier vor allem an meine beiden Laborkollegen Herrn Dr. Jürgen Bittner und Frau Dipl.-Chem. Sigrid Schüller, als auch an meine weiteren Mensa- und Kaffeerundenkameraden.

Abschließend möchte ich mich noch bei meinen Eltern für ihre großzügige Unterstützung während meines Studiums bedanken.

Symbols

α	polarisability [C m^2 V^{-1}]
β	scan rate [K min^{-1}]
γ_{cmc}	air-water surface tension at the critical micelle concentration [mN m^{-1}]
$\Delta H_a(\Theta)$	apparent heat of fusion of the penetrant liquid [J g^{-1}]
ΔH_f	heat of fusion under normal conditions [J g^{-1}]
ΔH_i	fusion enthalpy for a specific peak i [J]
ϵ_{r}	dielectric constant; relative permittivity
ϵ_{vis}	dielectric constant in the visible frequency range
η	dynamic viscosity [Pa s]
Θ	temperature [°C]
Θ_{c}	critical temperature [°C]
ξ_i	mass fraction of component i
ρ	density [kg m^{-3}]
τ	turbidity according to Rayleigh
ϕ	volume fraction of the dispersed phase
ϕ^{corr}	volume fraction of the dispersed phase corrected for the mutual water solubility in the supercritical continuous phase
ϕ_{p}	volume fraction of the percolation threshold
A_i	peak area of species i [pA s^{-1}, W K^{-1}]
D	diffusion coefficient [cm^2 s^{-1}]
k_i	rate constant of the i-th partial reaction
K_{eq}	thermodynamic equilibrium constant
$K_{\mathrm{i}}^{\mathrm{X}}$	inhibition constant for species X [mM]
K_{m}	Michaelis-Menten constant [mM]
$K_{\mathrm{m}}^{\mathrm{X}}$	Michaelis-Menten constant for species X [mM]
I	light intensity [W m^{-2}]
n_i	molar amount of component i [mol]
p	pressure [bar]
p_{c}	critical pressure [bar]
p_{t}	triple point pressure [bar]
p_{trans}	phase transition pressure [bar]
T	temperature [K]
T_{c}	critical temperature [K]
T_{t}	triple point temperature [K]
v	(initial) reaction rate [mM min^{-1}]
v_{f}	(initial) reaction rate in the forward direction [mM min^{-1}]
v_{r}	(initial) reaction rate in the reverse direction [mM min^{-1}]
v_{max}	maximal reaction rate under saturation conditions [mM min^{-1}]

v_{max}^{f}	maximal reaction rate in the forward direction [mM min^{-1}]
v_{max}^{r}	maximal reaction rate in the reverse direction [mM min^{-1}]
V, V_i	volume (of component i) [m^3]
W_0	molar ratio of water and surfactant
W_0^{corr}	molar ratio of water and surfactant corrected for the mutual water solubility in the supercritical continuous phase
[X]	molar concentration of reaction participant X [mM]

Abbreviations

$8FS(EO)_4$	sodium bis((1H,1H,2H,2H-heptadecafluorodecyl)-oxyethylene)-2-sulfosuccinate
AOT	Aerosol OT; sodium bis(2-ethylhexyl)-sulfosuccinate
ASES	aerosol solvent extraction system
C8C4	octyltributylammonium bromide
C8E5	pentaethylene glycol n-octyl ether
CaL	*Candida antarctica* lipase
ClPFPE	Fluorolink 7004
ClPFPE-NH_4	ammonium salt of Fluorolink 7004
di-HCF4	sodium bis(2,2,3,3,4,4,5,5-octafluoro-1-pentyl)-2-sulfosuccinate
DSC	differential scanning calorimetry
DELOS	depressurisation of an expanded organic solution
EPR	electron paramagnetic resonance
F7H7	Sodium salt of the sulfate monoester of 1,1,1,2,2,3,3,4,4,5,5,6,6,7,7-pentadecafluoro-pentadecan-8-ol
FFV	fractional free volume
FID	flame-ionisation detector
FTIR	Fourier-transform infrared
GAS	gas anti-solvent
GC	gas chromatography
GEFTA	German Society for Thermal Analysis
HPA	p-hydroxyphenylacetic acid
HPLC	high performance (or high pressure) liquid chromatography
HPMC	hydroxypropylmethyl cellulose
HPP	p-hydroxyphenylpropionic acid
IUPAC	International Union of Pure and Applied Chemistry
Ls-54	Dehypon Ls-54
MAC	maximal allowable concentration
MBG	microemulsion-based (organo-)gel
MES	2-(N-Morpholino)ethanesulfonic acid sodium salt

MmL	*Mucor miehei* lipase
NCF	near-critical fluid
NMR	nuclear magnetic resonance
o/w	oil-in-water
PGSS	particles from gas-saturated solutions (or suspensions)
PFPE	perfluoropolyether
PFPE-NH_4	ammonium salt of perfluoropolyether carboxylic acid
PFPE-TMAA	perfluoropolyether trimethylammonium acetate
PFPE-PO_4	perfluoropolyether phosphate
PTFE	poly(tetraflouroethylene)
QTH	quartz tungsten halogen lamp
RESS	rapid expansion of supercritical solution
RNA	ribonucleic acid
SANS	small-angle neutron scattering
SAXS	small-angle X-ray scattering
SAS	supercritical anti-solvent
$scCO_2$	supercritical carbon dioxide
SCF	supercritical fluid
SCWO	supercritical water oxidation
SEDS	solution enhanced dispersion by supercritical fluids
SFC	supercritical fluid chromatography
SFDE	supercritical fluid derivatisation and extraction
SFE	supercritical fluid extraction
SFP	supercritical fluid precipitation
scH_2O	supercritical water
TLC	thin layer chromatography
Tris	2-amino-2-(hydroxymethyl)-1,3-propanediol
VOC	volatile organic compound
w/c	water-in-carbon dioxide
w/o	water-in-oil

Contents

1 Introduction

Environmental awareness has grown considerably over the last decades. Increasing concerns regarding toxicity and environmental compatibility of chemicals have led to an environmental legislation which imposes ever-increasing regulations and restrictions concerning the use and disposal of (potentially) hazardous materials on the chemical industry. This in turn has resulted in intensified efforts to find sustainable alternatives for the current chemical processes. Today, these endeavours are known as "sustainable development" and "green chemistry".
These terms describe a new field in chemistry with the objective to prevent pollution by the reduction, avoidance or elimination of hazardous substances in the design, manufacture or application of chemical products. Objective of all research activities are chemical processes or products that are inherently of less or even no risk to the human health or the environment. Among other strategies for achieving these aims, the research on catalytic reaction processes and sustainable solvents is of special interest [1, 2, 3, 4].
In the field of catalysis, the use of enzymes in organic synthesis and in non-conventional solvents has become an interesting alternative to conventional chemical methods [5, 6]. Enzymes usually display high chemo-, regio-, and enantioselectivity, which makes them especially attractive for biocatalytic applications in pharmaceutical, cosmetic, and agricultural areas with increasing demand for enantiomerically pure and specifically functionalised chemical compounds. Non-conventional solvents allow the catalysis of reactions which are thermodynamically unfavourable in water or result in water-induced side-reactions. Moreover, these media permit the solubilisation of hydrophobic substrates for enzyme-catalysed reactions.
Apart from other non-conventional media, the use of enzymes solubilised in hydrated reverse micelles or water-in-oil microemulsions has been the subject of investigation in several studies [5]. In addition, microemulsion-based organogels, i.e. gelled microemulsion systems based on biopolymers, have recently attracted attention as solid-phase catalysts in organic solvents due to problems in product isolation and enzyme reuse in microemulsion systems [7, 8].
In parallel, liquid or supercritical carbon dioxide ($scCO_2$) has emerged as perhaps the most promising "green" solvent (apart from water): carbon dioxide is toxicologically harmless, not inflammable, readily available and inexpensive. Besides, it exhibits a moderate critical point ($\Theta_c = 30.98\,^{\circ}C$, $p_c = 73.773\,bar$ [9]) and tunable solvent and solvation properties by simple control of pressure and temperature [10].
The range of (potential) applications of $scCO_2$ is quite large [11]: apart from extraction and cleaning processes, it is used as solvent for spray coating and chemical reaction. The already mentioned low critical temperature makes $scCO_2$ moreover, an ideal solvent for heat-sensitive substances and biocatalysts.
Consequently, the field of investigations on enzyme catalysis in $scCO_2$ has been continuously growing since the mid-1980s [12, 13, 14], when Randolph et al. were the first to conduct an enzymatic reaction in $scCO_2$ using alkaline phosphatase [15]. So far, studies concerning enzymatic catalysis in $scCO_2$ were predominantly performed with solid (free) or conventionally immobilised enzymes.

However, a major drawback of $scCO_2$ is the fact that it exhibits very low solubilities for polar and ionic substances. In order to overcome this limitation, the use of microemulsions with special CO_2-philic surfactants has attracted attention. Microemulsions in $scCO_2$ allow one to dissolve hydrophilic substances such as proteins within the aqueous core of the microemulsion nanodroplets [16, 17]. Moreover, they can be applied for the preparation of nanoparticles of defined size [18]. Recently, enzymatic reactions in microemulsions in $scCO_2$ were reported in literature [19, 20, 21]. Until now, a large number of experimental and theoretical studies has been carried out in order to find both suitable and sustainable surfactants for stabilising the water-CO_2 interface [22].

This thesis concerns the potential application of organogels as enzyme immobilisation matrix for enzymatic reactions in $scCO_2$ aiming at the replacement of volatile organic solvents, e.g. isooctane, used in the conventional biocatalytic process by $scCO_2$.

For this purpose, lipases were encapsulated in microemulsion-based organogels and tested for their catalytic activity in $scCO_2$. Various parameters affecting the biocatalysis such as pressure, mass fraction of biopolymer, alcohol and carboxylic acid chain length were studied. Moreover, a kinetic study was performed in order to clarify the reaction mechanism and to determine apparent kinetic constants. Apart from classical microemulsions, so-called detergentless microemulsions were used for the preparation of enzyme-containing organogels and tested for their capability to catalyse esterification reactions in $scCO_2$. In addition, phytantriol-based organogels as a new type of immobilisation matrix were tested for their potential use as solid-phase catalysts.

Furthermore, solubility studies on surfactants and related molecules were undertaken in order to identify new surfactants for the formation of microemulsions in $scCO_2$.

2 Fundamentals

2.1 Supercritical fluids

In 1822, Baron Cagniard de la Tour was the first to observe the appearance of a supercritical phase by increasing the temperature of a pure substance in a sealed glass vessel so that the two distinct gas and liquid phases disappeared into one visual phase [23, 24]. This early discovery marks the first notation of a SCF (supercritical fluid). About half a century later, T. Andrews performed a thorough study on (supercritical) carbon dioxide. He introduced the term "critical point" and described the true nature of the supercritical state: "Carbonic acid at 35°·5, and under 108 atmospheres of pressure, stands nearly midway between the gas and the liquid; and we have no valid grounds for assigning it to one form of matter any more than to the other. (...) the gaseous and the liquid state are only distant stages of the same condition of matter, and are capable of passing into one another by a process of continuous change." [25]. Finally, J. B. Hannay and J. Hogarth were the first to consider SCFs as possible solvents for low-vapour-pressure solid materials. They undertook systematic solubility studies on SCFs [26, 27, 28] demonstrating that e.g. cobalt(II) chloride, ferric chloride and potassium chloride were soluble in supercritical ethane. Apart from observing that a very finely divided solid could be produced by rapidly reducing the pressure of a supercritical solution, they were able to show that the dissolving power of a SCF is pressure dependent. The tunable solvation behaviour as illustrated by their experiments is the basis for the growing modern-day research interest in supercritical fluids as solvents resulting in applications such as SFE (supercritical fluid extraction) and RESS (rapid expansion of supercritical solution) processes.
The remainder of this section provides an introduction to physicochemical properties and applications of supercritical fluids with special emphasis on supercritical carbon dioxide.

2.1.1 The supercritical state of pure substances

Pure chemical substances exist in different states of matter according to the actual values of the external state variables pressure p and temperature T. Figure 2.1 shows the phase diagram of carbon dioxide as a typical example of the phase diagram of a pure substance. It allows the determination of the number and the type of the aggregation states for any pair of values (p, T) of the state variables [29].
The regions, in which the substance occurs as a single phase, i. e. solid (s), liquid (l) or gaseous (g), are bounded by curves indicating the coexistence of two phases in mutual equilibrium. The sublimation curve represents the equilibrium between solid and gaseous phase and the melting curve visualises the equilibrium between solid and liquid, whereas the vapour-pressure curve indicates the coexistence of liquid and gas. The three curves intersect at the triple point, which indicates the condition under which all three phases of a substance exist in mutual equilibrium. All coexistence curves, except for the vapour-pressure curve, tend to infinity or eventually intercept another equilibrium curve. However, the vapour-pressure curve begins at the triple point

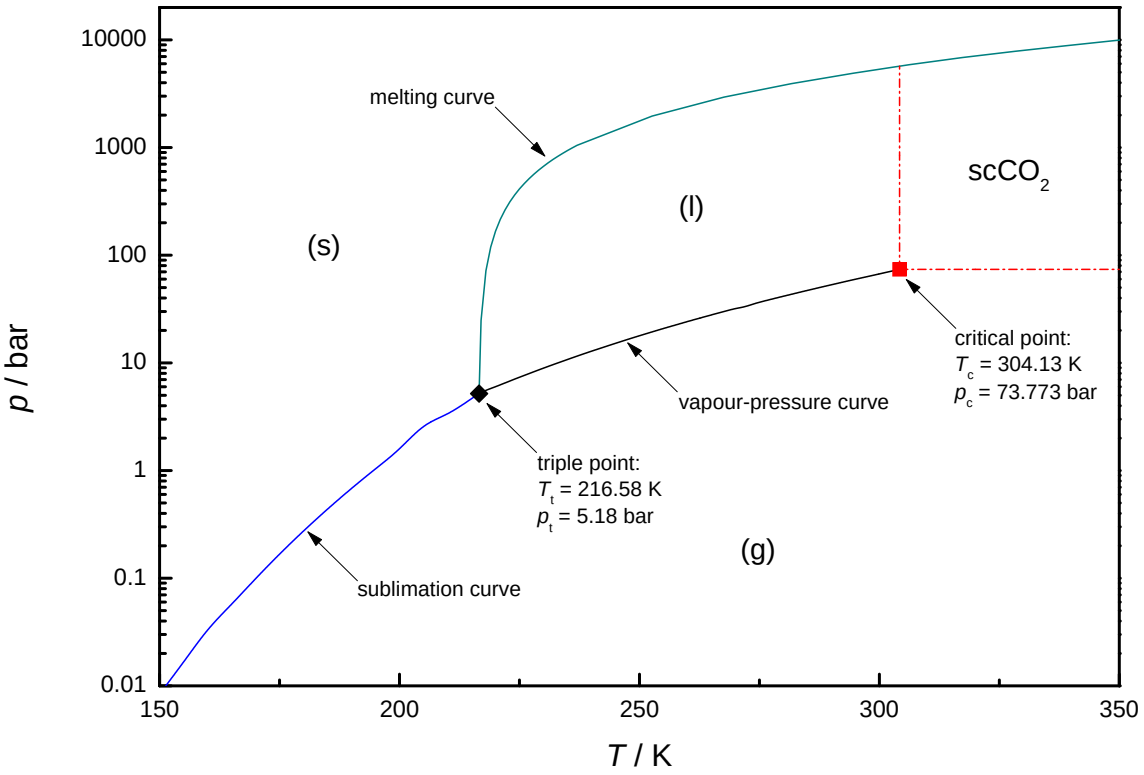

Figure 2.1: Phase diagram of carbon dioxide. Data taken from [9, 31, 32, 33].

and ends at the critical point. Increasing the temperature along this curve towards the critical point results not only in an increased pressure at which the two phases coexist, but also in a decreasing difference between the intensive properties of the liquid and the gaseous state. At the critical point, characterised by the substance-specific critical temperature T_c and pressure p_c, the densities and all other intensive properties of the liquid and the gaseous phase get identical. Consequently, the phase boundary between the liquid and the gas vanishes and both phases become indistinguishable at a temperature or a pressure beyond their critical values.

Thus, a pure substance is referred to as supercritical, if both the temperature, T, and the pressure, p, are above their critical values T_c and p_c, respectively. Additionally, the pressure has to be below the pressure p_s required to condense the fluid into a solid. This exception, omitted by the IUPAC definition, is necessary as the melting curve extends over the supercritical region [11, 30]. For example, the pressure required to solidify carbon dioxide at its critical temperature is only 5700 bar (cf. Figure 2.1).

Another commonly used expression is the term “near-critical fluid” (NCF). The near-critical region extends around the critical point but the description as near critical fluid is usually just used for fluids in the non-supercritical state.

2.1.2 Basic physical properties of supercritical fluids

The physical properties of SCFs vary over a wide range depending on pressure and temperature but are generally intermediate between those of gases and liquids [11, 35, 36]. Selected physical

Table 2.1: Comparison of the physical properties of gases, liquids, critical and supercritical fluids. Adapted with permission from [34]. Copyright 1987 VCH Verlagsgesellschaft.

Solvent	Density ρ/g cm^{-3}	Viscosity η/Pa s	Diffusion coefficient D/cm^2 s^{-1}
Gas [a]	$6 \cdot 10^{-4}$ - $2 \cdot 10^{-3}$	$1 \cdot 10^{-5}$ - $3 \cdot 10^{-5}$	0.1 - 0.4
Critical fluid [b]	0.2 - 0.5	$1 \cdot 10^{-5}$ - $3 \cdot 10^{-5}$	$7 \cdot 10^{-3}$
SCF [c]	0.4 - 0.9	$3 \cdot 10^{-5}$ - $9 \cdot 10^{-5}$	$2 \cdot 10^{-3}$
Liquid [a]	0.6 - 1.6	$2 \cdot 10^{-4}$ - $3 \cdot 10^{-3}$	$2 \cdot 10^{-6}$ - $2 \cdot 10^{-5}$

[a] $p = 1\,\text{bar}$, $\Theta = 25\,^\circ\text{C}$. [b] $p = p_\text{c}$, $\Theta = \Theta_\text{c}$. [c] $p = 4p_\text{c}$, $\Theta \approx \Theta_\text{c}$.

properties of SCFs in comparison to those of liquids and gases are shown in Table 2.1 revealing this Janus-faced nature of SCFs. The hybrid-like character arises from the fact that the liquid and the gaseous phase merge together at the critical point to form a single phase that can neither be attributed to the liquid nor the gaseous state.

The densities of SCFs are comparable to those of liquids and depend on both pressure and temperature as can be seen from Figure 2.2. Especially in the vicinity of the critical point they are very sensitive to small changes of the two state variables. As density is a measure of the solvating power of a solvent, changes of temperature and pressure can be used to continuously adjust the solubility in SCFs.

Increasing the pressure at constant temperature always results in an increased solubility due to rising density, whereas the effect of an isobaric temperature increase depends on the specific solute to be dissolved in the considered SCF. Below a system-specific inversion pressure lowering the temperature results in an enhanced solubility, whereas beyond this inversion pressure the opposite effect occurs [37, 38]. The explanation for this effect is the interplay between the vapour pressure of the solute and the density of the solvent, which are affected contrarily by the change of temperature. Raising the temperature results in a decreased density of the SCF, but in an increased vapour pressure of the solute. Below the inversion pressure the temperature-induced change of density prevails, whereas beyond the inversion point the change of vapour pressure predominates and leads to an improved solubility with rising temperature.

Another physical property which affects the solubility of substances in SCFs is the dielectric constant ϵ_r and, thus, the polarity of the solvent. The dielectric constant increases with pressure and behaves to some extent parallel to the density (cf. Figure 2.2 and Figure 2.3). Supercritical water (scH_2O; $T_\text{c} = 647.10\,\text{K}$, $\Theta_\text{c} = 373.95\,^\circ\text{C}$, $p_\text{c} = 220.64\,\text{bar}$ [9]) might serve as a good example for illustrating the tunable dielectric constant and polarity of SCFs: at 25 °C and 1 atm water has a dielectric constant of 78.4 [39], whereas scH_2O exhibits a dielectric constant of approx. 2 near the critical point and 32.1 at 10000 bar and 650 K [40]. Thus, water at ambient conditions is a polar solvent. On the other hand, scH_2O behaves as a more or less non-polar solvent with to some extent adjustable dielectric constant and polarity. Consequently, scH_2O shows a remarkable ability to dissolve non-polar organic compounds.

Both viscosity and diffusion coefficient represent transport properties of solvents affecting mass transfer rates. In general, viscosities of SCFs are similar to those of gaseous phases, whereas

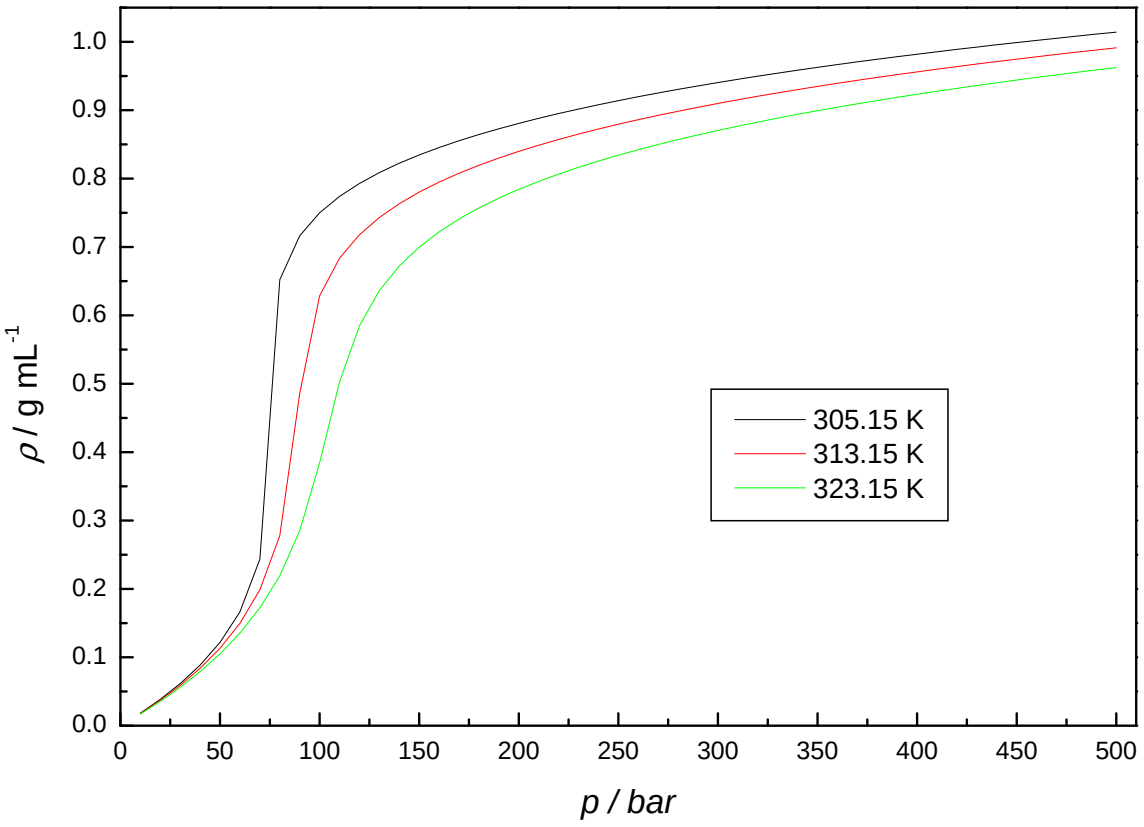

Figure 2.2: Density ρ of carbon dioxide as a function of pressure p at different temperatures. Data taken from [9].

the diffusion coefficients are intermediate between those for liquids and gases. This results in very low surface tensions, improved mass transport properties compared to liquids and low flow resistances. SCFs are more efficient in penetrating microporous solid structures and packed beds than liquids and solids tend to be dissolved faster in SCFs than in liquids.
Just like the density, viscosity and diffusion coefficient vary both with temperature and pressure. Density and viscosity increase with pressure accompanied by a decrease of the diffusion coefficient. This effect is less pronounced at higher pressures as density becomes less sensitive to pressure. In contrast, an isobaric increase of temperature generally results in an increase of the diffusion coefficient. However, changing the temperature at constant density seems to be negligible regarding diffusivity [11].

2.1.3 Technical applications of supercritical fluids

The special physical properties of SCFs as discussed in section 2.1.2 have resulted in several technical applications.
Among them, the supercritical fluid extraction (SFE) [35, 36, 38, 41, 42, 43, 44, 45, 46] is of particular importance. It is the most commonly used technical process employing SCFs and it is based on the high efficiency of SCFs in extracting substances from microporous solid

structures. The extracted component is dissolved in the fluid and the solution is removed from the feed material. Afterwards, the extracted species can be isolated by changing pressure and/or temperature and thus lowering its solubility in the particular SCF in use. This causes the solute to condense into a liquid or solid. Finally, the SCF can be recycled by recompressing it to extraction conditions.

The main advantages of SFE compared to conventional liquid extraction arise from the tunable solvation properties and the high recoverability of SCFs from the extract due to their high volatility. The separation of multiple substances dissolved from the extraction feed is often possible due to variable solvation properties and diverse solubilities of different solutes at the respective conditions. In addition, no harmful residues are left behind in the extracted substances if high volatile non-toxic SCFs are used.

Another technical application for SCFs is the supercritical fluid chromatography (SFC) [42, 47, 48, 49, 50]. Due to the outstanding properties of SCFs, the chromatography with supercritical fluids can be regarded as a hybrid between gas (GC) and liquid chromatography (LC). As the dissolving capacity of SCFs can be tuned continuously by changing pressure and/or temperature (cf. section 2.1.2), the partitioning between mobile and stationary phase can be influenced over a wide range, which allows the adjustment of separation conditions to a multitude of analytic problems. Consequently, its importance is based on the fact that it permits the separation and determination of compounds that are not conveniently handled by either gas or liquid chromatography. As gas chromatography is predominantly based on temperature control, it is an unsuitable method for the analysis of thermolabile substances. In contrast, SFC allows one to work pressure-controlled at low but constant temperatures and thus represents an applicable analytical method for these substances. Furthermore, it permits the analysis of non-volatile substances of high molecular weight, for which GC cannot be used due to the low densities of gases compared to SCFs. Advantages of SFC compared to LC arise from improved mass transport properties due to higher diffusion constants and from the fact that the separated substances can be easily obtained by simple reduction of pressure in the case of preparative chromatography. SFC has been applied to a wide variety of materials including natural products, drugs, foods, pesticides and herbicides, fossil fuels, explosives and propellants.

Apart from SFE and SCF, supercritical fluids are used for dyeing (supercritical fluid dyeing, SFD) [51, 52, 53, 54, 55, 56, 57] and impregnation [45, 58, 59, 60, 61, 62, 63] purposes. Both methods are based on the ability of SCFs to penetrate microporous structures, which allows the deposition of dissolved substances within the pores of solid materials by lowering the pressure. A further advantage of this technique is that both excess dyeing/impregnating agents and solvent can be easily recovered.

Furthermore, supercritical fluids are commonly used for the preparation of (extremely) fine particles. There are different techniques which are known under the generic term “supercritical fluid precipitation” (SFP). However, the terminology concerning the different SFP methods is not used uniformly in literature [64, 65, 66, 67]. The subsequent descriptions of the different SFP processes are based on [45, 65, 68].

One SFP technique is the so-called rapid expansion of supercritical solution (RESS). This process consists in solvating the product in a supercritical fluid and rapidly depressurising this solution through an adequate nozzle, which causes an extremely rapid nucleation of the product into a highly dispersed material. Known very long, the basic concept of the RESS method was first described by J. B. Hannay and J. Hogarth [26, 27, 28] (cf. section 2.1). The attractivity of

this process is rooted in the fact that it does not require further organic solvents. However, its application is limited to substances that present a reasonable solubility in the particular SCF in use.

A second type of SFP methods represent supercritical anti-solvent and related processes, which require a further (organic) solvent apart from the SCF. Consequently, the field of application for these methods is the processing of substances, which display poor solubilities in SCFs and thus do not permit the use of RESS. Furthermore, it is possible to deposit the processed substances on carriers (often polymers) which are present in the reaction vessel. This allows the formation active substance-loaded micro-/nano-spheres.

All supercritical anti-solvent and related processes have in common that the contact of a SCF with a solution of the product in a liquid organic solvent leads to a lowering of the solvent strength and thus to a supersaturation of the mixture as the SCF is (partially) dissolved in the organic solvent. This causes the solute to precipitate from the expanded solution. The various applications based on this so-called anti-solvent effect differ in the way the solution is exposed to the SCF.

In the case of the so-called gas anti-solvent (GAS) or supercritical anti-solvent (SAS) process, the liquid solution and the SCF are mixed in a high-pressure vessel by letting the SCF flow through the liquid solution. Another method called aerosol solvent extraction system (ASES) involves spraying of the solution through a nozzle into the SCF, while in the case of the solution enhanced dispersion by supercritical fluids (SEDS) process both solution and SCF are introduced together into a pressure and temperature controlled vessel by spraying them through the same nozzle with two coaxial passages.

Moreover, a third type of SFP methods can be applied for preparing fine particles. The respective technique is referred to as particles from gas-saturated solutions (or suspensions) (PGSS) or depressurisation of an expanded organic solution (DELOS). Here, a SCF is dissolved into a liquid substrate, or a solution of the substrate(s) in a solvent, or a suspension of the substrate(s) in a solvent followed by rapid depressurisation of this expanded solution through a nozzle which results in the formation of solid particles or liquid droplets according to the system. In contrast to the above mentioned anti-solvent processes, it is necessary that the solute does not precipitate upon the addition of the SCF. Accordingly, this technique can just be used if the solute-solvent couple does not show an anti-solvent effect.

In addition to the above mentioned technical applications, SCFs are also of interest for synthetical reactions because of their tunable solvation and mass transport properties. Thus a wide variety of reactions has been studied, among them: hydrogenations, hydroformylations, olefin metathesis reactions, radical reactions, Diels-Alder cylcoadditions, Friedel-Crafts alkylations, redox reactions, aldol additions, esterifications, polymerisation reactions, homogeneous and heterogeneous catalytic reactions, and enzymatic reactions [11, 14].

The physical properties of scH_2O have resulted in a special oxidation process called supercritical water oxidation (SCWO) [69, 70, 71, 72], which is mainly applied in the destruction of dangerous chemical wastes. As already stated in 2.1.2, scH_2O displays a remarkable solvating power for (non-polar) organic substances and gases such as oxygen. SCWO consists in the solvation of organic substances and compressed air in supercritical water, which results in a spontaneous and complete oxidation of the organic molecules by the aerial oxygen because of the high temperature ($\Theta_c = 373.95\,°C$ [9]). Hydrocarbons are degraded to water and carbon dioxide, while heteroatoms such as sulfur, chlorine and phosphorus in the organic molecules are converted to

the respective inorganic acids and nitrogen atoms yield ammonia, nitrous oxide, or nitrogen according to the oxidation conditions. As can be seen, the resulting oxidation products are at large relatively innocuous.

2.1.4 Supercritical carbon dioxide

2.1.4.1 Properties – advantages and disadvantages

Studies on SCFs have essentially focussed on four different fluids: carbon dioxide, ethane, ethene and water. Among them, supercritical carbon dioxide ($scCO_2$; $T_c = 304.13\,K$, $\Theta_c = 30.98\,°C$, $p_c = 73.773\,bar$ [9]) is the by far most widely used fluid. This fact is rooted in some advantages which $scCO_2$ offers in comparison with other SCFs [11].
$scCO_2$ exhibits a moderate critical temperature of 30.98 °C not far from room temperature (25 °C). As a consequence, $scCO_2$ is suitable for use as solvent for thermally labile natural substances or pharmaceutical agents. As many enzymes reach their activity maximum at temperatures just above the critical temperature of carbon dioxide, biocatalytic processes are a further field of possible applications for $scCO_2$.
The main advantage of $scCO_2$ lies in its toxicological and physiological safeness. Provided that the concentration of carbon dioxide is not too high, it can be regarded as non-toxic (MAC value: $9000\,mg\,m^{-3}$ [73]). Apart from air, nitrogen and water, carbon dioxide is the only substance which is explicitly excepted from the additive ban in foodstuffs [74] and does not have to be indicated to the consumer . The European Community (EC) Council directive 88/344/ECC, stating the regulations regarding the use of extraction solvents in the production of foodstuffs and food ingredients within the EC, classifies carbon dioxide as generally regarded as safe (GRAS). Besides, carbon dioxide can be removed without residue by release of pressure. Therefore, $scCO_2$ is of special interest for food technology, pharmaceutics and the production of cosmetics.
Furthermore, carbon dioxide is an environmentally benign and biocompatible solvent as it is ubiquitous in the atmosphere with a concentration of 0.03 % by volume [73] and 100 % biorecyclable trough photosynthetic pathways. Thus, carbon dioxide is regarded as an alternative to many organic solvents which are classified as volatile organic compounds (VOCs) and represent an environmental threat due to their volatility. Unlike many organic solvents, carbon dioxide is a relatively inert and non-flammable substance which contributes to the safety of processes using $scCO_2$ as solvent.
In addition, economic reasons plead for the use of $scCO_2$ as solvent. Carbon dioxide is priced – even highly purified – more reasonably (approx. $\$0.05\,kg^{-1}$ [75, 76]) than many organic solvents and is available in large quantities, as, at present, it is mainly recovered as a by-product of the industrial hydrogen and ammonia production. However, the sequestration of CO_2 from flue gases of power plants has increasingly gained importance in recent years. Alternatively, carbon dioxide can be extracted from the air.
An essential disadvantage of $scCO_2$ is the high critical pressure of 73.773 bar, which necessitates high engineering requirements and investments costs. As cost and apparative standards for the scale-up of practical applications are less demanding when liquid carbon dioxide is used at around its vapour pressure (approx. 25 °C, 60 bar), there is a tendency to use supercritical conditions only if necessary for processes such as fractionating or extraction.
A further drawback for the application of $scCO_2$ is the fact that carbon dioxide is not a completely inert solvent, as water in contact with CO_2 becomes acidic due to the formation and

Table 2.2: Schematic summary on the beneficial and adverse affects of chemical properties on the solubility of organic compounds in $scCO_2$. Adapted with permission from [35]. Copyright 1994 Springer-Verlag. Additional table entries according to [77].

Solubility enhancing	Solubility lowering
– unsaturations	– No. of carbon atoms
– branching	– aromaticity
– etherification	– aromatic substituents
– esterification	– OH groups
– fluoroalkyl groups	– COOH groups
– dimethyl siloxane groups	– halogen atoms apart from F
	– NH_2 groups
	– NO_2 groups

dissociation of carbonic acid. Accordingly, $scCO_2$ with admixed water is slightly corrosive and its applications are limited to reactions and separation processes where no pH-sensitive substances are involved. This restriction concerns particularly the use of enzymes in $scCO_2$ as many enzymes exhibit an optimum catalytic activity at higher pH values. Although it is possible to buffer the aqueous phase in such systems to a pH of about 5-7 [19, 78], the majority of enzymes with alkaline catalytic maximum do hardly come into consideration for catalysis in $scCO_2$. Only those enzymes can be used that are not denatured and display sufficient activity in the resulting acidic environment. Moreover, carbon dioxide tends to react with basic N–H functionalities in order to form amidocarbonic acids and carbamates [79]. This reaction capability of CO_2 restricts not only the usage of $scCO_2$ for the extraction and chromatography of amines, but is also problematic for the application of enzymes which frequently possess free amino groups in their active sites, as the formation of carbamates in presence of carbon dioxide is known to affect enzymatic activity [80, 81, 82, 83]. Besides, the coordination ability and reactivity of carbon dioxide towards various transition metal centers is well established [79, 84], which possibly causes problems for organometallic reactions in $scCO_2$.

Apart from the drawbacks mentioned above, the arguably most important disadvantage of $scCO_2$ is its hydrophobic, but not necessarily lipophilic character, which implies far-reaching restrictions for its applicability as solvent in technical processes, e.g. [76, 85, 86, 87]. Carbon dioxide exhibits very low solubilities for polar and ionic substances and for many (non-polar) compounds with high molecular weight. This behaviour arises from its very low values for the dielectric constant ϵ_r (cf. Figure 2.3) and for the polarisability α ($\alpha = 3.24 \cdot 10^{-40}\,C\,m^2\,V^{-1}$ [88]). Consequently, CO_2 is non-polar and has by far weaker intermolecular van der Waals interactions than those of lipophilic hydrocarbon solvents. This means that many substances such as polymers and many conventional surfactants with appreciable solubility in latter solvents show very poor solubilities in carbon dioxide. Although carbon dioxide is a low-dielectric fluid with no permanent dipole moment, it is also a Lewis acid and possesses a relatively large quadrupole moment. There are studies that suggest that CO_2 engages in quadrupole-quadrupole or quadrupole-dipole interactions with molecules that include certain types of polar functional groups such as esters,

ethers or hydrofluorocarbons, e.g. [87, 89]. Their results are used to explain why certain polymers with the respective functional groups show enhanced solubilities in $scCO_2$ in contrast to non-functionalised hydrocarbon polymers. Due to the complex behaviour of carbon dioxide as solvent, the terms "CO_2-philic" and "CO_2-phobic" have come into use in order to characterise the solvation properties of carbon dioxide and in order to classify substances according to their solubility in CO_2. Table 2.2 gives an overview on the influence of different chemical properties and functional groups on the solubility in $scCO_2$.

2.1.4.2 Strategies to enhance solubilities in supercritical carbon dioxide

As solubility limitations as described in section 2.1.4.1 are the main drawback for the application of $scCO_2$, the search for strategies to enhance solubilities – in particular of polar and ionic compounds – has been a major task in the $scCO_2$ research. In summary, the methods used to facilitate the dissolution of polar and ionic substances are based on two general principles: either increasing the polarity of the solvent or reducing the polarity of the compound to be dissolved in carbon dioxide [90].

2.1.4.2.1 Increase of solvent polarity

One possibility of increasing the polarity of carbon dioxide is to increase the density and thus the dielectric constant ϵ_r by raising the pressure or lowering the temperature as can be seen from Figure 2.3 (cf. also section 2.1.2). As thermolabile substances often require mild temperatures below 50 °C, the usually adjusted parameter in order to change solvent polarity is pressure.

Furthermore, an increase in solvent polarity and/or solvent strength of $scCO_2$ can also be achieved by admixture of one ore more cosolvents with higher polarity than CO_2. The added cosolvents are usually referred to as modifiers or entrainers. As $scCO_2$ is compatible and miscible with a great variety of common organic solvents, there are a lot of cosolvents to choose from in order to increase either the dielectric constant or the affinity towards certain compounds such as aromatic species. The most commonly used modifiers are short chain alcohols and among them methanol, although in some cases other entrainers such as hexane, toluene, aniline or diethylamine [92, 93] have been shown to be the more efficient additives. The modifier is usually added in a concentration range of 1-10 %. The more modifier is used, however, the less environmentally benign and sustainable the application gets despite the use of $scCO_2$ as chief component of the solvent. Furthermore, the application of less volatile cosolvents obviates one main advantage of carbon dioxide, which is the possibility to avoid solvent residues after depressurisation. Nevertheless, the addition of entrainers has proven to be a valuable tool for the modification of the solvent properties of $scCO_2$. This is not only based on the possibility to vary solvent polarity to a far greater extent than in pure $scCO_2$, but also on specific cosolvent-solute interactions and on effects on the leaching matrix in the case of SFE. As knowledge of the phase behaviour of the CO_2-modifier(s) mixtures is essential for process control and design, the investigation of phase equilibria has been a task of great interest. Reviews about systems studied in the last decades are given by Fornari et al. [94] and Dohrn and colleagues [95, 96].

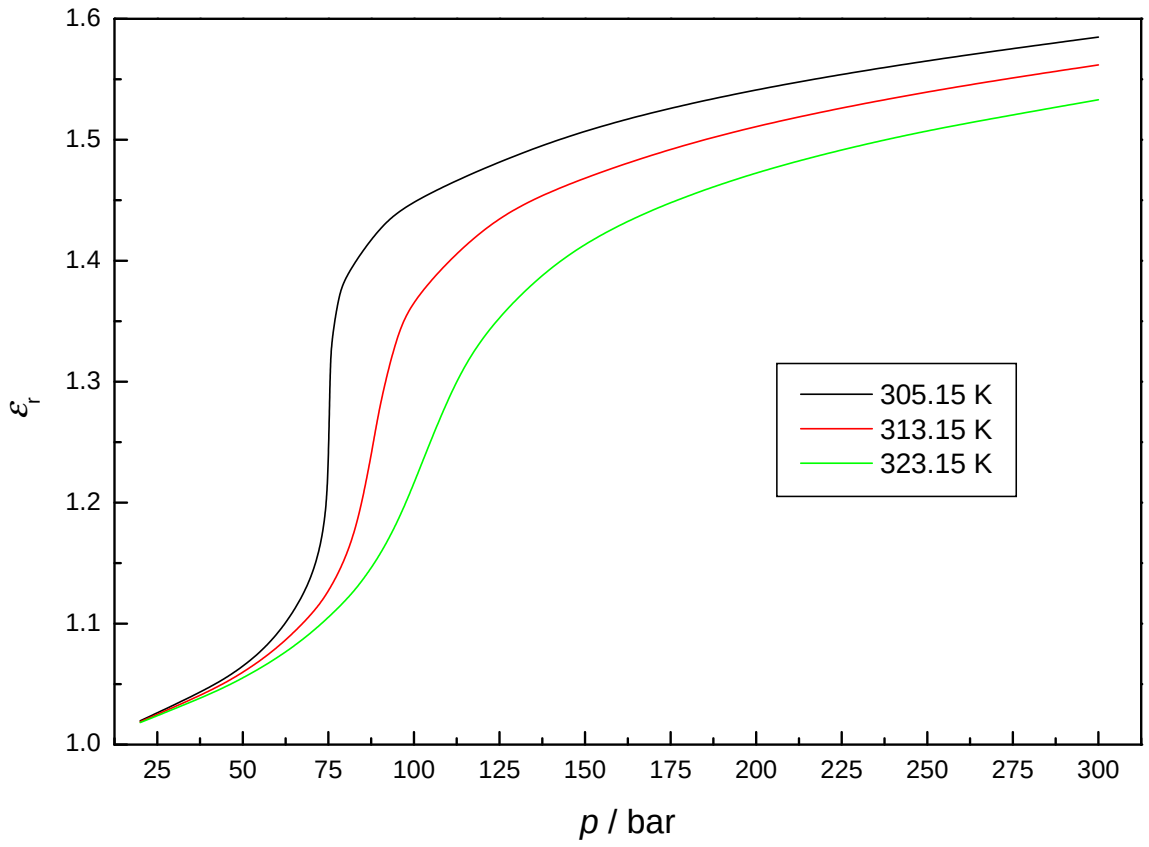

Figure 2.3: Dielectric constant ϵ_r of carbon dioxide as a function of pressure p at different temperatures. Data taken from [91].

2.1.4.2.2 Lowering the polarity of the compound to be dissolved

One method for enhancing the extraction efficiency of polar organics represents the in situ chemical modification under supercritical conditions, where polar groups (hydroxyl, carboxyl) are converted to less polar functionalities (ether, ester and sylil derivates) with CO_2-philic character. The resulting derivates are mostly more readily soluble in $scCO_2$. In case of SFE, this process is generally referred to as supercritical fluid derivatisation and extraction (SFDE) [97, 98].
Similarly, metals and their ions can be dissolved in $scCO_2$ by formation of organometallic compounds, as shown by Cai et al. [99], who developed a procedure for the simultaneous determination of butyltin and phenyltin compounds in sediment by in situ derivatisation with hexylmagnesium bromide in the extraction cell. A further instance is the speciation of organic and inorganic arsenic by GC after supercritical fluid extraction from sand supports with in situ derivatisation with thioglycolic acid methyl ester [100].
Another method for increasing the solubility of charged species in $scCO_2$ represents their neutralisation by ion-pair formation. The formed ion-pairs are less polar than the initial species and often tend to be soluble in carbon dioxide even without the addition of modifiers. The $scCO_2$ extraction of certain sulfonamides by means of ion-pair formation with trimethylphenylammonium as counterion has even proved to be more efficient than the corresponding extraction

Table 2.3: Industrial applications of supercritical carbon dioxide. Adapted with permission from [106]. Copyright 1996 Division of Chemical Education, Inc.

Process	Company
Decaffeination of coffee	Kaffee HAG AG
	Maxwell House
	Jacobs Suchard
Nicotin extraction (Tobacco)	Philip Morris
	Nippon Tobacco
	Fuji Flavor Co.
Hops extraction	SKW-Trostberg
	Barth and Co.
	Pitt–Des Moines
Extraction of aromas	CAL-Pfizer
Extraction of spices	Raps and Co.
Extraction of red pepper	Natural Care Byproducts
Extraction of pharmaceuticals from botanicals	Agrisana
Removal of lipids from bone	Bioland
Removal of oil from fiber optics rods	AT&T
Cleaning of aircraft gyrosopic components	U.S. Air Force

with methanol as solubility enhancer [101]. Further examples for the successful application of ion-pairing can be found in [102, 103].

Complex formation is a further method to increase the solubility of certain charged species such as metal ions in $scCO_2$. The ligands used for this purpose are generally dithiocarbamates, fluorinated dithiocarbamates, fluorinated β-diketones and ionisable crown ethers. An example for the latter ligand type is the tert.-butyl-substituted dibenzobistriazolo crown ether which permits the quantitative extraction of Hg^{2+} from sand, cellulose filter paper, and liquid samples by means of methanol-modified CO_2 under mild SFE conditions (60 °C, 200 atm), while other divalent metal ions, including Cd^{2+}, Co^{2+}, Mn^{2+}, Ni^{2+}, Pb^{2+} and Zn^{2+} are virtually unextractable under these conditions [104]. A strategy for the design of chelate ligands for $scCO_2$ is the attaching of CO_2-philic tail groups to conventional chelating agents [105]. In general, these modified CO_2-philic ligands can be used in the majority of the applications where their conventional analogues are used.

Finally, polar and ionic compounds can be dissolved in carbon dioxide by means of water-in-carbon dioxide microemulsions, where the water core of the microemulsion nanodroplets provides an appropriate environment for their incorporation. Details concerning microemulsions and reverse micellar systems in $scCO_2$ can be found in section 2.2.

2.1.4.3 Technical applications of liquid and supercritical carbon dioxide

As already stated in section 2.1.4.1, $scCO_2$ is the by far most widely used supercritical fluid. Consequently, many realised processes as described in section 2.1.3 utilise $scCO_2$ as solvent. This section gives a short survey of some selected technical applications of supercritical and liquid carbon dioxide besides SFC, SFD, supercritical fluid impregnation, and SFP.
The arguably best-known supercritical fluid extraction with $scCO_2$ as solvent is the decaffeination of coffee [36, 44], which is based on a patent developed by K. Zosel [107]. Due to its toxicological safeness and the fact that no solvent residue remains in the extract after depressurisation, the extraction with $scCO_2$ is frequently applied in food chemistry and pharmacy. Table 2.3 lists a few industrial processes. Further examples can be found in [108].
In recent years the cleaning of industrial component parts by means of $scCO_2$ has gained in importance, where carbon dioxide is used as a degreasing solvent in order to remove oily or fatty residuals from components within the manufacturing process. Possible fields of applications of CO_2-based cleaning processes include laser optical components, porous ceramic components, printed circuit boards, precision bearings, and machined parts. For example, Draper Laboratories (Cambridge, Massachusetts, USA) and Litton Industries (Salt Lake City, Utah, USA) use carbon dioxide in cleaning processes developed by CF Technologies (Hyde Park, Massachusetts, USA) for parts cleaning [109].
Moreover, $scCO_2$ is increasingly applied as a green alternative to conventional solvents for organic synthesis and polymerisation reactions. In 2002, Thomas Swan & Co. (Consett, U.K.) put a multipurpose plant into operation that uses carbon dioxide as reaction medium for hydrogenations, Friedel-Crafts alkylations and acylations, hydroformylations, and etherification reactions. Moreover, DuPont Fluoroproducts (Wilmington, Delaware, USA) started to use $scCO_2$ as solvent for the commercial production of poly(tetrafluoroethylene) resins in March 2002 [110]. Further potential applications in the field of polymer synthesis are precipitation polymerisations and surfactant-aided dispersion or emulsion polymerisations [10, 111].
Another industrial application is the so-called UNICARB process developed by Union Carbide (Danbury, Connecticut, USA). The UNICARB system uses $scCO_2$ as delivery solvent for spray coating materials, which allows the replacement of a substantial portion of the organic solvents present in conventional coating formulations. As a result, VOC emissions can be lowered while retaining coating sprayability [112].
Current research efforts include, inter alia, spin-coating of semiconductor wafers for the generation of high-quality thin films of CO_2-soluble photoresists for photolithography purposes [113] and the deposition of metals from $scCO_2$ solutions by chemical reduction of organometallic compounds [114, 115]. Following chemical vapour deposition, the latter process, which yields high purity films at low temperatures, is called chemical fluid deposition.

2.2 Microemulsions

2.2.1 Definition and properties

Microemulsions represent liquid, thermodynamically stable single-phase dispersions of two immiscible liquids and a dissolving intermediary. They are optically isotropic and either transparent or opalescent. The two immiscible liquids are generally water and an aliphatic hydrocarbon, which is usually referred to as oil, while the solubility promoter is either an ionic or a nonionic

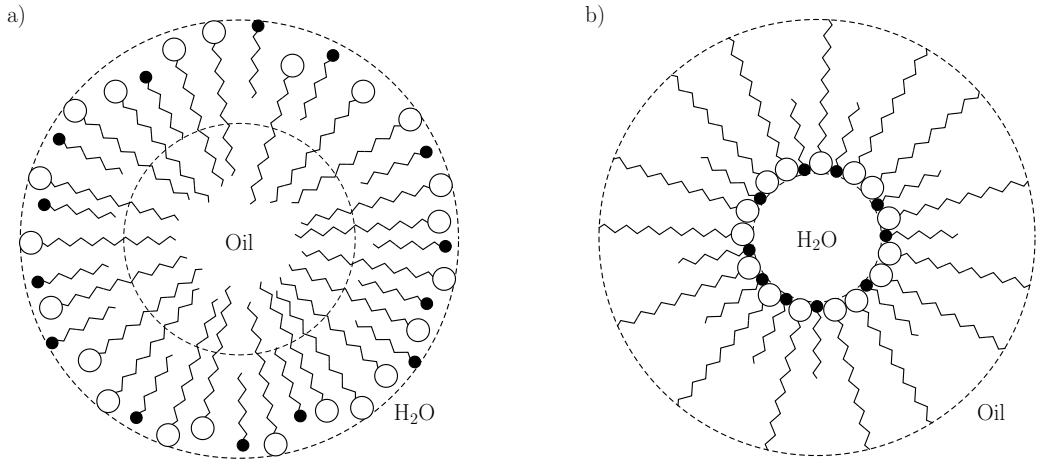

Figure 2.4: Schematic representation of nanodroplets in discrete microemulsions. a) Direct or o/w microemulsion. b) Reverse or w/o microemulsion. Tails with white "headgroups" represent surfactant molecules, while optionally admixed cosurfactants have black "headgroups". Adapted with permission from [116]. Copyright 1986 Springer-Verlag.

surfactant. However, some systems require the admixture of cosurfactants, which are mostly alcohols of medium chain length [117, 118, 119, 120, 121, 122, 123, 124].

Microemulsions are macroscopically homogeneous solutions which are microscopically heterogeneous. Concerning their structures two different models are discussed: discrete microemulsions and bicontinuous microemulsions.

Discrete microemulsions, as illustrated in Figure 2.4, consist of nanodroplets of one pseudophase (water or oil) dispersed in another pseudophase. Structures like that are generally found if one of the two immiscible liquids is present at much higher concentration than the second one and if only small amounts of amphiphile(s) are added to the system. The interface between the inner pseudophase (water or oil) and the outer or continuous dispersive pseudophase is stabilised by a monomolecular surfactant layer. The diameters of the dispersed nanodroplets are in the order of 10 nm to 100 nm. Thus, microemulsions are intermediate between micelles/micellar solutions (diameters < 10 nm) and (macro-)emulsions. Consequently, microemulsions are often described as swollen (reverse) micelles. According to their composition, a distinction is drawn between water-in-oil (w/o) and oil-in-water (o/w) microemulsions. In the case of liquid or supercritical carbon dioxide as continuous phase, the abbreviation w/c (water-in-CO_2) is commonly used for the respective microemulsions.

In the region of the phase diagram with comparable amounts of water and oil, bicontinuous sponge-like structures are observed, which are characterised by a morphology of interpenetrating domains of oil and water as shown in Figure 2.5.

In contrast to (macro-)emulsions, microemulsions are formed spontaneously, which can be attributed to the fact that interfacial tension is low enough to be compensated by the energy of dispersion. Besides, separation of the components is not possible by centrifugation.

As already stated, some microemulsions show the phenomenon of opalescence, which means that they scatter blue light more than red light. This effect can be attributed to Rayleigh scattering

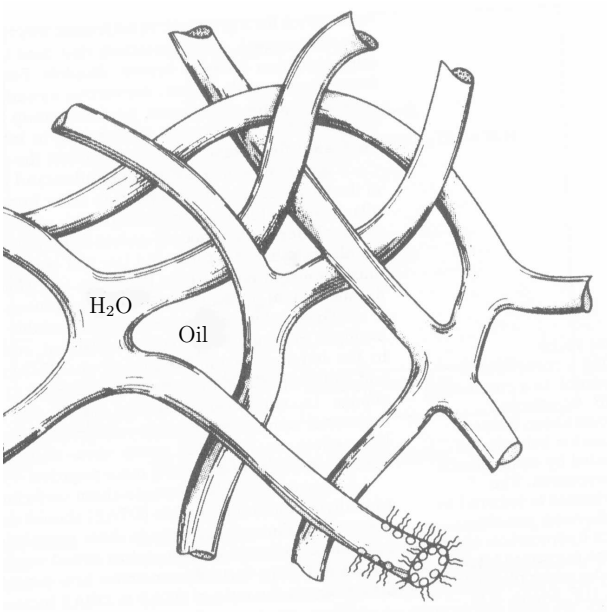

Figure 2.5: Schematic model of the interconnected conduits that compromise a bicontinuous microemulsion. Adapted with permission from [125]. Copyright 1986 American Chemical Society.

[126]. The turbidity τ is defined by

$$\exp(-\tau) = \frac{I_0 - I_{\text{sc}}^{\text{total}}}{I_0} \tag{2.1}$$

and describes the total relative amount of light scattered by a unit volume of the substance in all directions. I_0 is the intensity of the incident beam, while $I_{\text{sc}}^{\text{total}}$ is the loss of intensity with respect to the incident beam due to scattering. Furthermore, the turbidity τ depends on the wavelength λ of the scattered light:

$$\tau \propto \frac{1}{\lambda^4} \tag{2.2}$$

As can be seen from Equations (2.1) and (2.2), blue light is scattered more than red light due to its shorter wavelength λ.

2.2.2 Characterisation of ternary w/o microemulsions

Ternary w/o microemulsions consisting of surfactant, water and oil are generally characterised by the ratio W_0 of the molar amount of the surfactant to the molar water amount [127]:

$$W_0 = \frac{n_{\text{water}}}{n_{\text{surfactant}}} \tag{2.3}$$

According to Pileni [127] the term microemulsion corresponds to systems, where droplets containing a lot of water ($W_0 > 15$) are present, whereas aggregates containing just a small amount

of water ($W_0 < 15$) are usually called reverse (hydrated) micelles. In the latter case, the systems are often referred to as micellar solutions. However, in the literature there is frequently no clear distinction between these two cases and mostly the term microemulsion is used for the particular systems under investigation.
In addition, the volume fraction ϕ of the dispersed phase can be applied for the characterisation of ternary microemulsions. The volume fraction is defined as follows [128]:

$$\phi = \frac{V_{\text{water}} + V_{\text{surfactant}}}{V_{\text{water}} + V_{\text{surfactant}} + V_{\text{oil}}} \tag{2.4}$$

and for its calculation the microemulsion is regarded as ideal solution.
As water is slightly soluble in $scCO_2$ [129, 130], two modifications of the Equations (2.3) and (2.4) have been introduced for the characterisation of w/o microemulsions in $scCO_2$, which allow for this partial dissolution in the outer phase. The respective equations are

$$W_0^{\text{corr}} = \frac{n_{\text{water}} - n_{\text{water}}^{\text{CO}_2}}{n_{\text{surfactant}}} \tag{2.5}$$

$$\phi^{\text{corr}} = \frac{V_{\text{water}} - V_{\text{water}}^{\text{CO}_2} + V_{\text{surfactant}}}{V_{\text{water}} + V_{\text{surfactant}} + V_{\text{CO}_2}} \tag{2.6}$$

where $n_{\text{water}}^{\text{CO}_2}$ and $V_{\text{water}}^{\text{CO}_2}$ correspond to the water amount dissolved in the continuous $scCO_2$ phase.

2.2.3 Enzymatic catalysis in microemulsions and microemulsion-based gels

As already stated in chapter 1, the use of enzymes in organic synthesis and in non-conventional solvents has become an interesting alternative to conventional chemical methods [5, 6, 131]. One of the most intensively studied methods has been the technique of solubilising enzymes in hydrated reverse micelles or water-in-oil microemulsions where they may retain their catalytic ability. Consisting of small aqueous nanodroplets dispersed in a non-polar organic phase, microemulsions provide a water core where hydrophilic enzymes and reactants can be hosted, an interface where surface-active enzymes can be anchored, and a non-polar organic phase where hydrophobic substrates and products can be solubilised. Thus, microemulsions allow one to overcome solubility limitations of both hydrophilic and hydrophobic reactants. Furthermore, thermodynamic equilibrium in enzyme catalysed condensation and hydrolysis reactions can be shifted since the water concentration in microemulsions can be controlled to some extent. Of particular interest is the case of lipases (cf. section 2.3.3) since they display high stability and activity in this medium and may catalyse biotechnologically interesting synthetic reactions involving fatty acids apart from their physiological function to hydrolyse triglycerides [132]. Reviews concerning enzymatic reactions performed in microemulsions can be found in [5, 132, 133, 134]
Due to problems in product isolation and enzyme reuse in microemulsion systems, the use of microemulsion-based organogels (MBGs) has attracted attention. MBGs are rigid and stable in various non-polar organic solvents and may therefore be used for biotransformations in organic media. The gel matrix formed by a gelling agent, such as gelatin, fully retains the surfactant, water and enzyme components and can be handled as an immobilised biocatalyst that facilitates the diffusion of non-polar substrates and products. The preparation of MBGs was first reported

in 1986 [135, 136, 137]. Subsequent spectroscopic investigations [138, 139, 140] have shown that the microemulsion structure is well preserved in the gels, which are believed to contain a more or less networked bicontinuous structure stabilised by a surfactant layer that may co-exist with conventional w/o microemulsion droplets.
Robinson et al. [7, 8] were able to demonstrate that gelatin-based MBGs containing enzymes entrapped in an AOT microemulsion on the gel can be used as a new form of immobilised enzyme. Subsequent studies showed that MBGs formulated with gelatin can be used for the preparative-scale synthesis of miscellaneous esters and both regio- as well as stereoselectivity has been observed [7, 8, 141, 142, 143, 144, 145, 146, 147, 148, 149, 150]. Apart from gelatin, biopolymers such as agar, k-carrageenan and cellulose have been reported to form MBGs as an enzyme immobilisation matrix [151, 152, 153]. These gels overcome the restrictions to which the gelatin-based gels are subject with regard to biocatalytic applications, as they provide good mechanical and thermal stability and show high resistance to hydrophilic environments. A further approach to overcome the drawbacks of gelatin gels is to stabilise them by in situ polymerisation of tetraethoxysilane [154].

2.2.4 Detergentless microemulsions

It is known that alcohols can solubilise substantial amounts of water and oil and thus form isotropic solutions, which display a behaviour similar to that of microemulsions with regard to conductivity, ultracentrifugation, and light scattering despite the fact that the solutions do not contain surfactant [155, 156, 157, 158, 159, 160, 161]. In addition, these alcohol-based mixtures reproduce the phase behaviour of classical microemulsions. By analogy with latter systems, the ternary solutions, moreover, permit one to dissolve both hydrophobic and hydrophilic substances. Due to their resemblance to microemulsions, Smith et al. [155] introduced the designation "detergentless microemulsions" for these solutions. However, other authors prefer to refer to them as (surfactantless) microemulsion-like systems in order to draw a clear dividing line between them and conventional surfactant-based microemulsions [162].
Literature data concerning structure and microenvironment in surfactantless microemulsion-like systems are quite scarce and inconsistent [163, 164]. Khmelnitsky et al. [164] presented structural studies on a ternary system comprised of n-hexane, 2-propanol and water. Based on results from analytical ultracentrifugation and time-resolved fluorescence experiments, they concluded that the dispersed phase inside a limited area of the triangular phase diagram consists of aqueous nanodroplets as in classic microemulsion systems. Zoumpanioti et al. [163] conducted a fluorescence energy transfer study with *Mucor miehei* lipase and cis-parinaric acid as probes in order to determine the structure of detergentless microemulsions formulated with n-hexane, 1-propanol, and water in presence of enzyme. Their data indicated that the internal structure of the surfactant-free system differs from classical w/o microemulsions in the absence of well-defined reverse micelles where addition of water induces a swelling of the reverse micellar cores [163].
Just like conventional microemulsions, detergentless systems have been shown to serve as appropriate media for enzymatic catalysis in both oxidation and esterification reactions [165, 166, 167, 168]. Recently, Zoumpanioti et al. [165] reported on esterification reactions carried out in isooctane by means of lipase-containing surfactantless microemulsions immobilised on cellulose-based organogels as solid-phase catalysts.

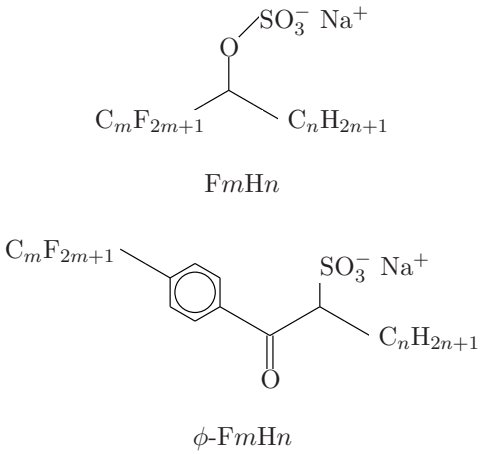

Figure 2.6: Constitutional formulas of hybrid sulfate surfactants FmHn and hybrid sulfonate surfactants ϕ-FmHn (FCm-HCn). F7H4: $m = 7$, $n = 4$. F7H7: $m = 7$, $n = 7$. F8H4: $m = 8$, $n = 4$. F8H8: $m = 8$, $n = 8$. ϕ-F4H4, FC4-HC4: $m = 4$, $n = 4$. ϕ-F6H2, FC6-HC2: $m = 6$, $n = 2$. ϕ-F6H4, FC6-HC4: $m = 6$, $n = 4$. ϕ-F6H6, FC6-HC6: $m = 6$, $n = 6$. ϕ-F6H8, FC6-HC8: $m = 6$, $n = 8$. Nomenclature of sulfonate surfactants according to Eastoe et al. (ϕ-FmHn) [185, 186] and according to Sagisaka et al. (FCm-HCn) [187, 188].

2.2.5 Surfactants for microemulsions in supercritical carbon dioxide

Preliminary studies by Consani and Smith [169] concerning the solubility of 130 common and commercially available surface active agents showed that most conventional surfactants are insoluble in CO_2. Among the tested surfactants, only a few nonionics exhibited reasonable solubility in CO_2. Based on the fact that fluorocarbons and carbon dioxide are compatible, Hoefling et al. [170] designed the first effective surfactants for application in CO_2. Subsequently, numerous research efforts have been made in order to find CO_2-philic surfactants in the last decade. Their results have highly contributed to the understanding of the relationship between structure and solubility in CO_2 as illustrated in Table 2.2.
This section intents to give a survey of "small molecule surfactants" [171] which are capable of stabilising water-in-carbon dioxide microemulsions. Polymeric amphiphile self-assembly in carbon dioxide solutions, cf. e.g. [85, 172, 173, 174, 175, 176, 177], use of stabilising agents for polymerisation reactions in CO_2, cf. e.g. [178, 179], and water-in-carbon dioxide emulsions, cf. e.g. [179, 180, 181, 182, 183, 184], are not taken into consideration.
A recent review concerning self assembly in (supercritical) carbon dioxide can be found in [22].

2.2.5.1 F7H7

The dichain hydrocarbon-fluorocarbon (hybrid) surfactant F7H7 is an amphiphile which allows the formation of swollen reverse micelles with substantial water content in supercritical and near-critical carbon dioxide. As can be seen from Figure 2.6, F7H7 is the sodium salt of the sulfate monoester of the partially fluorinated alcohol 1,1,1,2,2,3,3,4,4,5,5,6,6,7,7-pentadecafluoro-pentadecan-8-ol. While insoluble in $scCO_2$ without the presence of water, F7H7 can microemulsify

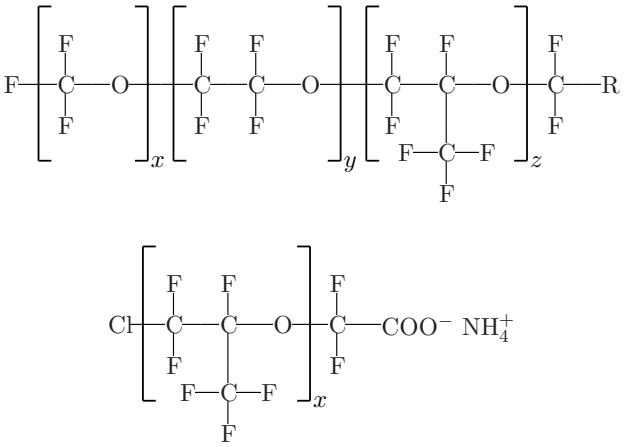

Figure 2.7: General constitutional formula of PFPE-based surfactants ($x + y + z \geq 4$; variable sequence of the repeating units) [192] and of ClPFPE-NH_4 [193]. PFPE-NH_4: R=COO^- NH_4^+ [194]. PFPE-PO_4: R=CH_2–O–CH_2–CH_2–$OPO(OH)_2$ [195, 196]. PFPE-TMAA: R=C(O)–NH–CH_2–$N^+(CH_3)_3$ CH_3COO^- [197].

slightly more than its own weight ($\sim$ 2 %) of water in carbon dioxide (25 °C, 231 bar), which corresponds to a water-to-surfactant ratio W_0^{corr} of 32 and is 10 times the amount soluble in pure compressed CO_2 [13].
Eastoe et al. [189] conducted small-angle neutron-scattering (SANS) experiments on F7H7-based microemulsions with a water-to-surfactant ratio W_0^{corr} of 33 (3 % (w/w) F7H7, 3.5 % (w/w) D_2O) in liquid carbon dioxide (25 °C, 500 bar). They were able to detect globular microemulsion droplets with an average core radius of 2.5 nm.
However, a major drawback for the usage of F7H7 is that the ester bond in the molecule is sensitive to hydrolysis due to the electron-withdrawing effect of the perfluorinated tail [13, 190].
Recently, Eastoe and colleagues [185, 186] extended their previous work on F7H7 by investigating the influence of variations in the chain length of fluorocarbon and/or hydrocarbon tail on the surfactant's ability to stabilise w/c microemulsion. They found that the equal chain compounds, F7H7 and F8H8, are more efficient than the asymmetric chain analogues such as F7H4 and F8H4.
Recently, Sagisaka and colleagues [187, 188] and Eastoe et al. [185, 186] reported on sulfonate hybrid surfactants (sodium 1-oxo-1-[4-(perfluoroalkyl)phenyl]-2-alkanesulfonates, ϕ-FmHn, FCm-HCn) to form microemulsions in $scCO_2$. In contrast to F7H7, these hydrocarbon-fluorocarbon amphiphiles have been shown to be highly resistant to hydrolysis [191].

2.2.5.2 Perfluoropolyether surfactants

Microemulsions or micellar solutions based on perfluoropolyether (PFPE) surfactants are the most often investigated micellar systems in $scCO_2$. Among the systems studied, anionic PFPE amphiphiles, which are predominantly ammonium carboxylates (PFPE-NH_4) are of particular importance, cf. for example [16, 17, 194, 198, 199, 200]. However, cationic PFPE, surfactants such as perfluoropolyether trimethylammonium acetate (PFPE-TMAA) have also been under investigation [197]. Furthermore, it has been shown that perfluoropolyether phosphates (PFPE-

PO_4; cf. section 2.2.5.3.1) [195, 196] and incompletely fluorinated derivates such as ClPFPE-NH_4 [201, 202] can be applied for the formation of microemulsions in $scCO_2$. Figure 2.7 gives an overall view on the constitutional formulas of the surfactants mentioned before.

Johnston et al. [16, 17] conducted Fourier-transform infrared (FTIR) spectroscopic experiments with PFPE-NH_4-based microemulsions in $scCO_2$, which showed that the water within the micellar core resembles bulk water. The bulk-like properties of the core water were confirmed by solvatochromic studies with methyl orange as probe. Moreover, Johnston et al. could demonstrate that hydrophilic proteins with high molecular weight such as bovine serum albumine and ionic compounds such as potassium permanganate or sodium dichromate can be dissolved in these microemulsions in $scCO_2$.

Further evidence for stable PFPE-NH_4-based micellar solutions with bulk-like water in carbon dioxide was provided by electron paramagnetic resonance (EPR) studies [194] and by small-angle neutron scattering (SANS) experiments [199] with deuterium oxide. The latter measurements revealed growing droplet core radii between 2.0 nm and 3.6 nm as the D_2O concentration increased from 0.8 % to 2.0 % (w/w) at a constant PFPE-NH_4 concentration of 2.1 % (w/w) in $scCO_2$ (35 °C, 192 bar $\leq p \leq$ 287 bar). More recently, Fremgen et al. [198] used nuclear magnetic resonance (NMR; ^1H and ^{19}F) and rotating frame-imaging NMR spectroscopy in order to observe spontaneous micelle formation in w/c microemulsions with PFPE-NH_4 as surface-active agent.

Droplet interactions in PFPE w/c microemulsions were investigated by both SANS [203] as well as conductivity [201, 204] studies. The results from neutron scattering exhibited that the respective attractive forces increase with decreasing pressure at constant temperature and with increasing temperature at constant pressure, respectively. This finding is consistent with cloud point measurements [194]. In the case of the conductance measurements, dynamic percolation [205, 206, 207] was identified at high volume fractions ϕ of the dispersed phase. Again, temperature and pressure dependence of the percolation thresholds exactly reflect the variation of attractive interdroplet interactions with both state variables. Furthermore, it could be shown that charge fluctuation models [208, 209, 210, 211] permit the calculation of droplet and core radii from conductivity measurements which are in good agreement to respective values obtained from SANS measurements [201].

As results from solvatochromic investigations [16, 17, 212] indicated that the pH within the dispersed aqueous phase drops to values of approx. 3 due to the formation of carbonic acid, Holmes et al. [78] inspected the applicability of several inorganic and/or organic buffers such as 2-(N-Morpholino)ethanesulfonic acid sodium salt (MES) for pH buffering within the water core of the microemulsion droplets. They were able to show that an increase in pH from approx. 3 to 5–7 can be achieved by admixture of suitable buffering agents. They also determined the influence of temperature, pressure, buffer type, buffer concentration, and ionic strength on the phase behaviour of the micellar system upon the addition of buffer. They found that the pressure-temperature phase boundaries for PFPE-NH_4-based w/c microemulsions are affected by the presence of buffer, as they are shifted to lower pressures and higher temperatures. This was explained by an increase of the rigidity of the interfacial region as a result of a closer packing of the polar surfactant headgroups because of an increased salinity of the dispersed phase.

Loeker et al. [202] screened PFPE-NH_4 surfactants of differing chain lengths but similar structure by means of in situ FTIR spectroscopy in order to study potential effects on their capability to form microemulsions in $scCO_2$. Among the systems studied, the ammonium carboxylate of

the PFPE acid Krytox FSL® with an average molecular weight of 2500 g mol^{-1} was the most efficient as indicated by the highest achieved water uptake. As both shorter and longer PFPE-NH_4 molecules were found to be less efficient, this was explained by the mentioned surfactant representing the best balance between hydro- and CO_2-philicity of all tested surfactants. Kinetic studies on the time dependence of the water uptake into the reverse micelles revealed, moreover, that a state of equilibrium is reached after about 24 h.
Kane et al. [21] were the first to conduct an enzymatic reaction within the water core of swollen reverse micelles stabilised by PFPE-NH_4 in supercritical carbon dioxide (35 °C, 100 bar $\leq p \leq$ 260 bar). They used cholesterol oxidase from *Pseudomonas fluorescens* for the oxidation of cholesterol to 4-cholesten-3-one in presence of catalase from *Aspergillus niger* which was added in order to destroy hydrogen peroxide created within the course of the oxidation reaction. The UV/vis-monitored reaction allowed the study of the effects of several process parameters such as water content, pressure, pH and incubation time. Another enzymatic reaction in PFPE-based microemulsions was reported by Irvin and John [20], who showed that horseradish peroxidase type II is capable of catalysing the polymerisation of p-cresol in a micellar system in liquid CO_2. As surfactant they used a mixture of PFPE-NH_4 and the corresponding free acid.
Although bioassays are indicative of a possible toxic effect of PFPE surfactants [213], many potential applications such as synthesis of metallic and semiconductor nanoparticles [18, 195, 196, 214], extraction of metals [215], and supercritical fluid dyeing [54, 216] have been the subject of investigation. Moreover, PFPE-based microemulsions in scCO_2 were shown to be novel media for both organic and inorganic reactions by Johnston et al. [17, 217, 218].
Recently, Lee et al. [219] demonstrated that perfluoropolyether surfactants are also capable of stabilising CO_2-in-water (c/w) microemulsions, which allow for the simultaneous solubilisation of certain fluorophilic, lipophilic molecules in the carbon dioxide nanodroplets and of hydrophilic substances in the dispersive water pseudophase. These systems could provide new opportunities in reaction, separation, and materials formation processes with carbon dioxide and water as solvents.

2.2.5.3 AOT and its derivates

AOT (sodium bis(2-ethylhexyl)-sulfosuccinate) and its analogues represent a group of surfactants which have given valuable insight into the design of CO_2-philic amphiphiles. Figure 2.8 gives an overview on the constitutional formulas of AOT and its derivates which have been the subject of investigation regarding both solubility in CO_2 and capability to stabilise w/c microemulsions.

2.2.5.3.1 AOT

The surfactant AOT (sodium bis(2-ethylhexyl)-sulfosuccinate) is an amphiphile which is commonly used for the preparation of microemulsions in organic solvents. Furthermore, AOT can be successfully applied for the same purpose in compressed alkanes [221].
Fulton et al. [222] were able to show that reverse micelles and microemulsions can be formed with AOT in supercritical ethane and propane. The systems studied consisted of 80-100 % alkane by weight and showed a strongly pressure-dependent phase and solubility behaviour. In particular, the molar water-to-surfactant ratio W_0 and thus the water content could be enhanced by increase of pressure. Further studies by Smith et al. [223, 224] reported on density, conductivity and phase behaviour measurements on AOT reverse micellar solutions in a variety of supercritical

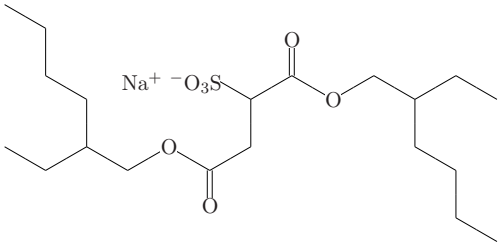

AOT

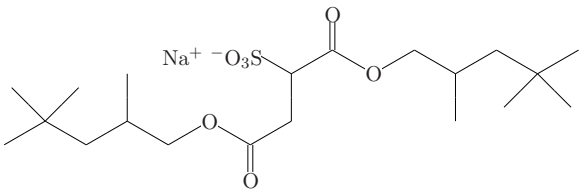

sodium bis(2,4,4-trimethyl-1-pentyl)-2-sulfosuccinate

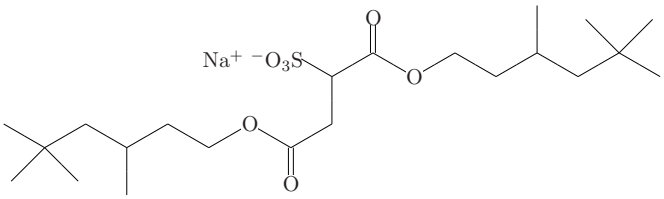

sodium bis(2,4,4-trimethyl-1-hexyl)-2-sulfosuccinate

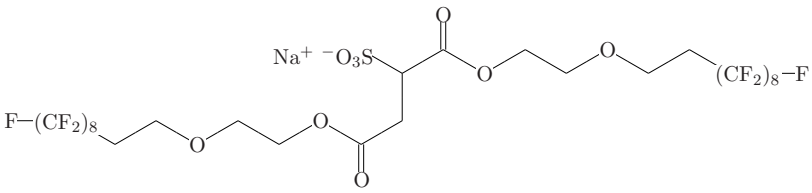

8FS(EO)$_4$

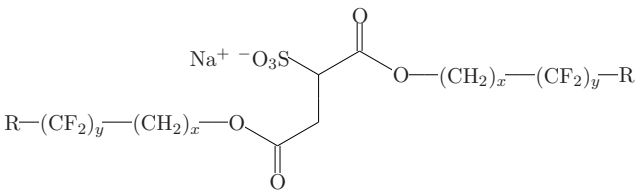

Figure 2.8: Constitutional formulas of AOT and its derivates. di-HCF2: $x = 1$, $y = 2$, R = H. di-HCF4: $x = 1$, $y = 4$, R = H. di-HCF6: $x = 1$, $y = 6$, R = H. di-CF2: $x = 1$, $y = 2$, R = F. di-CF3: $x = 1$, $y = 3$, R = F. di-CF4: $x = 1$, $y = 4$, R = F. di-CF6: $x = 1$, $y = 6$, R = F. di-CF8: $x = 1$, $y = 8$, R = F. di-CF4H: $x = 2$, $y = 4$, R = F. di-CF6H: $x = 2$, $y = 6$, R = F. di-CF8H, 8FS(EO)$_2$: $x = 2$, $y = 8$, R = F. Nomenclature of fluorinated surfactants according to [220] apart from 8FS(EO)$_2$ and 8FS(EO)$_4$ [187].

alkanes and noble gases. Ihara et al. [225] showed that AOT-based microemulsions in compressed n-pentane (50 °C, 50 atm) can be applied for the extraction of water-soluble vitamins from pharmaceutical preparations.
In contrast, AOT is not appropriate for the preparation of reverse micelles or microemulsions in liquid or supercritical carbon dioxide without an additional cosolvent or cosurfactant, as it is practically insoluble in carbon dioxide and exists in solution as a white waxy solid up to high pressures (25 °C to 100 °C, 400 bar) [13, 221]. Franco et al. [226] estimated the solubility of AOT in $scCO_2$ at less than 10^{-5} M (39 °C to 41 °C, 160 bar), while K. Jackson and J. L. Fulton [227] demonstrated that the dielectric constant in the visible spectral range, ϵ_{vis}, of the investigated supercritical and near-critical solvents has to be greater than 1.61 in order to dissolve 10 % (v/v) AOT at 25 °C. Accordingly, AOT cannot be solubilised in pure carbon dioxide due to the dielectric properties of this solvent. Yet, their study indicated that a possible strategy to dissolve AOT in $scCO_2$ was to add a cosolvent in order to raise the dielectric constant.
It was first shown by Ihara et al. [225] that AOT is indeed soluble in $scCO_2$ by addition of methanol or ethanol as modifier. Finally Hutton et al. [228, 229] demonstrated that reverse micellar solutions can be formed by addition of ethanol or n-pentanol in $scCO_2$ (175 bar to 250 bar; 40 °C to 70 °C). They conducted solvatochromic experiments with riboflavin as probe, which indicated that the microemulsion droplets contain a polar core with a dielectric constant of approx. 20. Consequently, they were not able to dissolve highly ionic compounds within the core of the swollen reverse micelles. An alternative possibility for the generation of w/c microemulsions with AOT in $scCO_2$ is the application of a cosurfactant, which was shown by Ji et al. [195] and Ohde et al. [196]. Both work groups used a perfluoropolyether phosphate as cosurfactant (cf. 2.2.5.2) for the synthesis of nanoparticles within microemulsions in $scCO_2$. Moreover, Liu et al. [230] reported on the use of 2,2,3,3,4,4,5,5-octafluoro-1-pentanol as cosurfactant in order to formulate AOT-based w/c microemulsions in $scCO_2$.

2.2.5.3.2 di-HCF4 and other fluorinated AOT derivates

In contrast to AOT, its fluorinated derivates have proven to be efficient surfactants which require neither additional cosolvents nor cosurfactants for the formation of microemulsions in near-critical and supercritical CO_2. Among them, sodium bis(2,2,3,3,4,4,5,5-octafluoro-1-pentyl)-2-sulfosuccinate (di-HCF4) is the arguably best-known surface-active agent.
Hoefling et al. [170] were the first to report on the good solubility of AOT derivates with two fluorinated alkyl tails. They could also show that the presence of this kind of surfactants permits the extraction of thymol blue from water with $scCO_2$.
First evidence for the existence of w/c microemulsions stabilised by 0.1 mol L^{-1} di-HCF4 was obtained by SANS measurements conducted by Eastoe et al. [231] in liquid carbon dioxide at a temperature of 15 °C and at pressures above 400 bar. The authors detected globular nanodroplets with core radii between 1.2 nm ($W_0 = 5$) and 3.7 nm ($W_0 = 30$) depending linearly on the molar water-to-surfactant ratio W_0.
Holmes et al. [19] reported on two enzymatic reactions conducted in di-HCF4-based microemulsions (30 mM di-HCF4, $W_0 = 10$) in compressed CO_2 at 20 °C and 450 bar: the hydrolysis of p-nitrophenyl butyrate catalysed by *Chromobacterium viscosum* lipase and the peroxidation of linoleic acid catalysed by soybean lipoxygenase. In order to improve the inherent condition of low pH in the water droplets upon pressurising with CO_2, the authors also examined several buffer substances for their potential application in w/c microemulsions. Among the buffering

agents tested, 2-(N-morpholino)ethanesulfonic acid sodium salt (MES) proved to be the most efficient in order to stabilise the pH in the range from 5–6 depending on buffer concentration, pressure, and temperature.

Subsequent investigations by J. Eastoe, D. C. Steytler, and colleagues [75, 220, 232, 233, 234] were concerned with structure-performance relationships of AOT analogues with varying chain lengths and fluorination degrees in CO_2. They could show that microemulsion stability and the efficiency of the tested surfactants as determined by cloud point/phase transition measurements are strongly influenced by subtle variations in the surfactant's molecular structure such as addition of extra methylene groups or replacement of the terminal CF_3– for HCF_2– groups. As can be seen from Table 2.4, their results indicate that di-CF4, di-CF4H and di-CF6, which exhibit the lowest phase boundaries, are the most efficient AOT analogues and thus display the highest compatibility with CO_2. Among them, di-CF4 seems to have the optimum chain length, which is also reflected in the results for di-CF4H and di-CF6H, with the longer compound requiring higher pressures. In addition, HCF_2-terminated surfactants, which exhibit a large dipole moment due to the substitution of fluorine by hydrogen, were found to be generally less efficient than those with CF_3-tips. Furthermore, the authors could demonstrate that the aqueous phase limiting surface tensions at the critical micelle concentration, γ_{cmc}, of the surfactants can be (linearly) correlated with the respective observed phase transition pressures p_{trans}: The lower the surfactant's surface tension γ_{cmc} is, the less pressure is required for the formation of stable microemulsions in CO_2, while surface active agents with two high surface tension such as AOT are even completely insoluble. Eastoe and coworkers pointed out that this finding might help to screen potential CO_2-philic surfactants by simple surface tension measurements in aqueous phase.

Erkey et al. [235, 236][1] used small-angle X-ray scattering (SANS) and cloud point measurements to characterise w/c microemulsions of di-HCF4 in $scCO_2$ for W_0 values between 0 and 20 at temperatures up to 55 °C and at pressures up to 350 bar. In summary, their results showed good agreement in phase behaviour and droplet size with previously published results [75, 220, 231, 233, 234].

In a recent study, Park et al. [237] investigated the influence of organic solvents such as acetonitrile and acetone on the phase behaviour of di-HCF4-based microemulsions in $scCO_2$.

Sagisaka et al. [187, 188, 238] gave details on further studies concerning structure-performance relationships of the fluorinated AOT analogues di-HCF4, di-HCF6, diHCF8, 8FS(EO)$_2$ (di-CF8H), and sodium bis((1H,1H,2H,2H-heptadecafluorodecyl)-oxyethylene)-2-sulfosuccinate (8FS(EO)$_4$). Among them, 8FS(EO)$_2$ was shown to have the highest microemulsion-forming potential despite its poor solubility in dry $scCO_2$. The reached W_0^{corr} value of approx. 32 for this surfactant is one of the highest values ever reported for w/c microemulsions. From comparisons with Krafft point and surface tension measurements in aqueous phases, the authors deduced that, apart from the limiting surface tension at the critical micelle concentration γ_{cmc}, the Krafft point temperature might be a further important parameter to be considered when predicting the ability of surfactants to stabilise microemulsions in $scCO_2$, since the most efficient surfactants were found to exhibit the highest Krafft temperatures.

[1] It should be noted that Erkey and colleagues use a different nomenclature for the homologous series of fluorinated AOT derivates in comparison to Eastoe et al. and Sagisaka et al. Data sets cannot be directly compared as there might be subtle differences in the chain-tip structures of the surfactants. In the present work, the nomenclature according to Eastoe et al. was adopted.

Table 2.4: Limiting air-water surface tensions at the critical micelle concentration, γ_{cmc}/mN m^{-1}, of various fluorinated AOT-derivates and their cloud point/phase transition pressures p_{trans} at 25 °C in liquid CO_2. Surfactant concentration: 0.05 mol L^{-1}. Molar water-to-surfactant ratio: $W_0 = 10$. For constitutional formulas of the respective surfactants cf. Figure 2.8. Adapted with permission from [220]. Copyright 2002 American Chemical Society. γ_{cmc} of AOT according to [234].

Surfactant	γ_{cmc}/mN m^{-1}	p_{trans}/bar
AOT	30.8 [a]	- [d]
di-HCF2	-	- [d]
di-HCF4	26.8 [a]	193
di-HCF6	24.1 [c]	164
di-CF2	-	- [d]
di-CF3	17.8 [a]	124
di-CF4	17.7 [b]	70
di-CF6	15.5 [c]	77
di-CF8	-	- [d]
di-CF4H	22.0 [a]	89
di-CF6H	25.8 [c]	139

Temperatures for tension measurements: [a] 25 °C, [b] 30 °C, [c] 40 °C. [d] No stable microemulsions observed.

2.2.5.3.3 Non-fluorinated AOT derivates

Apart from fluorinated AOT analogues, highly-methyl branched compounds such as sodium bis(2,4,4-trimethyl-1-pentyl)-2-sulfosuccinate and sodium bis(2,4,4-trimethyl-1-hexyl)-2-sulfosuccinate have been reported to be soluble in $scCO_2$ (33 °C, 250 bar) by Eastoe et al. [239]. The authors could further demonstrate that dry micellar solutions in $scCO_2$ (33 °C, 500 bar) with an overall surfactant concentration of 0.15 mol L^{-1} can be formed. The respective core radii as determined by SANS measurements were found to be between 1.4 nm and 2.0 nm. Besides, Eastoe and colleagues showed that sodium bis(2,4,4-trimethyl-1-hexyl)-2-sulfosuccinate allows dissolving of the highly polar dye dimidium bromide in $scCO_2$ (40 °C, 500 bar), while no dye uptake was observed in pure CO_2 or in presence of AOT.
Interestingly, both surfactants exhibit limiting air-water surface tensions at the critical micelle concentration, γ_{cmc}, of 27 mN m^{-1} and 28 mN m^{-1}, respectively. By analogy to the fluorinated AOT derivates, these values are again below the value measured for AOT confirming the finding that the surface tensions can be used as a guideline for solubility of surfactants and for microemulsion stabilities in $scCO_2$ (cf. Table 2.4 and section 2.2.5.3.2).

2.2.5.4 Anionic phosphate fluorosurfactants

Steytler et al. [240] were the first to test anionic phosphate fluorosurfactants for their ability to stabilise microemulsions in carbon dioxide. They synthesised ammonium phosphate analogues of

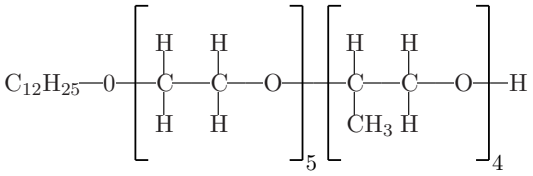

Figure 2.9: Constitutional formula of the surfactant Ls-54.

di-HCF4 and di-HCF6 (cf. section 2.2.5.3.2 and Figure 2.8), i.e. phosphate diesters of the same two fluorinated alcohols as in the respective succinates. Both surfactants, named di-HCF4-P and di-HCF6-P in accord to the previous nomenclature adopted for fluorosuccinates, were shown to stabilise w/c microemulsions. By analogy to their related AOT derivates, the longer chain di-HCF6-P was found to be more efficient with respect to microemulsion phase transition pressure.
Keiper and colleagues [241, 242] extended this work by synthesising fluorocarbon-hydrocarbon hybrid chain phosphates.
Recently, Xu et al. [243] reported on NMR and SANS studies on w/c microemulsions formed by phosphorous fluorosurfactants with structures similar to those phosphate amphiphiles used by Steytler et al. [240].

2.2.5.5 Nonionic surfactants

Besides ionic surfactants, nonionic surface active agents can also be used for the formation of reverse micellar solutions in $scCO_2$.
This was first shown by McFann and colleagues [86]. They applied solvatochromic probe and FTIR spectroscopy measurements in order to investigate the properties of micellar aggregates formed by pentaethylene glycol n-octyl ether (C8E5) with n-pentanol as cosolvent. The authors reached W_0^{corr} values of 12, but their further results showed that the micellar aggregates are rather small with a quite non-polar interior environment.
Recently, Liu et al. reported on two different non-fluorous surfactants, which were both shown to form microemulsions in $scCO_2$. One of them is the acetylenic glycol-based nonionic surfactant Dynol 604 from Air Products and Chemicals. The other one is the likewise nonionic surfactant (Dehypon) Ls-54, the constitutional formula of which is shown in Figure 2.9.
Concerning both surface active-agents Liu and coworkers conducted small-angle X-ray scattering experiments in addition to phase behaviour and solvatochromic studies [244, 245, 246, 247]. Their results proved the existence of water domains in both Dynol 604- and Ls-54-based $scCO_2$ microemulsions capable of dissolving both biomacromolecules such as lysozyme and methyl orange. Ls-54 SAXS data consistent with spherical micelles allowed the determination of reverse micelle radii between 2.04 nm and 2.52 nm depending on pressure and the achieved molar water-to-surfactant ratios W_0^{corr} between 2.0 and 8.0 [247]. The respective radii for Dynol 604 were estimated to be in the range of 7.4 nm to 7.8 nm at different pressures and water loadings [246].
In a continuative study on Ls-54, Liu et al. could, moreover, demonstrate that short-chain alcohols as cosurfactants can significantly reduce cloud point pressures [248]. In addition, Matthew and Becnel [249] measured diffusion coefficients of methyl orange dissolved in Ls-54-based micellar systems in CO_2.

Besides, two derivates of Ls-54, Ls-36 and Ls-45, were shown to stabilise microemulsions in $scCO_2$ by Liu et al. [250].
Recently, Sawada et al. [251] reported on w/c microemulsions formulated with nonionic polyethyleneglycol dialkylglycerol surfactants such as 2-(2-ethylhexyl)-1-octylglycerol ether.

2.3 Enzymes

Reactions in biological systems are mostly catalysed by specialised enzymes. Catalysis by these biocatalysts is necessary as non-catalysed chemical reactions are by far too slow to be effective under the conditions prevalent in most living cells – aqueous environments with neutral pH values and temperatures between 20 °C and 40 °C. Enzymes are characterised by an outstanding catalytic activity and specificity with regard to their substrates. Furthermore, enzymes display high regio- and enantioselectivity. As they easily outperform artificial catalysts in this respect, they have attracted much attention in pharmacy and agricultural chemistry, where the need for enantiomeric pure and specifically functionalised compounds is continuously growing.

2.3.1 Protein structure of enzymes

Apart from ribozymes, which are ribonucleic acid (RNA) molecules with catalytic functions in RNA processing, all enzymes are (modified) proteins which consist of one or more polypeptide chains called subunits. Biocatalysts made up of two or more subunits are termed oligomeric enzymes.
As the chemical and thus the catalytic potential of amino acid side chains is limited, many enzymes contain additional inorganic and/or organic compounds/groups, usually called cofactors, which provide further chemical and reactive properties and participate in the catalytic process. Therefore, so-called metalloenzymes comprise metal atoms or ions which represent efficient electron acceptors and donors in oxidation-reduction reactions. Besides metal ions, organic molecules which are referred to as coenzymes serve as cofactors. Some coenzymes are bound in an association/dissociation equilibrium to the enzymes, while others are covalently attached to the enzyme. In the latter case, the coenzymes are sometimes called prosthetic groups. They usually undergo cyclic reactions during the reaction course, but return to their initial state at the end of the catalytic process. In contrast, some non-covalently bound coenzymes are not regenerated during the reaction course and require separate reactions in order to revert to their initial state when not attached to the enzyme. As they resemble normal substrates, they can also be regarded as cosubstrates.
In summary, protein structure (of enzymes) can generally be classified into four structural levels [252, 253]: The so-called primary structure relates to the sequence of amino acids in a polypeptide chain with reference to the locations of disulfide bonds between cysteine side chains. It describes the complete covalent backbone in a polypeptide chain or protein and thus determines the higher structural elements as a result of the amino acid sequence. The secondary structure specifies the ordered arrangement of amino acids in localised regions of peptide chains. The two most common secondary structure segments are the right-handed α-helix and the β-pleated sheet. As a consequence of the localised definition of the secondary structure, a single polypeptide generally contains multiple secondary structural elements. The three-dimensional arrangement of all atoms in a peptide chain is referred to as ternary structure. For a monomeric protein

Table 2.5: Selection of some enzymatic reactions in $scCO_2$ catalysed by either free or immobilised enzymes.

Catalysed reaction	Enzyme	Ref.
Hydrolysis of p-nitrophenyl phosphate	alkaline phosphatase [a]	[15]
Transester. of methyl methacrylate by 2-ethylhexanol	*Candida cylindracea* lipase [a]	[80]
Oxidation of p-cresol and p-chlorophenol	polyphenol oxidase [b]	[254]
Transester. between triolein and stearic acid	*Rhizopus delemar* lipase [a]	[255]
Transester. between triolein and stearic acid	various lipases [c]	[256]
Oxidation of cholesterol	cholesterol oxidases [b]	[257]
Transester. of a N-acetyl-(L)-phenylalanine ester	*subtilisin Carlsberg* [a]	[258]
Esterification of oleic acid by ethanol	Lipozyme® [d]	[259]
Esterification of myristic acid by ethanol	Lipozyme® [d]	[260]
Esterification of oleic acid and rac-citronellol	*Candida cylindracea* lipase [b]	[261]
Enantioselective esterifcation of rac-ibuprofen	Lipozyme® IM 20 [d]	[262]
Acylation of glucose by lauric acid	*Candida rugosa* lipase [a]	[263]
Transester. between triolein and behenic acid	Lipozyme® IM [d]	[264]
Reduction of aromatic and cyclic ketones	alcohol deyhdrogenase [e]	[265]
Esterification of myristic acid by ethanol	crude hog pancreas lipase [a]	[266]
Esterification of isoamyl alcohol	crude hog pancreas lipase [a]	[267]

[a] free enzyme. [b] immobilised on glass beads (adsorptive and/or covalent). [c] adsorptive immobilised on Celite and Duolite. [d] *Mucor miehei* lipase immobilised on macroporous anionic resin beads. [e] immobilised resting cells of *Geotrichum candidum*.

consisting of a single polypeptide molecule, the ternary structure represents the highest structural level that is attained. Apart from non-covalent interactions, ionic and hydrogen bonds, disulfide bridges as mentioned before play a substantial role in the maintenance of the ternary structure. Finally, the quaternary structure characterises oligomeric proteins that consist of multiple subunits which are generally non-covalently linked.
The four levels of protein structure at large determine the characteristic shape of proteins, which is usually referred to as conformation. Depending on the environment, proteins and thus enzymes may exist in two or more different conformations. Conformational reshaping can be attributed to changes in the secondary, ternary and/or quaternary structure due to varied interaction forces as a result of environmental properties such as ionic strength, temperature and absence/presence of interfaces (cf. section 2.3.3).

2.3.2 Enzymatic reactions in supercritical carbon dioxide

Although Bourquelot and Bridel already reported on an enzymatic reaction in a non-aqueous solvent at the beginning of the last century [5, 268], it was not until the mid seventies that solvent systems apart from exclusively water have become the subject of extensive research [5, 6, 269, 270, 271, 272, 273, 274, 275]. In the period following, supercritical fluids have also

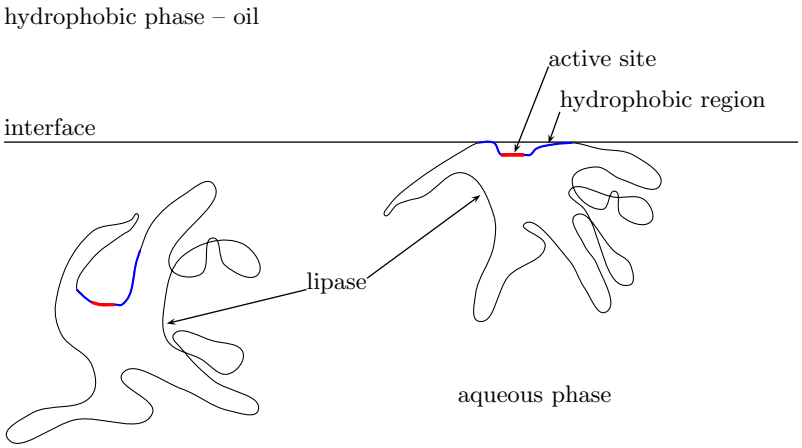

Figure 2.10: Schematic illustration of the interfacial activation of lipases [64].

been taken into consideration due to their solvation behaviour. Among them, special attention has been paid to $scCO_2$ because of its environmental compatibility and its low critical temperature of approx. 31 °C, which renders carbon dioxide an ideal solvent for heat-sensitive biocatalytic conversions. Consequently, enzymatic reactions in $scCO_2$ have been under investigation since 1985, when Randolph et al. were the first to conduct an enzymatic reaction in $scCO_2$ using alkaline phosphatase [15]. Apart from three reported reactions in microemulsions formulated with special CO_2-philic surfactants [19, 20, 21], the studies on biocatalysis in $scCO_2$ were predominantly performed with free (solid) or immobilised enzymes. The latter enzymes provide the advantage that they can be easily recovered and reused for further catalytic reactions in contrast to free enzymes. Table 2.5 gives a compilation of some investigated enzymatic reactions in $scCO_2$. Reviews about further systems studied are given by Perrut [12], Hartmann et al. [276] and Oakes et al. [14].
Of particular interest are the oxidation reactions as reported by Hammond et al. [254] and Randolph et al. [257], since they avail themselves of the fact that gases such as oxygen are completely miscible with supercritical fluids due to the partially gas-like character of SCFs. While oxygen displays very limited solubilities in organic and aqueous solvents [277], its concentration in $scCO_2$ can be continuously adjusted. Therefore, $scCO_2$ is a promising solvent for the oxidation of steroids, unsaturated fatty acids and other non-polar reductants.
As can be seen from Table 2.5, lipases have been most commonly used for studies on enzyme reactions in $scCO_2$. This is based on several advantages that lipases offer in comparison to other enzymes (cf. section 2.3.3). This work also reports on catalytic reactions in $scCO_2$ with lipases as enzymes.

2.3.3 Lipases and their interfacial activation

Lipases (acylglycerol acylhydrolases, EC 3.1.1.3) [278, 279, 280, 281] belong to the enzyme class of (serine) hydrolases. They are ubiquitous enzymes that catalyse the hydrolysis of triglycerides of higher fatty acids. However, their catalytic activity is not restricted to this type of substrates. Most lipases display a wide substrate spectrum and have the ability to reversibly hydrolyse various esters. Apart from their hydrolytic activity, they generally catalyse acyl transfer reactions,

where esters serve as acyl donors for the acylation of acyl acceptors such as alcohols, thiols and water (in the case of hydrolysis). Their pH optimum is generally between 5 and 9. Lipases differ from classic esterases in that their natural substrates are insoluble in water. Furthermore, esterases are just active in homogeneous aqueous phase, while lipases display maximal activity only at the water/oil interface.
The latter phenomenon is known as interfacial activation of lipases [282, 283, 284], which is based on (at least) two different conformational structures. The active site, which is also referred to as catalytic triad [285, 286], is located in a lipophilic region of the lipase. In aqueous environments, the triad is buried in the interior of the enzyme and covered by a hydrophilic lid-like structural element in order to avoid direct contact between the hydrophobic region and water. Accordingly, the lipase is inactive or displays just (very) low activity in this state. Furthermore, there is a structure in which the active site is exposed permitting the substrates to gain access to the catalytic region. The conformational change is induced by an oil/water or lipid/water interface, which initiates the structural rearrangement such as the movement of the lid in order to reveal the hydrophobic part. In a few cases, there is evidence for both the closed and the open form from X-ray investigations on crystal structures [287, 288, 289, 290, 284]. Figure 2.10 gives a schematic illustration of the interfacial activation.
Lipases are the most often applied biocatalysts in biotechnology and organic chemistry [5, 281, 291, 292, 293, 294]. This is not only based on their high chemo-, regio- and stereoselectivity, but also on their interfacial activation, because of which lipases represent a class of enzymes that is particularly suitable for the application in non-aqueous solvents including $scCO_2$ and in heterogeneous catalysis. Besides, they provide easy-to-study reactions as they usually do not require cofactors and as side reactions occur just exceptionally. In addition, lipases are readily available in large quantities since they are ubiquitous and can be isolated in high yields from microbial organisms such as fungi and bacteria. Finally, their use shows high commercial promise as many potential applications in the field of drugs, cosmetics and flavours exist.

2.3.4 Kinetics of unireactant enzymes

Enzyme kinetics is concerned with the factors that affect the rates of enzyme-catalysed reactions. The most important factors are pH, ionic strength and temperature apart from enzyme and ligand (substrates, products, inhibitors, and activators) concentrations. Their analysis allows not only the determination of the optimum conditions for catalysis, but can also give deeper insight into molecular mechanisms and into regulation processes in living cells. This section intents to give a short introduction on basic principles of enzyme kinetics illustrated by enzymatic reactions with only one substrate and product. The presentation is largely based on Refs. [252, 295, 296, 297, 298, 299] as sources of literature.

2.3.4.1 Michaelis-Menten Equation

The simplest case of an enzymatic reaction is an irreversible reaction with one substrate:

$$\mathrm{E} + \mathrm{A} \underset{k_{-1}}{\overset{k_1}{\rightleftharpoons}} \mathrm{EA} \xrightarrow{k_2} \mathrm{E} + \mathrm{P}$$

The enzyme E and the substrate A react together to form the enzyme-substrate complex EA,

which can irreversibly react to the product P and thus release the enzyme E or dissociate back to E and A.
The time-dependent variation of the concentrations [X] of all reaction participants X can be described as follows:

$$\frac{d[\mathrm{A}]}{dt} = -k_1[\mathrm{A}][\mathrm{E}] + k_{-1}[\mathrm{EA}] \tag{2.7}$$

$$\frac{d[\mathrm{E}]}{dt} = -k_1[\mathrm{A}][\mathrm{E}] + (k_{-1} + k_2)\,[\mathrm{EA}] \tag{2.8}$$

$$\frac{d[\mathrm{EA}]}{dt} = \quad k_1[\mathrm{A}][\mathrm{E}] - (k_{-1} + k_2)\,[\mathrm{EA}] \tag{2.9}$$

$$\frac{d[\mathrm{P}]}{dt} = \quad k_2[\mathrm{EA}] = v \tag{2.10}$$

v is the reaction velocity and k_i is the rate constant of the i-th partial reaction.
Provided that the overall reaction rate is limited by the breakdown of the EA complex to form the free enzyme and the product ($k_1 \approx k_{-1} \gg k_2$) and that the reaction velocity is measured during the early stages of the reaction, the system is in a so-called steady-state balance. In this state the enzyme-substrate complex forms at the same rate at which it decomposes and the following equation can be applied:

$$\frac{d[\mathrm{EA}]}{dt} = \frac{d[\mathrm{E}]}{dt} = 0 \tag{2.11}$$

The total enzyme concentration $[\mathrm{E}]_0$ can be expressed by:

$$[\mathrm{E}]_0 = [\mathrm{E}] + [\mathrm{EA}] \tag{2.12}$$

Thus, [EA] can be written as:

$$[\mathrm{EA}] = \frac{k_1[\mathrm{A}][\mathrm{E}]_0}{k_1[\mathrm{A}] + k_{-1} + k_2} \tag{2.13}$$

From Equations (2.10) and (2.13) follows for the reaction velocity:

$$v = \frac{d[\mathrm{P}]}{dt} = k_2[\mathrm{EA}] = \frac{k_2[\mathrm{A}][\mathrm{E}]_0}{\frac{k_{-1}+k_2}{k_1} + [\mathrm{A}]} \tag{2.14}$$

Substitution by

$$K_\mathrm{m} = \frac{k_{-1} + k_2}{k_1} \tag{2.15}$$

and

$$v_\mathrm{max} = k_2[\mathrm{E}]_0 \tag{2.16}$$

leads to the so-called Michaelis-Menten equation:

$$v = \frac{v_\mathrm{max}[\mathrm{A}]}{K_\mathrm{m} + [\mathrm{A}]} \tag{2.17}$$

where v_max is the maximum reaction velocity under saturation conditions and K_m is the Michaelis-Menten constant.

2.3.4.2 Reversible reactions

In case of a reversible enzymatic reaction course the reaction scheme can be depicted as follows:

$$\mathrm{E} + \mathrm{A} \underset{k_{-1}}{\overset{k_1}{\rightleftharpoons}} \mathrm{EA} \underset{k_{-2}}{\overset{k_2}{\rightleftharpoons}} \mathrm{E} + \mathrm{P}$$

This results in the following differential equation system:

$$\frac{d[\mathrm{E}]}{dt} = (k_{-1} + k_2)\,[\mathrm{EA}] - (k_1[\mathrm{A}] + k_{-2}[\mathrm{P}])\,[\mathrm{E}] \tag{2.18}$$

$$\frac{d[\mathrm{A}]}{dt} = (k_{-1} + k_2)\,[\mathrm{EA}] - k_1[\mathrm{A}][\mathrm{E}] \tag{2.19}$$

$$\frac{d[\mathrm{EA}]}{dt} = -(k_{-1} + k_2)\,[\mathrm{EA}] + (k_1[\mathrm{A}] + k_{-2}[\mathrm{P}])\,[\mathrm{E}] \tag{2.20}$$

$$\frac{d[\mathrm{P}]}{dt} = k_2[\mathrm{EA}] - k_{-2}[\mathrm{E}][\mathrm{P}] = v \tag{2.21}$$

Finally, the following equation can be derived for the reaction rate by means of the steady-state approach and Equation (2.12):

$$v = v_\mathrm{f} - v_\mathrm{r} = \frac{K_\mathrm{m}^\mathrm{P} v_\mathrm{max}^\mathrm{f}[\mathrm{A}] - K_\mathrm{m}^\mathrm{A} v_\mathrm{max}^\mathrm{r}[\mathrm{P}]}{K_\mathrm{m}^\mathrm{A} K_\mathrm{m}^\mathrm{P} + K_\mathrm{m}^\mathrm{P}[\mathrm{A}] + K_\mathrm{m}^\mathrm{A}[\mathrm{P}]} \tag{2.22}$$

where

$$K_\mathrm{m}^\mathrm{A} = \frac{k_{-1} + k_2}{k_1} \tag{2.23}$$

$$K_\mathrm{m}^\mathrm{P} = \frac{k_{-1} + k_2}{k_{-2}} \tag{2.24}$$

$$v_\mathrm{max}^\mathrm{f} = k_2[\mathrm{E}]_0 \tag{2.25}$$

$$v_\mathrm{max}^\mathrm{r} = k_{-1}[\mathrm{E}]_0 \tag{2.26}$$

K_m^A and K_m^P are the Michaelis-Menten constants for the respective compounds. v_f and v_r are the reaction velocities in the forward and the reverse direction, respectively, while $v_\mathrm{max}^\mathrm{f}$ and $v_\mathrm{max}^\mathrm{r}$ refer to the corresponding maximum reaction rates.
In the absence of product P ($[\mathrm{P}] = 0$) or of substrate A ($[\mathrm{A}] = 0$), the separated Michaelis-Menten equations for each reaction direction are obtained (cf. Equation (2.17)):

$$v_\mathrm{f} = \frac{v_\mathrm{max}^\mathrm{f}[\mathrm{A}]}{K_\mathrm{m}^\mathrm{A} + [\mathrm{A}]} \tag{2.27}$$

$$v_\mathrm{r} = \frac{v_\mathrm{max}^\mathrm{f}[\mathrm{P}]}{K_\mathrm{m}^\mathrm{P} + [\mathrm{P}]} \tag{2.28}$$

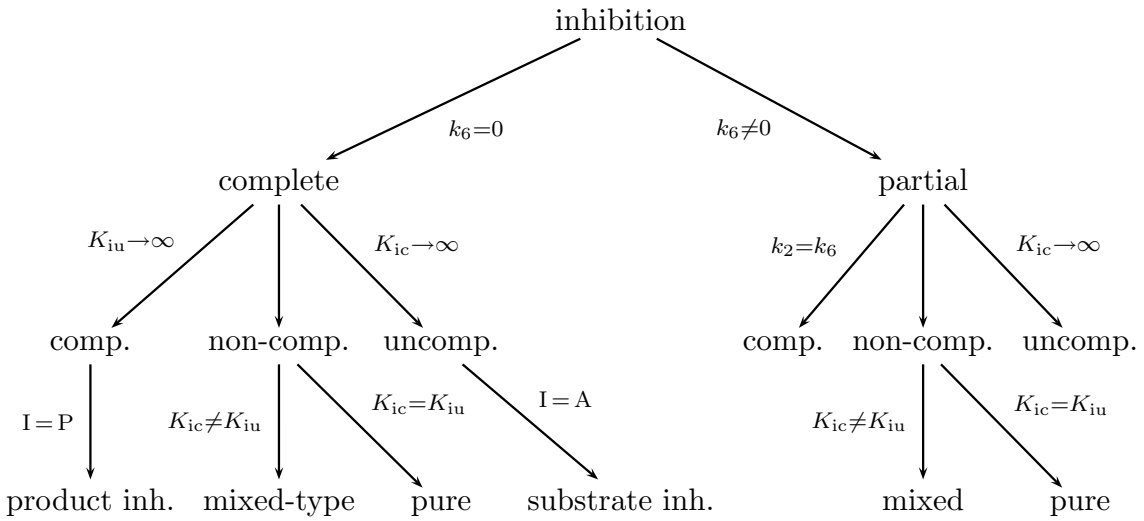

Figure 2.11: General survey of the most important types of reversible enzyme inhibition. comp.: competitive. non-comp.: non-competitive. uncomp.: uncompetitive. inh.: inhibition. Adapted with permission from [298]. Copyright 1994 VCH Verlagsgesellschaft.

2.3.4.3 Reversible enzyme inhibition

The term inhibition refers to the specific binding of ligands to defined (catalytic or regulatory) sites of enzymes which results in a reduction of the enzyme activity. The respective ligands are called inhibitors. Although other factors such as pH, temperature, ionic strength and solvent polarity can also inhibit enzyme activity, the resulting effects on reaction velocity are not embraced by the term "enzyme inhibition", as they are induced by non-specific impacts on the enzyme. Some inhibitors bind very strongly to the enzyme so that they are no longer removable from the binding site. The respective type of inhibition is characterised as irreversible, whereas a decrease in the reaction rate caused by detachable and/or displaceable ligands is referred to as reversible inhibition. Another distinction is drawn between complete and partial inhibition. In the latter case, the enzyme maintains an inhibitor-affected catalytic activity even after binding of the ligand, while in the case of the complete inhibition the enzyme-inhibitor complex does not display catalytic activity, which means that $k_6 = 0$ in Figure 2.11 and in Equation (2.33). Thus, complete inhibition is often referred to as dead-end inhibition, as enzyme-substrate complexes with bound inhibitor do not break down to form product.

2.3.4.3.1 General rate equation

The following scheme displays an enzymatic reaction scheme with partial non-competitive inhibition. The inhibitor I binds reversibly to the enzyme and affects the reaction velocity:

$$\begin{array}{ccccc} \mathrm{E} + \mathrm{A} & \underset{k_{-1}}{\overset{k_1}{\rightleftharpoons}} & \mathrm{EA} & \xrightarrow{k_2} & \mathrm{E} + \mathrm{P} \\ + \mathrm{I} & & + \mathrm{I} & & \\ k_3 \Big\| \; k_{-3} & & k_4 \Big\| \; k_{-4} & & \\ \mathrm{EI} + \mathrm{A} & \underset{k_{-5}}{\overset{k_5}{\rightleftharpoons}} & \mathrm{EAI} & \xrightarrow{k_6} & \mathrm{EI} + \mathrm{P} \end{array}$$

Two different dissociation constants, K_{ic} and K_{iu}, can be defined for the inhibitor I:

$$K_{\mathrm{ic}} = \frac{k_{-3}}{k_3} = \frac{[\mathrm{E}][\mathrm{I}]}{[\mathrm{EI}]} \tag{2.29}$$

$$K_{\mathrm{iu}} = \frac{k_{-4}}{k_4} = \frac{[\mathrm{EA}][\mathrm{I}]}{[\mathrm{EAI}]} \tag{2.30}$$

Allowing for the steady-state conditions and for the mass balance the following equation is obtained:

$$v = \frac{\left(v_{\max} + \frac{v^{\mathrm{i}}_{\max}[\mathrm{I}]}{K_{\mathrm{iu}}}\right)[\mathrm{A}]}{K_{\mathrm{m}}\left(1 + \frac{[\mathrm{I}]}{K_{\mathrm{ic}}}\right) + [\mathrm{A}]\left(1 + \frac{[\mathrm{I}]}{K_{\mathrm{iu}}}\right)} \tag{2.31}$$

where

$$v_{\max} = k_2[\mathrm{E}]_0 \tag{2.32}$$

$$v^{\mathrm{i}}_{\max} = k_6[\mathrm{E}]_0 \tag{2.33}$$

Although the presented case of a partial non-competitive inhibition does not occur frequently [298], it provides a general rate equation – Equation (2.31) – for deriving the respective equations for the most important inhibitions types as depicted in Figure 2.11. The remainder of this section focuses on three types of complete reversible enzyme inhibition: competitive, non-competitive, and uncompetitive

2.3.4.3.2 Competitive inhibition

In the case of competitive inhibition the inhibitor I combines with the free enzyme E in a manner that substrate binding is prevented as inhibitor and substrate are mutually exclusive. This can often be attributed to a true competition for the same enzyme site. Apart from reaction products, nonmetabolisable analogues or derivates of the true substrate and alternate substrates for the enzyme might act as competitive inhibitors.
The reaction scheme can be set up as follows:

$$\begin{array}{ccccc} \mathrm{E} + \mathrm{A} & \underset{k_{-1}}{\overset{k_1}{\rightleftharpoons}} & \mathrm{EA} & \xrightarrow{k_2} & \mathrm{E} + \mathrm{P} \\ + \mathrm{I} & & & & \\ k_3 \Big\| \; k_{-3} & & & & \\ \mathrm{EI} + \mathrm{A} & & & & \end{array}$$

Consequently, the equation for the reaction velocity can be derived from Equation (2.31) by omission of K_{iu} (i.e. $K_{\mathrm{iu}} \to \infty$ and $\frac{[\mathrm{I}]}{K_{\mathrm{ic}}} \to 0$):

$$v = \frac{v_{\max}[\mathrm{A}]}{K_{\mathrm{m}}\left(1 + \frac{[\mathrm{I}]}{K_{\mathrm{ic}}}\right) + [\mathrm{A}]} \tag{2.34}$$

2.3.4.3.3 Uncompetitive inhibition

An uncompetitive inhibitor is a ligand that binds reversibly to the enzyme substrate complex yielding an inactive EAI complex. Thus, the coordination site for the inhibitor is created by the interaction of substrate and enzyme in the EA complex. Complete uncompetitive inhibition is described by the following equilibria:

$$\begin{array}{ccccccc} \mathrm{E} & + & \mathrm{A} & \underset{k_{-1}}{\overset{k_1}{\rightleftharpoons}} & \mathrm{EA} & \xrightarrow{k_2} & \mathrm{E} + \mathrm{P} \\ & & & & + \mathrm{I} & & \\ & & & & k_4 \Big\| \; k_{-4} & & \\ & & & & \mathrm{EAI} & & \end{array}$$

By analogy with the competitive inhibition the rate equation can be obtained from Equation (2.31) as limit for $k_6 = 0$ and $K_{\mathrm{ic}} \to \infty$:

$$v = \frac{v_{\max}[\mathrm{A}]}{K_{\mathrm{m}} + \left(1 + \frac{[\mathrm{I}]}{K_{\mathrm{iu}}}\right)[\mathrm{A}]} \tag{2.35}$$

The scheme above shows that the maximal reaction rate $v_{\max}$ cannot be reached if inhibitor is present as some nonproductive EAI complex will always be formed. In contrast, it is possible to overcome the inhibition and to reach $v_{\max}$ by adding infinitely high (saturating) substrate concentrations in the case of the competitive inhibition.
A frequent example for uncompetitive inhibition is substrate inhibition where a second substrate molecule binds to the enzyme-substrate complex to form an inactive EAA complex. Consequently, the second substrate molecule can be formally regarded as an uncompetitive inhibitor.

2.3.4.3.4 Non-competitive inhibition

For the case of the complete non-competitive inhibition the subsequent scheme of equilibria can be applied:

$$\begin{array}{ccccccc} \mathrm{E} & + & \mathrm{A} & \underset{k_{-1}}{\overset{k_1}{\rightleftharpoons}} & \mathrm{EA} & \xrightarrow{k_2} & \mathrm{E} + \mathrm{P} \\ & + \mathrm{I} & & & + \mathrm{I} & & \\ k_3 \Big\| \; k_{-3} & & & & k_4 \Big\| \; k_{-4} & & \\ \mathrm{EI} & + & \mathrm{A} & \underset{k_{-5}}{\overset{k_5}{\rightleftharpoons}} & \mathrm{EAI} & & \end{array}$$

And from Equation (2.31) follows for the reaction velocity:

$$v = \frac{v_{\max}[\mathrm{A}]}{K_\mathrm{m}\left(1+\frac{[\mathrm{I}]}{K_\mathrm{ic}}\right)+\left(1+\frac{[\mathrm{I}]}{K_\mathrm{iu}}\right)[\mathrm{A}]} \tag{2.36}$$

Apparently, the non-competitive inhibition can be considered as a mixture of competitive and uncompetitive inhibition. Therefore it is very often referred to as mixed or mixed-type inhibition, while in the case of $K_\mathrm{ic} = K_\mathrm{iu}$ it is characterised as pure non-competitive inhibition, although some authors prefer the expression true non-competitive [300].

2.3.5 Steady-state kinetics of bireactant enzymes

In most enzymatic reactions two or more substrates are involved. An example is the case of lipases with two reactants and products. Therefore, this section deals briefly with two possible mechanisms for bireactant enzymes: Ordered Bi Bi and Ping Pong Bi Bi, respectively. Again, the presentation is based on Refs. [252, 295, 296, 297, 298, 299] as sources of literature.

2.3.5.1 Ordered Bi Bi System

In the case of an Ordered Bi Bi system the two substrates bind in a defined order to the enzyme in order to form a ternary central complex. This results in the following scheme of equilibria:

$$\mathrm{E} + \mathrm{A} \underset{k_{-1}}{\overset{k_1}{\rightleftharpoons}} \mathrm{EA}$$

$$\mathrm{EA} + \mathrm{B} \underset{k_{-2}}{\overset{k_2}{\rightleftharpoons}} \mathrm{EAB} \rightleftharpoons \mathrm{EPQ} \underset{k_{-3}}{\overset{k_3}{\rightleftharpoons}} \mathrm{EQ} + \mathrm{P}$$

$$\mathrm{EQ} \underset{k_{-4}}{\overset{k_4}{\rightleftharpoons}} \mathrm{E} + \mathrm{Q}$$

Figure 2.12 shows an alternative representation of the mechanism, which was introduced by Cleland [295, 296].

The equation for the reaction velocity is given by:

$$v = \frac{v^\mathrm{f}_{\max} v^\mathrm{r}_{\max}\left([\mathrm{A}][\mathrm{B}] - \frac{[\mathrm{P}][\mathrm{Q}]}{K_\mathrm{eq}}\right)}{v^\mathrm{r}_{\max} K^\mathrm{A}_\mathrm{i} K^\mathrm{B}_\mathrm{m} + v^\mathrm{r}_{\max} K^\mathrm{B}_\mathrm{m}[\mathrm{A}] + v^\mathrm{r}_{\max} K^\mathrm{A}_\mathrm{m}[\mathrm{B}] + v^\mathrm{r}_{\max}[\mathrm{A}][\mathrm{B}] + \alpha_1 + \alpha_2 + \alpha_3} \tag{2.37}$$

$$= \frac{v^\mathrm{f}_{\max}\left([\mathrm{A}][\mathrm{B}] - \frac{[\mathrm{P}][\mathrm{Q}]}{K_\mathrm{eq}}\right)}{K^\mathrm{A}_\mathrm{i} K^\mathrm{B}_\mathrm{m} + K^\mathrm{B}_\mathrm{m}[\mathrm{A}] + K^\mathrm{A}_\mathrm{m}[\mathrm{B}] + [\mathrm{A}][\mathrm{B}] + \frac{\alpha_1}{v^\mathrm{r}_{\max}} + \frac{\alpha_2}{v^\mathrm{r}_{\max}} + \frac{\alpha_3}{v^\mathrm{r}_{\max}}} \tag{2.38}$$

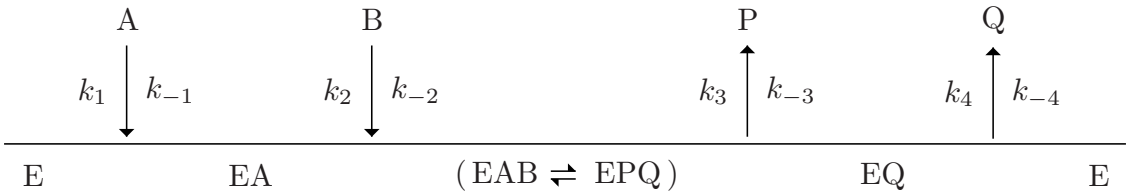

Figure 2.12: Cleland notation of an Ordered Bi Bi reaction (cf. e.g. [297]). A, B: substrates. P, Q: products. E: free enzyme. EA: enzyme-substrate complex. EQ: enzyme-product complex. EAB: enzyme-substrate-substrate complex: EPQ: enzyme-product-product complex.

where

$$\alpha_1 = \frac{v_{\max}^{\mathrm{f}}}{K_{\mathrm{eq}}} \left(K_{\mathrm{m}}^{\mathrm{Q}}[\mathrm{P}] + K_{\mathrm{m}}^{\mathrm{P}}[\mathrm{Q}] + [\mathrm{P}][\mathrm{Q}] \right) \tag{2.39}$$

$$\alpha_2 = \frac{v_{\max}^{\mathrm{r}} K_{\mathrm{m}}^{\mathrm{A}}[\mathrm{B}][\mathrm{Q}]}{K_{\mathrm{i}}^{\mathrm{Q}}} + \frac{v_{\max}^{\mathrm{r}}[\mathrm{A}][\mathrm{B}][\mathrm{P}]}{K_{\mathrm{i}}^{\mathrm{P}}} \tag{2.40}$$

$$\alpha_3 = \frac{v_{\max}^{\mathrm{f}}}{K_{\mathrm{eq}}} \left(\frac{K_{\mathrm{m}}^{\mathrm{Q}}[\mathrm{A}][\mathrm{P}]}{K_{\mathrm{i}}^{\mathrm{A}}} + \frac{[\mathrm{B}][\mathrm{P}][\mathrm{Q}]}{K_{\mathrm{i}}^{\mathrm{B}}} \right) \tag{2.41}$$

$K_{\mathrm{m}}^{\mathrm{X}}$ is the Michaelis-Menten constant, while $K_{\mathrm{i}}^{\mathrm{X}}$ is the inhibition constant for the respective species X. $v_{\max}^{\mathrm{f}}$ and $v_{\max}^{\mathrm{r}}$ refer to the maximum reaction rates in forward and reverse direction, respectively. Furthermore, K_{eq} represents the thermodynamic equilibrium constant for the overall reaction. If $[\mathrm{P}] = 0$ and $[\mathrm{Q}] = 0$, Equation (2.38) can be simplified to give the initial reaction rate in the absence of products:

$$v = \frac{v_{\max}[\mathrm{A}][\mathrm{B}]}{K_{\mathrm{i}}^{\mathrm{A}} K_{\mathrm{m}}^{\mathrm{B}} + K_{\mathrm{m}}^{\mathrm{B}}[\mathrm{A}] + K_{\mathrm{m}}^{\mathrm{A}}[\mathrm{B}] + [\mathrm{A}][\mathrm{B}]} \tag{2.42}$$

2.3.5.2 Ping Pong Bi Bi System

Another possible mechanism for enzymatic reactions with two substrates is the so-called Ping Pong Bi Bi mechanism. The expression "Ping Pong" refers to the fact that a product is released between the ordered addition of two substrates. Hence, the reaction scheme can be set up as follows:

$$\mathrm{E} + \mathrm{A} \underset{k_{-1}}{\overset{k_1}{\rightleftharpoons}} \mathrm{EA} \rightleftharpoons \mathrm{E^*P} \underset{k_{-2}}{\overset{k_2}{\rightleftharpoons}} \mathrm{E^*} + \mathrm{P}$$

$$\mathrm{E^*} + \mathrm{B} \underset{k_{-3}}{\overset{k_3}{\rightleftharpoons}} \mathrm{E^*B} \rightleftharpoons \mathrm{EQ} \underset{k_{-4}}{\overset{k_4}{\rightleftharpoons}} \mathrm{E} + \mathrm{Q}$$

Again, an alternative representation is given in Figure 2.13. As can be seen, this mechanism involves two different stable enzyme forms. The free enzyme E and a modified enzyme $\mathrm{E^*}$,

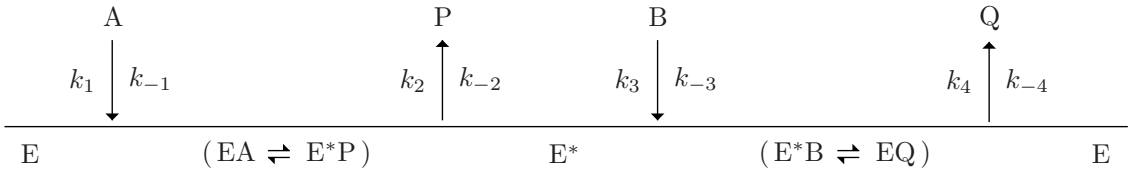

Figure 2.13: Cleland notation of a Ping Pong Bi Bi reaction (cf. e.g. [297]). A, B: substrates. P, Q: products. E: free enzyme. E*: modified enzyme. EA: enzyme-substrate complex. EQ: enzyme-product complex. E*B: modified enzyme-substrate complex. E*P: modified enzyme-product complex.

which is usually substituted by a reactive group of substrate A. In addition, two sets of central complexes occur during the reaction sequence.
The reaction velocity v is given by:

$$v = \frac{v^{\mathrm{f}}_{\max} v^{\mathrm{r}}_{\max} \left([\mathrm{A}][\mathrm{B}] - \frac{[\mathrm{P}][\mathrm{Q}]}{K_{\mathrm{eq}}} \right)}{v^{\mathrm{r}}_{\max} K^{\mathrm{B}}_{\mathrm{m}} [\mathrm{A}] + v^{\mathrm{r}}_{\max} K^{\mathrm{A}}_{\mathrm{m}} [\mathrm{B}] + v^{\mathrm{r}}_{\max} [\mathrm{A}][\mathrm{B}] + \alpha_1 + \alpha_2 + \alpha_3} \tag{2.43}$$

$$= \frac{v^{\mathrm{f}}_{\max} \left([\mathrm{A}][\mathrm{B}] - \frac{[\mathrm{P}][\mathrm{Q}]}{K_{\mathrm{eq}}} \right)}{K^{\mathrm{B}}_{\mathrm{m}} [\mathrm{A}] + K^{\mathrm{A}}_{\mathrm{m}} [\mathrm{B}] + [\mathrm{A}][\mathrm{B}] + \frac{\alpha_1}{v^{\mathrm{r}}_{\max}} + \frac{\alpha_2}{v^{\mathrm{r}}_{\max}} + \frac{\alpha_3}{v^{\mathrm{r}}_{\max}}} \tag{2.44}$$

where

$$\alpha_1 = \frac{v^{\mathrm{f}}_{\max}}{K_{\mathrm{eq}}} \left(K^{\mathrm{Q}}_{\mathrm{m}} [\mathrm{P}] + K^{\mathrm{P}}_{\mathrm{m}} [\mathrm{Q}] + [\mathrm{P}][\mathrm{Q}] \right) \tag{2.45}$$

$$\alpha_2 = \frac{v^{\mathrm{r}}_{\max} K^{\mathrm{A}}_{\mathrm{m}} [\mathrm{B}][\mathrm{Q}]}{K^{\mathrm{Q}}_{\mathrm{i}}} \tag{2.46}$$

$$\alpha_3 = \frac{v^{\mathrm{f}}_{\max} K^{\mathrm{Q}}_{\mathrm{m}} [\mathrm{A}][\mathrm{P}]}{K_{\mathrm{eq}} K^{\mathrm{A}}_{\mathrm{i}}} \tag{2.47}$$

In the absence of products ([P] = [Q] = 0) the equation for the initial reaction velocity can be reduced to:

$$v = \frac{v_{\max} [\mathrm{A}][\mathrm{B}]}{K^{\mathrm{B}}_{\mathrm{m}} [\mathrm{A}] + K^{\mathrm{A}}_{\mathrm{m}} [\mathrm{B}] + [\mathrm{A}][\mathrm{B}]} \tag{2.48}$$

3 Instrumentation

This chapter provides an account of the high-pressure instrumentation. As [64] gives an extensive description of the apparatus as found at the beginning of this work, the focus is set on subsequent changes and improvements. In addition, still existing apparative problems and limitations are discussed.

3.1 Survey of the high-pressure apparatus

The Figures 3.1 and 3.2 show an outline of the high-pressure apparatus in two different configurations for injection purposes.
The main items of the high-pressure installation are two high-pressure stainless steel cells with volumes of 100 mL (cf. section 3.2.1) and 32.1 mL (cf. section 3.2.2), respectively, providing three sapphire windows (S1, S2, and S3 in Figures 3.1 and 3.2) for spectroscopic measurements and visual observation of the cell contents. Details concerning the spectroscopic equipment can be found in section 3.5.
The main difference between the two cells – apart from their different volume – is the fact that the lid of the 100 mL cell provides a packless magnetic drive stirrer (MD in Figure 3.2; cf. section 3.7), while the lid of the 32.1 mL high-pressure cell is equipped with an additional sapphire window unit (S4 in Figure 3.1) for the visual observation of the interior of the high-pressure cell. The constructional compatibility of the two cells permits the use of the 32.1 mL cell with the lid of the 100 mL cell in high-pressure experiments and vice versa.
The pressure in the system is generated in the pressurising section by means of a dosing pump (DP in Figures 3.1 and 3.2; cf. section 3.4.1) which is fed with liquid carbon dioxide from a steel cylinder with immersion pipe. The pressurising section is spatially separated from the high-pressure cell by an air-operated valve (PV in Figures 3.1 and 3.2). Two check valves (CV1 and CV2 in Figures 3.1 and 3.2) prevent contamination of the dosing pump and the pressurising section, respectively, by the cell contents. Moreover, two rupture discs (B1 and B2 in Figures 3.1 and 3.2) protect the apparatus from pressures above the maximum allowable value.
For pressure measurement, the apparatus is equipped with two analogue pressure gauges (M1 and M2 in Figures 3.1 and 3.2) and two digital pressure transmitters (PT1 and PT2 in Figures 3.1 and 3.2; cf. section 3.4.2).
The cell assembly is placed in an air thermostat allowing pre-thermostatting of the carbon dioxide in the pressurising section by means of a heat exchanger (not shown in Figures 3.1 and 3.2; cf. [64]) and of the (substrate) solutions in the sample loop. Additionally, the cell temperature can be regulated (cf. section 3.3.2) via a thermostatting jacket (TJ in Figures 3.1 and 3.2) by a cryostat. The temperature inside the high-pressure cell is monitored via a Pt resistance thermometer (Pt100 in Figures 3.1 and 3.2; cf. section 3.3.1).
Both temperature and pressure in the high-pressure apparatus can be controlled by a computer control programme named "CO_2Spec".

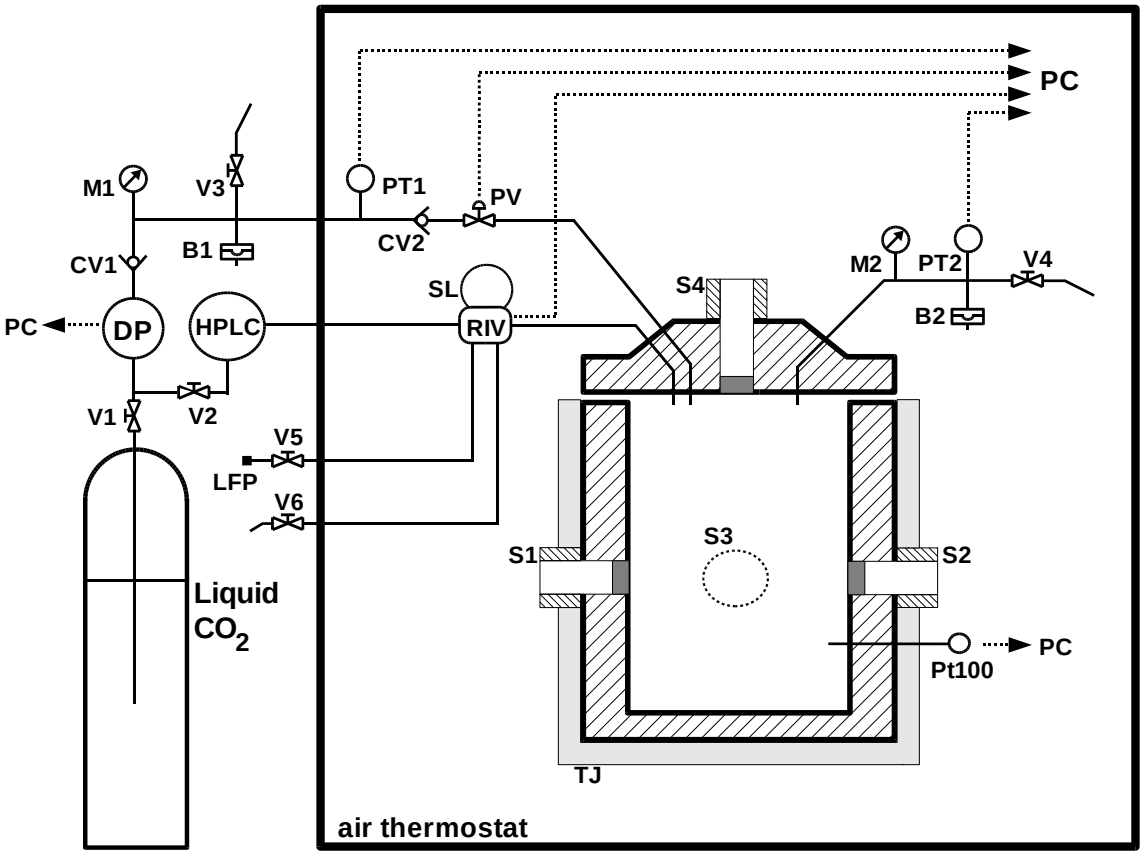

Figure 3.1: Outline of the high-pressure apparatus – 1. DP: dosing pump. V1 - V6: high-pressure valve. CV1 - CV2: check valve. PV: air-operated valve. B1 - B2: rupture discs. M1 - M2: analogue manometer. PT1 - PT2: pressure transducer. Pt100: Pt resistance thermometer. S1 - S4: sapphire window. HPLC: Gilson M305 HPLC pump. RIV: Rheodyne injection valve. SL: sample loop. LFP: loop filling port. TJ: additional cell thermostatting. PC: computer.

As already mentioned before, there are two different apparative configurations for injection purposes:

On the one hand, substrates can be injected by pumping fresh carbon dioxide by means of a Gilson HPLC pump (HPLC; cf. section 3.6.1.1) through the sample loop (SL) at the injection valve (RIV) into the high-pressure cell as illustrated in Figure 3.1. This injection method results in an increase of pressure in the cell due to additional carbon dioxide.

Alternatively, a Knauer HPLC pump (HPLC; cf. section 3.6.1.2) can be used to inject substrate solutions at constant pressure by flushing the sample loop (SL) at the injection valve (RIV) with circulated carbon dioxide from the high-pressure cell. As shown in Figure 3.2, a high-pressure inline filter (IF) should be used in order to protect the HPLC pump from damage due to solid particles when circulating carbon dioxide solutions containing insoluble or slightly soluble substances.

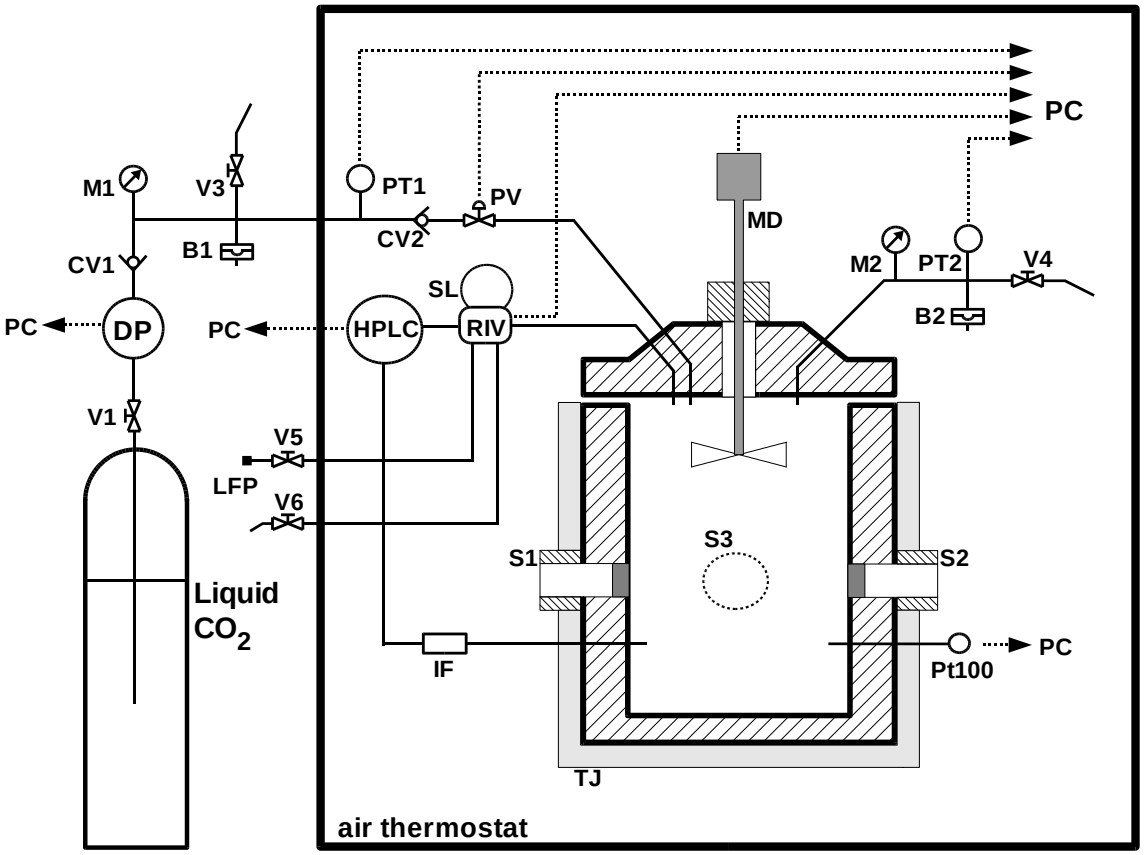

Figure 3.2: Outline of the high-pressure apparatus – 2. DP: dosing pump. V1 - V6: high-pressure valve. CV1 - CV2: check valve. PV: air-operated valve. B1 - B2: rupture discs. M1 - M2: analogue manometer. PT1 - PT2: pressure transducer. Pt100: Pt resistance thermometer. S1 - S3: sapphire window. HPLC: Knauer K-120 HPLC pump. RIV: Rheodyne injection valve. SL: sample loop. LFP: loop filling port. IF: high-pressure inline filter. MD: MagneDrive stirrer. TJ: additional cell thermostatting. PC: computer.

3.2 High-pressure cells

3.2.1 100 mL high-pressure cell

The 100 mL stainless steel fixed volume high-pressure cell (cf. [64] and Figures A.1 and A.2) was supplied by Bio-Ingenieurtechnik GmbH (Engelsdorf, Germany). It is designed for a maximum pressure of 500 bar at a maximum temperature of 60 °C.

The lid of the cell, which provides four M16x1.5 connecting ports, can be installed at a mounting plate inside the air thermostat. Due to this fixed position, the 1/4 inch high-pressure tubings for CO_2 supply, venting and injection are connected to the lid by means of SITEC high-pressure tube connectors (M16x1.5; part nos. 720.0310 and 720.0320; SITEC-Sieber Engineering AG, Maur/Zürich, Switzerland). A screwed port in the centre of the lid allows, moreover, the installation of a packless magnetic drive stirrer (cf. section 3.7 for details).

For high-pressure experiments, the lower part of the cell is attached to the lid by means of eight M12 anti-fatigue bolts which have to be tightened with 23 Nm using a torque wrench. The pressure-proof sealing of the cell is accomplished by a 39x2.2 mM PTFE O-ring.
The lower part of the cell provides three additional M16x1.5 screwed ports, which allow one to connect additional high-pressure tubings apart from the installation of a Pt100 resistance thermometer (cf. section 3.3.1) for measuring the temperature inside the cell. For example, one of this ports can be used for the withdrawal of CO_2 from the cell for the injection with circulated carbon dioxide as shown in Figure 3.2.
For spectroscopic purposes (cf. section 3.5), the high-pressure cell is equipped with two opposed 6 mm sapphire window units (part no. 742.0021; SITEC-Sieber Engineering AG), which are held in place by M20x1.5 gland nuts and have been modified with lenses (cf. [64]) for the application with optical fibres (cf. section 3.5.2). A third non-modified 6 mm sapphire window in perpendicular position to the already mentioned window units permits visual observation and may be utilised for future fluorescence spectroscopy.

3.2.2 32.1 mL high-pressure cell

Apart from the 100 mL high-pressure cell, a 32.1 mL stainless steel fixed volume view cell can be used for experiments with liquid and supercritical carbon dioxide. This cell was designed and constructed in the present work in cooperation with the faculty's fine mechanical workshop. A subsequent construction inspection and first pressure test by the TÜV Süddeutschland (Bau und Betrieb; Niederlassung Regensburg) proved that it complies with homologation specifications for high-pressure vessels in agreement with relevant legal regulations.
The construction of the second high-pressure vessel was undertaken in order to overcome experimental restrictions and problems with regard to 100 mL cell causing a high consumption of chemicals due to its volume. This results not only in high costs but also in difficulties in providing sufficient amounts with invariable high purity of those substances which have to be synthesised/prepared in the laboratory. For example, conductivity investigations [201] on ClPFPE-NH_4-based microemulsions in $scCO_2$ required more than 36 g surfactant per measurement for the highest reached W_0 values of approx. 0.33. Allowing for the limited size of the sample loops (cf. section 3.6.2), the high volume imposes, moreover, restraints concerning attainable concentrations of substrates after their injection. Besides, the 100 mL cell provides only limited possibilities for the observation of the cell content as just a small part of the cell is visible due to the position and the small diameter (6 mm) of the sapphire window.
However, the major objective of the construction of the cell was not only to reduce the volume and to enhance observation possibilities but also to maintain constructional compatibility to the 100 mL vessel regarding the lids and the tubing connections in order to avoid complex modifications inside the air thermostat when replacing the lids at the mounting plate inside the air thermostat.
The lid (cf. Figures A.8, A.10, and A.9) of the new cell provides four M16x1.5 connecting ports for the connection of the 1/4 inch high-pressure tubings for CO_2 supply, venting and injection by means of a M16x1.5 gland nut (cf. Figure A.11). A threaded hole in the centre of the lid permits, moreover, the installation of an additional 6 mm sapphire window unit (part no. 742.0021; SITEC-Sieber Engineering AG) for the observation of the cell contents.
The smaller volume of the new cell (cf. Figures A.3, A.4, A.5, A.6, A.7, and A.8) in comparison to the 100 mL high-pressure cell, was achieved by a smaller diameter in the lower part of the

cell and a reduced height. In contrast to the 100 mL high-pressure vessel, the lower part of the 32.1 mL cell provides only two additional M16x1.5 screwed ports for the Pt100 resistance thermometer (cf. section 3.3.1) and an additional 1/4 inch tubing. For spectroscopic purposes (cf. section 3.5) and visual observation of the cell contents, the second high-pressure cell is likewise equipped with two opposed 6 mm sapphire windows (part no. 742.0021; SITEC-Sieber Engineering AG) modified with lenses (cf. [64]) and a third non-modified 6 mm sapphire window in perpendicular position to the aforementioned window units.
Due to extended thread heights in the new cell (cf. Figure A.8), the standard glands nuts by the SITEC-Sieber Engineering AG for the M16x1.5 and M20x1.5 screwed ports cannot be used. Engineering drawings of nuts suitable for the 32.1 mL cell can be found in section A.
Sealing of the 32.1 mL high-pressure cell is accomplished as described in section 3.2.1 for the 100 mL cell.
Despite the improved observation possibilities due to the additional window unit in the lid of the 32.1 mL high-pressure cell, it must be noted that the observation of the cell contents is still limited and problematic because of the small diameter (6 mm) of the sapphire windows.

3.3 Temperature measurement and temperature regulation

3.3.1 Temperature measurement

The temperature in the air thermostat is measured by a Pt100 screw-in resistance thermometer (Schwille Elektronik GmbH, Kirchheim, Germany) whose electrical signal is digitised by a digital indicator (Digital 280, Philips Prozeß- und Maschinenautomation GmbH, Kassel, Germany). For accuracy improvement, a two-point input signal adjustment concerning the digital indicator was carried out. Iced and boiling water were chosen as reference points. In order to eliminate the influence of the atmospheric pressure on melting and boiling temperature, the exact temperatures of both reference points were determined by means of a precision thermometer F250 (Automatic Systems Laboratories, Milton Keynes, United Kingdom). The latter thermometer permits the determination of temperatures with a maximum error of ±0.025 K between −50 °C and 250 °C. Assuming an error of ±0.1 K for the two-point signal adjustment and allowing for the uncertainty of the F250 precision thermometer, the maximal error of the temperature measurement inside the air thermostat can be assessed at [64]:

$$\Delta\Theta_{\text{air thermostat}} = \pm 0.2\,\text{K} \tag{3.1}$$

For the determination of the temperature inside the cell, a Pt100 two-wire system resistance thermometer (part no. 770.5331-26, SITEC-Sieber Engineering AG, Maur/Zürich, Switzerland) is available. This sensor can be installed in the lower part of the high-pressure cells by means of a M16x1.5 screwed joint. In order to provide the control progamme "CO_2Spec" with the cell temperature, the analogue signal of the Pt100 sensor can be digitised either via a digital indicator Digital 280 as used for the Pt100 resistance thermometer of the air thermostat or via a low-temperature thermoregulated circulator (F32-HD, JULABO Labortechnik GmbH, Seelbach, Germany), which feeds the thermostatting jacket of the cell.
The latter temperature measurement by means of the cryostat was established in the present work. The real temperature Θ_{cell} inside the cell is calculated by the control programme "CO_2Spec"

from the temperature value Θ_{in} provided by the circulator. The conversion is based on the following linear equation:

$$\Theta_{\text{cell}} = a_1 \cdot \Theta_{\text{in}} + a_2 \tag{3.2}$$

The parameters a_1 and a_2 in Equation (3.2) were derived from an input signal adjustment performed in a temperature range from 5 °C to 60 °C in steps of 5 K. As reference, a high precision calibration thermometer [301] with a standard deviation of 0.01 K was used. Allowing for the uncertainty of the latter thermometer and for the rounding to two decimal places by the control programme, the maximal error for the temperature measurement inside the cell can be assessed at:

$$\Delta\Theta_{\text{cell, F-32HD}} = \pm 0.05\,\text{K} \tag{3.3}$$

If the digital indicator Digital 280 is used for digitising, the maximal error of the temperature measurement in the high-pressure can be estimated accordingly to the two-point signal adjustment for the temperature sensor in the air thermostat [64]:

$$\Delta\Theta_{\text{cell, Digital 280}} = \pm 0.2\,\text{K} \tag{3.4}$$

3.3.2 Temperature regulation

The temperature regulation of the air thermostat permits a temperature control to ±0.1 K and works as follows: The control programme "CO_2Spec" compares every second the adjusted value for the temperature with its actual value. If the temperature exceeds the desired value, the control programme switches on the heater inside the air thermostat. If the temperature is higher than the desired temperature, the cooler of the air thermostat is turned on. When the temperature reaches the adjusted set value, the heater and the cooler, respectively, are switched off.
At the beginning of this work, no direct regulation of the cell temperature was possible (cf. [64]). The following two options for controlling the temperature inside the cell were established by means of the already mentioned cryostat and the thermostatting jackets:
On the one hand, the temperature inside the cell can be adjusted by manual setting of the water bath temperature cryostat and, thus, of the water which circulates through the thermostatting jackets of the high pressure cell. However, this method is not very precise and requires frequent interventions by the user in order to obtain a constant temperature inside the cell.
Alternatively, the measurement of the cell temperature by means of the cryostat (cf. section 3.3.1) allows one to use the external PID-regulation mechanism of the low-temperature thermoregulated circulator. In this case, the cryostat independently regulates the temperature inside the cell allowing a temperature control to within less than ±0.1 K. In order to reach the correct desired cell temperature, $\Theta_{\text{cell, desired}}$, the signal adjustment according to Equation (3.2) has to be taken into account. Consequently, the temperature, Θ_{out}, to be set in the cryostat for external regulation is calculated by the control programme according to the following equation

$$\Theta_{\text{out}} = \frac{\Theta_{\text{cell, desired}} - a_2}{a_1} \tag{3.5}$$

3.4 Dosing pump, pressure measurement and pressure regulation

3.4.1 Dosing pump

For pressurising the system, a Dosapro Milton Roy (Pont-Saint-Pierre; France) dosing pump (DP in Figure 3.1 and 3.2) with the type designation MD.140.S(F).4.M.690/J (supplied by MPT; Rodgau; Germany) is applied. It provides a maximum output of 1.6 L/h at a maximum allowable output pressure of 600 bar. Furthermore, it allows the continuously variable manual adjustment of the feed rate via a micrometer screw affecting the length of the piston stroke. For its self-protection, the pump is equipped with a relief valve which prevents generation of pressures above 690 bar.
The dosing pump is driven by a three-phase motor of type K21R 71 K 4 (supplied by VEM motors GmbH, Zwickau, Germany) with a maximum power of 0.25 kW and a maximal rotational frequency of 1400 min^{-1}.

3.4.2 Pressure measurement

Apart from two analogue pressure gauges (M1 and M2, respectively, in Figure 3.1 and 3.2), the high-pressure apparatus is equipped with two pressure transmitters (Haenni Mess-Systeme GmbH; Stuttgart; Germany; Model ED 517/314.211/165) which allow the determination of the pressure in the pressurising section (PT1 in Figure 3.1 and 3.2) as well as in the high-pressure cell (PT2 in Figure 3.1 and 3.2). Their principle of measurement is based on a thin film diaphragm which displays a variable resistance with respect to its pressure dependent camber. The transducers permit differential pressure measurements in relation to atmospheric pressure up to a maximum pressure of 600 bar. Their operating temperature range is −10 °C to 80 °C, whereas the compensated temperature range extends from 20 °C to 50 °C. The latter temperature span refers to the range where the pressure transmitters comply with the specifications stated in the data sheet [302]. The reference temperature for calibration and testing purposes is 25 °C.
Allowing for linearity, hysteresis, repeatability, zero thermal drift, and span thermal drift, the temperature dependent maximum measuring error $\Delta p_{\mathrm{ED\ 517}}(\Theta)$ of the pressure transmitters within the compensated temperature range can be calculated as follows:

$$\Delta p_{\mathrm{ED\ 517}}(\Theta) = \pm \left(4.2 + 4.32 \frac{|\Theta - 25\,^{\circ}\mathrm{C}|}{10\,^{\circ}\mathrm{C}} \right) \mathrm{bar} \tag{3.6}$$

Apart from $\Delta p_{\mathrm{ED\ 517}}(\Theta)$, the instrument error of the digital indicator (Digital 280, Philips Prozeß- und Maschinenautomation GmbH, Kassel, Germany) used for digitising the analogue signal of the pressure transmitters has to be taken into account [64, 303]:

$$\Delta p_{\mathrm{Digital\ 280}} = \pm 0.6\,\mathrm{bar} \tag{3.7}$$

Consequently, the overall maximal error for the pressure measurement $\Delta p(\Theta)$ is given by:

$$\Delta p(\Theta) = \pm \left(4.8 + 4.32 \frac{|\Theta - 25\,^{\circ}\mathrm{C}|}{10\,^{\circ}\mathrm{C}} \right) \mathrm{bar} \tag{3.8}$$

Within the temperature compensated range, the maximal pressure error for the whole measuring span from 1 bar up to 600 bar passes through a minimum of ±4.8 bar at the reference temperature of 25 °C and displays a maximum of ±15.0 bar at 50 °C. For the most commonly used experimental temperature of 35 °C, it amounts to ±9.1 bar.

3.4.3 Pressure regulation

For the maintenance of constant pressure conditions during experiments, the control programme "CO_2Spec" provides a pressure regulation mode which automatically compensates temporary pressure loss as a result of sporadic leakages or temperature changes by appropriate activation/deactivation of the dosing pump and the air operated valve (PV in Figures 3.1 and 3.2), respectively. In addition, the regulation permits pressurising of the system in order to reach the desired working pressure.
The regulation is based on three adjustable parameters which can be set in the control programme by the user: required pressure in the cell as controlled condition, overpressure in the pressurising section, and tolerance threshold. The latter parameter refers to the shortfall of the required pressure which is tolerated by the system. The overpressure provides the necessary cracking pressure for the check valve (CV2 in Figures 3.1 and 3.2) in order to permit immediate free flow in the direction of the cell when readjusting cell pressure.
In principle, the pressure regulation works as follows: By analogy to the temperature regulation (cf. section 3.3.2), the control programme compares every second the actual pressure values in the cell and in the pressurising section with the control parameters. If the pressure in the pressurising section falls below the adjusted overpressure, the control programme turns on the dosing pump. The pump is turned off after restoration of the required overpressure. If the pressure in the cell drops below the tolerance threshold, the air operated valve is opened. This results in an increase of pressure in the cell, as carbon dioxide flows into the vessel due to the overpressure in the pressurising section. If this pressure compensation causes the pressure in the pressurising section to fall below the adjusted overpressure, the control programme, moreover, switches the dosing pump on. When the pressure reaches and exceeds, respectively, the tolerance threshold, the pneumatic valve is closed. The optionally actuated pump is turned off by the programme as soon as the overpressure is restored.
In order to avoid too high-pressure increases in the pressurising section and thus substantial deviations from the desired pressure, it is necessary to reduce the output of the dosing pump as described in section 3.4.1. While pressurising or changing the pressure of the system requires high feed rates (preferably 100 %), smaller rates between 50 % and 70 % have turned out to be more effective for pressure regulation. Provided that the parameters and the pump output are appropriately chosen, the regulation mode allows the adjustment of the required pressure with a control accuracy of ± 1 % at pressures above 100 bar.
Apart from pressurising and maintaining constant pressure in the cell, the pressure regulation mode provides security features. In case of steep pressure drops in the cell as a result of rupture of bursting discs or O-rings, it ensures that the dosing pump is deactivated and that the air operated valve is closed in order to prevent loss of CO_2 from the steel gas bottle. Besides, the temperature regulation is turned off. Furthermore, it takes measures if the cell pressure exceeds the maximum allowable value of 500 bar.

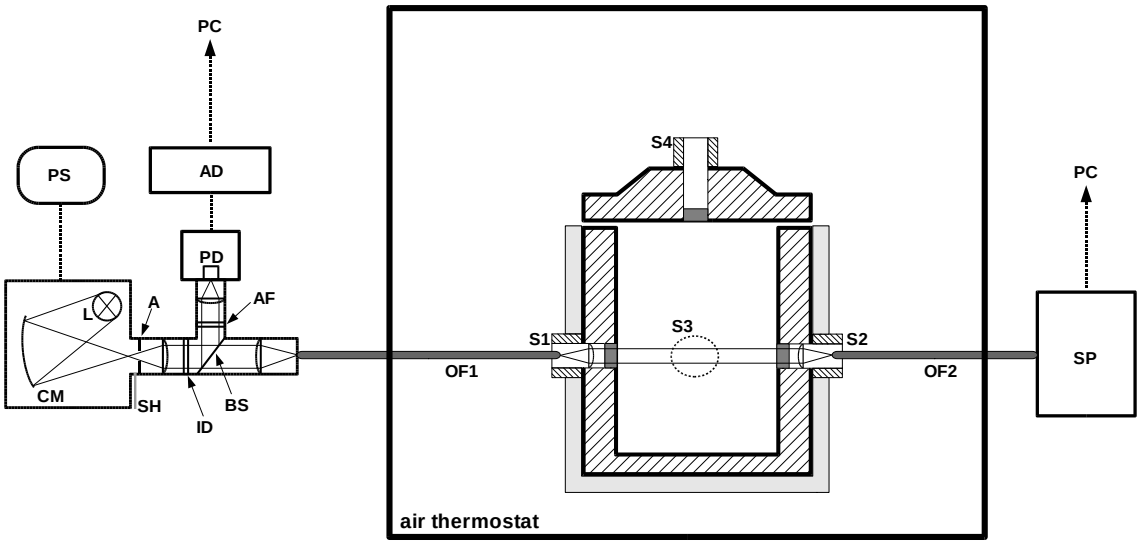

Figure 3.3: Outline of the high-pressure apparatus – spectroscopic equipment. PS: power supply for lamp. L: lamp. CM: concave mirror. SH: shutter. A: aperture. ID: iris diaphragm. BS: beam splitter. AF: attenuation filter. PD: photo diode. AD: Analogue-to-Digital converter. OF1 - OF2: optical fibre. S1 - S3: sapphire window. SP: diode array spectrophotometer. PC: computer.

3.5 UV/VIS spectroscopy

A schematic representation of the equipment for UV/VIS spectroscopy gives Figure 3.3.

3.5.1 Light sources

Two different lamps are available as light sources for UV/VIS spectroscopy, which, moreover, provide the necessary light for visual observation of the cell content. One of them is a 150 W xenon short arc lamp provided by Osram (Munich) with the type designation XBO 150 W/1. A constant wattage regulated voltage generator containing an integral high-voltage RF ignitor (Oriel; Stratford, Connecticut, USA; model no. 8510-2) serves as a power supply for this lamp type. Alternatively, a 100 W tungsten halogen lamp (QTH) mounted in the same cabinet (Oriel; model no. 7340) as the xenon arc lamp can be used. The second lamp is fed by a constant voltage regulator (Gossen; Erlangen; Germany) with the required direct current.

The emitted light of both lamps is directed to a beam splitter by means of an optical system compromised of a folding concave mirror, a shutter, an aperture, a lens, and an iris diaphragm. The beam splitter diverts 5 % of the initial light intensity to a photo diode via an attenuation filter. After digitising, the signal of the photo diode allows the mathematical elimination of intensity fluctuations of the light source within the control programme "CO_2Spec". The remaining light, which is not diverted by the beam splitter, is focussed and passed into an optical fibre via an adequate adapter.

3.5.2 Optical fibres

Two optical fibres allow guiding the light from the radiation sources (cf. section 3.5.1) to the high-pressure cell and the transmitted light from the cell to the spectrophotometer (cf. section 3.5.3).
The two used light conductors are multi-fibre optical waveguides (Carl Zeiss Jena; Jena; Germany) with a length of 2 m and a core diameter of 3 mm. Due to their fibre type LUV 105 they are also appropriate for spectrophotometric measurements in the UV-range. Metallic end sleeves (ZEISS type each) allow the fixation at the respective optical devices.
Alternatively, a third optical fibre is available, which is a 1.8 m quartz (215 nm - 1100 nm) monofibre optic (Carl Zeiss Jena; Jena). Its diameter of the core amounts to 0.6 mm and its end sleeves are of the same type as those of the two optical fibres mentioned above.

3.5.3 Diode array spectrophotometer

For spectrophotometry a single-beam simultaneous spectrophotometer of type MCS 220 (Carl Zeiss; Oberkochen; Germany) with a diode array consisting of 512 discrete silicon diodes can be utilised. It permits spectral measurements in a wavelength range from 200 nm to 600 nm with integration times between 5.6 ms and 42.6 ms. Spectral decomposition is accomplished by means of a holographic concave reflection grating characterised by a blaze wavelength of 230 nm. Typically, a practical resolving power of approx. 2.4 nm is achieved by the photometer.
An integrated 12-bit analogue-to-digital converter digitises the spectrophotometer signal and facilitates the data transfer to the computer via a parallel interface-card. The control programme "CO_2Spec" allows the immediate graphical display of the measured spectrum. Besides, it is possible to observe the time-dependence of the spectrum in order to measure kinetics by means of UV/VIS spectroscopy.

3.6 Injection

3.6.1 HPLC pumps

Two HPLC pumps are at disposal for injection purposes.

3.6.1.1 Gilson M 305

On the one hand, a single-piston Gilson (Middleton, Wisconsin; USA) M305 HPLC pump (supplied by ABIMED Anyalsen-Technik; Langenfeld; Germany) can be used for the injection of substrate solutions by pumping fresh carbon dioxide through the sample loop at the injection valve into the high-pressure cell (cf. Figure 3.1). The applied cooled pump head 10SC is dimensioned for a maximum output pressure of 600 bar at a maximal input pressure of 100 bar and allows flow rates between 0.050 mL/min and 10 mL/min. Due to its serial interface architecture, external control by the computer is not possible at the present stage (cf. [64]).

3.6.1.2 Knauer K-120

On the other hand, a double-piston Knauer (Berlin; Germany) WellChrom K-120 HPLC pump is available for the injection of substrate solution by flushing the sample loop at the injection valve

with circulated carbon dioxide from the high-pressure cell (cf. Figure 3.2). The maximum operating pressure of this pump is 400 bar at flow rates between 0.001 mL/min and 9.999 mL/min. As this pump provides a standard serial interface, external control by the computer is possible, which permits a completely automated injection in combination with the computer controlled injection valve as described below.
Despite positive test results (cf. [64]), the above mentioned injection type by means of the Knauer HPLC pump turned out to be unreliable with a failure rate of 80-90 % (no observable flow).

3.6.2 Injection valve and sample loops

The injection valve is a stainless steel 2-position, 6-port high-pressure motorised switching valve with the type designation LabPRO 7000 (Rheodyne; Rhonert Park, California; USA; supplied by ABIMED Analysen-Technik; Langenfeld; Germany) and a maximum operating pressure of 345 bar. It provides a serial interface which allows one to switch the valve's positions by means of the computer as an alternative to manual operation.
Sample loops for the injection valve as described above are available with volumes between 5 μL and 5 mL.

3.7 Stirring and mixing

A packless magnetic drive stirrer (MagneDrive II; part no. 0.75 02 SS 06 A; Autoclave Engineers AE, Erie, Pennsylvania, USA; supplied by Schmidt, Kranz & Co. GmbH, Velbert-Langenberg, Germany) attached at the lid of the 100 mL high-pressure cell can be used for intermixing the cell contents. It is designed for a maximum rotational speed of 3000 U min^{-1} and a maximal torque of 1.808 Nm.
The packless magnetic drive stirrer is driven via a V-belt by a three-phase motor of type M80A2 (ATM Antriebstechnik GmbH, Zwickau, Germany) with a maximum power of 0.75 kW and a maximal rotational frequency of 3000 min^{-1}.
Further details concerning this stirrer type can be found in [64].
Alternatively, a magnetic stirrer can be used to intermix the cell contents.

3.8 Conductivity measurement

3.8.1 Conductivity bridge

The alternating current conductance bridge consists of a symmetric Wheatstone bridge with a Wagner earth circuit, a frequency generator, and a high precision resistance decade. The frequency generator permits measurements in a frequency range between 10 Hz and 10 kHz. The resistance decade (part no. 1433-29, QuadTech Inc., Maynard, USA; supplied by CME CompuMess Elektronik GmbH, Unterschleißheim, Germany) allows balancing of the bridge resistors up to $1.11111 \cdot 10^5\,\Omega$ with a resolution of 0.01 Ω. The determination of even higher resistances is facilitated by shunting a $1 \cdot 10^5\,\Omega$ precision resistor. Besides, additional capacitor decades can be connected in parallel to the Wheatstone bridge in case of very high capacities to be measured.

Because of metrological reasons, the serial arrangement of electrolyte resistance R_E and capacity C_P is transformed to a parallel connection [304]. For the balanced bridge follows:

$$R_E = \frac{R(\nu)}{1 + (2\pi\nu R_E C_P)^{-2}} \tag{3.9}$$

$$C(\nu) = \frac{C_P}{1 + (2\pi\nu R_E C_P)^2} \tag{3.10}$$

$$\tag{3.11}$$

where $R(\nu)$ is the resistance and $C(\nu)$ is the electric capacity. As can be seen from the equations above, balancing of the conductance bridge depends on the adjusted measuring frequency ν. Hence, the exact resistance of the electrolyte R^{ex} is usually obtained by extrapolation to infinite frequency. For this purpose, several mathematical methods have been proposed in literature. Robinson and Stokes [305] have suggested Equation (3.12), which has shown to be effective for conductance measurements with grey platinised electrodes. Jones and Christian [306] have recommended Equation (3.13), while Hoover [307] has introduced Equation (3.14) with a variable exponent for ν. Furthermore, Nicol and Fuoss [308] have proposed Equation (3.15), which represents a combination of the Equations (3.12) and (3.13).

$$R(\nu) = R^{ex} + a\nu^{-1} \tag{3.12}$$

$$R(\nu) = R^{ex} + a\nu^{-\frac{1}{2}} \tag{3.13}$$

$$R(\nu) = R^{ex} + a\nu^{-b} \tag{3.14}$$

$$R(\nu) = R^{ex} + a\nu^{-\frac{1}{2}} + b\nu^{-1} \tag{3.15}$$

3.8.2 Electrodes

In a previous study, the electric conductivity of ClPFPE-NH_4-based microemulsions in $scCO_2$ was investigated [201]. The 100 mL view cell was set up for electrical conductivity measurements by means of a single annular Pt electrode (height 3 mm, diameter 20 mm) which was concentrically mounted at the top of the high pressure cell with the help of a Kel-F mounting. The electrode was connected with a wheatstone bridge as described in the previous section via an high-pressure electric single connector (part no. 770.8350, SITEC-Sieber Engineering AG). In order to avoid stray fields and additional earth impedances, the metallic view cell itself connected to earth was, moreover, used as the second electrode.
In the present work, two new electrode types (cf. Figure 3.4 and Figures A.15 and A.16, respectively) were designed and constructed in cooperation with the faculty's fine mechanical workshop. The construction of these electrodes vessel was undertaken in order to overcome experimental limitations and problems with regard to the old electrode type as described above.
The new electrodes can be mounted in the M20x1.5 screwed ports of the high-pressure cells replacing the respective sapphire window unit. As in the case of the old electrode type, the view cells have to be used as second electrode in order to avoid stray fields and additional earth impedances.

Figure 3.4: Photograph of the high-pressure electrodes

Main advantage of the new electrodes are their smaller electrode surfaces resulting in higher cell constants and, thus, allowing to measure a wider conductivity range as compared to the old electrode.
Both new electrodes have been tested up to a maximal pressure of 450 bar at 35 °C without failure. However, since no conductivity measurements were performed in the present work, there is no data available concerning the long-term stability of the electrodes. Possible critical areas are the soldering joints between nickelised Macor and the stainless steel parts of the electrodes. This is particularly the case for the electrode II (cf. Figure A.16) where sealing is established by means of these soldering joints. In the case of the other electrode (cf. Figure A.15), Macor is just used to provide a defined electrode surface, while sealing is achieved by means of a cone. As can be seen from Figure 3.4, the latter electrode, however, requires a PTFE heatshrinking tube for electric isolation from the high-pressure cell.

4 Syntheses

4.1 Synthesis of di-HCF4

The sodium salt of bis(2,2,3,3,4,4,5,5-octafluoro-1-pentyl)-2-sulfosuccinate (di-HCF4) was prepared in a two-step synthesis via the intermediate product bis(2,2,3,4,4,5,5-octafluoro-1-pentyl) maleate and bis(2,2,3,4,4,5,5-octafluoro-1-pentyl) fumarate, respectively.

4.1.1 Synthesis of bis(2,2,3,4,4,5,5-octafluoro-1-pentyl) maleate

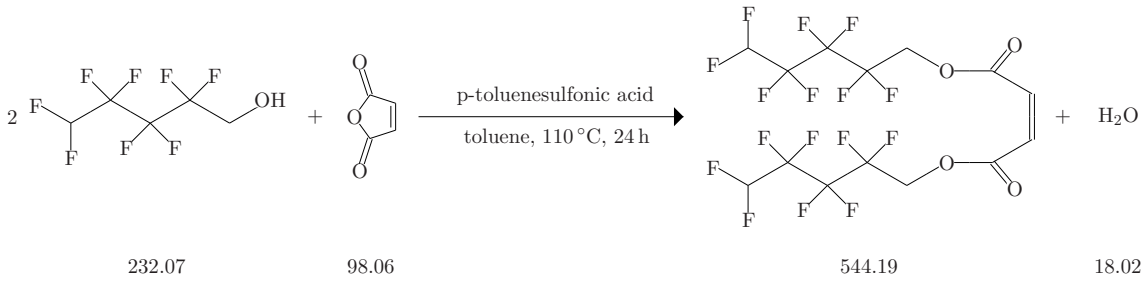

Figure 4.1: Synthesis of bis(2,2,3,4,4,5,5-octafluoropentyl) maleate

Bis(2,2,3,4,4,5,5-octafluoropentyl) maleate was synthesised according to Yoshino et al. [309]. A mixture of 19.6 g (200 mmol) maleic anhydride (for synthesis, Merck), 101.0 g (435 mmol) 2,2,3,4,4,5,5-octafluoropentanol (98 %, Aldrich), and p-toluenesulfonic acid monohydrate (7.6 g, 40 mmol) as catalyst was refluxed under stirring in 750 mL toluene at 110 °C for 24 h. In order to shift the reaction equilibrium of the esterification reaction, the water liberated in the course of the reaction was azeotropically removed and separated from the reaction flask by means of a water trap. Subsequently, the warm reaction mixture was washed 5 times with water (80 °C). After evaporation of the solvent, the remaining orange liquid was fractionated under reduced pressure to yield a colorless liquid product (yield: 69.5 g, 63.9 %).
^{1}H-NMR (250 MHz, THF-D8): δ [ppm] = 4.87 (t(t), J = 14.2 (1.4) Hz, 4H, –CF_2–CH_2–O), 6.56 (s, 2H, =CH), 6.57 (t(t), J = 50.9 (5.5) Hz, 2H, –CF_2–CHF_2).

4.1.2 Synthesis of bis(2,2,3,4,4,5,5-octafluoro-1-pentyl) fumarate

Bis(2,2,3,4,4,5,5-octafluoropentyl) fumarate was synthesised according to Downer et al. [232]. A mixture of 26.7 g (220 mmol) N,N-dimethylaniline (for synthesis, Merck), 51.1 g (220 mmol) 2,2,3,4,4,5,5-octafluoropentanol (98 %, Aldrich), and 16.8 g (110 mmol) fumaryl chloride (for synthesis, Merck) was refluxed under stirring in anhydrous THF (500 mL) for 48 h under nitrogen. After removal of the solvent, the reaction mixture was dissolved in diethyl ether. The resulting solution was sequentially washed 8 times with 10% HCl and 5 times with saturated aqueous

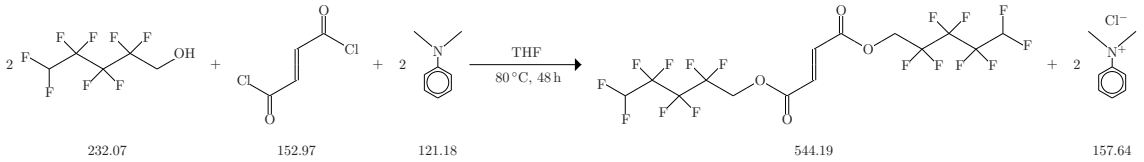

Figure 4.2: Synthesis of bis(2,2,3,4,4,5,5-octafluoropentyl) fumarate

$NaHCO_3$ solution. The ethereal extracts were dried over anhydrous $MgSO_4$, filtered, and diethyl ether was removed by rotary evaporation. Subsequent distillation at reduced pressure yielded a pale yellow to colorless liquid which solidified on cooling within several days (yield: 30.6 g, 25.6 %).
^{1}H-NMR (250 MHz, THF-D8): δ [ppm] = 4.87 (t, J = 14.2 Hz, 4H, –CF_2–CH_2–O), 6.59 (t(t), J = 51.0 (5.0) Hz, 2H, –CF_2–CHF_2), 6.98 (s, 2H, =CH).

4.1.3 Synthesis of the sodium salt of bis(2,2,3,3,4,4,5,5-octafluoro-1-pentyl)-2-sulfosuccinate

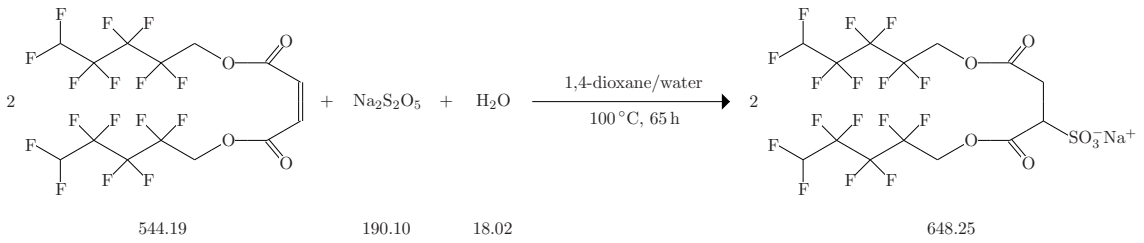

Figure 4.3: Synthesis of the sodium salt of bis(2,2,3,3,4,4,5,5-octafluoro-1-pentyl)-2-sulfosuccinate

The sodium salt of bis(2,2,3,3,4,4,5,5-octafluoro-1-pentyl)-2-sulfosuccinate (di-HCF4) was synthesised by modification of the procedures given by Yoshino et al. [309], Downer et al. [232], and Liu and Erkey [235]. Alternative syntheses for di-HCF4 can be found in [310] and [311], respectively. The synthesis described below can also be conducted with bis(2,2,3,3,4,4,5,5-octafluoro-1-pentyl) fumarate as educt.
A solution of 3.4 g (17.9 mmol) sodium metabisulfite (extra pure, Merck) in 65 mL water was added to a solution of 20.0 g (36.8 mmol) bis(2,2,3,3,4,4,5,5-octafluoro-1-pentyl) maleate in 174 mL 1,4-dioxane. The resulting mixture was refluxed under stirring at 98 °C for 65 h. After evaporation of the dioxane/water mixture, the residual solid was dried under vacuum for 24 h. Subsequently, a Soxhlet extraction was conducted with dry diethyl ether as solvent in order to remove residual inorganic material. After evaporation of the ether, the white solid product was recrystallised several times from a chloroform/ethanol mix. A white powder was obtained after drying under vacuum at 60 °C for 36 h.
^{1}H-NMR (400 MHz, THF-D8): δ [ppm] = 3.20 (d(d), J = 17.9 (4.5) Hz, 1H, –CO–CH_2–), 3.28 (d(d), J = 17.9 (10.6) Hz, 1H, –CO–CH_2–), 4.14 (d(d), J = 10.6 (4.5) Hz, 1H, –CH(SO_3Na)–), 4.66 – 4.89 (m, –CF_2–CH_2–O), 6.73 (t(t), J = 51.0 (5.6) Hz, 1H, –CF_2–CHF_2), 6.77 (t(t), J = 50.9 (5.8) Hz, 1H, –CF_2–CHF_2).

4.2 Synthesis of C8C4

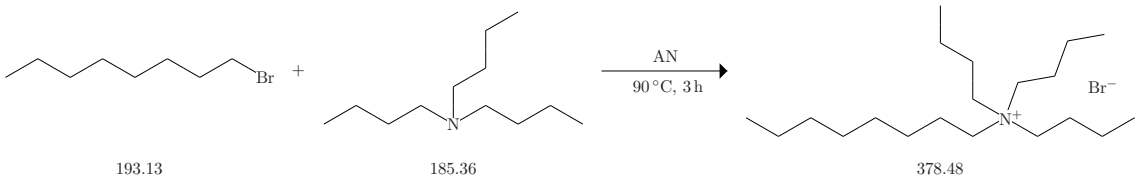

Figure 4.4: Synthesis of octyltributylammonium bromide (C8C4)

Octyltributylammonium bromide (C8C4) was synthesised by modification of the procedure given by Drifford et al. [312].
A mixture of 62.5 g (337 mmol) freshly distilled tributylamine (for synthesis; Merck) and 65 g (337 mmol) 1-bromooctane (for synthesis, Merck) was refluxed under stirring in dry acetonitrile (AN, 125 mL) at 90 °C for 3 h under nitrogen. Upon cooling to room temperature, phase separation occurred allowing to separate a slightly yellow liquid product phase from unreacted educts and solvent. After drying under vacuum in order to remove residual AN, a slightly yellow liquid was obtained.
Crystallisation of C8C4 was achieved by the following procedure: ethyl acetate was added to the liquid product and removed by evaporation under vacuum after mixing. The repeated treatment with ethyl acetate resulted (sometimes) in the crystallisation of C8C4. A white product was obtained after further vacuum drying.
Further efforts to purify and recrystallise the obtained product were not made. Recrystallisation in diethyl ether and ethyl acetate was impossible due to the fact that a pale yellow phase separated from solvent was obtained in both cases (cf. also [312]).
NMR measurements showed that reaction times longer than 3 h result in a significant amount of by-products, which might be caused by transalkylation reactions. It should be noted that the second phase containing significant amounts of unreacted educts might be used to start a new synthesis according to the synthesis procedure given above. This reuse might, however, yield C8C4 with more impurities.
^{1}H-NMR (300 MHz, $CDCl_3$): δ [ppm] = 0.81 (t, 3H, –CH_2–C$\underline{H}_3$), 0.95 (t, 9H, –CH_2–C$\underline{H}_3$), 1.15 – 1.50 (m, 16H, –CH_2–), 1.55 – 1.71 (m, 8H, –CH_2–), 3.2 – 3.4 (m, 8H, N-CH_2–).
^{13}C-NMR (75.5 MHz , $CDCl_3$): δ [ppm] = 59.22 (N–CH2–), 59.07 (N–CH2–), 31.59 , 29.06, 29.00, 26.38, 24.22, 22.55, 22.28, 19.76 (all: CH2–$\underline{C}$H2–CH2), 14.03 (–CH3), 13.70 (–CH3).

4.3 Synthesis of DPnBPrSO$_3$Na

In this work, the term DPnBPrSO$_3$Na is used as abbreviation for the following mixture of isomeric salts: sodium salt of 5,8-dimethyl-4,7,10-trioxatridecane-1-sulfonic acid, sodium salt of 5,9-dimethyl-4,7,10-trioxatridecane-1-sulfonic acid, sodium salt of 6,8-dimethyl-4,7,10-trioxatridecane-1-sulfonic acid, and sodium salt of 6,9-dimethyl-4,7,10-trioxatridecane-1-sulfonic acid.
13.9 g (72.9 mmol) Dowanol DPnB (bis(isopropylene glycol) butyl ether, $\geq$ 98.5 %, Aldrich, mixture of isomers) was added dropwise under stirring to a suspension of 3.5 g sodium hydride (for synthesis 60 % suspension in paraffin oil, Merck) in 100 mL anhydrous THF cooled by an

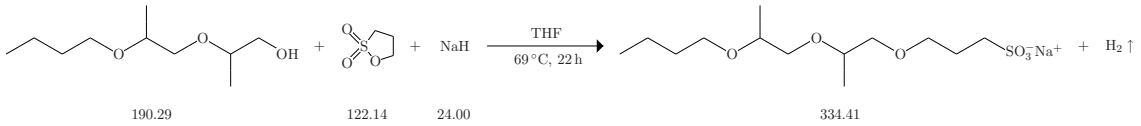

Figure 4.5: Synthesis of DPnBPrSO$_3$Na

ice bath. After half an hour stirring at room temperature, a solution of 12.4 g (101 mmol) freshly distilled 1,3-propanesultone (99 %, Lancaster) in 50 mL dry THF was slowly added to the mixture, which was then refluxed at 69 °C for 22 h. The reaction mixture was allowed to cool down to room temperature and water was added in order to destroy unreacted sodium hydride. After evaporation of the solvent, the residual solid was dissolved in water and the resulting mixture was extracted with 1-butanol (addition of salt necessary in order to achieve phase separation). Subsequently, the 1-butanol was removed by rotary evaporation, the residuals were again dissolved in water and an extraction with diethyl ether was performed by means of a liquid-liquid extractor (addition of salt necessary in order to achieve phase separation). After evaporation of the ether and drying under vacuum, a white waxlike solid product was obtained. Further efforts to purify the product were not made.
^{1}H-NMR (400 MHz, D_2O): δ [ppm] = 0.75 (t, 3H, J = 7.4 Hz, –CH_2–C$\underline{H}_3$), 0.98 – 1.00 (m, 6H, –CH–C$\underline{H}_3$), 1.15 – 1.25 (m, 2H, –CH_2–), 1.35 – 1.44 (m, 2H, –CH_2), 1.80 – 1.87 (m, 2H, –CH_2–), 2.80 – 2.84 (m, 2H, –CH_2–), 3.29 – 3.61 (m, 10H, –C$\underline{H}$(CH_3)–, –CH_2).

4.4 Preparation ClPFPE-NH_4

ClPFPE-NH_4, the ammonium salt of Fluorolink 7004 (ClPFPE-NH_4; cf. Figure 2.7 for constitutional formula), was prepared according to [64, 201, 313].
100 mL aqueous ammonia solution (extra pure, $\geq$ 32 % acidimetric, Merck) was slowly added to 50 mL Fluorolink 7004 (Ausimont Italy, Lot number BL14299, equivalent molecular weight 600) at room temperature. After stirring for half an hour, the temperature was raised to approx. 65 °C for 24 h in order to remove excess ammonia and water. The waxlike surfactant was then dried under vacuum for several days at 65 °C. The final water content of the surfactant, as determined by Karl-Fischer-titration in anhydrous methanol, was 0.14% (w/w). Because of its hygroscopic properties, ClPFPE-NH_4 was stored in a Schlenk flask under dry nitrogen.

5 Enzymatic reactions in $scCO_2$

5.1 Organogels as enzyme immobilisation matrix

As already stated in section 2.2, organogels based on both classical and detergentless microemulsions have recently attracted attention as enzyme immobilisation matrix for reactions in non-aqueous conventional solvents such as isooctane or n-hexane. In the present work, the catalytic ability of lipases encapsulated in these microemulsion-based organogels with $scCO_2$ as external solvent was the subject of investigation. Moreover, initial tests concerning organogels based on phytantriol as a new type of immobilisation matrix were performed in both isooctane and $scCO_2$.

5.1.1 Microemulsion-based organogels

For the investigation of lipase-catalysed reactions with microemulsion-based organogels (MBGs) as immobilisation matrix, lipases from *Candida antarctica* and *Mucor miehei* were encapsulated in lecithin as well as AOT water-in-oil (w/o) MBGs formulated with either hydroxypropylmethyl cellulose (HPMC) or gelatin. Based on results obtained from initial activity tests in $scCO_2$, the focus for further investigations was set on HPMC-lecithin MBGs with entrapped *C. antarctica* lipase.
The effect of various parameters such as pressure, mass fraction of biopolymer, alcohol and carboxylic acid chain length was studied in $scCO_2$. Results are discussed with reference to experiments performed with isooctane as external solvent. In addition, a kinetic study of MBG encapsulated *C. antarctica* lipase in $scCO_2$, based on a simple model esterification reaction, was undertaken to clarify the reaction mechanism and to determine the apparent kinetic constants. Furthermore, differential scanning calorimetry (DSC) measurements were carried out in order to characterise the state of water within the MBGs in more details.

5.1.1.1 Experimental

5.1.1.1.1 Materials

Lipases. Lipases from *C. antarctica* and *M. miehei*, respectively, were supplied by Fluka. The lipase B from *C. antarctica* (CaL) had a specific activity of $9.2\,\mathrm{U\,mg^{-1}}$ (Lot & Filling Code: 47202/1 3203023). 1 U corresponds to the amount of enzyme which liberates 1 mmol butyric acid per minute at pH 8.0 and 40 °C using tributyrine as substrate. The specific activity of the *M. miehei* lipase (MmL) was $242\,\mathrm{U\,mg^{-1}}$ (Lot & Filling Code: 49325/1 11502). In the case of the lipase from *M. miehei*, 1 U refers to the amount of enzyme which liberates 1 mmol oleic acid per minute at pH 8.0 and 40 °C using trioleine as substrate.

Chemicals. Table 5.1 gives a survey of the chemicals utilised for the experiments concerning enzymatic reactions with MBGs. In addition, carbon dioxide (99.995 %) was obtained from

Linde and used without further purification. All gels and buffer solutions were prepared with Millipore Milli-Q water.

5.1.1.1.2 Preparation of microemulsion-based gels

Preparation of Tris/HCl buffer and enzyme stock solutions. A 200 mM Tris/HCl pH 7.5 buffer was used for all experiments with lipase-containing organogels. For buffer preparation, a solution of 6.6 g Tris in approx. 150 mL water was adjusted to pH 7.5 by addition of 1 mol L^{-1} hydrochloric acid followed by diluting to 250 mL in a volumetric flask. The effect of dilution on the adjusted pH value was negligible.
The pH was measured by means of a "Titroline alpha" automatic titrator (Schott-Geräte GmbH, Hofheim, Germany) with a N62 pH combination electrode (Schott-Geräte GmbH). Calibration was done with standard buffers of pH 7.00 and pH 4.00 (CertiPUR, Merck) at room temperature. Enzyme stock solutions were prepared by dissolving appropriate amounts of CaL and MmL, respectively, in adequate amounts of Tris/HCl buffer pH 7.5. In order to avoid repeated freeze-thaw cycles, the stock solutions were frozen at −20 °C in aliquots of 30 µL.

Preparation of microemulsions. Lecithin microemulsions for HPMC based gels were prepared by adding appropriate amounts of lipase in 200 mM Tris/HCl pH 7.5 buffer to a solution of 4.8 % (w/w) lecithin (used as received) in isooctane containing 5.0 % (v/v) 1-propanol. In order to formulate AOT microemulsions, appropriate amounts of lipase in 200 mM Tris/HCl pH 7.5 buffer were added to a 200 mM solution of AOT in isooctane. The final water content of the latter system was 3.5 % (v/v) yielding a molar hydration ratio $W_0 = [H_20]/[AOT]$ of approx. 10.
In the case of lecithin microemulsions for gelatin organogels, appropriate amounts of buffer containing lipase were added to a solution of 22.2 % (w/w) lecithin in isooctane containing 32 % (v/v) 1-propanol and 26.5 % (v/v) water. Respective AOT microemulsions were prepared by addition of lipase containing buffer to a solution of 17.8 % (w/w) AOT in n-hexane containing 7.3 % (v/v) water.

Preparation of gels. The MBGs were prepared by introducing appropriate amounts of microemulsion containing lipase to a mixture of biopolymer and water. In the case of HPMC gels, 1.02 mL of lecithin or AOT microemulsion containing 1.20 mg CaL or 0.22 mg MmL was gelled with 1.0 g HPMC and 2.0 mL water at room temperature. The gelatin gels were prepared by gelling 4.0 mL AOT or 3.6 mL lecithin microemulsion with 1.4 g gelatin and 1.8 mL water. The gelatin-water mixtures were preheated to 55 °C, stirred until homogeneous and then allowed to cool. Organogels were formed by addition of the microemulsion at 35 °C. Data concerning the exact amounts of enzyme in the respective gelatin-based MBGs is given in Table 5.2.

5.1.1.1.3 Lipase-catalysed reactions

Carbon dioxide as external solvent. Lipase-catalysed reactions with carbon dioxide as external solvent were carried out in the 32.1 mL high-pressure cell (cf. section 3.2.2). The high-pressure apparatus was additionally equipped with a Gilson M305 HPLC pump (cf. section 3.6.1.1) and a Rheodyne injection valve (cf. section 3.6.2) for the injection of substrates by pumping fresh carbon dioxide through the sample loop into the cell and thus reaching the adjusted reaction

Table 5.1: Survey of the chemicals used for the experiments with microemulsion-based organogels.

Chemical	Purity and/or specification	Supplier
AOT [a]	BioChemika MicroSelect, $\geq 99\,\%$ (TLC)	Fluka
1-butanol	for analysis, $\geq 99.5\,\%$ (GC)	Merck
1-butyl laurate	$\geq 99\,\%$ (GC)	Aldrich
decanoic acid	for synthesis, $\geq 98\,\%$ (GC)	Merck
1-ethanol	absolute, Baker analyzed, 99.9 % (GC)	Baker
ethyl acetate	for analysis, $\geq 99.5\,\%$ (GC)	Merck
ethyl acetoacetate	for synthesis, $> 98\,\%$ (GC)	Merck
ethyl crotonate	for synthesis, $> 98\,\%$ (GC)	Merck
gelatin	powder food grade	Merck
geraniol	purum, $\geq 96\,\%$ (GC)	Fluka
1-heptanol	for synthesis, $> 99\,\%$ (GC)	Merck
n-hexane	extra pure, $\geq 95\,\%$ (GC)	Merck
hexanoic acid	for synthesis, $\geq 98\,\%$ (GC)	Merck
1-hexanol	for synthesis, $> 98\,\%$ (GC)	Merck
HPA [b]	for synthesis, $> 98\,\%$ (acid.)	Merck
HPMC [c]	viscosity 3500-5600 cP [d]	Sigma
HPP [e]	for synthesis, $\geq 98\,\%$ (HPLC)	Merck
hydrochloric acid	$1\,\mathrm{mol\,L^{-1}}$ standard solution	Roth
isooctane	for analysis, $\geq 99.5\,\%$ (GC)	Merck
lauric acid	$\geq 99.5\,\%$ (GC)	Sigma
lecithin	$\approx 40\,\%$ (TLC) phosphatidylcholine	Sigma
myristic acid	for synthesis, $\geq 98\,\%$ (GC)	Merck
nerol	technical, $\sim 95\,\%$ (GC)	Fluka
1-nonanol	for synthesis, $> 98\,\%$ (GC))	Merck
octanoic acid	for synthesis, $> 99\,\%$ (GC)	Merck
1-octanol acid	for synthesis, $> 99\,\%$ (GC)	Merck
1-pentanol	for synthesis, $> 98\,\%$ (GC)	Merck
1-propanol	for analysis, $\geq 99.5\,\%$ (GC)	Merck
2-propanol	for analysis, $\geq 99.7\,\%$ (GC)	Merck
Tris [f]	for analysis, 99.8 %–100.1 % (acid.)	Merck
vinyl acetate	for synthesis, $> 99\,\%$ (GC)	Merck

acid.: acidimetric. [a] Aerosol OT; sodium bis(2-ethylhexyl)-sulfosuccinate. [b] p-hydroxyphenylacetic acid. [c] hydroxypropylmethyl cellulose. [d] 2 % aqueous solution, 20 °C. [e] p-hydroxyphenylpropionic acid. [f] 2-amino-2-(hydroxymethyl)-1,3-propanediol.

pressure. An outline of the apparatus is given in Figure 3.1. Further details concerning the instrumentation can be found in chapter 3.

In order to ensure complete injection of substrates, injections were performed assuming laminar flow, i.e. that the amount/volume of carbon dioxide used to flush the sample loop was at least 3.5 times higher than the nominal volume of the sample loop (cf. [64]).

The freshly prepared gels were loaded into the high-pressure cell, which was then sealed. The temperature was adjusted to about 0.8 K below the final temperature as pressurising results in a temperature increase. After increasing the pressure by feeding the cell with CO_2, the reactions were started by injecting appropriate amounts of lauric acid and 1-propanol solubilised in small amounts of isooctane. The solutions were not stirred during reaction. Analysis of the reactions was done by GC after depressurising and sample recovery. Details concerning GC equipment and conditions can be found in appendix B. For the HPMC gels the reaction temperature was 35 °C, whereas in the case of the gelatin gels a temperature of 25 °C was chosen (liquid CO_2).

Kinetic measurements were carried out batchwise: sets of identical samples with freshly prepared, new gels were sealed in the high-pressure cell and the reactions were stopped at certain predefined time intervals. Reproducibility tests showed that all measured conversions were reproducible within ±2 %, most of them even within less than ±1 %.

Isooctane as external solvent. In addition to the experiments in $scCO_2$, lipase-catalysed reactions were also studied in isooctane as a reference system at ambient pressure. The experiments with isooctane as external conventional organic solvent were performed at 35 °C as described by Delimitsou et al. [153].

The lipase-containing MBGs were placed into Schott bottles and the reactions were initiated by adding a pre-thermostated isooctane-phase containing the substrates at different concentrations to the MBG. At fixed time intervals samples of 50 µL each were taken and analysed by GC as described above for the case of lipase-catalysed reactions with $scCO_2$ as external solvent (cf. appendix B).

5.1.1.1.4 Determination of kinetic parameters

Parametric identification of maximum velocity, Michaelis-Menten constants and inhibition constants was done from the equation for the initial reaction rate in absence of product. The program used for identification was based on a Levenberg-Marquardt algorithm.

5.1.1.1.5 Biocatalyst reuse

In order to determine the stability of the CaL immobilised in the HPMC organogels with lecithin microemulsion, the gels were reused in consecutive independent batches in $scCO_2$. Each batch reaction was continued for 3 h at 35 °C. The total volume of the batch was 32.1 mL in each case. After each run, the organogels containing lipase were washed twice with 10 mL isooctane and a new catalytic reaction was started in $scCO_2$ as described before. The same series of experiments was also performed in the reference system isooctane at 35 °C and with 32.1 mL total volume.

Table 5.2: Esterification of 103 mM lauric acid and 207 mM 1-propanol: Survey of the preliminary tests on enzyme activity in MBGs with $scCO_2$ as solvent. % conversion of lauric acid to 1-propyl laurate. Reaction time: 3 h unless otherwise stated.

Polymer	Surfactant	Lipase	m_{Lipase}/mg	% conversion
HPMC [a]	lecithin	CaL	1.20	36.5
		MmL	0.22	11.5
	AOT	CaL	1.20	10.7
		MmL	0.22	1.6
gelatin	lecithin [b]	CaL	0.90	1.8
		MmL	0.17	2.2
	AOT	CaL [b]	7.19	17.0
		MmL [c]	1.32	9.0
		MmL [d]	1.39	36.8

[a] 35 °C, 110 bar. [b] 25 °C, 150 bar. [c] 25 °C, 175 bar. [d] 25.2 °C, 130 bar, gelation with 4.6 mL AOT microemulsion, reaction time: 7 h.

5.1.1.1.6 DSC measurements

Differential scanning calorimetry (DSC) measurements on gels of different composition were performed using a SETARAM Micro DSC III (SETARAM Scientific & Industrial Equipment, Caluire, France). Phase transitions of water in these gels were studied in a temperature range from −20 °C to 25 °C with a scan rate of 0.5 K min^{-1}.

5.1.1.2 Results

5.1.1.2.1 Choice of system

In the present work, the ability of HPMC as well as gelatin organogels based on both AOT as well as lecithin microemulsions to catalyse esterification reactions in $scCO_2$ was investigated. As model reaction the esterification lauric acid and 1-propanol was chosen. The preliminary tests were performed with gel compositions similar to those published recently [151, 152, 153]. Efforts to optimise gel compositions were not attempted. A reaction temperature of 25 °C was chosen for gelatin MBGs in order to avoid melting of the gels under pressure.
It was observed that the carbon dioxide solution above the HPMC MBGs remains transparent, whereas in the case of the gelatin gels turbidity appears when the amount of microemulsion in the gel exceeded 55 % (w/w). After injection of the substrate solution the carbon dioxide phase becomes turbid independently of the microemulsion contents in the gels. This is observed for both gelatin and HPMC gels.
The preliminary tests with carbon dioxide as solvent showed that both enzymes were catalytically active in MBGs based on either HPMC or gelatin and in microemulsions containing either AOT or lecithin (cf. Table 5.2). After having accomplished the reactions in the carbon dioxide environment, all gels were tested in a subsequent esterification reaction with isooctane as solvent according to the procedure given in section 5.1.1.1.3. These tests showed that the catalytic

Table 5.3: Survey of the preliminary tests on the enzyme activity in HPMC-lecithin MBGs containing CaL with $scCO_2$ (35 °C, 110 bar) as solvent. % conversion of miscellaneous tested esterification and transesterification reactions. Reaction time: 3 h unless otherwise stated. [lauric acid] = 103 mM, [propanol] = 207 mM, and [1st Reactant] = 100 mM unless otherwise stated.

1st reactant	2nd reactant	% conversion
geraniol	lauric acid	1.8
nerol	lauric acid	-
HPA [a]	1-propanol	- [b]
HPP [c]	1-propanol	- [b]
1-butyl laurate [d]	1-propanol	8.9
vinyl acetate [e]	1-propanol	28.2

[a] reaction time: 12 h. [b] not detectable. [c] reaction time: 6 h. [d] 88.4 mM. [e] 202 mM.

activity of the enzyme was maintained in all gels excluding any deleterious effect of carbon dioxide on the lipase.

According to results compiled in Table 5.2, the most appropriate system is the HPMC organogel formulated with lecithin microemulsion and CaL as catalyst. Consequently, the focus for further investigations was set on this particular gel type.

In addition to the model reaction, esterification reactions with different alcohols such as geraniol or nerol, or different acids such as the phenolic acids p-hydroxyphenylacetic acid (HPA) and p-hydroxyphenylpropionic acid (HPP) were conducted in $scCO_2$ (cf. Table 5.3). In the case of geraniol and nerol, the 1-propanol in the microemulsion was replaced by 2-propanol in order to avoid substrate competition. Analysis of the esterification of HPA and HPP, respectively, with 1-propanol was not possible, as neither acids nor esters could be detected after sampling.

Furthermore, transesterification reactions were conducted with $scCO_2$ as external solvent in order to test the catalytic ability of the immobilised CaL to catalyse this specific reaction type. The following esters were chosen for the reaction with 1-propanol: butyl laurate, vinyl acetate, ethyl acetate, ethyl acetoacetate and ethyl crotonate. However, the latter two esters did not show any conversion with isooctane as solvent within 3 h and the reaction of ethyl acetate was very slow. Therefore, transesterification reactions in $scCO_2$ were just performed with butyl laurate and vinyl acetate (35 °C, 110 bar). The results from the transesterification reactions can be found in Table 5.3.

5.1.1.2.2 Effect of pressure

Figure 5.1 shows the effect of pressure on the reaction profiles of the esterification of lauric acid with 1-propanol and thus on the initial reaction velocities in $scCO_2$ at 35 °C. The initial rate decreases with increasing pressure from 110 bar to 200 bar, and a further raise of pressure does not affect the reaction velocity anymore.

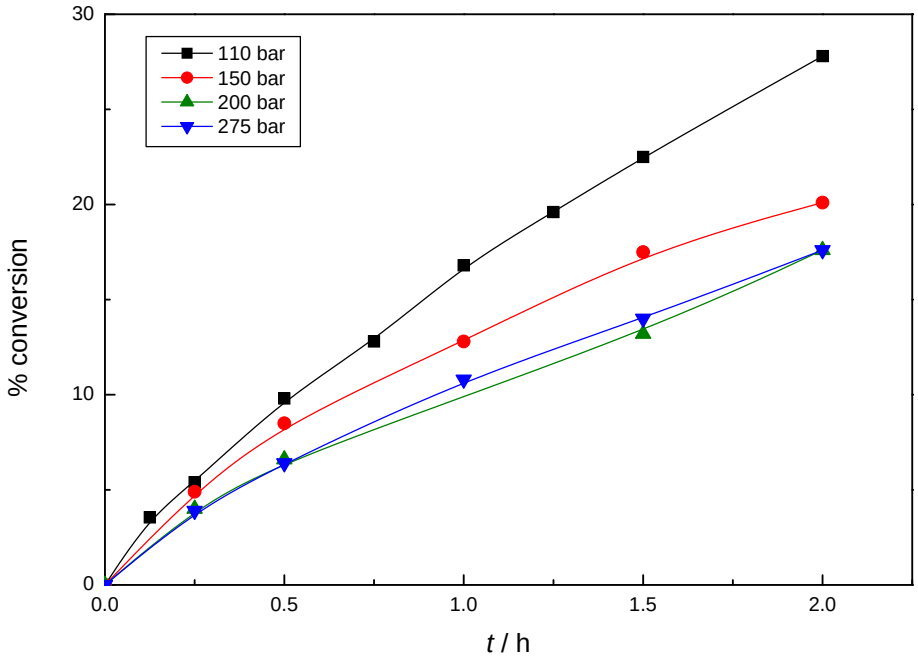

Figure 5.1: Influence of pressure on the reaction profiles of the esterification of 103 mM lauric acid and 207 mM 1-propanol catalysed by CaL encapsulated in a HPMC-lecithin MBG containing 1.2 mg enzyme at 35 °C in $scCO_2$.

5.1.1.2.3 Kinetic analysis

Figure 5.2 shows the initial reaction profile of the esterification of 103 mM lauric acid with various concentrations of 1-propanol catalysed by CaL immobilised in a HPMC-lecithin MBG containing 1.2 mg enzyme at 35 °C and 110 bar in $scCO_2$. Typical profiles are observed with the produced amounts of ester increasing upon increase of the alcohol concentration up to 207 mM. A further increase of the 1-propanol concentration results in a decrease of the initial rate. The same can be seen in Figure 5.3 which displays the initial rate as function of the alcohol concentration at different constant lauric acid concentrations. Again, too high alcohol concentrations lead to an inhibitory effect.

A Lineweaver-Burk double reciprocal plot of the initial rate vs. the 1-propanol concentration in the non-inhibitory alcohol concentration range is shown in Figure 5.4. As can be seen, a set of parallel lines is obtained. Furthermore, Figure 5.5 shows the double reciprocal plot of the initial velocity as a function of the lauric acid concentration. Again, the plots appear to be parallel for alcohol concentrations up to 207 mM.

5.1.1.2.4 Effect of substrate chain length

The influence of alcohol and acid carbon chain length was studied in both $scCO_2$ and isooctane as a reference system. For the determination of the changes in the reaction rate in $scCO_2$ with varying chain length, the conversions after 3 h were chosen. Since the amount of produced ester is supposed to increase more or less linearly in this time interval, the differences in the

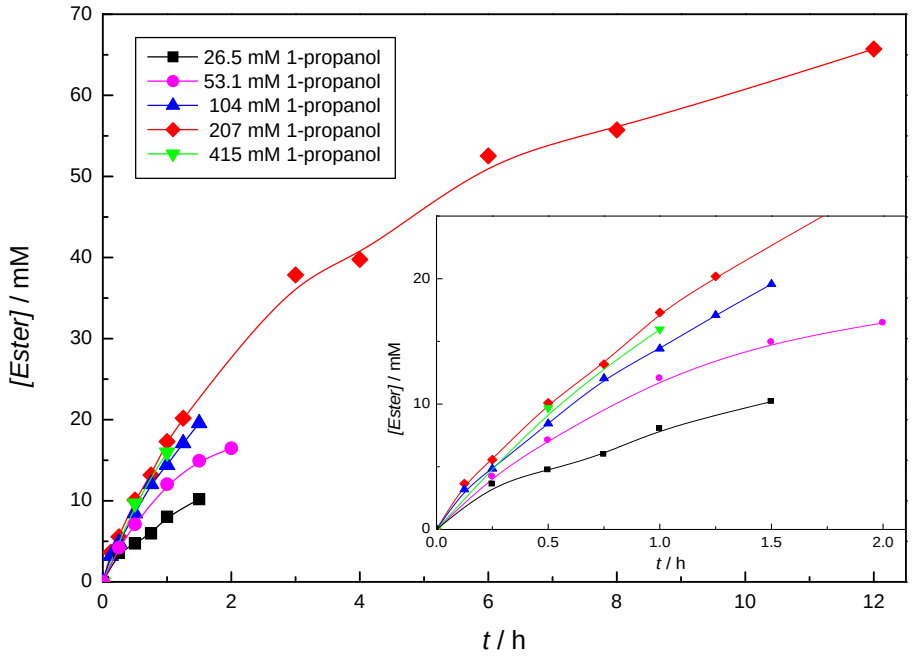

Figure 5.2: Reaction profile of the esterification of 103 mM lauric acid and 1-propanol catalysed by CaL immobilised in a HPMC-lecithin MBG containing 1.20 mg enzyme at 35 °C and 110 bar in $scCO_2$. The insert represents a magnification of the first two 2 h.

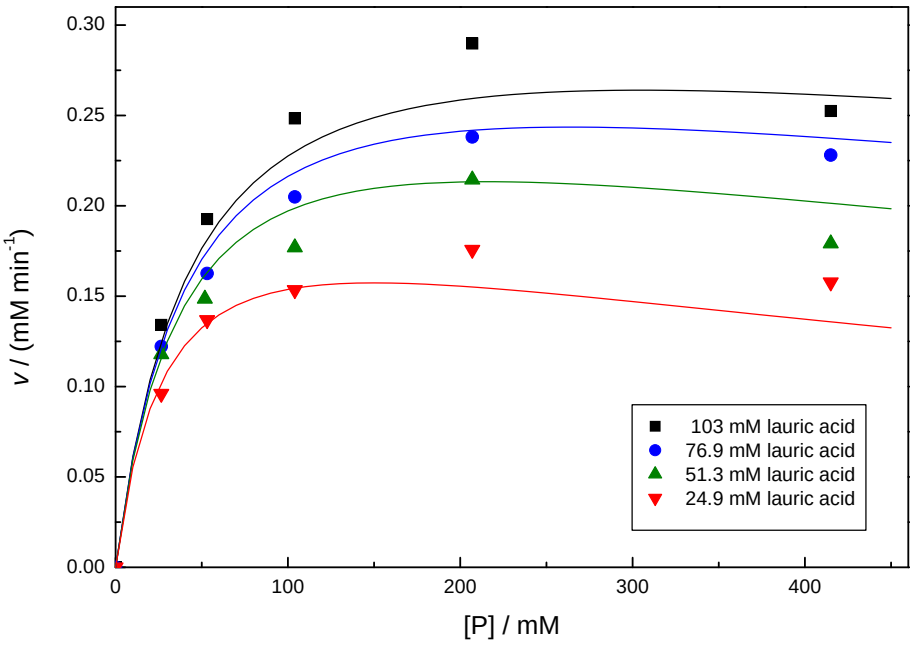

Figure 5.3: Effect of the 1-propanol concentration, [P], on the initial reaction velocity, v. Esterification of 1-propanol by lauric acid at different fixed concentrations of lauric acid in $scCO_2$ at 110 bar and 35 °C. Lines calculated according to the kinetic model (cf. Equation (5.1) and Table 5.5).

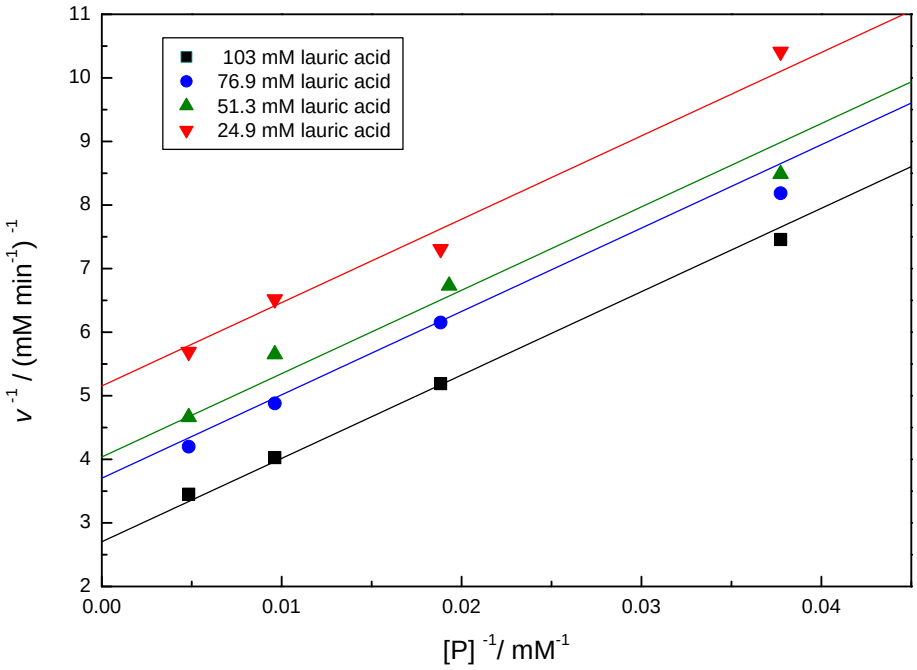

Figure 5.4: Double reciprocal plot of the initial reaction velocity, v, as a function of the 1-propanol concentration, [P], at different fixed concentrations of lauric acid in $scCO_2$ at 110 bar and 35 °C.

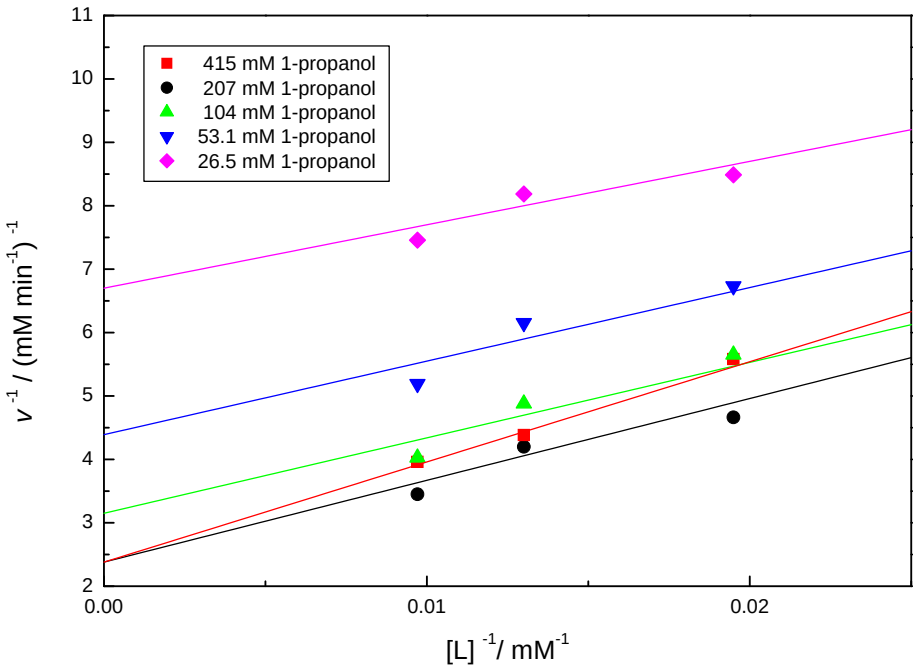

Figure 5.5: Double reciprocal plot of the initial reaction velocity, v, as a function of the lauric acid concentration, [L], at different fixed concentrations of 1-propanol in $scCO_2$ at 110 bar and 35 °C.

conversion after 3 h are assumed to correlate to different initial rates. With regard to the observed reproducibilities in $scCO_2$, the chosen time interval of three hours is considered to be long enough for secure differentiation of the results above possible error. For the experiments in the reference system, the initial rates for the different alcohols and acids were determined from the initial slope of the reaction profile.
The effect of alcohol chain length was studied by following the esterification of lauric acid with a series of n-alcohols as shown in Figure 5.6. In order to avoid competition reactions with the internal alcohol of the microemulsion of the organogel, 2-propanol was used for the microemulsion formulation. This secondary alcohol cannot be converted by CaL under these conditions. It can be seen that in $scCO_2$ there is an increase of the reaction rate from ethanol to 1-butanol. This maximum is followed by a sharp decline and a slow increase towards the long chain alcohols. In isooctane the observed pattern is similar. Only the maximum is shifted from 1-butanol to 1-propanol.
In order to determine the effect of the fatty acid chain length, esterification reactions of a series of acids with 1-propanol were conducted. As can be seen in Figure 5.7, the results revealed a diverse behavior in the two media. In $scCO_2$, there is a tendency towards increasing reaction velocity with increasing number of carbon atoms, whereas in isooctane the initial rate decreases in the same direction.

5.1.1.2.5 Effect of gel composition

Figure 5.8 shows the effect of changes of the gel composition on the initial rate of the esterification of lauric acid and 1-propanol in both $scCO_2$ (110 bar) as well as isooctane as solvent at 35 °C. As can be seen, an increase of the HPMC mass fraction, ξ_{HPMC}, of the gel and thus a decrease of the water content, ξ_{H_2O}, results in an increased initial reaction rate.
In addition, experiments on freezing and melting of water in HPMC gels of different polymer and thus different water concentration were performed by DSC measurements on freshly prepared MBGs in a temperature range from −20 °C to +25 °C. In order to resolve overlapping bands, a peak-analysis was accomplished with the DSC data (cf. appendix C.1 and Figure 5.9).
The existing amounts of different water types were estimated from the peak areas by using an equation for the temperature dependent heat of fusion for water derived from thermoporometry studies [314, 315] (cf. appendix C.2). Preceding DSC measurements on the pure microemulsions displayed no melting and freezing events in the studied temperature range.
Table 5.4 shows the results for the DSC analysis, which allow the identification of three different states of water by DSC. The highest melting point at approx. −2 °C can be assigned to bulk-like water which is free water with no or very weak interactions with the polymer. In addition, there are two different types of interfacial water with weaker (melting point of approx. −5 °C to −7 °C; type I) and stronger (melting point approx. −14 °C; type II) interactions with the polymer. The results compiled in Table 5.4 also hint at a fourth type of water in the gel matrix, as not all water is found by the DSC measurements. This water structure can be classified as non freezable, bound water with the strongest polymer interactions of all water types.

5.1.1.2.6 Biocatalyst reuse

In order to get a first impression of the operational stability of the HPMC-lecithin gels containing CaL, they were used three consecutive times. Conversions per gram of gel after successive

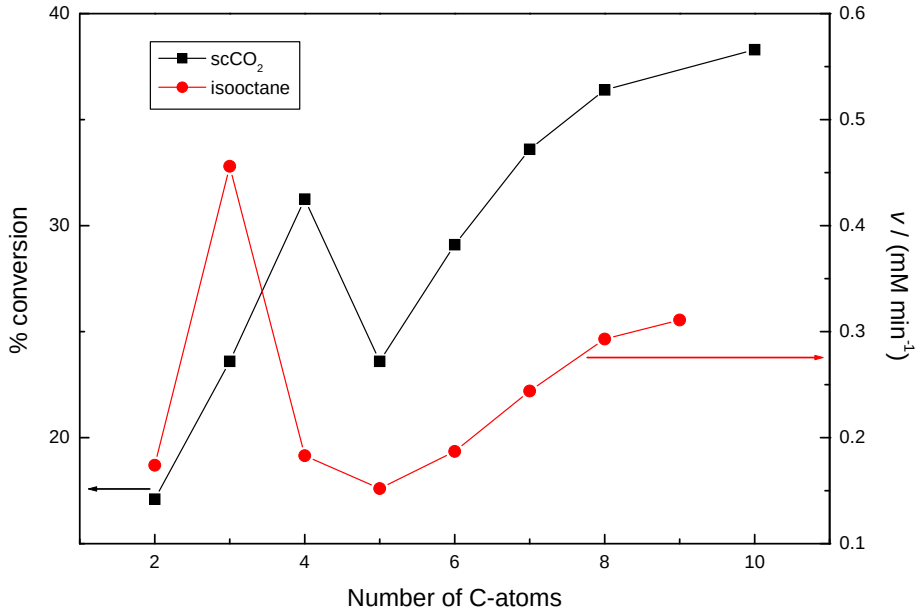

Figure 5.6: Effect of the alcohol chain length on the conversion after three hours reaction time in $scCO_2$ (35 °C; 110 bar) and on the initial rate, v, in isooctane (35 °C). Esterification of different primary alcohols (100 mM each) with 100 mM lauric acid catalysed by CaL immobilised in HPMC-containing lecithin MBG.

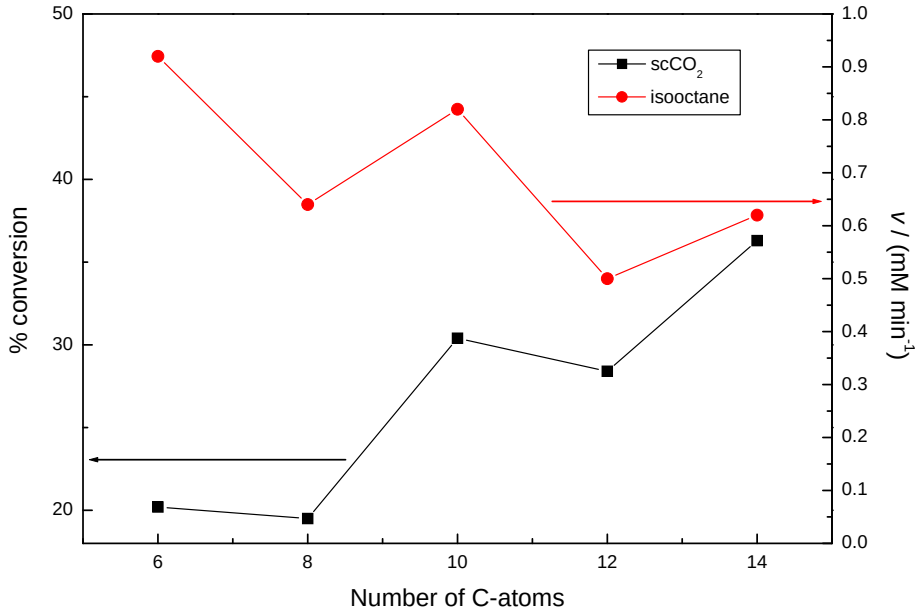

Figure 5.7: Effect of the acid chain length on the conversion after three hours reaction time in $scCO_2$ (35 °C; 110 bar) and on the initial rate, v, in isooctane (35 °C). Esterification of different acids (100 mM each) with 200 mM 1-propanol catalysed by CaL immobilised in HPMC-containing lecithin MBG.

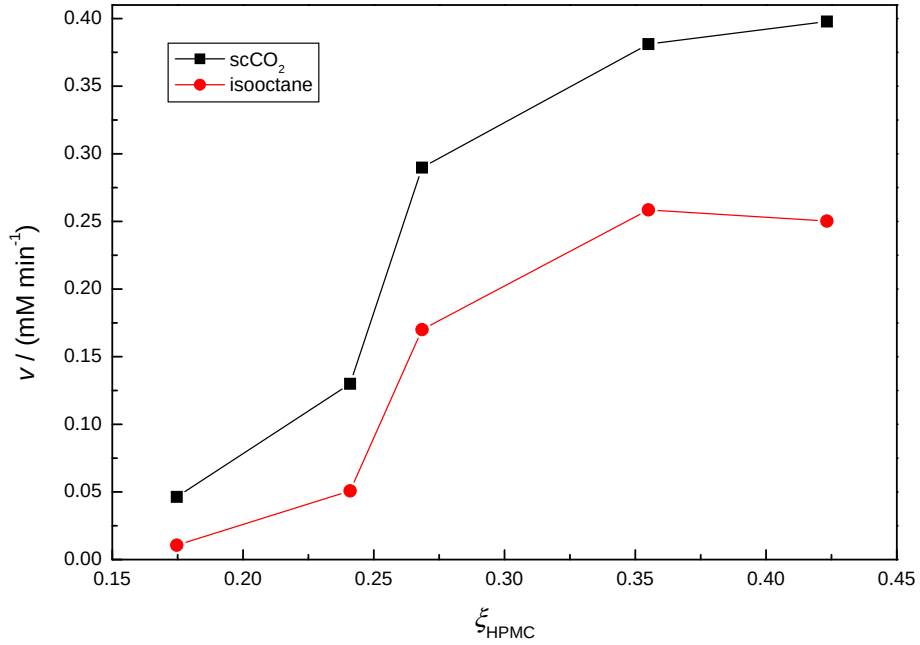

Figure 5.8: Influence of the HPMC mass fraction, ξ_{HPMC}, on the synthetic activity of CaL in lecithin-based MBGs containing 1.20 mg enzyme. Esterification of 100 mM lauric acid and 200 mM 1-propanol at 35 °C in $scCO_2$ and isooctane, respectively.

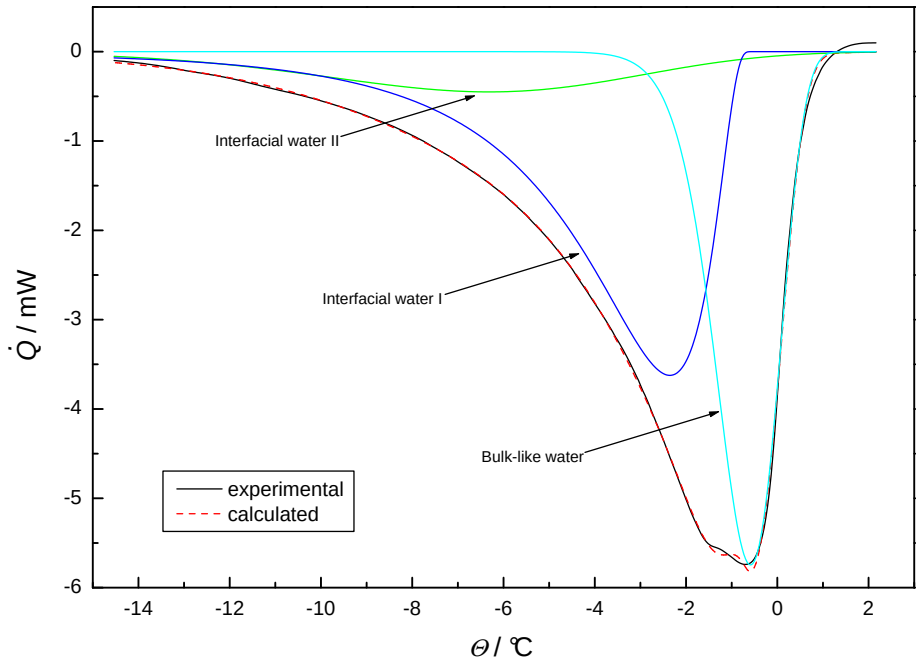

Figure 5.9: DSC measurement on a HPMC-lecithin MBG ($\xi_{\mathrm{HPMC}} = 0.27$, $\xi_{H_2O} = 0.53$): heat flow, $\dot{Q}$, as function of temperature, Θ (scan rate: 0.5 K min^{-1}). Experimental data and calculated curves for the different water types according to the accomplished peak-analysis.

Table 5.4: DSC measurements on HPMC-lecithin MBGs with increasing HPMC fraction, ξ_{HPMC}, and thus decreasing water content, ξ_{H_2O}. Results from heating experiments starting from −20 °C with a scan rate of 0.5 K min^{-1}. Onset temperatures of the different water peaks and estimated fractions χ_i with respect to the total water amount in the gel matrix.

ξ_{HPMC}	ξ_{H_2O}	Bulk-like water		Interfacial water I		Interfacial water II	
		Onset / °C	χ_B	Onset / °C	χ_I	Onset / °C	χ_{II}
0.18	0.70	−1.4	0.39	−4.8	0.56	-	-
0.27	0.53	−2.2	0.26	−6.7	0.47	−13.9	0.15
0.42	0.42	-	-	−7.5	0.30	−13.9	0.40

operational steps are shown in Figure 5.10.
In the case of $scCO_2$ a mass loss of gel occurs while pressure is released. The gel is partly flushed out and crushed into smaller particles while it is pressed through the outlet of the cell resulting in smaller gel particles with each reuse. While the reaction products can easily be collected, the recovery of the gel is difficult and not complete at least with the high-pressure apparatus used. The smaller the gel particles get, the less complete the gel recovery becomes. For the second use the available gel mass recovered was 83 % of the initial gel mass, while for the third application it was just 45 %. After the second reuse the amount of gel was too small to start a fourth cycle.

5.1.1.3 Discussion

5.1.1.3.1 Choice of system

As Table 5.2 shows, HPMC and gelatin MBGs based on both lecithin as well as AOT microemulsions are active in $scCO_2$. However, the gels are not completely inert in this medium under the particular reaction conditions chosen, as the solutions above the gel get turbid. This might indicate that some components are partially extracted from the gel. Nevertheless, all gels exhibit catalytic activity.
As can be seen in Figure 5.8, the esterification between lauric acid and 1-propanol catalysed by CaL in HPMC-lecithin organogels in $scCO_2$ displayed initial rates higher than those in the reference system isooctane. In terms of conversion this reaction yielded 36.5 % after 3 h. Such a conversion can be considered to be quite high as compared to data reported on similar enzymatic reactions in carbon dioxide. Srivastava et al. [266] reported just 18 % conversion for the reaction between myristic acid and ethanol in a batch reaction with a total volume of 6 mL using 10 mg of crude lipase, an enzyme quantity which is eight times higher than in the present study. Steytler et al. [316] presented the esterification of lauric acid with butanol catalysed by supported *Candida* lipase with a conversion of about 20 % within 3 h. Here again, the quantity of enzyme used is very high with 2.4 g in a reactor volume of 120 mL. Furthermore, comparing to other studies [259, 262] concerning lipase catalysed reactions in $scCO_2$, it seems that one of the main advantages of MBGs is the very small quantity of enzyme required for the efficient catalysis of such reactions (here: 1.20 mg).

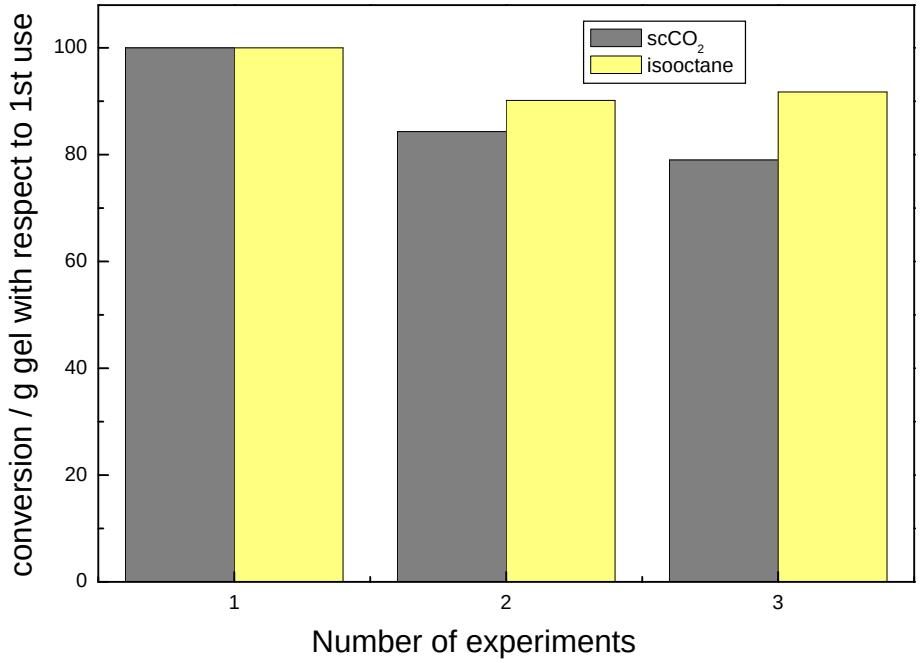

Figure 5.10: Catalytic activity of CaL immobilised in a HPMC-lecithin MBG containing 1.20 mg enzyme towards repeated synthesis of 1-propyl laurate. Esterification of 100 mM lauric acid and 200 mM 1-propanol.

The experiments with the phenolic acids HPA and HPP reveal a general restriction for the use of HPMC-based MBGs. Although these two acids can be esterified with 1-propanol catalytically in lecithin microemulsions containing CaL, the use of HPMC-based MBGs is not possible as the acids are absorbed and can no longer be detected in the solutions above the gels. This can be directly observed for both acids in reactions in isooctane with continuous sampling after predefined time-intervals, as the amount of acid detected by GC is continuously decreasing until complete absorption. Consequently, HPMC MBGs can not be applied for esterification reactions of acids that show too strong interactions with the gel matrix.
Furthermore, the HPMC-lecithin MBGs with CaL lipase are capable to catalyse transesterification reactions in $scCO_2$. However, the initial test with the gels in isooctane showed that not all esters might be suitable for catalytic transesterification with the MBG system investigated. For esters with additional functional groups or double bonds within the alkyl chain no conversion was observed after three hours of reaction time. Similarly, the branched alcohols geraniol and nerol containing a double bond react very slowly.

5.1.1.3.2 Effect of pressure

The effect of pressure on enzymatic reactions in $scCO_2$ has been the subject of investigation in several studies. However, the influence of pressure on this kind of reactions is still not fully understood due to contradictory results [317].
Randolph et al. [257] reported a linear increase of the oxidation rate of cholesterol with increasing pressure in the range from 80 bar to 100 bar, when using $scCO_2$ saturated with the substrate.

This was explained by an increase of cholesterol solubility as well as an increase of the cholesterol aggregation in the particular pressure range. Similarly, Steytler et al. [316] observed an increase in the esterification rate of lauric acid with butanol catalysed by *Candida* lipase B when the pressure was increased stepwise from 150 bar to 500 bar. The authors attributed this effect to a higher adsorption of the synthesised ester on the enzyme bed as the solvent capacity of $scCO_2$ decreases with decreasing pressure. Furthermore, Miller et al. [318, 319] reported an increase of reaction rate with pressure. They studied the interesterification of trilaurin and myristic acid in $scCO_2$ saturated with the substrates at pressures in the range from 80 bar to 110 bar. Again, this increase was contributed to the increase of solubility of the substrates in the carbon dioxide. In contrast, Vermuë et al. [320] observed a decline of the reaction rate in the transesterification of nonanol and ethyl acetate when rising the pressure in the system. The same observation was made by Erickson et al. [321], who studied the transesterification between trilaurin and palmitic acid catalysed by immobilised lipase of *Rhizopus arrhizus* in $scCO_2$ and supercritical ethane, respectively. They found the same behaviour in both solvents and deduced that the decrease in the reaction rate with increasing pressure is not a pH effect, since ethane is not acidic in contrast to CO_2. In conclusion, they attributed the pressure effect to changes of the reactants' partitioning between the supercritical fluid and the vicinity of the enzyme. Likewise, Rantakylä and Aaltonen [262] reported a decrease of reaction rate with rising pressure in the enantioselective esterification of racemic ibuprofen with 1-propanol catalysed by Lipozyme IM 20.
Finally, Ikushima et al. [322] and Nakaya et al. [317] observed even a peak of the initial rate at the vicinity of the critical point of carbon dioxide. They studied the esterification of n-valeric acid by citronellol catalysed by *Candida cylindracea* lipase at 35 °C and the transesterification between triolein and stearic acid catalysed by Lipozyme IM at 50 °C, respectively.
Recapitulating, Nakaya et al. [317] stated that at pressures above the critical region an increase of pressure results in an increase of reaction rate, if the amount of substrates is higher than the solubility limit, as this results in increasing substrate concentrations with pressure. On the other hand, an increase of pressure results in a decline of reaction velocity in the case of concentrations below saturation.
In the present study the reason for the decrease of the reaction rate with increasing pressure might be similar to the explanation by Erickson et al. [321]. The rising pressure is accompanied by an increase of the solvating power of $scCO_2$, which means that the solubility of lauric acid and 1-propanol in the supercritical phase rises. Due to this solvation effect, the partitioning of the substrates between the supercritical fluid, the oil phase of the microemulsion in the gel and the immediate vicinity of the enzyme is changed. The enzyme environment is depleted with regard to the substrates, which causes a decline in the reaction rate. As soon as the partitioning of the substrates is virtually shifted to the supercritical phase, a further increase of pressure should no longer result in a further depletion in the enzyme environment, i.e. that the initial rate should no longer be affected by the rise of pressure. The plateau observed in Figure 5.1 is in accordance with the latter hypothesis.

5.1.1.3.3 Kinetic analysis

The results of the kinetic analysis (cf. section 5.1.1.2.3) indicate that a Ping Pong Bi Bi mechanism with dead-end inhibition by alcoholic substrate (1-propanol) occurs in this system. The same mechanism has been proposed for various esterification or transesterification reactions catalysed by both free and immobilised lipases:

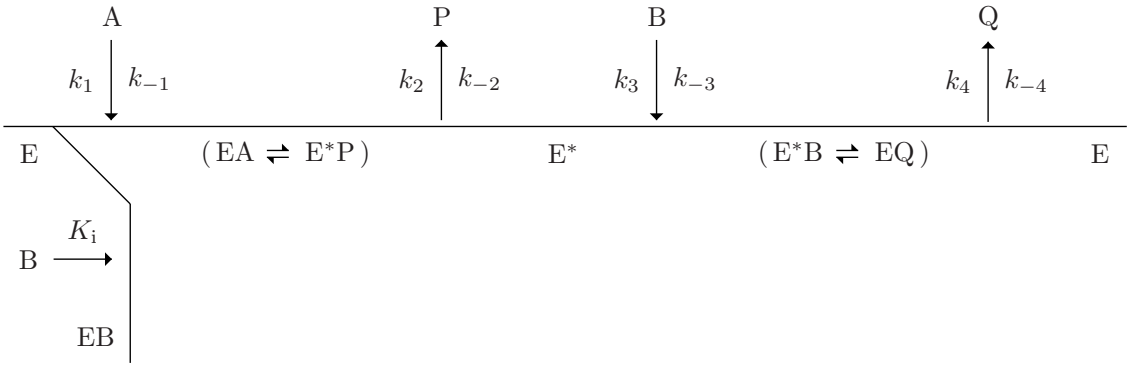

Figure 5.11: Cleland notation of a Ping Pong Bi Bi reaction with dead-end inhibition by excess of alcohol (cf. e.g. [149, 297]). A: lauric acid. B: 1-propanol. P: water. Q: product – 1-propyl laurate. E: free lipase. E*: modified lipase. EA: lipase-lauric acid complex. EB: lipase-propanol dead-end complex. E*P: modified lipase-water complex. E*B: modified lipase-propanol complex. EQ: lipase-propyl laurate complex.

Stamatis et al. [323] suggested this mechanism for the esterification of lauric acid and (-)-menthol catalysed by free *Penicillium simplicissimum* lipase in an AOT-based microemulsion in isooctane. Kinetic studies by Condoret et al. concerning the esterification of oleic acid and ethanol [324, 325] and the transesterification of propyl acetate and geraniol [259, 326, 327] by immobilised *M. miehei* lipase (Lipozyme) revealed a Ping Pong Bi Bi mechanism with inhibition by excess of alcohol (ethanol and geraniol, respectively) for both n-hexane and $scCO_2$ as reaction medium. Furthermore, this reaction mechanism has also been proposed for lipases encapsulated in MBGs: Jenta et al. [141] investigated the synthesis of octyl decanoate catalysed by *Chromobacterium viscosum* lipase immobilised in AOT microemulsion-based organogels formulated with gelatin. Recently, Delimitsou et al. [153] reported on the esterification of lauric acid and 1-propanol by means of a HPMC MBG containing an AOT microemulsion with *M. miehei* lipase.
According to the Ping Pong Bi Bi mechanism model, the lipase reacts with the lauric acid to form a lipase-acid complex, which is then transformed to a carboxylic lipase by release of water. A subsequent nucleophilic attack of the alcohol on this intermediate results finally in the regeneration of the enzyme and the release of the ester. A possible explanation for the alcohol inhibitory effect might be the following hypothesis: 1-propanol reacts with the free lipase, a dead-end complex is formed, and the lipase cannot further participate in the reaction. Figure 5.11 shows the Cleland notation for this kind of mechanism. The general rate equation [297] is given in Equation (5.1), where v is the initial velocity, v_{max} is the maximum velocity under saturation conditions, K_m^A and K_m^B are the Michaelis-Menten constants of the acid and the alcohol, respectively, and K_i^B is the inhibition constant for the substrate inhibition by the alcohol.

$$v = \frac{v_{max}[A][B]}{K_m^A[B]\left(1 + \frac{[B]}{K_i^B}\right) + K_m^B[A] + [A][B]} \tag{5.1}$$

The kinetic constants were determined by fitting the experimental data to Equation (5.1) by non-linear regression and values are given in Table 5.5. In Figure 5.3, symbols represent experimental

Table 5.5: Apparent kinetic constants for $scCO_2$ according to Equation (5.1). Esterification of lauric acid and 1-propanol catalysed by CaL encapsulated in a HPMC-lecithin MBG containing 1.2 mg enzyme at 35 °C and 110 bar in $scCO_2$. A and B refer to the substrates lauric acid and 1-propanol, respectively.

Apparent kinetic constants	HPMC-lecithin MBG in $scCO_2$
K_m^A/mM	22.9 ± 6.80
K_m^B/mM	56.4 ± 10.8
K_i^B/mM	367 ± 205
v_{max}/mM min^{-1}	0.420 ± 0.039

data, whereas lines represent the kinetic model according to Equation (5.1).
The determined kinetic constants represent apparent ones, as the esterification does not take place in a homogeneous medium and the constants are probably affected by internal diffusion, i.e. substrate transport from the surface of the organogel to the microenvironment of the enzyme. In spite of the unstirred solution, the influence of the diffusion within the solvent should be small because of the high diffusivity in supercritical fluids [11].
Plots (not shown) of the measurements in isooctane according to the Figures 5.3, 5.4 and 5.5 likewise indicate that a Ping Pong Bi Bi mechanism occurs. However, due to the poor reproducibility fitting of the data according to Equation (5.1) results in error bars greater than the numerical values of the respective kinetic constants. Thus, a direct comparison between the kinetic constants in the two different solvents can not be accurately drawn.

5.1.1.3.4 Effect of substrate chain length

Reactions of various alcohols in both media indicated no significant differences concerning the effect of the alcohol chain length on the initial rates in $scCO_2$ and isooctane, respectively, except for the case of 1-propanol. It is known that the different partitioning of alcoholic substrates in various phases of the system influences the catalytic behavior of lipases in AOT or lecithin microemulsions [328]. Thus, differences in the reaction rates for different alcohols can be attributed to the diverse partitioning of the alcohols between the (organic) solvent and the microenvironment of the immobilised lipase.
Consequently, the observed maximum in the reaction rate for 1-butanol in $scCO_2$ can be attributed to the high solubility of this alcohol in the vicinity of the enzyme displaying the good co-surfactant property of this alcohol. Similar observations have been made in other studies on the effect of alcohol chain length on lipase activity. Sawant et al. stated a maximum in the initial rate for 1-butanol for both immobilised *M. miehei* lipase [329] as well as for soluble Lipolase 100 L in a biphasic reaction system [330]. In addition, Delimitsou et al. [153] reported the same finding for *M. miehei* lipase immobilised in a HPMC-containing AOT MBG at 25 °C with isooctane as external solvent.
However, in the present study the maximum in isooctane is shifted to 1-propanol. Allowing for the fact that the microemulsions of the organogels were formulated with 2-propanol in order to avoid competition reactions, a possible explanation might be the following hypothesis: an

exchange of the inner (2-propanol) and the outer (1-propanol) alcohol proceeds in isooctane leading to a higher concentration of the reactant in the microenvironment of the enzyme and consequently to a maximum for 1-propanol, whereas this substitution does not occur to the same extent in $scCO_2$ hindering the external 1-propanol from reaching the enzyme. This would also explain the maximum for 1-butanol found in the above mentioned study on *M. miehei* lipase immobilised on HPMC-containing AOT MBG [153], a system that does not contain an internal alcohol in the microemulsion of the gel.
Investigations concerning the influence of acid chain length on the initial rate of esterifications catalysed by lipases immobilised on MBGs have not yet been reported in the literature. So far, just the differences in the final yield of ester have been investigated with respect to changes in the alkyl chain length of the acids [7, 149, 152].
In the case of acids with different chain length, the behavior in $scCO_2$ and isooctane is completely different. In $scCO_2$ the initial rate increases with increasing chain length, whereas in isooctane there is a decline of the reaction rate towards longer acids. Again, this can be attributed to a different partitioning of the acids between the solvent and the microenvironment of the enzyme. The longer the chains of the acids become, the more alkane-like they behave, which results in an increasing solubility in isooctane and a decreasing solubility in $scCO_2$. This means that in $scCO_2$ the concentration of the acids in the vicinity of the enzyme increases with increasing chain length leading to higher reaction rates. In contrast, the surrounding of the enzyme is depleted, if the solvent is isooctane.
Furthermore, it seems that the reaction system consisting of the enzyme immobilised on the MBG prefers the acids with 6, 10, and 14 C-atoms to the acids with 8 and 12 C-atoms, as the initial rates for the latter acids are lower compared to the former ones. Obviously, this is not affected by the change in the solvent as it can be seen from both curves in Figure 5.7.

5.1.1.3.5 Effect of gel composition

Figure 5.8 indicates an increase in the reaction rate with increasing HPMC mass fraction. The same has already been reported for the catalytic esterification of lauric acid and 1-hexanol using agar- or HPMC-based organogels containing *M. miehei* lipase entrapped in an AOT microemulsion [153]. The effect was observed for both solvent-free reactions (1-hexanol as solvent) as well as reactions carried out in isooctane. In addition, a similar behavior has been reported on the esterification of 1-propanol with lauric acid catalysed by *Rhizomucor miehei* as well as *C. antarctica* lipase in organogels formulated with lecithin microemulsions [152].
The different states of water in (hydro-)gels based on cellulose or cellulose derivatives have been the subject of investigations by many authors. A review was given by Ford and Mitchell [331]. The majority of authors discusses models of gel structures displaying three different states of water. These are generally bound water, free (unbound) water and weakly bound or interfacial water [331]. Taniguchi and Horigome [332] described four different states of water in cellulose acetate membranes, namely completely free water, free water interacting weakly with the polymer, bound water which can contain salts, and bound water which rejects salts.
The present DSC measurements on organogels also hint at four different states of water in a similar way as those mentioned above. It was found that the different water types of the organogel matrix depended on the HPMC mass fraction. The matrix of the gel with the highest water content shows bulk-like water and interfacial water I, whereas the gel with the highest HPMC fraction contains just the two types of interfacial water. The gel with medium composition dis-

plays all three different water types in lower concentration with respect to the two gels mentioned before. The initial rates of the enzymatic reaction correlate with this change in water structure: increasing interfacial water II and thus decreasing bulk-like water content leads to an increase of the reaction rate. A possible explanation for this behavior might be that the diffusion of the reactants to the enzyme located in the microemulsion through the gel matrix is less impeded by weaker interactions with the more strongly bound and thus more apolar water. A similar conclusion was drawn for changes in the semipermeability of cellulose membranes [332] and the modulation of drug release from cellulose matrix tablets, where the interactions between drugs and the hydrating gel layer around the tablets seem to be at least partly responsible for changes in the drug release [331].
Another explanation might be a change of the total surface area of the gels. Although all gels were cut into several pellets of approx. equal size, the gels differ quite strongly from each other in the outward appearance. HPMC gels with high water content are cohesive and are in a way similar to gelatin-based MBGs. In contrast, the gels with high HPMC content appear to consist of many loose gel particles sticking together. Hence the change from low to high HPMC fraction might lead to an increase of the total surface area of the gels and might thus minimise diffusion distances in the gel.
The influence of the surface area of MBGs on the reaction rate has first been observed by Jenta et al. [8]. They reported that granulated gelatin-based gels with a AOT microemulsion containing *Chromobacterium viscosum* lipase behave differently from pelleted MBGs of the same composition. The observed initial rates were generally higher for the granulated gels having a higher surface area per unit volume than the pellets. They attributed this effect to the importance of diffusion distances. Furthermore, Hedström et al. [333] conducted a study on the influence of the gel surface area on the initial rate of gelatin AOT MBGs with *C. antarctica* lipase and were able to show that the extrapolated initial rate of hypothetical pellet gels with infinitely large areas are in good agreement with those obtained for granulated MBGs representing gels where diffusion distances are minimised.

5.1.1.3.6 Biocatalyst reuse

The operational stability of an immobilised enzyme, i.e. the ability to reuse it, is an important parameter determining the economic viability of a biocatalytic process. As can be seen in Figure 5.10, the lipase activity in both solvents is quite well preserved. It should be noted that in the case of $scCO_2$ the mass loss due to the sudden depressurising of the high-pressure cell, leads by itself to a decline of activity as the total enzyme concentration in the cell decreases. Nevertheless, the slight decrease of activity is comparable in both solvents, i.e. $scCO_2$ obviously does not negatively influence the operational stability of the HPMC gels containing lipase.
However, due to the limited number of reuses the experiments can just give preliminary and rough initial insight to the operational stability of the CaL immobilised on the HPMC-lecithin MBG. In order to get a further impression of the reusability of the organogels, the number of reuses should be increased and the MBGs should also be investigated in a continuous reaction-separation process. This seems a realistic scenario for a future scale up of the MBG use in $scCO_2$ in which no depressurising steps would deteriorate the biocatalyst. At the present stage of the high-pressure apparatus these experiments could not be carried out as the equipment does neither allow continuous sampling nor continuous addition of substrates under constant pressure (cf. section 3.6).

5.1.1.4 Conclusion

The present study demonstrates that microemulsion-based organogels formulated with HPMC and gelatin can be used as solid-phase catalysts in liquid and supercritical carbon dioxide as external solvents for substrates. Lipase hosted in MBGs retains its ability to catalyse esterification reactions of fatty acids and alcohols and transesterifications in these media. Furthermore, the initial rates of the model esterification reaction of lauric acid and 1-propanol are higher in $scCO_2$ than in the corresponding isooctane system.

With a focus on HPMC-based organogels formulated with lecithin microemulsions containing *C. antarctica* lipase, it has been shown that the mechanism of the chosen model esterification of lauric acid and 1-propanol seems to be of the Ping Pong Bi Bi type with dead-end inhibition by excess of alcohol. In addition, the effect of pressure on the initial rate of the esterification displayed a similar behaviour as described in literature for reactant concentrations below saturation. The influence of alcohol and acid chain length on the initial rate revealed significant differences between isooctane and $scCO_2$. This can be attributed to different partitioning of the reactants in the two solvents. In contrast, the effect of gel composition on the reaction rate is similar in both solvents. Further, DSC measurements on the gels of different composition gave additional insight into the observed increase of reaction velocity with increasing polymer fraction.

Biocatalyst reuse experiments in $scCO_2$ showed that the slight decrease of activity is similar to that observed in isooctane. Provided that continuous reaction-separation processes lead to similar conclusions, the combination of MBGs with the solvent $scCO_2$ represents a promising "green" reaction system for bioconversions. It should be noted that in such a combination the amount of less green substances such as the constituents of the microemulsion and the enzyme is very small.

In summary, the potential of reusable MBGs in biocatalytic processes involving enzymes with high biotechnological value can be combined with the tunable solvent and solvation properties of $scCO_2$ and hence with the superior reaction-separation processes based on supercritical fluids.

5.1.2 Organogels based on detergentless microemulsions

Recently, Zoumpanioti et al. [165] reported on the ability of lipases immobilised in detergentless HPMC MBGs to catalyse esterification reactions in isooctane. The present work provides an extension of their work to $scCO_2$ as external solvent. Results are discussed with reference to the results obtained from the investigation of the catalytic behaviour of MBG-encapsulated CaL in $scCO_2$ (cf. section 5.1.1) and to the findings of Zoumpanioti et al. [165].

5.1.2.1 Experimental

5.1.2.1.1 Materials

The following materials were used for the investigation of lipase catalysed reactions with organogels based on detergentless microemulsions: CaL, carbon dioxide, n-hexane, HPMC, hydrochloric acid, isooctane, lauric acid, 1-propanol, Tris, and Millipore Milli-Q water. Details concerning their (chemical) properties and sources of supply can be found in section 5.1.1.1.1.

5.1.2.1.2 Preparation of organogels

Organogels based on detergentless microemulsions were prepared as described by Zoumpanioti et al. [165]. The actual detergentless microemulsion/gel composition chosen for the experiments with $scCO_2$ refers to the one which displayed the highest activity with isooctane as external solvent according to the study by Zoumpanioti et al.

Preparation of detergentless microemulsions. Detergentless microemulsion-like systems for HPMC-based organogels were prepared by adding 20.0 µL 200 mM Tris/HCl pH 7.5 buffer (cf. section 5.1.1.1.2) containing 1.20 mg of CaL to a binary solution comprised of 472 µL n-hexane and 508 µL 1-propanol. Subsequent vigorous shaking for several seconds yielded stable transparent solutions.

Gelation of detergentless microemulsions. The lipase-containing organogels were prepared by introducing appropriate amounts of surfactantless microemulsion to a mixture of HPMC and water in a similar manner as described in section 5.1.1.1.2 for the HPMC organogels with lecithin-based microemulsions. In a typical experiment, an entire detergentless microemulsion prepared as described above was gelled with 1.0 g HPMC and 2.0 mL water at room temperature.

5.1.2.1.3 Lipase-catalysed reactions

Esterification reactions in $scCO_2$ catalysed by CaL immobilised in organogels based on detergentless microemulsions were carried out as described in section 5.1.1.1.3 for the HPMC organogels based on conventional microemulsions. All experiments were performed at 35 °C and 110 bar.

5.1.2.1.4 Biocatalyst reuse

Reuse experiments with detergentless MBGs in $scCO_2$ were performed as described in section 5.1.1.1.5 for HPMC-lecithin organogels.

5.1.2.2 Results

5.1.2.2.1 Reaction profiles

In the present study, the ability of CaL immobilised in detergentless MBGs to catalyse esterification reactions in $scCO_2$ was investigated. As in the case of the experiments concerning the catalytic behaviour of MBG-encapsulated lipases with $scCO_2$ as external solvent, the condensation of lauric acid and 1-propanol was chosen as model esterification reaction.
Figure 5.12 shows the initial reaction profile of the esterification of 103 mM lauric acid and 207 mM 1-propanol catalysed by CaL entrapped in a HPMC-based detergentless MBG containing 1.2 mg lipase. The profile is shown in comparison to the profile obtained for the same amount of enzyme immobilised in a HPMC organogel based on a conventional lecithin microemulsion (cf. section 5.1.1.2.3 and Figure 5.2).

5.1.2.2.2 Biocatalyst reuse

In order to obtain initial data concerning the operational stability of CaL entrapped in detergentless MBGs, three consecutive batch reactions were carried out in $scCO_2$.

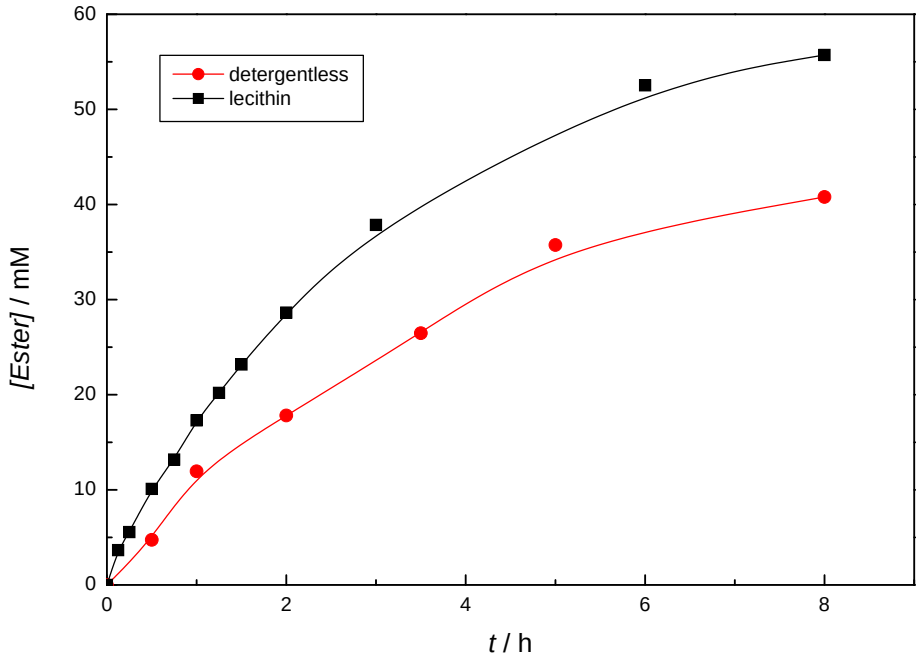

Figure 5.12: Reaction profiles for the esterification of 103 mM lauric acid and 207 mM 1-propanol catalysed by CaL immobilised in HPMC-based organogels: comparison between detergentless and lecithin-based microemulsion.

Figure 5.13 shows the conversions per gram of gel after successive operational steps in comparison to the results obtained for the reuse of HPMC lecithin MBGs in $scCO_2$ (cf. section 5.1.1.2.6 and Figure 5.10).
As in the case of the latter organogels, the pressure release after each batch reaction results in a loss of gel. The available amount of gel for the second use was 90 % of the initial gel mass, while for the third reaction cycle it was just 44 %. The mass of gel recovered after the second reuse was likewise insufficient in order to start of a fourth cycle.

5.1.2.3 Discussion

As can be seen from Figure 5.12, CaL immobilised in surfactantless HPMC MBGs exhibits a lower catalytic activity in $scCO_2$ than CaL entrapped in HPMC organogels based on a lecithin microemulsions. However, Figure 5.13 indicates that the activity of the lipase is better preserved in the detergentless organogel than in the lecithin-based MBG. Despite the fact that a loss of gel mass and thus of enzyme occurs, the conversion per gram of gel even increases, whereas in the case of the conventional MBG the activity decreases.
A similar behaviour has been reported by Zoumpanioti et al. [165] for esterification reactions with isooctane as external solvent. The authors investigated lipases (CaL and *M. miehei* lipase, respectively) immobilised in HPMC MBGs based on both various detergentless microemulsion-like systems and AOT microemulsions. They reported that the reaction rate of the ester synthesis after 7 runs (24 h reaction time) decreased by approx. 15 % in detergentless MBGs and by approx. 30 %-50 % in AOT-based MBGs. In the case of CaL entrapped in a detergentless MBG,

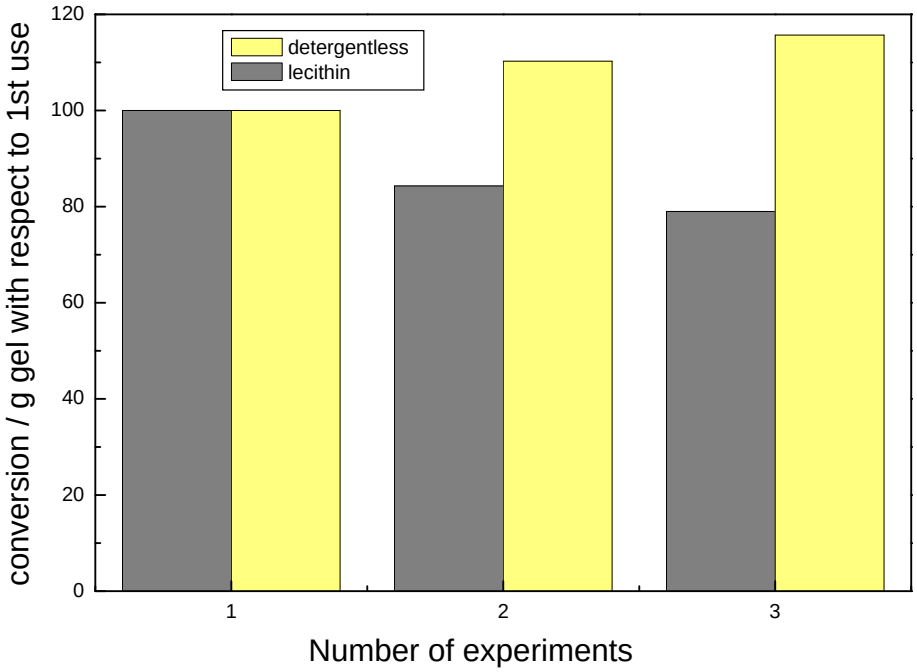

Figure 5.13: Catalytic activity of CaL immobilised in HPMC MBGs containing 1.20 mg enzyme towards repeated synthesis of 1-propyl laurate in $scCO_2$: comparison between detergentless and lecithin-based microemulsion. Esterification of 103 mM lauric acid and 207 mM 1-propanol at 35 °C and 110 bar.

the authors even found an increase of the initial rate during the first 5 batch reactions, before a loss of activity occurred. Moreover, Zoumpanioti et al. investigated the storage stability of the immobilised lipases and found that the surfactantless MBGs exhibited a significantly higher catalytic activity than the conventional MBGs after a storage period of 6 months at 4 °C. The authors concluded that the catalytic activity of both lipases was better preserved in surfactantless MBGs than in AOT-based MBGs.

5.1.2.4 Conclusion

In the present study, *C. antarctica* immobilised in organogels based on detergentless microemulsions was tested for catalytic activity in $scCO_2$. It was found that the entrapped lipase retains its ability to catalyse esterification reactions. Accordingly, the respective gels can be utilised as solid-phase catalysts in this reaction medium.

In summary, the surfactantless MBGs represent an alternative to organogels based on conventional microemulsions, particularly as the results obtained so far in both isooctane and $scCO_2$ indicate that detergentless MBGs exhibit a better operational and storage stability than organogels formulated with classical microemulsions. However, as already stated for the HPMC-lecithin MBGs (cf. section 5.1.1.4), the limited number of reuse experiments in $scCO_2$ requires further investigations concerning this topic.

5.1.3 Phytantriol-based organogels

Phytantriol (3,7,11,15-tetramethyl-1,2,3-hexadecanetriol) is a well-known active ingredient for the cosmetics industry [334, 335, 336, 337].
It improves the moisture retention properties of hair and skin and acts as penetration enhancer for other care chemicals such as panthenol, vitamins, and amino acids. The latter active substances display an increased caring effect due to a more effective deposition in hair and skin. Accordingly, phytantriol is applied in formulations for skin (vitamin) creams, sun care agents, shampoos, hair rinses, and hair treatments.
In the present study, initial tests concerning the potential application of phytantriol-based organogels as enzyme immobilisation matrix were performed with both isooctane and $scCO_2$ as external solvent. Phytantriol-based gels represent a new type of organogels, which can prepared by gelation of a mixture of phytantriol and water (or buffer containing lipase) with HPMC as gelling agent. The investigation of these lipase-containing gels aims at the avoidance of any (volatile) organic solvent in the preparation and application of organogels as solid-phase catalysts: in contrast to MBGs, which contain substantial amounts of organic solvent(s) in their microemulsion part, organogels based on phytantriol would allow enzyme-catalysed reactions in $scCO_2$ in the absence of organic solvents.
In order to get a first impression of the parameters affecting the catalytic activity of enzyme-containing phytantriol-based organogels, the initial tests with entrapped lipase from *M. miehei* were predominantly performed with isooctane as external solvent. As in the case of the MBGs, the esterification of lauric acid and 1-propanol was chosen as model reaction. Apart from the operational stability, the influence of the mass fractions of biopolymer and phytantriol on the initial reaction velocity was studied. Furthermore, activity tests in $scCO_2$ were performed.

5.1.3.1 Experimental

5.1.3.1.1 Materials

Phytantriol (technical, $\geq 85\,\%$ (GC)) was obtained from Fluka and used without further purification.
In addition, carbon dioxide, HPMC, hydrochloric acid, isooctane, MmL, lauric acid, 1-propanol, Tris, and Millipore Milli-Q water were used for the experiments with phytantriol-based organogels. Details concerning their (chemical) properties and sources of supply can be found in section 5.1.1.1.1. Unless otherwise stated, the lipase had a specific activity of $242\,U\,mg^{-1}$ (cf. section 5.1.1.1.1).

5.1.3.1.2 Preparation of gels

Preparation of phytantriol-based organogels. The phytantriol-based organogels were prepared by mixing appropriate amounts of phytantriol with 20.0 µL 200 mM Tris/HCl pH 7.5 buffer (cf. section 5.1.1.1.2) containing MmL followed by gelation of this mixture with 1.0 g HPMC and 2.0 mL water at room temperature. Due to the high viscosity of phytantriol, the intermixing of the buffer solution and the phytantriol was established by means of a spatula.

Preparation of hydrogels. Apart from phytantriol-based organogels, lipase-containing aqueous gels formulated without the addition of phytantriol were used for the investigation of the effect of the phytantriol mass fraction on the enzymatic activity.
These so-called hydrogels were prepared by addition of 20.0 µL 200 mM Tris/HCl pH 7.5 buffer (cf. section 5.1.1.1.2) containing MmL to a mixture of 1.0 g HPMC and 2.0 mL water at room temperature followed by vigorous mixing by means of a spatula.

5.1.3.1.3 Lipase-catalysed reactions

Isooctane as external solvent. Lipase-catalysed reactions with phytantriol-based organogels in isooctane were carried out as described in section 5.1.1.1.3 for the microemulsion-based organogels.

Carbon dioxide as external solvent. Except for the addition of the substrates, lipase-catalysed reactions with phytantriol-based organogels in $scCO_2$ were carried out as described in section 5.1.1.1.3 for the microemulsion-based organogels. Appropriate amounts of lauric acid were added to the freshly prepared gels before sealing the cell. Consequently, the reactions were started by the injection of pure 1-propanol.

5.1.3.1.4 Biocatalyst reuse

For the determination of the operational stability of the MmL immobilised in phytantriol-based HPMC organogels, the gels were reused in consecutive independent batch reactions in isooctane. Each reaction was continued for 24 h at 35 °C, and the total volume of the batch was 32.1 mL in each case. In order to remove products and unreacted substrates, the organogels containing lipase were washed three times with 30 mL isooctane after each run.

5.1.3.2 Results

5.1.3.2.1 Preliminary tests

The aim of this study was to test phytantriol-based organogels with regard to their potential application as enzyme immobilisation matrix for catalytic reactions. As first reaction medium isooctane was chosen for the esterification of lauric acid and 1-propanol. The preliminary tests showed that MmL entrapped in this new kind of organogel is catalytically active. Typical reaction profiles (data not shown) could be obtained.
It was observed that the solutions above the gels became slightly turbid. Analysis of the reaction by GC (cf. appendix B.2.3) revealed that the turbidity was caused by the extraction of phytantriol from the gel, the amount of eluted phytantriol increasing during the reaction course. This loss of phytantriol is accompanied by a change of the outward appearance of the gel: the freshly prepared organogel is cohesive and sticky, while the used (after 24 h reaction time) gel seems to consist of many loose gel particles sticking together. On that score, the latter gel resembles conventional HPMC-lecithin MBGs (cf. section 5.1.1.3.5). However, subsequent reuse experiments with the phytantriol-based organogels showed that the catalytic behaviour was maintained in the gels despite the elution of phytantriol.
Due to these findings, special attention was focussed on the extraction of phytantriol in all following experiments concerning gel composition and reuse.

5.1.3.2.2 Effect of gel composition

The effect of the gel composition on the catalytic activity of the immobilised enzyme was investigated in two different series of experiments. The MmL used for both series had a specific activity of 146.880 U mg^{-1} (Lot & Filling Code: 16008/1 22003179).
As in the case of the classical MBGs (cf. 5.1.1.2.5), the influence of changes of the HPMC mass fraction, ξ_{HPMC}, on the initial rate was investigated. For the respective series of experiments, mixtures of 1.00 g phytantriol and 20.0 µL 200 mM Tris/HCl pH 7.5 buffer containing 0.24 mg MmL were gelled with HPMC/water mixtures with different biopolymer concentrations.
Figure 5.14 shows the effect of the HPMC mass fraction on the catalytic activity of MmL entrapped in a phytantriol-based organogel at 35 °C with isooctane as external solvent: at low HPMC concentration an increase of the HPMC mass fraction, ξ_{HPMC}, of the gel and thus a decrease of the water content, ξ_{H_2O}, results in a drastic increase of the initial reaction rate, while changes in the HPMC concentration at higher mass fractions ($\xi_{HPMC} \geq 0.25$) do virtually not affect the reaction velocity.
In addition, the influence of changes in the phytantriol mass fraction, $\xi_{phytantriol}$, on the enzymatic activity at a certain constant matrix composition was the subject of investigation in isooctane. In this case, the organogels were prepared by gelation of appropriate amounts of phytantriol and 20.0 µL 200 mM Tris/HCl pH 7.5 buffer containing 0.24 mg MmL gelation with 1.0 g HPMC and 2.0 mL water.
Figure 5.15 reveals that the enzyme activity strongly depends on the phytantriol mass fraction, $\xi_{phytantriol}$: at low phytantriol content the initial rate increases with increasing phytantriol concentration, while it is practically not influenced by changes in the phytantriol amount at higher mass fractions ($\xi_{phytantriol} \geq 0.25$). As can be seen, the MmL immobilised in hydrogels formulated without the addition of phytantriol displays the least activity.
With regard to the observed elution of phytantriol, a GC analysis was performed in order to estimate the eluted amount after 24 h reaction time as a function of the initial phytantriol mass fraction. These measurements indicate that approx. 75 % of the phytantriol used for the preparation of the gel is extracted and dissolved in the external solvent, independently of the initial phytantriol concentration in the gel.

5.1.3.2.3 Biocatalyst reuse

Figure 5.16 shows the operational stability of MmL entrapped in a phytantriol-based organogel towards the repeated batchwise esterification between 100 mM lauric acid and 200 mM 1-propanol in isooctane at 35 °C.
As far as the elution of phytantriol is concerned, it was observed that significant amounts of extracted phytantriol after 24 h reaction time could be detected for the first two reaction cycles. In the subsequent batch reactions only traces of phytantriol could be found in the solutions above the gel.

5.1.3.2.4 Reactions with supercritical carbon dioxide as external solvent

In addition to the esterification reactions in isooctane, activity tests in $scCO_2$ as external solvent were performed with the lipase-containing phytantriol-based organogels. With regard to the already mentioned problems in the recovery of (detergentless) MBGs (cf. section 5.1.1.2.6 and

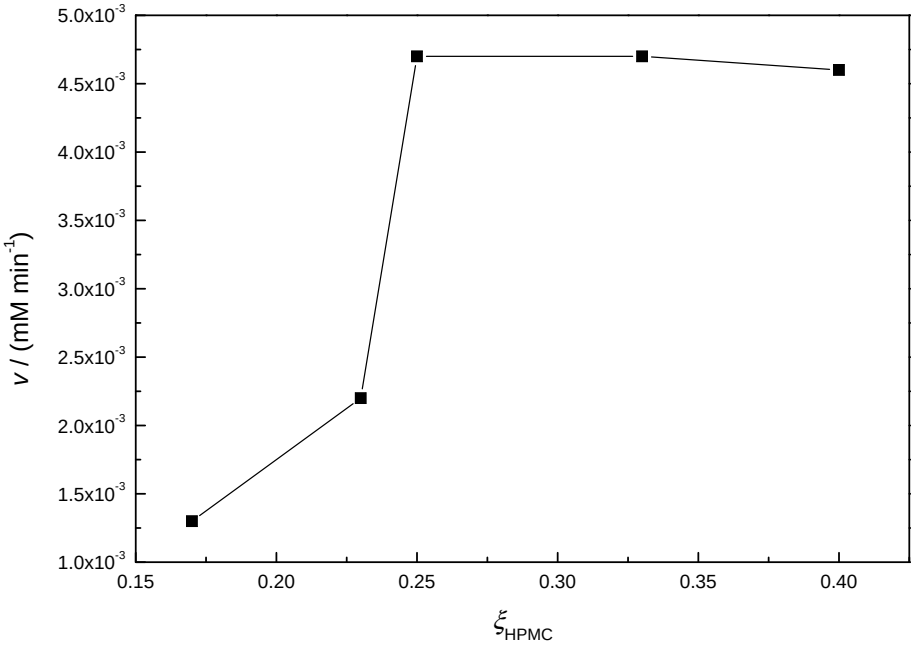

Figure 5.14: Influence of the HPMC mass fraction, ξ_{HPMC}, on the catalytic activity of MmL (146.880 U mg^{-1}; Lot & Filling Code: 16008/1 22003179) in phytantriol-based organogels containing 0.24 mg enzyme. Esterification of 100 mM lauric acid and 200 mM 1-propanol at 35 °C in isooctane.

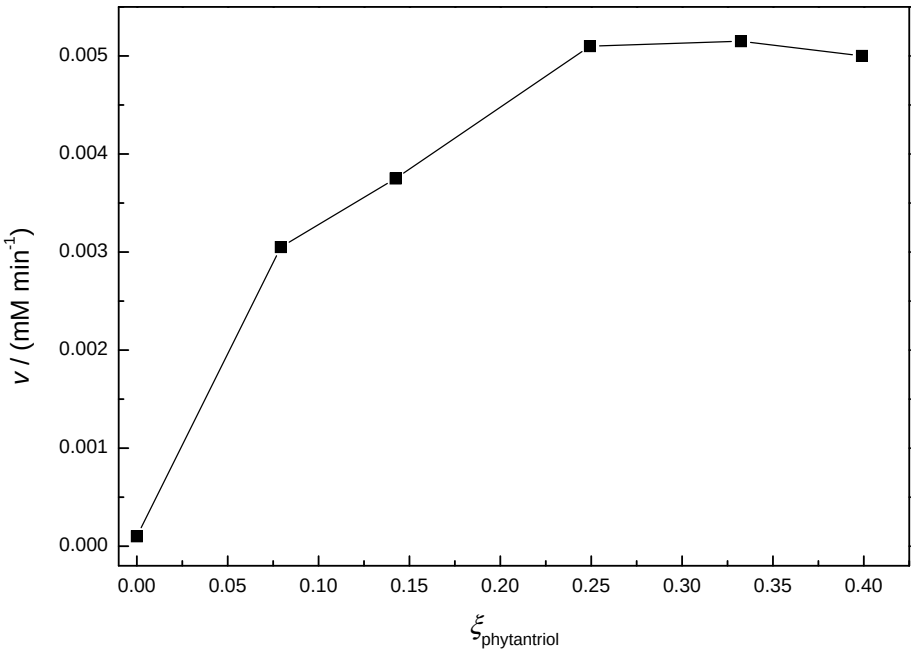

Figure 5.15: Influence of the phytantriol mass fraction, $\xi_{\mathrm{phytantriol}}$, on the catalytic activity of MmL (146.880 U mg^{-1}; Lot & Filling Code: 16008/1 22003179) in phytantriol-based organogels containing 0.24 mg enzyme. Esterification of 100 mM lauric acid and 200 mM 1-propanol at 35 °C in isooctane.

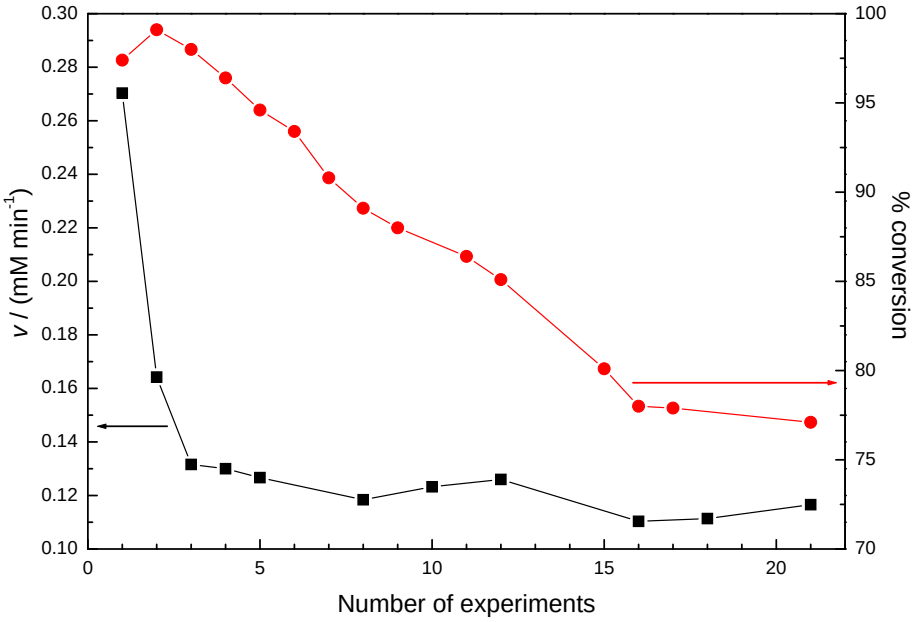

Figure 5.16: Initial rates and conversions after 24 h towards repeated synthesis of 1-propyl laurate catalysed by MmL immobilised in a phytantriol-based HPMC organogel containing 0.22 mg enzyme. Esterification of 100 mM lauric acid and 200 mM 1-propanol at 35 °C in isooctane.

section 5.1.2.2.2), reuse experiments in $scCO_2$ were not carried out, particularly as the same loss of gel could be observed with the phytantriol-based gels when depressurising.
The reaction profile for the esterification of 103 mM lauric acid and 207 mM 1-propanol catalysed by MmL entrapped in a phytantriol-based HPMC organogel containing 0.22 mg enzyme at 35 °C and 110 bar in $scCO_2$ as external solvent is given in Figure 5.17.

5.1.3.3 Discussion

5.1.3.3.1 Preliminary tests

MmL immobilised in phytantriol-based organogel is catalytically active in isooctane as external solvent. However, the gels are not inert in this medium, as phytantriol is extracted from the gel. It should be noted that the elution of phytantriol might result in a slight loss of enzyme despite the fact that the gels exhibit catalytic activity in subsequent reactions.
In the present study, no efforts were attempted to optimise both gel composition and preparation with regard to the observed phytantriol extraction. Further work is, thus, required in order to determine whether a variation of these two parameters allows the minimisation of the phytantriol loss.

5.1.3.3.2 Effect of gel composition

As can be seen from Figures 5.14 and 5.15, the enzymatic activity of MmL entrapped in phytantriol-based organogels depends strongly on the composition of the gel.

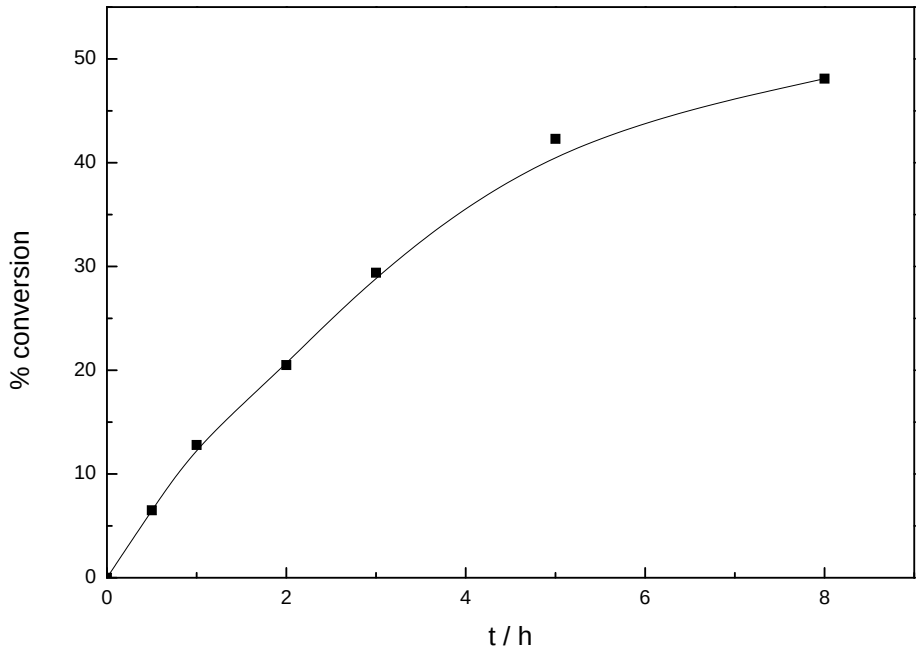

Figure 5.17: Reaction profile of the esterification of 103 mM lauric acid and 207 mM 1-propanol catalysed by MmL immobilised in a phytantriol-based HPMC organogel containing 0.22 mg enzyme at 35 °C and 110 bar in $scCO_2$.

Figure 5.14 indicates – at least partly – an increase in the reaction rate with increasing HPMC mass fraction. A similar behaviour has been observed for the HPMC-lecithin MBGs studied in this present work (cf. section 5.1.1.2.5) and has also been described for other MBGs in literature [152, 153].
The MmL in the hydrogel displays a significantly lower reaction rate in comparison to the organogels formulated with phytantriol indicating that the presence of phytantriol increases the catalytic activity of the enzyme. A possible explanation for this effect might be that the phytantriol/water system is capable of providing an oil/water interface for the interfacial activation (cf. section 2.3.3) of the lipase. This hypothesis is in agreement with phase behaviour studies on the phytantriol/water system by Barauskas and Landh [334]. For high phytantriol concentrations the authors observed a reversed micellar structure providing a large interfacial area. However, it should be noted that – at the present stage – there is no evidence whether this particular structure is present or preserved in the gels.

5.1.3.3.3 Biocatalyst reuse

As can be seen from Figure 5.16, the initial rate displays a decrease by more than 60 % after the first two runs. This initial decline in the MmL activity can be ascribed to the observed significant loss of phytantriol due to its elution from the gel. As already shown by the measurements concerning the gel composition, the phytantriol concentration on the gel strongly affects the enzymatic activity of the lipase. In addition, the elution of phytantriol might be to some extent accompanied by the loss of enzyme.

After this drastic decline, the reaction velocity remains quite constant during the subsequent batch reactions. The initial rate observed after twenty conversions remains at an acceptable level for the duration of the experiment with the velocity being approx. 88 % of the value observed for the third run.
In contrast to the reaction rates, the final conversions after 24 h reaction time show only slight decrease by less than 25 % after 21 runs.
In summary, the activity of the MmL on the phytantriol-based organogel is quite well preserved as a comparison with literature shows:
Rees et al. [7] investigated the operational stability of *Chromobacterium viscosum* lipase immobilised in AOT-based gelatin MBGs towards the repeated synthesis of octyl decanoate in n-heptane at 25 °C. The authors reported a decrease of the initial rate by 25 % after 15 catalytic cycles over a 30-day period. However, individual batch reactions were run to only approx. 10 % final substrate conversion. In a subsequent study on the same MBG system, Jenta et al. [8] allowed the consecutive batch reactions to proceed to equilibrium. The authors observed an activity decrease by approx. 40 % with each run, although the final conversions remained at approx. 90 % throughout the whole series of 5 reuse experiments.
Zhou et al. [149] conducted a kinetic study on the catalytic behaviour of *Candida lypolytical* encapsulated in gelatin-containing AOT MBGs. They observed a decline in the final conversions by 10 % after allowing the MBGs to proceed for ten runs carried out over a 20-day period.
Fadnavis et al. [147] working with lipase from *Pseudomonas cepacia* encapsulated in crosslinked gelatin-AOT MBGs reported that their MBG system could be recycled 25 times with less than 10 % loss of activity after 25 runs.
Delimitsou et al. [153] investigated the activity of *M. miehei* lipase entrapped in HPMC MBGs based on microemulsions formulated with lecithin and AOT, respectively. They observed a decline in the reaction rate by approx. 15 % for the HPMC-lecithin MBGs and by approx. 25 % for the HPMC-AOT MBGs after six consecutive reaction cycles.

5.1.3.3.4 Reactions with supercritical carbon dioxide as external solvent

As can be seen from the reaction profile given in Figure 5.17, MmL entrapped in phytantriol-based organogels exhibits catalytic activity in $scCO_2$. Consequently, phytantriol-based organogels might be used as a solid-phase catalysts in $scCO_2$. However, it should be noted that biocatalyst reuse experiments in $scCO_2$ are required in order to assess their economic viability.

5.1.3.4 Conclusion

Initial tests concerning the ability of *M. miehei* immobilised in phytantriol-based organogels to catalyse esterification reactions in isooctane and $scCO_2$ were undertaken.
Despite the fact that an extraction of phytantriol from the gel occurred, reuse experiments with isooctane as external solvent showed that the operational stability in the phytantriol-based organogels is quite well preserved as compared to observed stabilities for MBG-encapsulated lipases. Moreover, it was found that both the phytantriol and the HPMC content of the gel strongly influence the catalytic activity of the entrapped *M. miehei* lipase.
The so far conducted experiments on this new type of organogel indicate that phytantriol-based gels might be an alternative to conventional MBGs as enzyme immobilisation matrix: although the gels are not stable as far as the loss of phytantriol in isooctane is concerned, they exhibit a

quite good operational stability. Furthermore, the chemicals used for the preparation of the gel are all environmentally compatible, and immobilised enzymes exhibit catalytic activity in $scCO_2$. Future research activities should include further reactions in $scCO_2$ with regard to operational stability and optimisation of both composition and gelation/preparation of the gels in order to minimise/avoid phytantriol loss. Moreover, the structure of the gels should be the subject of investigation in order to gain information concerning the enzyme surrounding.

5.2 Reactions in microemulsions

Recent studies [19, 20, 21] have demonstrated that microemulsions in liquid and supercritical carbon dioxide might be a suitable reaction medium for cell-free enzymatic biotransformations. In the present work, lipase from *C. antarctica* was tested for catalytic activity in microemulsions formed with three well-known CO_2-philic surfactants in $scCO_2$.

5.2.1 Experimental

5.2.1.1 Materials

For the experiments concerning enzyme-catalysed reactions in microemulsions in $scCO_2$, the following CO_2-philic (cf. section 2.2.5) surfactants were used: the nonionic Dehypon Ls-54, and the ionic amphiphiles di-HCF4 and ClPFPE-NH_4. The latter two were prepared as described in chapter 4, while (Dehypon) Ls-54 ($> 99.5\,\%$) was obtained from Cognis and used as received.
In addition, CaL, carbon dioxide, hydrochloric acid, isooctane, lauric acid, 1-propanol, Tris, and Millipore Milli-Q water were utilised. Details concerning their (chemical) properties and sources of supply can be found in section 5.1.1.1.1.

5.2.1.2 Lipase-catalysed reactions

Lipase-catalysed reactions in microemulsions in $scCO_2$ were carried out in the 32.1 mL high-pressure cell (cf. section 3.2.2). Injections of substrate were performed as described in section 5.1.1.1.3 for the enzymatic reactions with MBGs as immobilisation matrix. An outline of the apparatus can be found in Figure 3.1.
Appropriate amounts of surfactant, Tris/HCl pH 7.5 buffer (cf. section 5.1.1.1.2) containing CaL and lauric acid were loaded into the high-pressure cell, which was then sealed. The cell temperature was adjusted to about 1 K below the final reaction temperature of 35 °C since pressurising leads to a temperature increase in the high-pressure cell. After increasing the pressure by feeding the cell with CO_2, the reactions were started by injecting appropriate amounts of 1-propanol. The solutions were stirred during reaction by means of a magnetic stirrer. Analysis of the reactions was done by GC after venting and sample recovery. Details concerning GC conditions can be found in appendix B.

5.2.2 Results

The present study intended to test CaL with regard to its ability to catalyse esterification reactions in microemulsions in $scCO_2$. For this purpose, the condensation between lauric acid and 1-propanol was chosen as model reaction. As surfactants for the formation of the microemulsions

Table 5.6: Survey of the performed tests on the enzyme activity of CaL in microemulsions formulated with CO_2-philic surfactants in $scCO_2$ (35 °C). % conversion of the esterification between lauric acid and 207 mM 1-propanol. Surf.= Surfactant. [lauric acid] = 51 mM unless otherwise stated.

Surfactant	[Surf.]/mM	W_0	m_{Lipase}/mg	p/bar	t/h	% conversion
ClPFPE-NH_4	9.0	10	3.0	120	5	87.9
di-HCF4 [a]	48	11	9.0	250	8	< 1 %
Ls-54	20	10	6.0	250	3	39.3
	20 [a]	10	6.0	250	6	50.1
– [b]	–	–	3.0	250	5	72.1

[a] 103 mM lauric acid, reaction started by the injection of appropriate amounts of lauric acid and 1-propanol solubilised in small amounts of isooctane. [b] reaction in absence of surfactant(s). 3.0 mg CaL in 50 µL Tris/HCl pH 7.5 buffer added to the cell prior to sealing.

in $scCO_2$ the well-known CO_2-philic surfactants (cf. section 2.2.5) Ls-54, di-HCF4, and ClPFPE-NH_4 were applied. Table 5.6 gives a survey of the observed conversions in the systems studied. The compositions for the microemulsion systems compiled in Table 5.6 were chosen according to phase behaviour and conductivity studies on the respective surfactants [201, 235, 236, 247]. Transparent solutions were obtained for surfactants after pressurising and injection. In the case of ClPFPE-NH_4, the resulting microemulsion exhibited opalescence (cf. section 2.2.1), i.e. that the system showed a blue color when observed perpendicularly to the incident light.
However, in all microemulsion systems a slightly brownish precipitate could be observed at the walls of the high-pressure cell. In order to identify the precipitate, control experiments in absence of different microemulsion components were performed revealing that the precipitate was (wet) lipase. This finding is in agreement with the fact that lyophilised CaL as obtained from Fluka is slightly brown. Moreover, the least amount of precipitated enzyme was observed for the ClPFPE-NH_4 microemulsion, the system with the least lipase content.
In addition, the control experiments showed that precipitation of the lipase likewise occurs in the absence of surfactants and that the precipitated enzyme is active in $scCO_2$, as can be seen in Table 5.6.

5.2.3 Discussion

The results compiled in Table 5.6 indicate that the observed esterification of lauric acid with 1-propanol in microemulsion systems based on ClPFPE-NH_4 and Ls-54, respectively, in $scCO_2$ can be attributed to the catalytic activity of solid (precipitated) enzyme. However, it should be noted that there might still be some catalytically active lipase dissolved in the microemulsion.
In the case of the di-HCF4-based microemulsion, it seems, moreover, that the fluorinated surfactant inhibits the catalytic activity of the used CaL. A similar observation has been reported by Bittner [64]. The author studied the compatibility of miscellaneous lipases with the fluorosurfactant PFPE-NH_4 and found that most enzymes were inhibited by the surfactant.
A possible explanation for the precipitation of the lipase in all microemulsion systems studied

might be that the high amount of enzyme used could not be sufficiently solubilised/stabilised within the aqueous droplets of the microemulsions. Kane et al. [21] investigating the catalytic ability of cholesterol oxidase in PFPE-based microemulsions in $scCO_2$ used approx. 1.5 µg of enzyme in total volume of 3.5 mL. Similarly, Holmes et al. [19] worked with a total enzyme amount of approx. 6.5 µg in their study of a lipase-catalysed hydrolysis in a di-HCF4-based microemulsion in liquid carbon dioxide.
However, the use of less enzyme seems problematic with the high-pressure apparatus at the present stage: a possible precipitation of the lipase might be overseen due to the limited possibilities for observing the cell contents. Moreover, since the results obtained so far indicate that the lipase is also active in the absence of surfactant, it would not be possible to differentiate between a reaction catalysed by lipase encapsulated in the microemulsion droplets and a reaction catalysed by the free precipitated enzyme. Consequently, no further experiments concerning the catalytic activity of CaL in microemulsions in $scCO_2$ were performed.
In order to allow a clear differentiation in this case, it would be necessary to prove that the lipase is present in the microemulsion droplets while the reaction proceeds. A possible method for this purpose could be fluorescence spectroscopy with fluorescence-labelled enzymes.

5.2.4 Conclusion

C. antarctica lipase was tested for catalytic activity in microemulsion systems based on ionic (PFPE-NH_4 and di-HCF4) and nonionic (Ls-54) surfactants in $scCO_2$. The performed experiments showed that the used lipase could not be sufficiently solubilised within the internal phase of the microemulsions resulting in the precipitation of the enzyme. Accordingly, the observed enzymatic activity was attributed to the precipitated solid lipase. Evidence for enzymatic catalysis by lipase entrapped in the microemulsion was not found.
Due to its catalytic activity, the free (solid) lipase might serve as a reference system for further investigations on enzymatic reactions with organogels as immobilisation matrix in $scCO_2$.

6 Solubility studies

In addition to enzymatic reactions in $scCO_2$, solubility studies on surfactants and related molecules were performed in $scCO_2$ in order to find new surfactants for the stabilisation of w/c microemulsions. Since toxicological results are indicative of a potential toxic effect of CO_2-philic fluorinated surfactants such as PFPE [213], only non-fluorinated substances were taken into consideration.

6.1 Experimental

6.1.1 Materials

Dowanol DPM (bis(isopropylene glycol) methyl ether, mixture of isomers, 99 %) and Dowanol DPnB (bis(isopropylene glycol) butyl ether, mixture of isomers, $\geq$ 98.5 %) were obtained from Aldrich, and Triton X-45 from Fluka.
Octyltributylammonium bromide (C8C4) and $DPnBPrSO_3Na$, an ionic derivative of Dowanol DPnB, were synthesised as described in chapter 4.
Ralufon F 5-13 (approx. 80 % active substance) was provided by Raschig (Ludwigshafen, Germany). Akypo LF1 ($\geq$ 89 % active substance, max. 10 % water) was obtained from Kao Chemicals (Emmerich, Germany), while Emulsogen CIO 050 (containing 10.6 % water) was provided by Clariant.
In addition, carbon dioxide, 1-pentanol, and water were used for the solubility studies. Details concerning their (chemical) properties and sources of supply can be found in section 5.1.1.1.1.

6.1.2 Solubility experiments in carbon dioxide

Solubility experiments concerning surfactants and related molecules were carried out in the 32.1 mL high-pressure cell unless otherwise stated. Cell contents were mixed by means of a magnetic stirrer. The injection system was disconnected from the high-pressure apparatus.
The substance to be tested for its solubility in carbon dioxide and optionally water and/or co-surfactant were loaded into the cell which was then sealed. Due to the fact that pressurising results in a temperature increase, the cell temperature was adjusted to approx. 0.8 K below the measurement temperature of 35 °C. Starting from an initial pressure of 100 bar, the pressure in the cell was then raised in steps of 50 bar up to a maximum of 450 bar. Subsequently, the temperature in the cell was lowered to 25 °C at a constant pressure of 450 bar. Observations regarding solubility were usually made 15-30 min after each change in pressure or temperature.

6.2 Results

A survey of the qualitative experiments concerning the solubility of surfactants and related molecules in $scCO_2$ can be found in Table 6.1. Figure 6.1 shows the constitutional formulas of

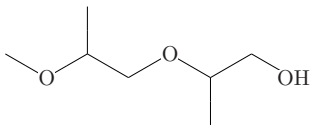

Dowanol DPM

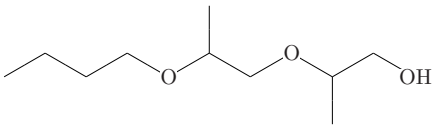

Dowanol DPnB

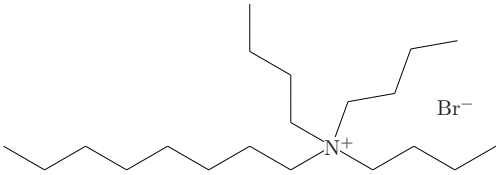

C8C4

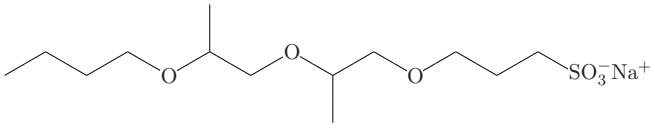

DPNBPrSO$_3$Na

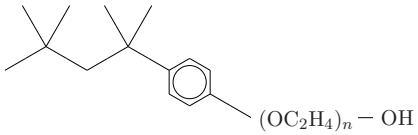

Triton X-45

$$C_{13}H_{27} — (OC_2H_4)_5 — O — CH_2 — CH_2 — CH_2 — SO_3^- \ Na^+$$

Ralufon F 5-13

$$C_8H_{17} - (OC_2H_4)_6 — O — CH_2 — COOH$$

Akypo LF1

$$C_nH_{2n+1} — (OC_2H_4)_5 — O — CH_2 — COOH$$

Emulsogen CIO 050

Figure 6.1: Constitutional formulas of the substances used for the solubility studies on surfactants and related molecules. Dowanol DPM, Dowanol DPnB, and DPnBPrSO$_3$Na: mixture of isomers. Triton X-45: $n =\sim 5$. Emulsogen CIO 050: $n = 6{,}8$.

Table 6.1: Survey of the qualitative solubility studies on surfactants and related molecules in $scCO_2$

Substance	$m_{Substance}$/g	Cosurfactant	$m_{Cosurfactant}$/g	m_{H_2O}/g	Molar ratio [a]	Observations
Dowanol DPM [b]	19.5	–	–	–	– : – : –	transparent single phase
Dowanol DPnB [c]	18.3	–	–	–	– : – : –	transp. single phase ($\geq$ 150 bar)
C8C4	0.30	–	–	–	– : – : –	biphasic, droplets
C8C4	0.30	–	–	0.14	1 : – : 10	biphasic, droplets
C8C4	0.30	1-pentanol	1.40	–	1 : 20 : –	biphasic, droplets
C8C4	0.30	1-pentanol	1.40	0.14	1 : 20 : 10	biphasic, droplets
$DPnBPrSO_3Na$	0.30	–	–	–	– : – : –	white solid (flakes)
$DPnBPrSO_3Na$	0.30	–	–	0.16	1 : – : 10	white solid, foam after venting
$DPnBPrSO_3Na$	0.30	1-pentanol	1.58	–	1 : 20 : -	white solid
$DPnBPrSO_3Na$	0.30	1-pentanol	1.58	0.16	1 : 20 : 10	turbid, droplets
$DPnBPrSO_3Na$	0.30	DPnB	0.68	–	1 : 4 : –	white solid
$DPnBPrSO_3Na$	0.30	DPnB	3.42	–	1 : 20 : –	white solid
$DPnBPrSO_3Na$	0.30	DPnB	0.68	0.16	1 : 4 : 10	white solid, foam after venting
$DPnBPrSO_3Na$	0.15	DPnB	0.34	0.08	1 : 4 : 10	white solid, foam after venting
Ralufon F 5-13 [d]	2.06	–	–	0.80	– : – : –	biphasic, droplets
Akypo LF1 [e]	2.10	–	–	–	– : – : –	biphasic, droplets
Akypo LF1 [f]	2.10	–	–	0.80	– : – : –	turbid, droplets
Emulsogen CIO 050 [g]	2.10	–	–	–	– : – : –	biphasic, droplets
Triton X-45 [h]	2.41	–	–	1.70	1 : – : 18	biphasic, droplets

[a] Molar ratio: substance : cosolvent : water. [b] 100 mL high-pressure cell. Only 35 °C. [c] 100 mL high-pressure cell. 50 °C. [d] 100 mL high-pressure cell. Only 35 °C. Molar ratio not calculated since technical product contains significant amounts of water and ethoxylated fatty alcohols as by-products. [e] 100 mL high-pressure cell. [f] 100 mL high-pressure cell. 50 °C. Molar ratio not calculated since technical product contains significant amounts of water. [g] 100 mL high-pressure cell. [h] 100 mL high-pressure cell. 50 °C.

the substances under investigation.
The isobaric lowering of the temperature from 35 °C to 25 °C was done assuming that an increase in the density of the carbon dioxide phase might result in a increased solubility of the investigated substance (cf. section 2.1.2 and [37, 38]).

6.3 Discussion

As can be seen from Table 6.1, most of the tested surfactants and related molecules are not soluble in carbon dioxide under the specific conditions chosen.
Only Dowanol DPM and Dowanol DPnB allowed the formation of clear transparent single phase solutions indicating their highly CO_2-philic structure. Dowanols being ethers of alcohols with bis(isopropylene glycol) are known as solvo-surfactants or hydrotropic detergents, i.e. that they combine properties of solvents with those of surfactants [338, 339]. They can, thus, be applied as solvents, cosolvents, cosurfactants, or real surfactants depending on temperature or/and on their molecular composition [338]. Due to their solvo-surfactant characteristics and their CO_2-philic structure, they might be used as cosolvents or cosurfactants with liquid or supercritical carbon dioxide in order to enhance the solubilities of less CO_2-philic or CO_2-phobic substances and to promote the ability of hydrocarbon surfactants to form w/c microemulsions (cf. section 2.1.4.2 and Table 2.2). Accordingly, Dowanol DPnB was used as cosurfactant for the present solubility studies apart from 1-propanol.
Due to the CO_2-philic behaviour of Dowanol DPM and DPnB, respectively, $DPnBPrSO_3Na$ was synthesised (cf. section 4.3) as an ionic derivative of Dowanol DPnB. The solubility experiments showed that $DPnBPrSO_3Na$ in absence/presence of 1-propanol and Dowanol DPnB, respectively, is insoluble in $scCO_2$ and does not allow the dispersion of water within reverse micelles in supercritical and liquid carbon dioxide. Ralufon F 5-13 having a similar structure does, likewise, not seem to form reverse microemulsions in $scCO_2$. It should be noted that so far no single-tail ionic surfactants, apart from perfluoropolyether or other fluorinated [340] amphiphiles, have been reported to stabilise w/c microemulsions.
Octyltributylammonium bromide (C8C4) was chosen for the solubility tests due to weak tail-tail interactions as indicated by the low melting point of approx. 35 °C. The results indicate that C8C4 is insoluble in $scCO_2$ and may not be used as a hydrocarbon surfactant for the stabilisation of w/c (micro-)emulsions. The addition of cosurfactant does obviously not influence its solubility in $scCO_2$.
Moreover, Triton X-45 seems to be incapable of forming a w/c microemulsion. This finding is in agreement with a recent study by Eastoe et al. [341]. Although Triton-type surfactants with similar structure were reported to be soluble in liquid and supercritical carbon dioxide, the authors stated that all tested amphiphiles were not capable of dispersing significant amounts of water in hydrated reverse micelles or microemulsion droplets.
The polyethyleneglycol n-alkyl ether carboxylic acids, Akypo LF1 and Emulsogen CIO 050, were found to be insoluble in $scCO_2$. Structurally similar straight-chain nonionic polyethylene glycol n-alkyl ethers such as C8E5 [86] and C12E3 [221] were reported to form aggregates in carbon dioxide. However, no significant water uptake was observed and the formation of micelles often required the addition of a cosolvent or cosurfactant. It might, thus, be that the addition of cosurfactants such as 1-propanol increases the solubility of the tested carboxylic acids.
In the present study, the substances for the solubility tests were predominantly chosen for the

sole reason that they have CO_2-philic groups in their constitutional structure. Recent data from empirical structure-activity relationship studies have, however, allowed the establishment of predictive concepts and parameters which might permit a systematic search for/design of new CO_2-philic surfactants for their potential application in $scCO_2$.
Recently, Johnston and coworkers [342] proposed an index for surface activity at a water-CO_2 interface based on the fractional free volume (FFV) available to carbon dioxide in the tail region. It was suggested that the free fraction volume can be calculated as follows:

$$\mathrm{FFV} = 1 - \frac{V_\mathrm{t}}{tA_\mathrm{h}} \tag{6.1}$$

where V_t is the van der Waals volume of the surfactant tail, A_h is the interfacial area per headgroup/surfactant molecule, and t is the thickness of the interface. For a given surfactant, the FFV factor can be estimated from literature values [22].
Johnston et al. [342] proposed that amphiphiles with a low FFV should represent the most CO_2-philic surfactants and should, thus, promote the formation of w/c microemulsions. A comparison of phase transition pressures reported in literature and calculated FFV values for thirteen different surfactants revealed a clear correlation between low FFV and low phase transition pressures as indicator for high surfactant activity at the water-CO_2 interface.
Moreover, Dupont et al. [186] concluded in a recent study that the free fractional volume (FFV) might be a useful parameter for finding/designing new CO_2-philic surfactants. The authors reported that their findings concerning phase behaviour of different hydrocarbon-fluorocarbon surfactants were in agreement with calculated FFV for the respective surfactants.
Another recently established parameter is the so-called hydrophilic-CO_2-philic balance (HCB) [181], an analogue to the hydrophilic-lipophilic balance in conventional oil/water systems. The HCB is given by [184, 343]

$$\frac{1}{\mathrm{HCB}} = \frac{E_\mathrm{TC} - E_\mathrm{TT} - E_\mathrm{CC}}{E_\mathrm{HW} - E_\mathrm{HH} - E_\mathrm{WW}} \tag{6.2}$$

where E_{ij} (positive quantity) represents the various interaction energies between carbon dioxide (C), surfactant tails (T), surfactant headgroups (H), and water (W).
Low HCB values result in the formation of w/c microemulsions or (macro-)emulsions [184]. As can be seen from Equation (6.2), this condition is favoured by increasing the tail-CO_2 interactions (high E_TC) while lowering the tail-tail interactions (low E_TT) [184].
A recent computer simulation study by Stone et al. [344] indicated that energetic interactions between fluorinated tails and carbon dioxide are comparable to those between hydrocarbon tails and carbon dioxide. However, it was found that the tail-tail interactions, E_TT, are much stronger for hydrocarbon tails than for fluorocarbon ones.
Consequently, the observed capability of branched, "stubby" nonionic surfactants to stabilise w/c microemulsions [343] and the solubility of branched AOT derivates in $scCO_2$ [239] can be – at least partly – attributed to reduced tail-tail interactions of branched surfactants due to limited tail overlays [184].
Da Rocha and Johnston [345] measured the interfacial tension at the water-CO_2 interface with a dissolved PFPE surfactant. They were able to show that the interfacial tension has to be lowered to a typical value for microemulsions of approx. $1\,\mathrm{mN\,m^{-1}}$ in order to obtain a w/c microemulsion stabilised by the PFPE amphiphile. Recently, Dupont et al. [186] suggested

that the water-poly(dimethylsiloxane) interface might be used as a model system for interfacial tension measurements in order to avoid such measurements for the water-CO_2 interface when screening for new CO_2-philic surfactants.
Moreover, studies on fluorinated AOT-like surfactants [75, 187, 188, 220, 232, 233, 234, 238] indicated that both surface tension and Krafft point measurements in aqueous solutions might be further parameter to predict the ability of surfactants to form/stabilise microemulsions in $scCO_2$.

6.4 Conclusion

Surfactants and related molecules were tested for their solubility in $scCO_2$ in order to identify new surfactants for the formation of w/c microemulsions.
Dowanol DPM and Dowanol DPnB were shown to be highly soluble in $scCO_2$. Because of their solvo-surfactant properties, they might be used as cosolvents and cosurfactants, respectively, for further investigations concerning the capability of surfactants to form reverse microemulsions in $scCO_2$.
Apart from the above mentioned Dowanols, the tested surfactants, C8C4, DPnBPrSO_3Na, Akypo LF1, Ralufon F 5-13, and Emulsogen CIO 050, were not found to be soluble in $scCO_2$ or to stabilise w/c microemulsions. It should, however, be noted that the surfactants might be soluble under different conditions or with other/additional cosurfactant(s).
Recent advances concerning a parametric and predictive description of the ability of surfactants to form microemulsions in $scCO_2$ might allow a systematic screening of new (hydrocarbon) surfactants or the specific synthesis of such amphiphiles.

7 Summary

In the present thesis, the catalytic ability of lipases encapsulated in microemulsion-based organogels with $scCO_2$ as external solvent was the subject of investigation.
Lipases from *C. antarctica* and *M. miehei* were encapsulated in AOT as well as in lecithin water-in-oil (w/o) microemulsion-based organogels (MBGs). These gels were formulated with either hydroxypropylmethyl cellulose (HPMC) or gelatin. The esterification of lauric acid and 1-propanol catalysed by these MBGs was examined in supercritical carbon dioxide ($scCO_2$; 35 °C, 110 bar) as solvent for the substrates.
Preliminary tests showed that both enzymes were catalytically active in MBGs based on either HPMC or gelatin and in microemulsions containing either AOT or lecithin. Furthermore, it was found that these gels are capable of catalysing transesterification reactions.
Starting from the initial tests as described above, the focus was set on HPMC-based MBGs containing *C. antarctica* lipase immobilised in a lecithin microemulsion for further investigations. Apart from kinetic measurements various parameters like pressure, alcohol and acid chain length, and gel composition were investigated with regard to the reference solvent isooctane.
Kinetic studies showed that the ester synthesis catalysed by the immobilised *C. antarctica* lipase occurs via a Ping Pong Bi Bi mechanism in which only inhibition by excess of alcohol was identified. Values of all kinetic parameters were determined. In addition, the effect of pressure on the initial reaction rate in $scCO_2$ exhibited a similar behaviour as described in literature for free or conventional immobilised enzymes and for reactant concentrations below saturation. The influence of the alcohol and acid chain length on the initial rate revealed significant differences between $scCO_2$ and isooctane, which can be attributed to a diverse partitioning of the reactants in the two solvents.
The effect of gel composition on the enzymatic reaction was found to be similar in both solvents and displayed an increase of the reaction rate with increasing biopolymer fraction and, thus, decreasing water content of the gel matrix. In order to get further insight to changes within the gel matrix, differential scanning calorimetry (DSC) measurements on freezing and melting of water in the gel matrix were performed. They displayed changes in the water types present at different water contents, which can be correlated to changes in the initial reaction rate.
As the operational stability of an immobilised enzyme, i.e. the ability to reuse, is an important parameter determining the economic viability of a biocatalytic process, initial reuse experiments were conducted with the HPMC-lecithin gels containing *C. antarctica* lipase. They showed that the slight decrease of activity in carbon dioxide is similar to that observed in isooctane.
In addition, the catalytic activity of HPMC MBGs containing *C. antarctica* lipase immobilised in so-called detergentless microemulsions comprised of n-hexane, 1-propanol, and buffer solution was investigated in $scCO_2$. It could be shown that this type of MBG is likewise active in $scCO_2$. Biocatalyst reuse experiments indicate that detergentless MBGs exhibit a better operational and storage stability than organogels formulated with classical microemulsions.
Phytantriol-based organogels as a new type of immobilisation matrix were tested for their potential application as solid-phase catalysts with both isooctane and $scCO_2$ as external solvents.

It was shown that *M. miehei* lipase immobilised in such organogels is capable of catalysing the esterification of 1-propanol and lauric acid in both solvents. Typical reaction profiles could be observed. However, the preliminary tests in isooctane revealed that within 24 h approx. 75 % of the phytantriol used for the preparation of the gel is dissolved in the external solvent.
The effect of the gel composition on the catalytic activity was investigated in two different series of experiments. The variation of the phytantriol content of the gels showed that the reaction rate increases with increasing phytantriol mass fractions at low phytantriol concentrations. A comparison of the observed initial rates with those obtained for hydrogels indicated, moreover, that the phytantriol/water system is capable of providing an oil/water interface for the interfacial activation of the lipase. As far as the HPMC-mass fraction is concerned, the effects were similar to those observed for the organogels with conventional microemulsions.
In order to determine the operational stability of the *M. miehei* lipase immobilised in phytantriol-based organogels, reuse experiments were conducted in isooctane. They showed that the catalytic activity is quite well preserved despite the fact that the already mentioned loss of phytantriol occurs.
Moreover, *C. antarctica* lipase was tested for catalytic activity in microemulsion systems based on ionic (PFPE-NH_4 and di-HCF4) and nonionic (Ls-54) surfactants in $scCO_2$. However, no evidence for enzymatic catalysis by lipase solubilised in the microemulsions was found.
Furthermore, qualitative solubility studies on surfactants and related molecules were performed in $scCO_2$ in order to identify new surfactants for the formation of w/c microemulsions. While Dowanol DPM and Dowanol DPnB exhibited high solubility in $scCO_2$, the tested surfactants, C8C4, $DPnBPrSO_3Na$, Akypo LF1, Ralufon F 5-13, and Emulsogen CIO 050, were not found to be soluble in $scCO_2$ or to stabilise w/c microemulsions.

A Engineering drawings

The Figures A.1 and A.2 show scans of the engineering drawings of the 100 mL high-pressure cell (cf. section 3.2.1). The drawings were provided by: Bio-Ingenieurtechnik GmbH (Engelsdorf, Germany).
All other drawings in this section were prepared by means of the computer programme AutoCAD [346]:
Detailed engineering drawings of the 32 mL high-pressure cell can be found in the Figures A.3 (top view), A.4 (horizontal section), A.5 (vertical section HS1), A.6 (vertical section HS2), A.7 (vertical section HS3) and A.8 (detail drawings E1 and E2). The Figures A.9 (top view) and A.10 (vertical sections DS1, DS2, and DS3) show drawings of the lid of the 32 mL high-pressure cell.
The Figures A.11, A.12, A.13, and A.14 show drawings of various gland nuts for the different screwed ports of the high-pressure cells.
Plans of the high-pressure electrodes (cf. section 3.8.2) for conductivity studies can be found Figures A.15 and A.16.

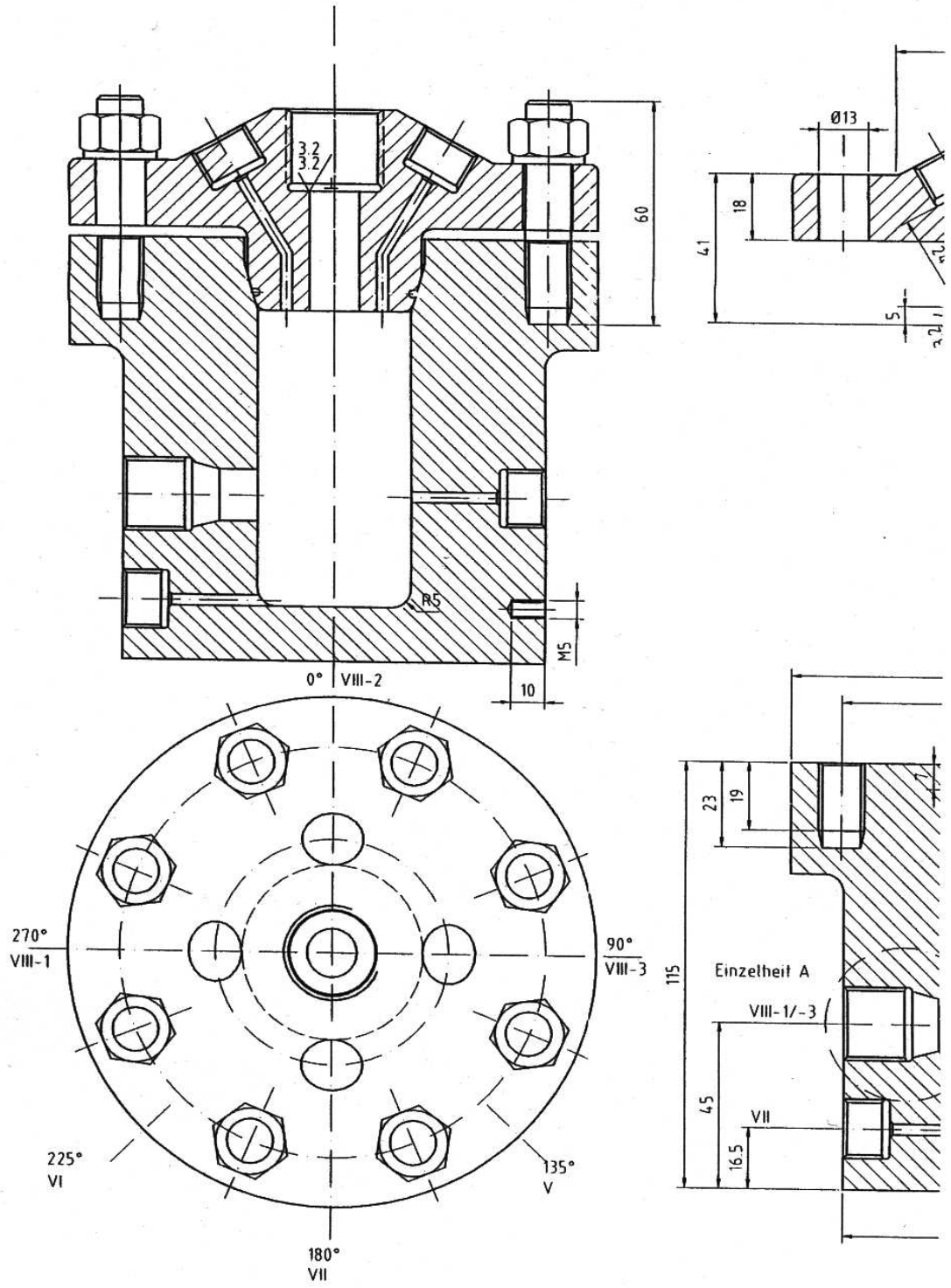

Figure A.1: Drawings of the 100 mL stainless steel high-pressure cell – part 1.

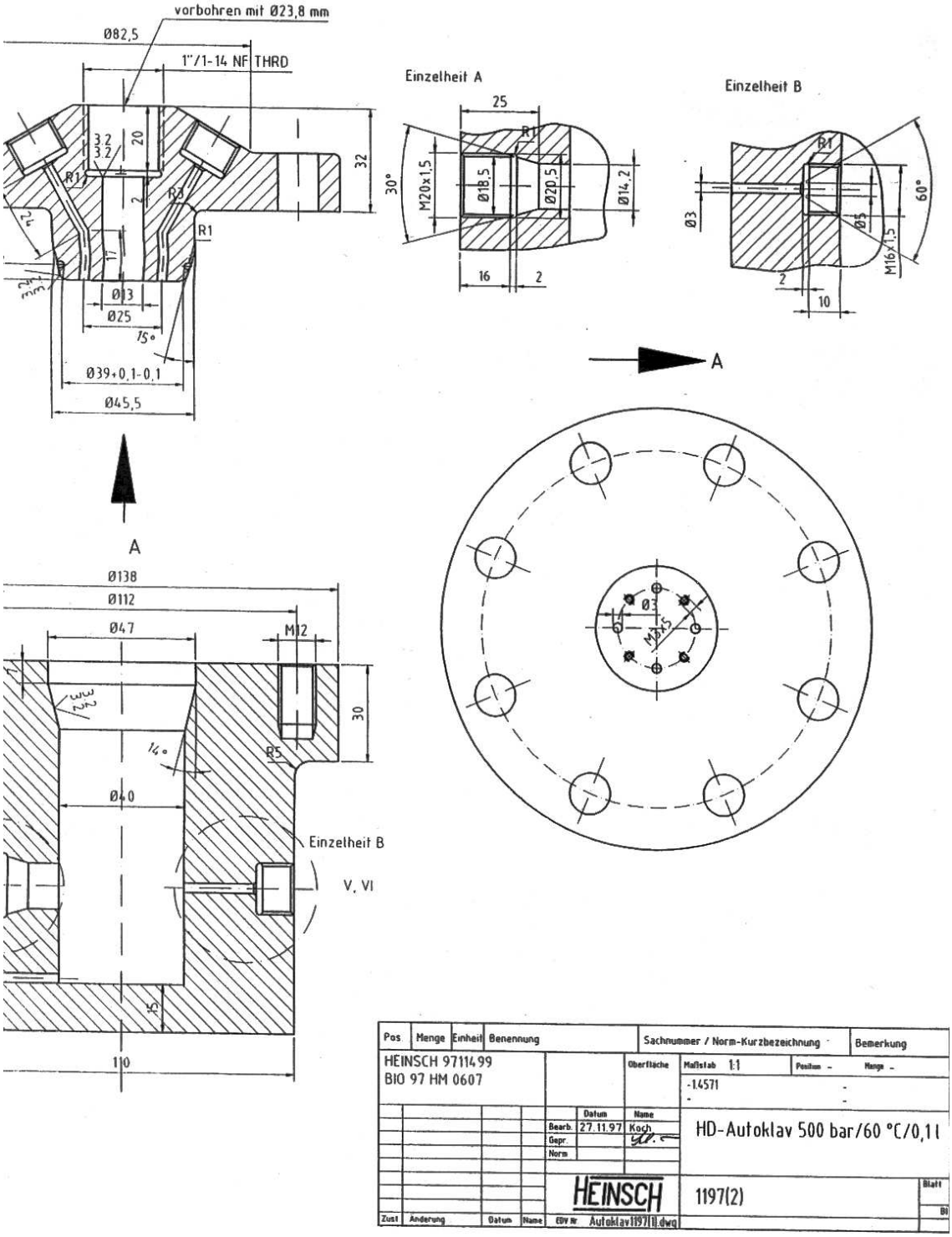

Figure A.2: Drawings of the 100 mL stainless steel high-pressure cell – part 2.

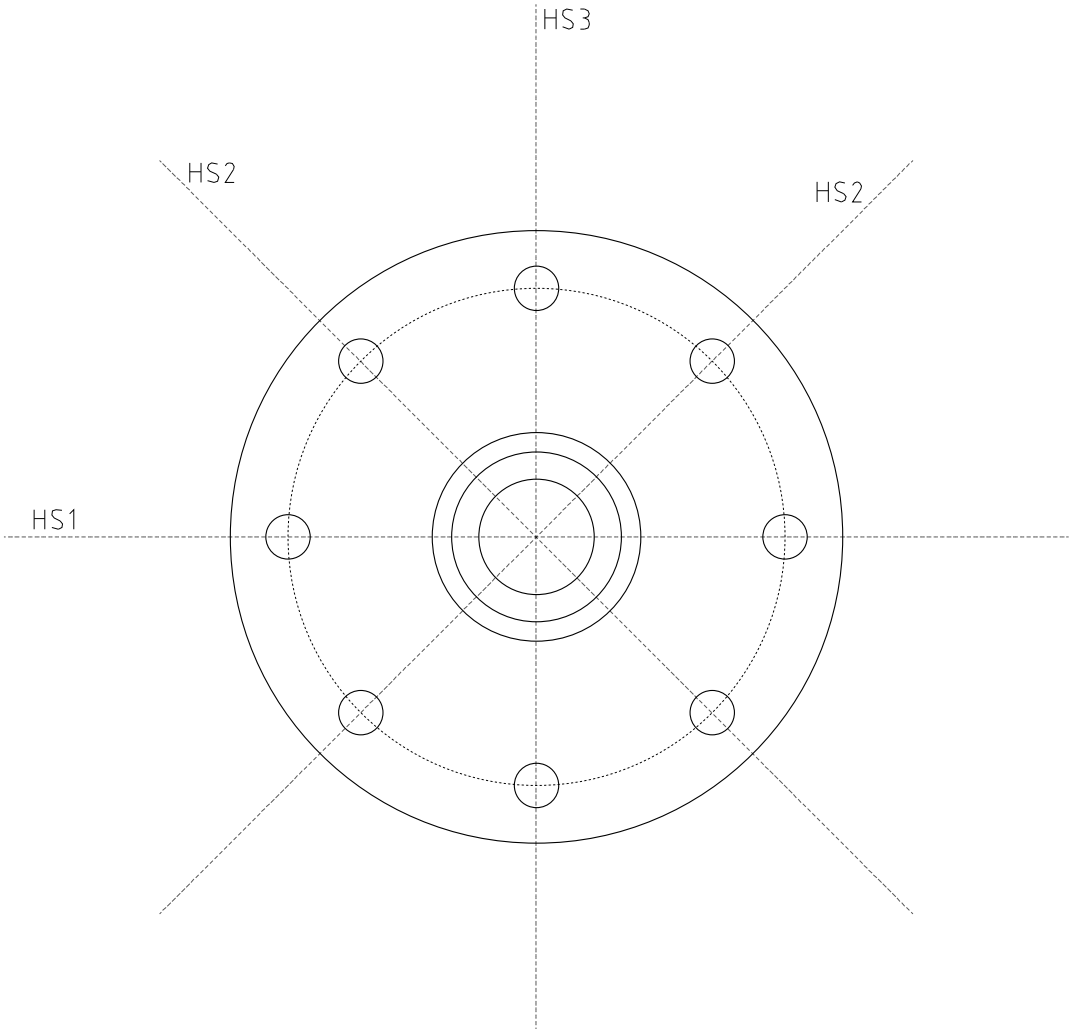

Figure A.3: Top view on the 32.1 mL stainless steel high-pressure cell.

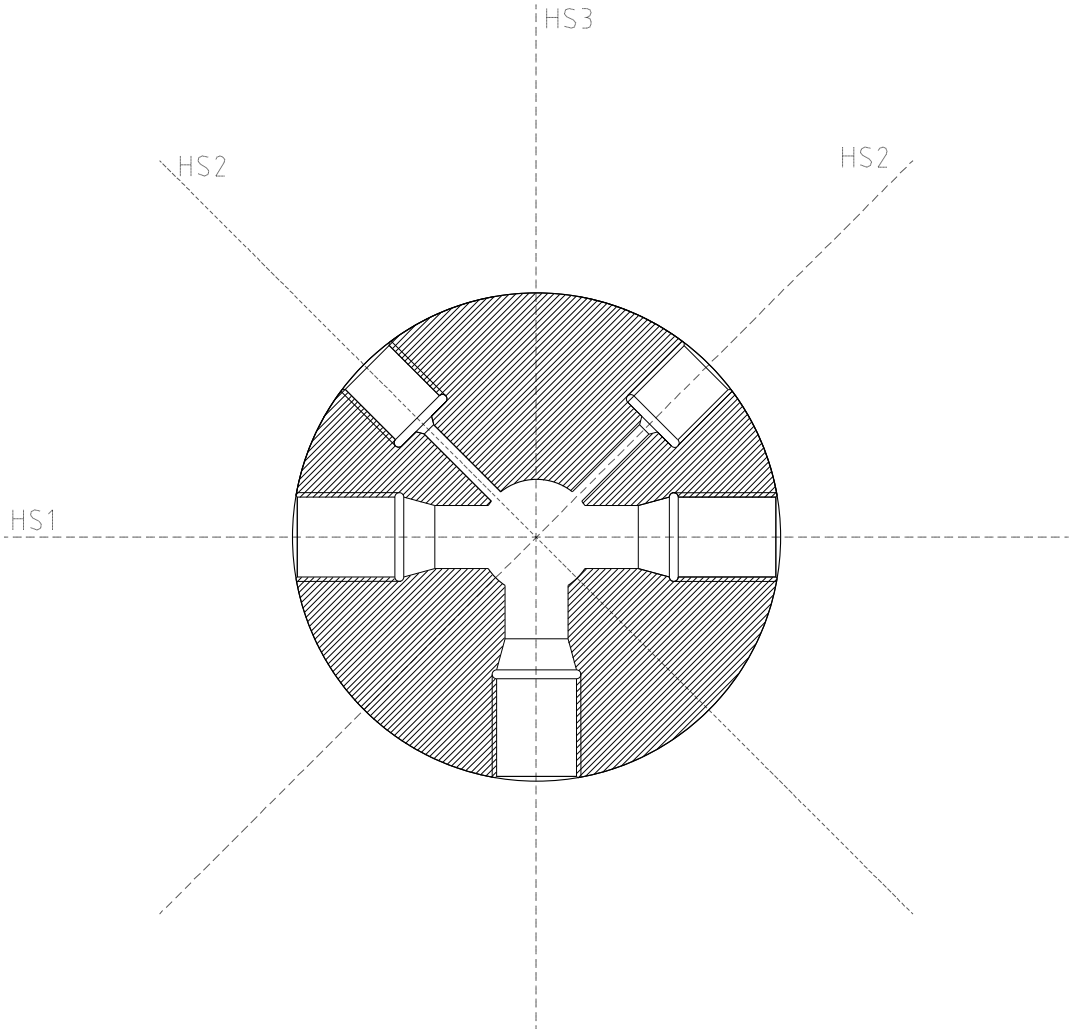

Figure A.4: Horizontal section (29 mm above the bottom) through the 32.1 mL stainless steel high-pressure cell.

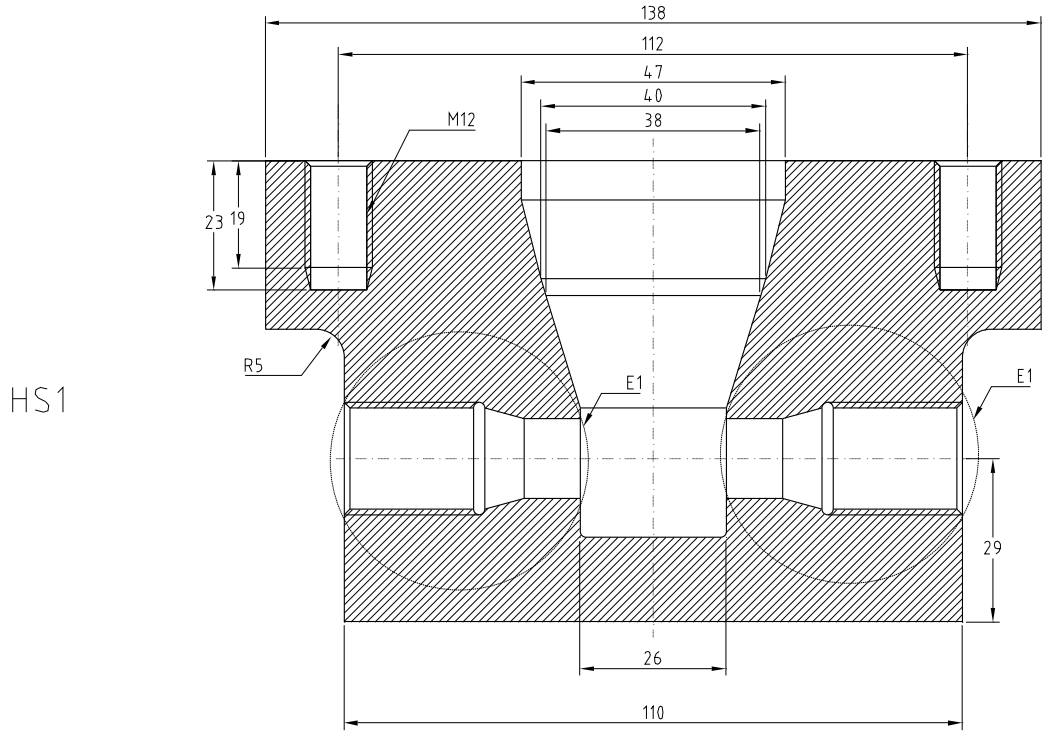

Figure A.5: Sectional drawing HS1 of the 32.1 mL stainless steel high-pressure cell.

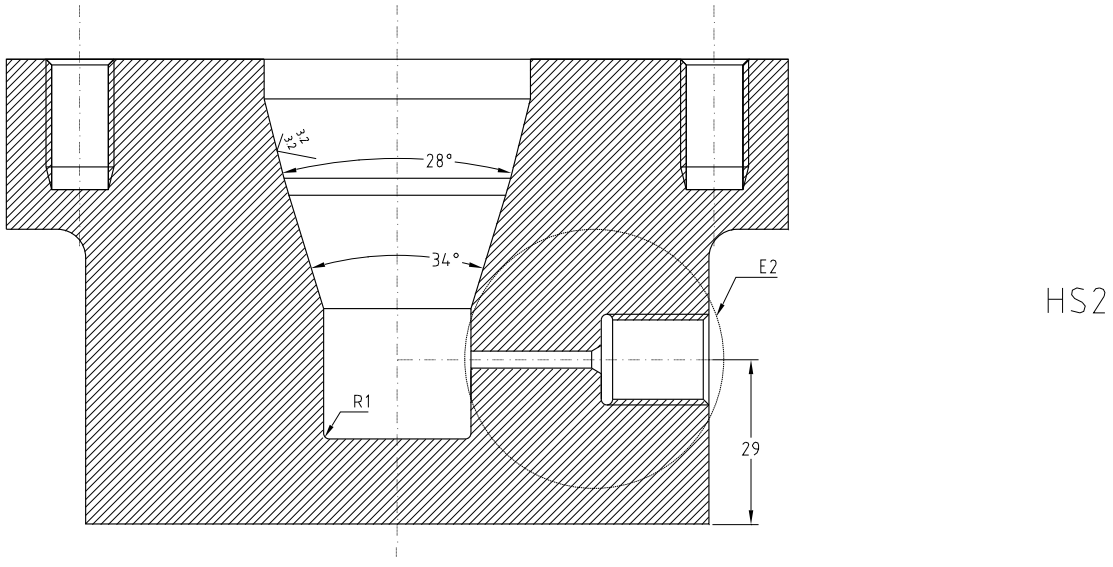

Figure A.6: Sectional drawing HS2 of the 32.1 mL stainless steel high-pressure cell.

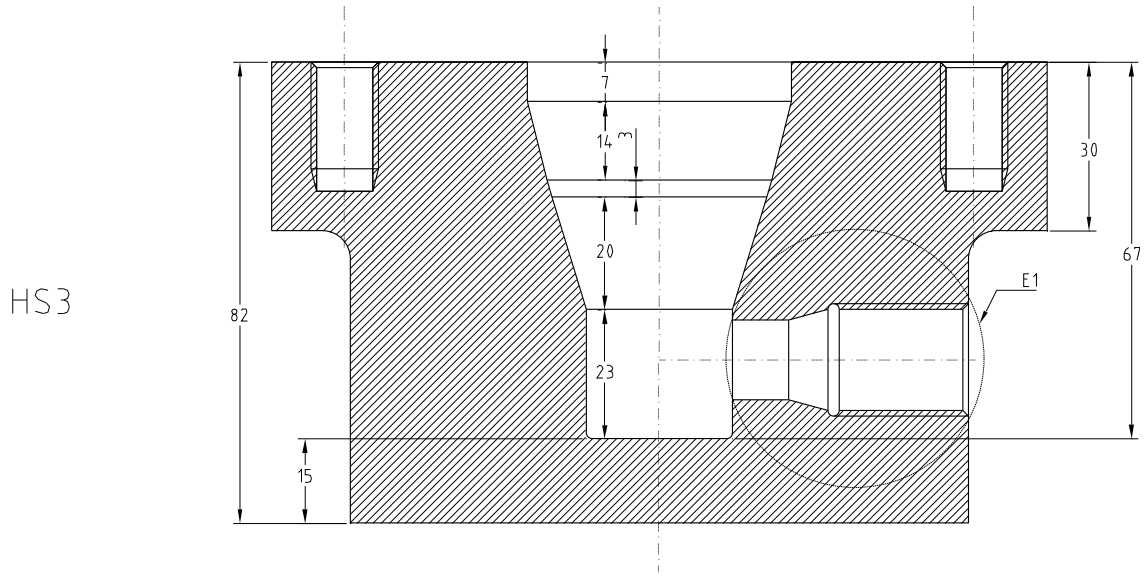

Figure A.7: Sectional drawing HS3 of the 32.1 mL stainless steel high-pressure cell.

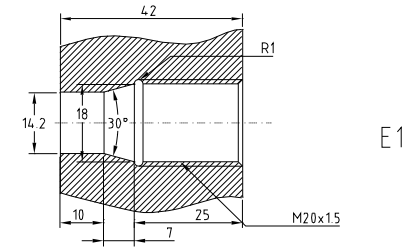

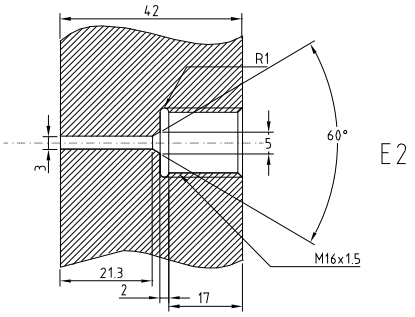

Figure A.8: Detail drawings E1 and E2 of the 32.1 mL stainless steel high-pressure cell.

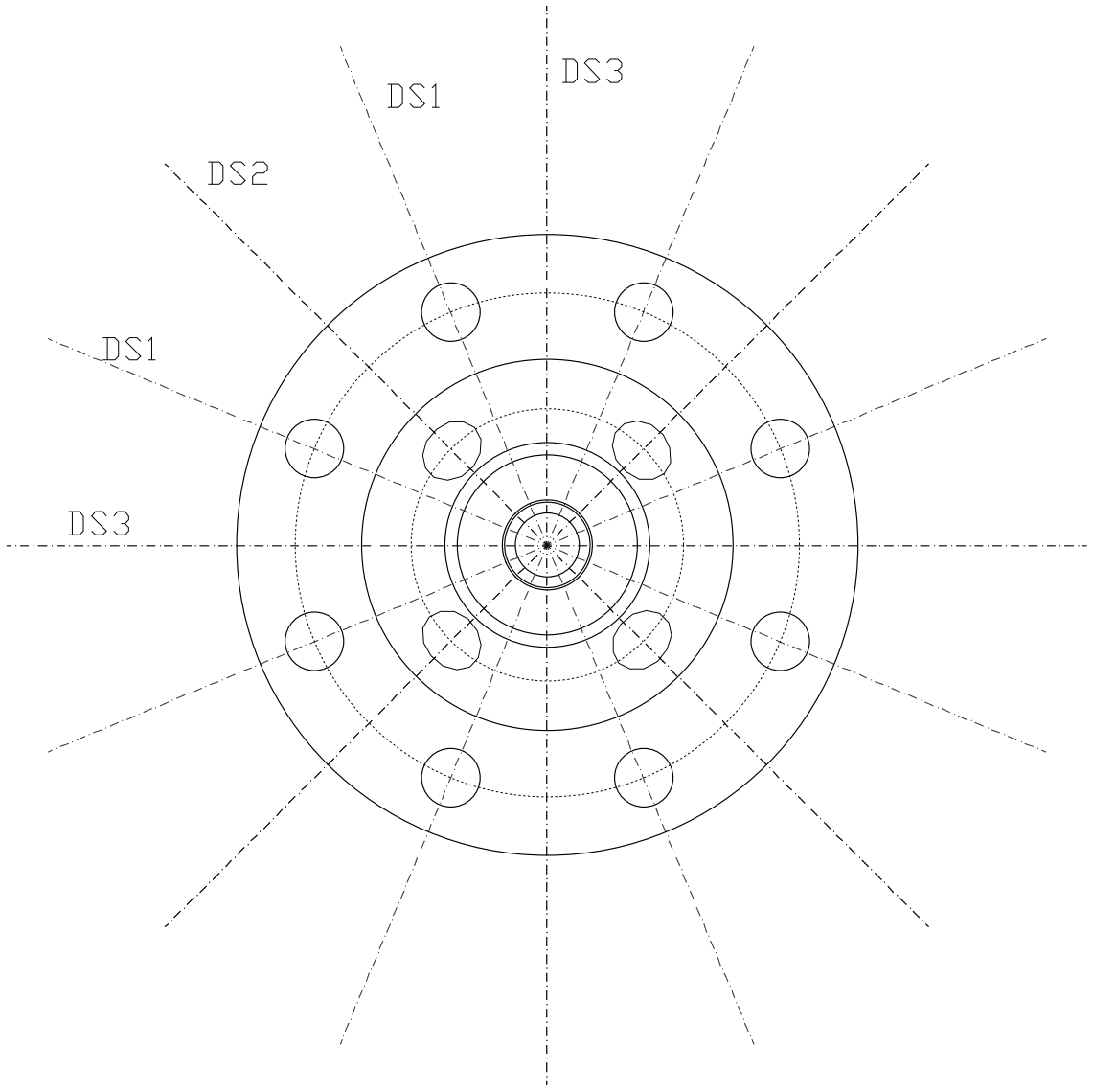

Figure A.9: Top view on the lid of the 32.1 mL stainless steel high-pressure cell.

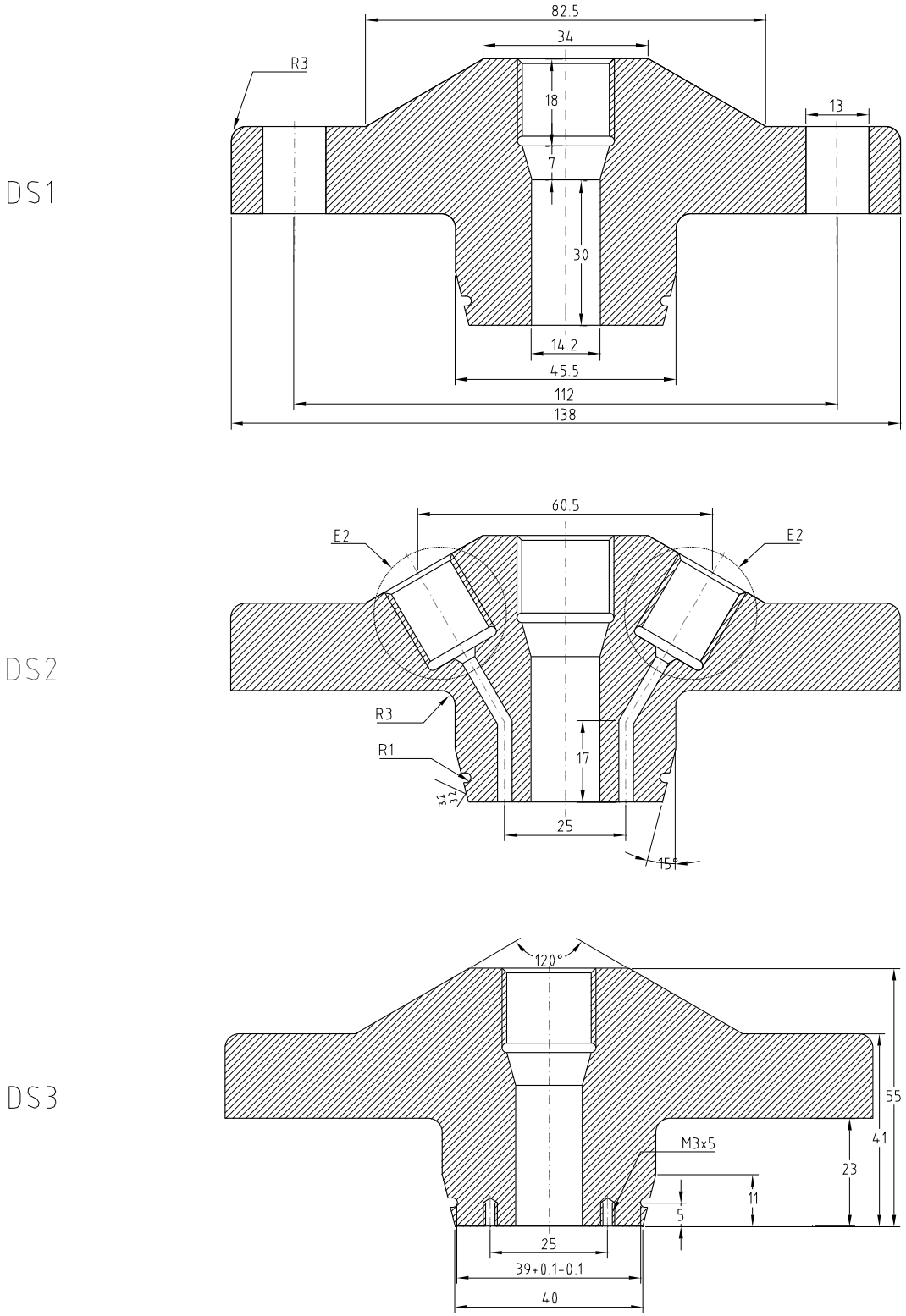

Figure A.10: Sectional drawings DS1, DS2, and DS3 of the lid of the 32.1 mL stainless steel high-pressure cell.

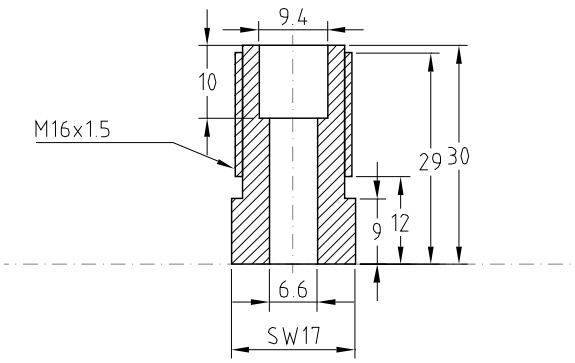

Figure A.11: Stainless steel gland nut for the 1/4 inch high-pressure tube connections of the 32.1 mL cell.

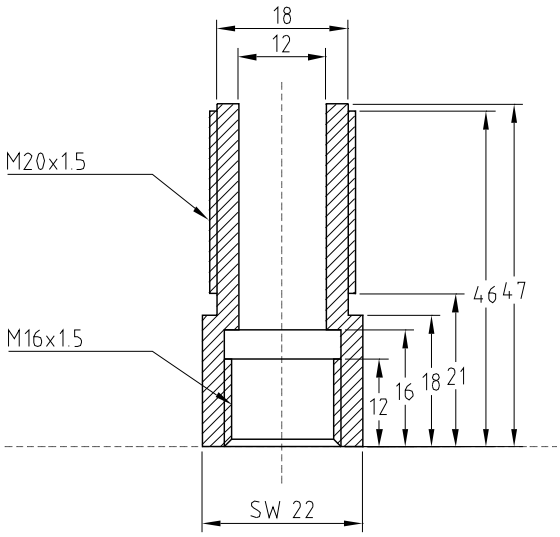

Figure A.12: Stainless steel gland nut used for the sapphire window units for the 32.1 mL high-pressure cell.

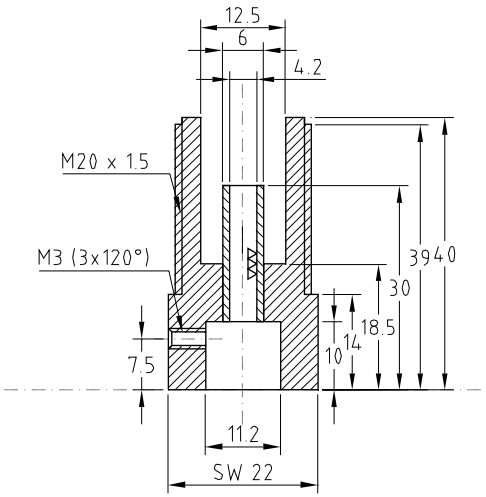

Figure A.13: Alternative stainless steel gland nut for the sapphire window units for the 32.1 mL high-pressure cell. It allows the fixation of optical fibres with metallic end sleeves (ZEISS type) by means of a setscrew.

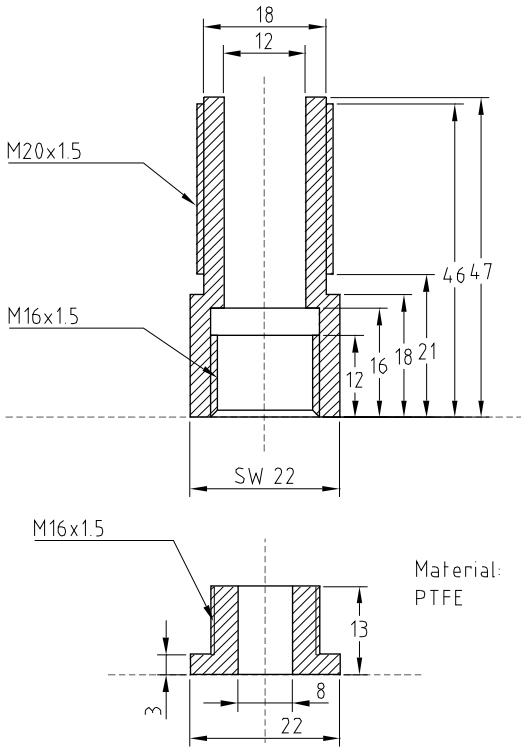

Figure A.14: Exploded drawing of the stainless steel gland nut for the high-pressure electrodes.

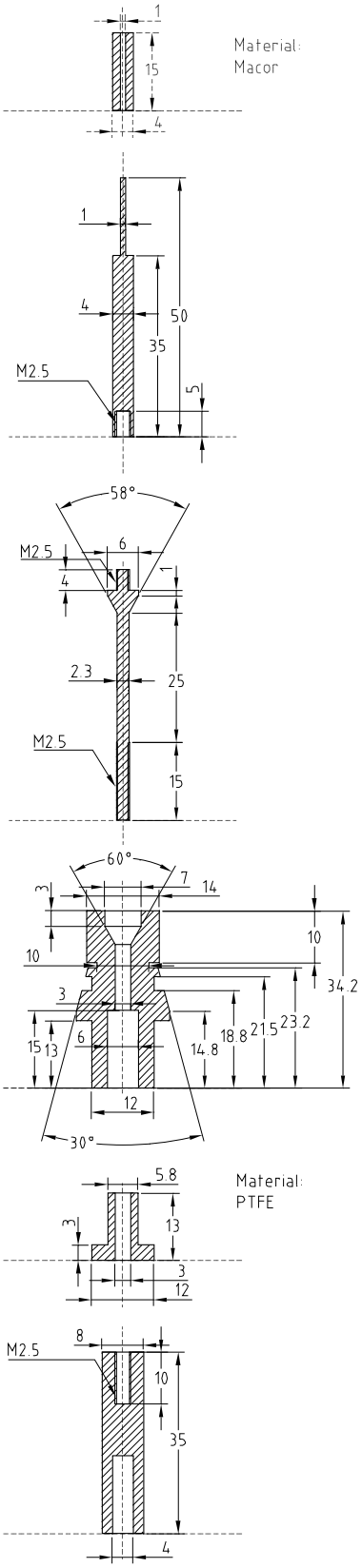

Figure A.15: High-pressure electrode I for conductivity measurements – exploded drawing.

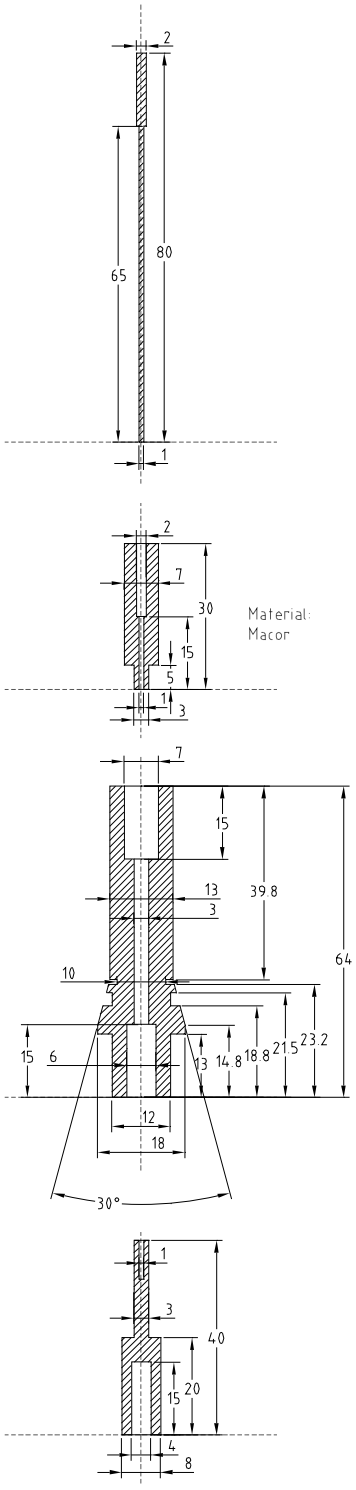

Figure A.16: High-pressure electrode II for conductivity measurements – exploded drawing.

B GC conditions and reaction analysis

B.1 GC equipment

Analysis of enzymatic reactions was performed on a HP 6890 GC system with a flame-ionisation detector (FID). The used separation column was a HP-5 ((5 %-Phenyl)-methylpolysiloxane; nominal length: 30 m; nominal diameter: 0.32 mm; nominal film thickness: 0.025 µm; HP Part No. 19091J-413) capillary column. Data acquisition and analysis were accomplished using HP ChemStation (version A.06.01) software.

B.2 GC conditions for reaction analysis

This section gives the GC conditions for the analysis of the chosen model esterification reaction between 1-propanol and lauric acid. The conditions for the reaction evaluation depend on the particular organogel used for the encapsulation of the enzyme as leaching of certain gel components such as AOT and phytantriol occurs. As solvent for the reaction samples isooctane was used.

B.2.1 Organogels based on lecithin or detergentless microemulsions

Table B.1 shows the GC conditions for the analysis of the esterification of 1-propanol and lauric acid catalysed by lipase immobilised in organogels based on lecithin or detergentless microemulsions.

B.2.2 Organogels based on AOT microemulsions

In the case of AOT MBGs, traces of AOT leached from the gels require the modification of the oven conditions in order to purge the AOT from the capillary column (cf. Table B.2). The settings for the inlet, the column, and the detector do not have to be changed (cf. Table B.1).

B.2.3 Phytantriol-based organogels

As can be seen in Table B.3 the GC oven settings have also to be modified due to the leaching of phytantriol from the organogels. As in the case of AOT MBGs, the settings for the inlet, the column, and the detector do not have to be changed (cf. Table B.1).
The GC settings for the phytantriol-based organogels were also used for the analysis of the enzyme catalysed reactions in w/c microemulsions. However, the run time had to be modified in this case depending on the surfactant used for the formation of the microemulsion in $scCO_2$.

B.3 Reaction analysis

Conversions of esterification reactions were calculated by using the following formula:

$$\text{conversion} = \frac{A_{\text{ester}}}{A_{\text{acid}} + A_{\text{ester}}} \tag{B.1}$$

where A_i represents the peak area of ester and acid, respectively, as determined by GC measurements.

Table B.1: GC conditions for the analysis of the esterification of 1-propanol and lauric acid: enzyme immobilisation in organogels based on lecithin or detergentless microemulsions.

Oven	Initial temperature	200 °C
	Initial time	5.00 min
	Run time	5.00 min
	Equilibration time	1.00 min
Inlet	Mode	Split
	Initial temperature	280 °C
	Pressure	59.1 kPa
	Split ratio	50.298 : 1
Column	Capillary column	cf. section B.1
	Mode	Constant flow
	Initial flow	0.9 mL min^{-1}
	Nominal initial pressure	59.1 kPa
Detector (FID)	Temperature	300 °C
	Hydrogen flow	40 mL min^{-1}
	Air flow	450 mL min^{-1}
	Mode	Constant makeup flow
	Makeup flow	45.0 mL min^{-1}
	Makeup gas type	Nitrogen
	Lit offset	2.0 pA

Table B.2: GC conditions for the analysis of the esterification of 1-propanol and lauric acid: enzyme immobilisation in organogels based on AOT microemulsions.

Oven	Initial temperature	200 °C
	Initial time	5.00 min
	Ramp – Rate	25.0 K min^{-1}
	Ramp – Final temperature	250 °C
	Ramp – Final time	5 min
	Run time	12.00 min
	Equilibration time	1.00 min
Inlet	Mode	Split
	Initial temperature	280 °C
	Pressure	59.1 kPa
	Split ratio	50.298 : 1
Column	Capillary column	cf. section B.1
	Mode	Constant flow
	Initial flow	0.9 mL min^{-1}
	Nominal initial pressure	59.1 kPa
Detector (FID)	Temperature	300 °C
	Hydrogen flow	40 mL min^{-1}
	Air flow	450 mL min^{-1}
	Mode	Constant makeup flow
	Makeup flow	45.0 mL min^{-1}
	Makeup gas type	Nitrogen
	Lit offset	2.0 pA

Table B.3: GC conditions for the analysis of the esterification of 1-propanol and lauric acid: enzyme immobilisation in phytantriol-based organogels.

Oven	Initial temperature	200 °C
	Initial time	5.00 min
	Ramp – Rate	25.0 K min^{-1}
	Ramp – Final temperature	250 °C
	Ramp – Final time	18.00 min
	Run time	25.00 min
	Equilibration time	1.00 min
Inlet	Mode	Split
	Initial temperature	280 °C
	Pressure	59.1 kPa
	Split ratio	50.298 : 1
Column	Capillary column	cf. section B.1
	Mode	Constant flow
	Initial flow	0.9 mL min^{-1}
	Nominal initial pressure	59.1 kPa
Detector (FID)	Temperature	300 °C
	Hydrogen flow	40 mL min^{-1}
	Air flow	450 mL min^{-1}
	Mode	Constant makeup flow
	Makeup flow	45.0 mL min^{-1}
	Makeup gas type	Nitrogen
	Lit offset	2.0 pA

C Analysis of the DSC data

C.1 Peak analysis

Peak analysis of the DSC data was done by fitting the experimental data to a linear combination of three asymmetric Gaussian bands. The fitting algorithm was based on non-linear iterative least square procedures as proposed by Frasier and Suzuki [347]. For the mathematical description of a single skewed Gaussian band the following function, $Y = f(X)$, was chosen [348]:

$$Y = Y_0 \cdot \exp\left[-\ln 2 \cdot \left\{\ln\left(1 + 2b\left(X - X_0\right)/\Delta X_{1/2}\right)/b\right\}^2\right] \tag{C.1}$$

where Y_0 represents the peak height, and X_0 the peak position. In contrast to a symmetrical Gaussian band, the parameter $\Delta X_{1/2}$ does not represent the half band width but its value may be estimated from the experimental data by the expression

$$\Delta X_{1/2} = \frac{\left(X_\mathrm{U} - X_\mathrm{L}\right) b}{\sinh\left(b\right)} \tag{C.2}$$

where X_L and X_U are the upper and lower X value at which Y falls to $\frac{1}{2}Y_0$. The value of the parameter b can be estimated from the observed data using the following equation:

$$b = sinh^{-1}\left[\frac{\left(X_\mathrm{U} - X_0\right)^2 - \left(X_\mathrm{L} - X_0\right)^2}{2\left(X_\mathrm{U} - X_0\right)\left(X_\mathrm{L} - X_0\right)}\right] \tag{C.3}$$

The area A beneath a skewed Gaussian band as described by Equation (C.1) is given by

$$A = \frac{1}{2}\sqrt{\frac{\pi}{\ln 2}} Y_0 \Delta X_{1/2} \cdot \exp\left[b^2/\left(4\ln 2\right)\right] \tag{C.4}$$

Onset temperatures for each peak were determined as described in the recommendations of the German Society for Thermal Analysis (GEFTA) [349, 350, 351, 352, 353].

C.2 Analysis of the water peaks

As already stated in section 5.1.1.2.5, the determination of the existing amounts of the different water types was accomplished by means of an equation derived from thermoporometry studies. Thermoporometry is a widely used calorimetric method for the determination of pore size distributions based on the melting point depression of substances confined within small pores. A detailed theoretical basis for the quantitative analysis of such measurements was provided in

1977 by Brun et al. [314, 315]. Reviews concerning thermoporometry studies can be found in [354, 355, 356, 357].
Amongst other mathematical terms, Brun et al. [314, 315] derived the following equation for the temperature dependent apparent heat of fusion $\Delta H_a(\Theta)$ of the penetrant liquid:

$$\Delta H_a(\Theta) = \Delta H_f + C \cdot \Delta\Theta + D \cdot (\Delta\Theta)^2 \tag{C.5}$$

ΔH_f is the heat of fusion of the same liquid under normal conditions ($332\,\mathrm{J\,g^{-1}}$ for water). $\Delta\Theta$ refers to the melting point depression and is negative for lowered melting points. The parameters C and D generally depend on whether the measurement was performed while cooling or heating the sample, on the pore geometry, and on the penetrant liquid.
In the present case, it was assumed that the water is constrained within cylindrical pores inside the MBGs. Consequently, the numerical values of the constants C and D for the performed heating experiments are given by:

$$C = 11.39\,\mathrm{J\,g^{-1}\,K^{-1}} \tag{C.6}$$

$$D = 0.155\,\mathrm{J\,g^{-1}\,K^{-2}} \tag{C.7}$$

The fusion enthalpy, ΔH_i, for a specific peak i is given by:

$$\Delta H_\mathrm{i} = \frac{A_\mathrm{i}}{\beta} \tag{C.8}$$

where A_i is the peak area and β is the scan rate applied for the DSC measurement.
The melting point depression $\Delta\Theta_\mathrm{i}$ of the peak is given by its onset temperature. The amount of water m_i for this specific peak can, thus, be calculated by the following equation:

$$m_\mathrm{i} = \frac{\Delta H_\mathrm{i}}{\Delta H_a(\Delta\Theta_\mathrm{i})} \tag{C.9}$$

Allowing for the known mass of gel used for the DSC experiment and the known composition of the gel, Equation C.9 permits the calculation of the mass fraction χ_i of the specific water type in the gel (cf. Table 5.4).

List of Figures

List of Tables

Bibliography

[1] P. T. Anastas, J. C. Warner. *Green Chemistry: Theory and Practice*, Oxford University Press, Oxford (1998)

[2] P. T. Anastas, T. C. Williamson (Eds.). *Green Chemistry: Frontiers in Benign Chemical Syntheses and Processes*, Oxford University Press, Oxford (1998)

[3] P. T. Anastas, T. C. Williamson. *Green Chemistry: An Overview*, in: P. T. Anastas, T. C. Williamson (Eds.). *ACS Symposium Series 626 – Green Chemistry: Designing Chemistry for the Environment*, pp. 1-17, American Chemical Society, Washington (1996)

[4] J. Clark, D. Macquarrie (Eds.). *Handbook of Green Chemistry and Technology*, Blackwell Science, Oxford (2002)

[5] A. Ballesteros, U. Bornscheuer, A. Capewell, D. Combes, J. Condoret, K. Koenig, F. N. Kolisis, A. Marty, U. Menge, T. Scheper, H. Stamatis, A. Xenakis. Review article: Enzymes in non-conventional phases, *Biocatal. Biotransform.* 13, 1-42 (1995)

[6] G. Carrea, S. Riva. Properties and synthetic applications of enzymes in organic solvents, *Angew. Chem. Int. Ed.* 39, 2226-2254 (2000)

[7] G. D. Rees, M. D. G. Nascimento, T. R. J. Jenta, B. H. Robinson. Reverse enzyme synthesis in microemulsion-based organogels, *Biochim. Biophys. Acta* 1073, 493-501 (1991)

[8] T. R. Jenta, G. Batts, G. D. Rees, B. H. Robinson. Biocatalysis using gelatin microemulsion-based organogels containing immobilized *Chromobacterium viscosum* lipase, *Biotechnol. Bioeng.* 53, 121-131 (1997)

[9] E. W. Lemmon, M. O. McLinden, D. G. Friend. *Thermophysical Properties of Fluid Systems*, in: P. J. Linstrom, W. G. Mallard (Eds.). *NIST Chemistry Webbook, NIST Standard Reference Database 69*, National Institute of Standards and Technology, Gaithersburg MD (März 2003), http://webbook.nist.gov

[10] S. L. Wells, J. DeSimone. CO_2 Technology Platform: An Important Tool for Environmental Problem Solving, *Angew. Chem. Int. Ed.* 40, 518-527 (2001)

[11] P. G. Jessop, W. Leitner (Eds.). *Chemical Synthesis Using Supercritical Fluids*, Wiley-VCH, Weinheim (1999)

[12] M. Perrut. Enzymic reactions in supercritical carbon dioxide, *Colloque INSERM* 224, 401-410 (1992)

[13] K. Harrison, J. Goveas, K. P. Johnston, E. A. O'Rear. Water-in-Carbon Dioxide Microemulsions with a Fluorocarbon-Hydrocarbon Hybrid Surfactant, *Langmuir* 10, 3536-3541 (1994)

[14] R. S. Oakes, A. A. Clifford, C. M. Rayner. The use of supercritical fluids in synthetic organic chemistry, *J. Chem. Soc., Perkin Trans. 1*, 917-941 (2001)

[15] T. W. Randolph, H. W. Blanch, J. M. Prausnitz, C. R. Wilke. Enzymic catalysis in a supercritical fluid, *Biotechnol. Lett.* 7, 325-328 (1985)

[16] K. P. Johnston, K. L. Harrison, M. J. Clarke, S. M. Howdle, M. P. Heitz, F. V. Bright, C. Carlier, T. W. Randolph. Water-in-carbon dioxide microemulsions: an environment for hydrophiles including proteins, *Science* 271, 624-626 (1996)

[17] M. J. Clarke, K. L. Harrison, K. P. Johnston, S. M. Howdle. Water in Supercritical Carbon Dioxide Microemulsions: Spectroscopic Investigation of a New Environment for Aqueous Inorganic Chemistry, *J. Am. Chem. Soc.* 119, 6399-6406 (1997)

[18] J. D. Holmes, P. A. Bhargava, B. A. Korgel, K. P. Johnston. Synthesis of Cadmium Sulfide Q Particles in Water-in-CO_2 Microemulsions, *Langmuir* 15, 6613-6615 (1999)

[19] J. D. Holmes, D. C. Steytler, G. D. Rees, B. H. Robinson. Bioconversions in a Water-in-CO_2 Microemulsion, *Langmuir* 14, 6371-6376 (1998)

[20] G. C. Irvin Jr., V. T. John. Materials Synthesis via Water-in-Dense CO_2-Microemulsions: A Novel Reaction Medium, *Proc.: NOBBCChE* 25, 59-67 (1998)

[21] M. A. Kane, G. A. Baker, S. Pandey, F. V. Bright. Performance of Cholesterol Oxidase Sequestered within Reverse Micelles Formed in Supercritical Carbon Dioxide, *Langmuir* 16, 4901-4905 (2000)

[22] J. Eastoe, S. Gold. Self-assembly in green solvents, *Phys. Chem. Chem. Phys.* 7, 1352-1362 (2005)

[23] C. Cagniard de la Tour. Exposé de quelques résultats obtenus par l'action combinée de la chaleur et de la compression sur certains liquides, tels que l'eau, l'alcool, l'éther sulfurique et l'essence de pétrole rectifiée, *Ann. Chim. Phys.* 21, 127-132 (1822)

[24] C. Cagniard de la Tour. Supplément au Mémoire de M. Cagniard de la Tour, imprimé page 127 de ce Cahier des Annales, *Ann. Chim. Phys.* 21, 178-182 (1822)

[25] T. Andrews. On the Continuity of the Gaseous and Liquid States of Matter, *Philos. Trans. R. Soc. London* 159, 575-590 (1869)

[26] J. B. Hannay, J. Hogarth. On the Solubility of Solids in Gases, *Proc. Roy. Soc.* 29, 324-326 (1879)

[27] J. B. Hannay, J. Hogarth. On the Solubility of Solids in Gases, *Proc. Roy. Soc.* 30, 178-188 (1880)

[28] J. B. Hannay. On the Solubility of Solids in Gases, II., *Proc. Roy. Soc.* 30, 484-489 (1880)

[29] G. M. Barrow. *Physikalische Chemie – Gesamtausgabe*, 6th Edition, Bohmann, Wien (1984)

[30] A. D. McNaught (Ed.). *Compendium of Chemical Terminology. IUPAC Recommendations*, Blackwell Science Ltd., Oxford (1997)

[31] S. Angus, B. Armstrong, K. M. de Reuck (Eds.). *International Thermodynamic Tables of the Fluid State – Carbon Dioxide*, Pergamon Press, Oxford (1976)

[32] P. W. Bridgman. Change of phase under pressure – I. The phase diagram of eleven substances with especial reference to the melting curve, *Phys. Rev.* 3, 153-203 (1914)

[33] J. D. Grace, G. C. Kennedy. The melting curve of five gases up to 30 kb, *J. Phys. Chem. Solids* 28, 977-982 (1967)

[34] G. Brunner. Stofftrennung mit überkritischen Gasen (Gasextraktion), *Chem. Ing. Tech.* 59, 12-22 (1987)

[35] M. D. Luque de Castro, M. Valcárcel, M. T. Tena. *Analytical Supercritical Fluid Extraction*, Springer-Verlag, Heidelberg (1994)

[36] M. McHugh, V. Krukonis. *Supercritical Fluid Extraction – Principles and Practice*, Butterworth Publishers (1986)

[37] A. Birtigh, G. Brunner. Abscheidung aus überkritischen Gasen, *Chem. Ing. Tech.* 67, 829-835 (1995)

[38] T. Clifford. *Fundamentals of Supercritical Fluids*, Oxford University Press, New York (1999)

[39] W. J. Ellison, K. Lamkaouchi, J.-M. Moreau. Water: a dielectric reference, *J. Mol. Liq.* 68, 171-279 (1996)

[40] D. P. Fernandez, A. R. H. Goodwin, E. W. Lemmon, J. M. H. L. Sengers, R. C. Williams. A formulation for the static permittivity of water and steam at temperatures from 238 K to 873 K at pressures up to 1200 MPa, including derivatives and Debye-Hueckel coefficients, *J. Phys. Chem. Ref. Data* 26, 1125-1166 (1997)

[41] F. V. Bright, M. E. P. McNally (Eds.). *ACS Symposium Series 488 – Supercritical Fluid Technology: Theoretical and Applied Approaches in Analytical Chemistry*, American Chemical Society, Washington (1992)

[42] B. A. Charpentier, M. R. Sevenants (Eds.). *ACS Symposium Series 366 – Supercritical Fluid Extraction and Chromatography*, American Chemical Society, Washington (1988)

[43] K. P. Johnston, J. M. L. Penninger (Eds.). *ACS Symposium Series 406 – Supercritical Fluid Science and Technology*, American Chemical Society, Washington (1989)

[44] M. B. King, T. R. Bott (Eds.). *Extraction of natural products using near-critical fluids*, Blackie Academic & Professional, Glasgow (1993)

[45] M. Perrut. Supercritical fluids applications in the pharmaceutical industry, *S. T. P. Pharma Sciences* 13, 83-91 (2003)

[46] G. M. Schneider, E. Stahl, G. Wilke (Eds.). *Extraction with Supercritical Gases*, Verlag Chemie, Weinheim (1980)

[47] T. L. Chester, J. D. Pinkston, D. E. Raynie. Supercritical fluid chromatography and extraction, *Anal. Chem.* 70, 301R-319R (1998)

[48] T. L. Chester, J. D. Pinkston. Supercritical Fluid and Unified Chromatography, *Anal. Chem.* 76, 4606-4613 (2004)

[49] B. Wenclawiak (Ed.). *Analysis with Supercritical Fluids: Extraction and Chromatography*, Springer-Verlag, Heidelberg (1992)

[50] C. M. White (Ed.). *Modern Supercritical Fluid Chromatography*, Dr. Alfred Hüthig Verlag, Heidelberg (1988)

[51] E. Bach, E. Cleve, E. Schollmeyer. Past, present and future of supercritical fluid dyeing technology – an overview, *Rev. Progr. Color.* 32, 88-102 (2002)

[52] P. L. Beltrame, A. Castelli, E. Selli, A. Mossa, G. Testa, A. M. Bonfatti, A. Seves. Dyeing of cotton in supercritical carbon dioxide, *Dyes and Pigments* 39, 335-340 (1998)

[53] M. R. De Giorgi, E. Cadoni, D. Maricca, A. Piras. Dyeing polyester fibres with disperse dyes in supercritical CO_2, *Dyes and Pigments* 45, 75-79 (2000)

[54] J. H. Jun, K. Sawada, M. Ueda. Application of perfluoropolyether reverse micelles in supercritical CO_2 to dyeing process, *Dyes and Pigments* 61, 17-22 (2004)

[55] A. S. Özcan, A. A. Clifford, K. D. Bartle, D. M. Lewis. Dyeing of cotton fibers with disperse dyes in supercritical carbon dioxide, *Dyes and Pigments* 36, 103-110 (1998)

[56] K. Sawada, T. Takagi, M. Ueda. Solubilization of ionic dyes in supercritical carbon dioxide: a basic study for dyeing fiber in non-aqueous media, *Dyes and Pigments* 60, 129-135 (2004)

[57] A. Schmidt, E. Bach, E. Schollmeyer. The dyeing of natural fibers with reactive disperse dyes in supercritical carbon dioxide, *Dyes and Pigments* 56, 27-35 (2003)

[58] C. Cinquemani, V. Heil, J. Jakob. Supercritical impregnation of technical high weight absorbent, *GIT Fachz. Lab.* 47, 748-750 (2003)

[59] J. N. Hay, K. Johns. Supercritical fluids – a potential revolution in wood treatment and coating, *Surf. Coat. Int.* 83, 106-110 (2000)

[60] I. Kikic, F. Vecchione. Supercritical impregnation of polymers, *Curr. Opin. Solid State Mater. Sci.* 7, 399-405 (2003)

[61] L. N. Nikitin, M. O. Gallyamov, R. A. Vinokur, A. Y. Nikolaec, E. E. Said-Galiyev, A. R. Khokhlov, H. T. Jespersen, K. Schaumburg. Swelling and impregnation of polystyrene using supercritical carbon dioxide, *J. Supercrit. Fluids* 26, 263-273 (2003)

[62] J. Sauk, J. Byun, H. Kim. Grafting of styrene on to Nafion membranes using supercritical CO_2 impregnation for direct methanol fuel cells, *J. Power Sources* 132, 59-63 (2004)

[63] S. Yoda, A. Hasegawa, H. Suda, Y. Uchimaru, K. Haraya, T. Tsuji, K. Otake. Preparation of a platinum and palladium/polyimide nanocomposite film as a precursor of metal-doped carbon molecular sieve membrane via supercritical impregnation, *Chem. Mater.* 16, 2363-2368 (2004)

[64] J. Bittner. *Aufbau einer Hochdruckapparatur zur absorptionsspektrophotometrischen Untersuchung von Reaktionen, Mikroemulsionen und mizellären Lösungen in flüssigem und überkritischem Kohlendioxid*, Dissertation, Universität Regensburg (2002), http://www.opus-bayern.de/uni-regensburg/volltexte/2002/109/

[65] J. Jung, M. Perrut. Particle design using supercritical fluids: Literature and patent survey, *J. Supercrit. Fluids* 20, 179-219 (2001)

[66] E. Reverchon. Supercritical antisolvent precipitation of micro- and nano-particles, *J. Supercrit. Fluids* 15, 1–21 (1999)

[67] M. Sihvonen, E. Järvenpää, V. Hietaniemi, R. Huopalahti. Advances in supercritical carbon dioxide technologies, *Trends Food Sci. Technol.* 10, 217-222 (1999)

[68] M. Perrut, J. Clavier. Supercritical Fluid Formulation: Process Choice and Scale-up, *Ind. Eng. Chem. Res.* 42, 6375-6383 (2003)

[69] S. Minett, K. Fenwick. Supercritical water oxidation – the environmental answer to organic waste disposal?, *Eur. Water Management* 4, 54-56 (2001)

[70] H. Schmieder, J. Abeln. Supercritical water oxidation: State of the art, *Chem. Eng. Technol.* 22, 903-908 (1999)

[71] T. B. Thomason, G. T. Hong, K. C. Swallow, W. R. Killilea. The MODAR supercritical water oxidation process, *Innovative Hazardous Waste Treatment Technology Series* 1, 31-42 (1990)

[72] S. Yesodharan. Supercritical water oxidation: an environmentally safe method for the disposal of organic wastes, *Curr. Sci.* 82, 1112-1122 (2002)

[73] A. F. Hollemann, N. Wiberg. *Lehrbuch der anorganischen Chemie*, 101st Edition, Walter de Gruyter, Berlin (1995)

[74] Gesetz über den Verkehr mit Lebensmitteln, Tabakerzeugnissen, kosmetischen Mitteln und sonstigen Bedarfsgegenständen (Lebensmittel- und Bedarfsgegenständegesetz – LMBG) in der Fassung vom 09.09.1997 (BGBl. I, S. 2296), zuletzt geändert durch Artikel 4 und Artikel 5 G vom 13.05.2004 (BGBl. I, S. 934)

[75] J. Eastoe, A. Dupont, D. C. Steytler. Fluorinated surfactants in supercritical CO_2, *Curr. Opin. Colloid Interface Sci.* 8, 267-273 (2003)

[76] E. L. V. Goetheer, M. A. G. Vostman, J. T. F. Keurentjes. Opportunities for Process Intensification using Reverse Micelles in Liquid and Supercritical Carbon Dioxide, *Chem. Eng. Sci.* 54, 1589-1596 (1999)

[77] A. V. Yazdi, E. J. Beckman. Design, Synthesis, and Evaluation of Novel, Highly CO_2-Soluble Chelating Agents for Removal of Metals, *Ind. Eng. Chem. Res.* 35, 3644-3652 (1996)

[78] J. D. Holmes, K. J. Ziegler, M. Audriani, C. T. J. Lee, P. A. Bhargava, D. C. Steytler, K. P. Johnston. Buffering the Aqueous Phase pH in Water-in-CO_2 Microemulsions, *J. Phys. Chem. B* 103, 5703-5711 (1999)

[79] W. Leitner. Reactions in Supercritical Carbon Dioxide ($scCO_2$), *Top. Curr. Chem.* 206, 107-132 (1999)

[80] S. Kamat, J. Barrera, E. J. Beckman, A. J. Russell. Biocatalytic synthesis of acrylates in organic solvents and supercritical fluids: I. Optimization of enzyme environment, *Biotechnol. Bioeng.* 40, 158-166 (1992)

[81] S. Kamat, G. Critchley, E. J. Beckman, A. J. Russell. Biocatalytic synthesis of acrylates in organic solvents and supercritical fluids: III. Does carbon dioxide covalently modify enzymes?, *Biotechnol. Bioeng.* 46, 610-620 (1995)

[82] G. H. Lorimer, M. R. Badger, T. J. Andrews. The activation of ribulose-1,5-bisphosphate carboxylase by carbon dioxide and magnesium ions. Equilibria, kinetics, a suggested mechanism, and physiological implications, *Biochemistry* 15, 529-536 (1976)

[83] G. H. Lorimer, H. M. Miziorko. Carbamate formation on the ε-amino group of a lysyl residue as the basis for the activation of ribulosebisphosphate carboxylase by CO_2 and Mg^{2+}, *Biochemistry* 19, 5321-5328 (1980)

[84] W. Leitner. The coordination chemistry of carbon dioxide and its relevance for catalysis : a critical survey, *Coord. Chem. Rev.* 153, 257-284 (1996)

[85] T. A. Hoefling, R. R. Beitle, R. M. Enick, E. J. Beckman. Design and Synthesis of Highly CO_2-Soluble Surfactants and Chelating Agents, *Fluid Phase Equil.* 83, 203-212 (1993)

[86] G. J. McFann, K. P. Johnston, S. M. Howdle. Solubilization in nonionic reverse micelles in carbon dioxide, *AIChE J.* 40, 543-555 (1994)

[87] R. Fink, D. Hancu, R. Valentine, E. J. Beckman. Toward the Development of "CO_2-philic" Hydrocarbons. 1. Use of Side-Chain Functionalization to Lower the Miscibility Pressure of Polydimethylsiloxanes in CO_2, *J. Phys. Chem. B* 103, 6441-6444 (1999)

[88] D. R. Lide (Ed.). *CRC Handbook of Chemistry and Physics – 76th Edition 1995-1996*, CRC Press, Boca Raton (1995)

[89] F. Rindfleisch, T. P. DiNoia, M. A. McHugh. Solubility of Polymers and Copolymers in Supercritical CO_2, *J. Phys. Chem.* 100, 15581-15587 (1996)

[90] M. D. Luque de Castro, M. T. Tena. Strategies for supercritical fluid extraction of polar and ionics compounds, *Trends Anal. Chem.* 15, 32-37 (1996)

[91] T. Moriyoshi, T. Kita, Y. Uosaki. Static Relative Permittivity of Carbon Dioxide And Nitrous Oxide up to 30 MPa, *Ber. Bunsenges. Phys. Chem.* 97, 589-596 (1993)

[92] S. B. Hawthorne, D. J. Miller. Extraction and recovery of organic pollutants from environmental solids and Tenax-GC using supercritical carbon dioxide, *J. Chromatogr. Sci.* 24, 258-264 (1986)

[93] J. J. Langenfeld, S. B. Hawthorne, D. J. Miller, J. Pawliszyn. Effects of temperature and pressure on supercritical fluid extraction efficiencies of polycyclic aromatic hydrocarbons and polychlorinated biphenyls, *Anal. Chem.* 65, 338-344 (1993)

[94] R. E. Fornari, P. Alessi, I. Kikic. High pressure fluid phase equilibria: experimental methods and systems investigated (1978-1987), *Fluid Phase Equilib.* 57, 1-33 (1990)

[95] R. Dohrn, G. Brunner. High-pressure fluid-phase equilibria: experimental methods and systems investigated (1988-1993), *Fluid Phase Equilib.* 106, 213-282 (1995)

[96] M. Christov, R. Dohrn. High-pressure fluid phase equilibria: experimental methods and systems investigated (1994-1999), *Fluid Phase Equilib.* 202, 153-218 (2002)

[97] J. W. Hills, H. H. Hill, T. Maeda. Simultaneous supercritical fluid derivatization and extraction, *Anal. Chem.* 63, 2152-2155 (1991)

[98] R. Hillmann, K. Bachmann. Online supercritical fluid derivatization and extraction - capillary gas chromatography of polar compounds, *J. High Resolut. Chromatogr.* 17, 350-352 (1994)

[99] Y. Cai, R. Alzaga, J. M. Bayona. In situ Derivatization and Supercritical Fluid Extraction for the Simultaneous Determination of Butyltin and Phenyltin Compounds in Sediment, *Anal. Chem.* 66, 1161-1167 (1994)

[100] B. W. Wenclawiak, M. Krah. Reactive supercritical fluid extraction and chromatography of arsenic species, *Fresenius J. Anal. Chem.* 351, 134-138 (1995)

[101] M. T. Tena, M. D. Luque de Castro, M. Valcarcel. Improved supercritical fluid extraction of sulfonamides, *Chromatographia* 40, 197-203 (1995)

[102] M. M. Jimenez-Carmona, M. T. Tena, M. D. Luque de Castro. Ion-pair-supercritical fluid extraction of clenbuterol from food samples, *J. Chromatogr. A* 711, 269-276 (1995)

[103] J. A. Field, D. J. Miller, T. M. Field, S. B. Hawthorne, W. Giger. Quantitative determination of sulfonated aliphatic and aromatic surfactants in sewage sludge by ion-pair/supercritical fluid extraction and derivatization gas chromatography/mass spectrometry, *Anal. Chem.* 64, 3161-3167 (1992)

[104] S. Wang, S. Elshani, C. M. Wai. Selective extraction of mercury with ionizable crown ethers in supercritical carbon dioxide, *Anal. Chem.* 67, 919-923 (1995)

[105] A. V. Yazdi, C. Lepilleur, E. J. Singley, W. Liu, F. A. Adamsky, R. M. Enick, E. J. Beckman. Highly carbon dioxide soluble surfactants, dispersants and chelating agents, *Fluid Phase Equilib.* 117, 297-303 (1996)

[106] C. L. Phelps, N. G. Smart, C. M. Wai. Past, Present, and Possible Future Applications of Supercritical Fluid Extraction Technology, *J. Chem. Educ.* 73, 1163-1168 (1996)

[107] K. Zosel (Erfinder). *Verfahren zur Entcoffeinierung von Kaffee*. Patent, Offenlegungsschrift 2 005 293, Aktenzeichen: P 20 05 293.1, Anmeldetag: 05.02.1970, Offenlegungstag: 18.11.1971, Anmelder: Studiengesellschaft Kohle mbH (Mülheim)

[108] L. T. Taylor. *Supercritical Fluid Extraction*, John Wiley & Sons, New York (1996)

[109] S. Moore, S. Samdani, G. Ondrey, G. Parkinson. New Roles for Supercritical Fluids, *Chem. Eng.* 101, 3: 32-34 (1994)

[110] DECHEMA – Gesellschaft für Chemische Technik und Biotechnologie e.V. Press release 18th May 2003: Supercritical Fluids – Green and Effectiv.
http://www.dechema.de/9___Supercritical_Fluids-lang-en.html

[111] S. A. Cretté, J. M. DeSimone. Neueste Anwendungen von komprimiertem Kohlendioxid, *Nachr. aus der Chemie* 49, 462-466 (2001)

[112] J. F. Brennecke. New applications of supercritical fluids, *Chem. Ind.* 21, 831-834 (1996)

[113] E. N. Hoggan, D. Flowers, K. Wang, J. M. DeSimone, R. G. Carbonell. Spin Coating of Photoresists Using Liquid Carbon Dioxide, *Ind. Eng. Chem. Res.* 43, 2113-2122 (2004)

[114] J. J. Watkins, J. M. Blackburn, T. J. McCarthy. Chemical Fluid Deposition: Reactive Deposition of Platinum Metal from Carbon Dioxide Solution, *Chem. Mater.* 11, 213-215 (1999)

[115] D. P. Long, J. M. Blackburn, J. J. Watkins. Chemical fluid deposition: a hybrid technique for low-temperature metallization, *Adv. Mater.* 12, 913-915 (2000)

[116] U. Pfüller. *Mizellen – Vesikel – Mikroemulsionen. Tensidassoziate und ihre Anwendungen in Analytik und Biochemie – Anleitung für die chemische Laboratoriumspraxis*, Vol. 22, Springer-Verlag, Berlin (1986)

[117] G. Brezesinski, H.-J. Mögel. *Grenzflächen und Kolloide – Physikalisch-chemische Grundlagen*, Spektrum, Heidelberg (1993)

[118] S.-H. Chen, R. Rajagopalan (Eds.). *Micellar Solutions and Microemulsions: Structure, Dynamics and Statistical Thermodynamics*, Springer-Verlag, New York (1990)

[119] D. F. Evans und H. Wennerström. *The Colloidal Domain: where Physics, Chemistry, Biology and Technology Meet*, 2nd Edition, Wiley-VCH, New York (1999)

[120] P. C. Hiemenz. *Principles of Colloid and Surface Chemistry*, 2nd Edition, Marcel Dekker, New York (1986)

[121] L.-M. Prince (Ed.). *Microemulsions – Theory and Practice*, Academic Press, New York (1977)

[122] H. L. Rosano, M. Clausse (Eds.). *Microemulsion Systems*, Marcel Dekker, New York (1987)

[123] S. A. Safran. *Theory of Structure and Phase Transitions in Globular Microemulsions*, in: S.-H. Chen, R. Rajagopalan (Eds.). *Micellar Solutions and Microemulsions: Structure, Dynamics and Statistical Thermodynamics*, Springer-Verlag, New York (1990)

[124] J.-L. Salager. *Microemulsions*, in: U. Zoller, G. Broze (Eds.). *Surfactant Science Series Vol. 82 – Handbook of Detergents. Part A: Properties*, pp. 253-302, Marcel Dekker, New York (1999)

[125] S. J. Chen, D. F. Evans, B. W. Ninham, D. J. Mitchell, F. D. Blum, S. Pickup. Curvature as a Determinant of Microstructure and Microemulslons, *J. Phys. Chem.* 90, 842-847 (1986)

[126] K. Shinoda, H. Kunieda. *How to Formulate Microemulsions with Less Surfactant*, in: L.-M. Prince (Ed.). *Microemulsions – Theory and Practice*, Academic Press, New York (1977)

[127] M. P. Pileni. Reverse Miceles as Microreactors, *J. Phys. Chem.* 97, 6961 -6973 (1993)

[128] C. Mathew, Z. Saidi, J. Peyrelasse, C. Boned. Viscosity, conductivity, and dielectric relaxation of waterless glycerol-sodium bis(2-ethylhexyl)sulfosuccinate-isooctane microemulsions: the percolation effect, *Phys. Rev. A* 43, 873-882 (1991)

[129] J. Chrastil. Solubility of solids and liquids in supercritical gases, *J. Phys. Chem.* 86, 3016-3021 (1982)

[130] M. B. King, A. Mubarak, J. D. Kim, T. R. Bott. The mutual solubilities of water with supercritical and liquid carbon dioxide, *J. Supercrit. Fluids* 5, 296-302 (1992)

[131] Y. L. Khmelnitsky, J. O. Rich. Biocatalysis in nonaqueous solvents, *Curr. Opin. Chem. Biol.* 3, 47-53 (1999)

[132] H. Stamatis, A. Xenakis, F. N. Kolisis. Bioorganic reactions in microemulsions: the case of lipases, *Biotechnol. Adv.* 17, 293-318 (1999)

[133] B. Orlich, R. Schomacker. Enzyme catalysis in reverse micelles, *Adv. Biochem. Eng. Biotechnol.* 75, 185-208 (2002)

[134] N. L. Klyachko, A. V. Levashov. Bioorganic synthesis in reverse micelles and related systems, *Curr. Opin. Colloid Interface Sci.* 8, 179-186 (2003)

[135] G. Haering, P. L. Luisi. Hydrocarbon gels from water-in-oil microemulsions, *J. Phys. Chem.* 90, 5892-5895 (1986)

[136] C. Quellet, H. F. Eicke. Mutual gelation of gelatin and water-in-oil microemulsions, *Chimia* 40, 233-238 (1986)

[137] C. Quellet, H. F. Eicke. Some comments on the gelation of gelatin containing water/oil microemulsions, *J. Phys. Chem.* 91, 4211-4112 (1987)

[138] P. J. Atkinson, M. J. Grimson, R. K. Heenan, A. M. Howe, A. R. Macke, B. H. Robinson. Microemulsion-based gels: a small-angle neutron scattering study, *Chem. Phys. Lett.* 151, 494-498 (1988)

[139] P. J. Atkinson, B. H. Robinson, A. M. Howe, R. K. Heenan. Structure and stability of microemulsion-based organo-gels, *J. Chem. Soc., Faraday Trans.* 87, 3389-3397 (1991)

[140] C. Quellet, H.-F. Eicke, W. Sager. Formation of microemulsion-based gelatin gels, *J. Phys. Chem.* 95, 5642-5655 (1991)

[141] T. R. Jenta, G. Batts, G. D. Rees, B. H. Robinson. Kinetic studies of *Chromobacterium viscosum* lipase in AOT water-in-oil microemulsions and gelatin microemulsion-based organogels, *Biotechnol. Bioeng.* 54, 416-427 (1997)

[142] S. Backlund, F. Eriksson, L. T. Kanerva, M. Rantala. Selective enzymic reactions using microemulsion-based gels, *Colloids Surf., B* 4, 121-127 (1995)

[143] S. Backlund, F. Eriksson, S. Karlsson, G. Lundsten. Enzymic esterification and phase behavior in ionic microemulsions with different alcohols, *Colloid Polym. Sci.* 273, 533-588 (1995)

[144] G. D. Rees, B. H. Robinson, G. R. Stephenson. Preparative-scale kinetic resolutions catalyzed by microbial lipases immobilized in AOT-stabilized microemulsion-based organogels: cryoenzymology as a tool for improving enantioselectivity, *Biochim. Biophys. Acta* 1259, 73-81 (1995)

[145] K. Nagayama, K. Tada, K. Naoe, M. Imai. *Rhizopus delemar* Lipase in Microemulsion-based Organogels: Reactivity and Rate-Limiting Study, *Biocatal. Biotransform.* 21, 321-324 (2003)

[146] K. Nagayama, N. Yamasaki, M. Imai. Fatty acid esterification catalyzed by *Candida rugosa* lipase in lecithin microemulsion-based organogels, *Biochem. Eng. J.* 12, 231-236 (2002)

[147] N. W. Fadnavis, R. Luke Babu, G. Sheelu, A. Deshpande. 'Gelozymes' in organic synthesis: synthesis of enantiomerically pure (S)-2-hydroxy-(3-phenoxy)phenylacetonitrile with lipase immobilized in a gelatin matrix, *Tetrahedron: Asymmetry* 11, 3303-3309 (2000)

[148] K. Soni, D. Madamwar. Ester synthesis by lipase immobilized on silica and microemulsion based organogels (MBGs), *Process Biochem.* 36, 607-611 (2001)

[149] G. Zhou, G. Li, J. Xu, Q. Sheng. Kinetic studies of lipase-catalyzed esterification in water-in-oil microemulsions and the catalytic behavior of immobilized lipase in MBGs, *Colloids Surf., A* 194, 41-47 (2001)

[150] K. Nagayama, M. Imai. Enhanced activity of *Mucor javanicus* lipase in polyoxyethylene sorbitan trioleate containing microemulsion-based organogels, *J. Mol. Catal. B: Enzym.* 34, 44-50 (2005)

[151] H. Stamatis, A. Xenakis. Biocatalysis using microemulsion-based polymer gels containing lipase, *J. Mol. Catal. B: Enzym.* 6, 399-406 (1999)

[152] A. Pastou, H. Stamatis, A. Xenakis. Microemulsion-based organogels containing lipase: application in the synthesis of esters, *Prog. Colloid Polym. Sci.* 115, 192-195 (2000)

[153] C. Delimitsou, M. Zoumpanioti, A. Xenakis, H. Stamatis. Activity and stability studies of *Mucor miehei* lipase immobilized in novel microemulsion-based organogels, *Biocatal. Biotransform.* 20, 319-327 (2002)

[154] M. Schuleit, P. L. Luisi. Enzyme immobilization in silica-hardened organogels, *Biotechnol. Bioeng.* 72, 249-253 (2001)

[155] G. D. Smith, C. E. Donelan, R. E. Barden. Oil-continuous microemulsions composed of hexane, water, and 2-propanol, *J. Colloid Interface Sci.* 60, 488-496 (1977)

[156] N. F. Borys, S. L. Holt, R. E. Barden. Detergentless water/oil microemulsions. III. Effect of potassium hydroxide on phase diagram and effect of solvent composition on base hydrolysis of esters, *J. Colloid Interface Sci.* 71, 526-532 (1979)

[157] B. A. Keiser, D. Varie, R. E. Barden, S. L. Holt. Detergentless water/oil microemulsions composed of hexane, water, and 2-propanol. 2. Nuclear magnetic resonance studies, effect of added NaCl, *J. Phys. Chem.* 83, 1276-1280 (1979)

[158] G. Lund, S. L. Holt. Detergentless water/oil microemulsions. IV. The ternary pseudo-phase diagram for and properties of the system toluene/2-propanol/water, *J. Am. Oil Chem. Soc.* 57, 264-267 (1980)

[159] J. Lara, G. Perron, J. E. Desnoyers. Heat capacities and volumes of the ternary system benzene-water-2-propanol, *J. Phys. Chem.* 85, 1600-1605 (1981)

[160] B. A. Keiser, S. L. Holt. Reactions in detergentless microemulsions: incorporation of copper(II) into meso-tetraphenylporphine ((TPP)H_2) in a water/oil microemulsion, *Inorg. Chem.* 21, 2323-2327 (1982)

[161] J. E. Puig, D. L. Hemker, A. Gupta, H. T. Davis, L. E. Scriven. Interfacial tensions and phase behavior of alcohol-hydrocarbon-water-sodium chloride systems, *J. Phys. Chem.* 91, 1137-1143 (1987)

[162] A. Xenakis, Personal communication

[163] M. Zoumpanioti, H. Stamatis, V. Papadimitriou, A. Xenakis. Spectroscopic and catalytic studies of lipases in ternary hexane-1-propanol-water surfactantless microemulsion systems, *Colloids Surf., B* 47, 1-9 (2005)

[164] Y. L. Khmelnitsky, A. van Hoek, C. Veeger, A. J. W. G. Visser. Detergentless microemulsions as media for enzymatic reactions: spectroscopic and ultracentrifugation studies, *J. Phys. Chem.* 93, 872-878 (1989)

[165] M. Zoumpanioti, M. Karali, A. Xenakis, H. Stamatis. Lipase biocatalytic processes in surfactantless microemulsion-like ternary systems and related organogels, *Enzyme Microb. Technol.*, accepted

[166] Y. L. Khmelnitsky, R. Hilhorst, C. Veeger. Detergentless microemulsions as media for enzymatic reactions. Cholesterol oxidation catalyzed by cholesterol oxidase, *Eur. J. Biochem.* 176, 265-271 (1988)

[167] E. N. Vulfson, G. Ahmed, I. Gill, I. A. Kozlov, P. W. Goodenough, B. A. Law. Alterations to the catalytic properties of polyphenol oxidase in detergentless microemulsions and ternary water-organic solvent mixtures, *Biotechnol. Lett.* 13, 91-96 (1991)

[168] E. Topakas, H. Stamatis, P. Biely, D. Kekos, B. J. Macris, P. Christakopoulos. Purification and characterization of a feruloyl esterase from *Fusarium oxysporum* catalyzing esterification of phenolic acids in ternary water-organic solvent mixtures, *J. Biotechnol.* 102, 33-44 (2003)

[169] K. A. Consani, R. D. Smith. Observations on the solubility of surfactants and related molecules in carbon dioxide at 50 °C, *J. Supercrit. Fluids* 3, 51-65 (1990)

[170] T. A. Hoefling, R. M. Enick, E. J. Beckman. Microemulsions in Near-Critical and Supercritical CO_2, *J. Phys. Chem.* 95, 7127-7129 (1991)

[171] J. M. DeSimone, J. S. Keiper. Surfactants and self-assembly in carbon dioxide, *Curr. Opin. Solid State Mater. Sci.* 5, 333-341 (2001)

[172] T. A. Hoefling, D. A. Newman, R. M. Enick, E. J. Beckman. Effect of Structure on the Cloud-Point Curves of Silicone-Based Amphiphiles in Supercritical Carbon Dioxide, *J. Supercrit. Fluids* 6, 165-171 (1993)

[173] D. A. Newman, T. A. Hoefling, R. R. Beitle, E. J. Beckman, R. M. Enick. Phase Behavior of Fluoroether-Functional Amphiphiles in Supercritical Carbon Dioxide, *J. Supercrit. Fluids* 6, 205-210 (1993)

[174] R. Fink, E. J. Beckman. Phase behavior of siloxane-based amphiphiles in supercritical carbon dioxide, *J. Supercrit. Fluids* 18, 101-110 (2000)

[175] T. Sarbu, T. J. Styranec, E. J. Beckman. Non-fluorous polymers with very high solubility in supercritical CO_2 down to low pressures, *Nature* 405, 165-168 (2000)

[176] T. Sarbu, T. J. Styranec, E. J. Beckman. Design and Synthesis of Low Cost, Sustainable CO_2philes, *Ind. Eng. Chem. Res.* 39, 4678-4683 (2000)

[177] F. Triolo, A. Triolo, R. Triolo, J. D. Londono, G. D. Wignall, J. B. McClain, D. E. Betts, S. Wells, E. T. Samulski, J. M. DeSimone. Critical Micelle Density for the Self-Assembly of Block Copolymer Surfactants in Supercritical Carbon Dioxide, *Langmuir* 16, 416-421 (2000)

[178] M. Z. Yates, G. Li, J. J. Shim, S. Maniar, K. P. Johnston, K. T. Lim, S. Webber. Ambidextrous Surfactants for Water-Dispersible Polymer Powders from Dispersion Polymerization in Supercritical CO_2, *Macromolecules* 32, 1018-1026 (1999)

[179] K. P. Johnston. Block copolymers as stabilizers in supercritical fluids, *Curr. Opin. Colloid Interface Sci.* 5, 351-356 (2000)

[180] S. R. P. da Rocha, P. A. Psathas, E. Klein, K. P. Johnston. Concentrated CO_2-in-Water Emulsions with Nonionic Polymeric Surfactants, *J. Colloid Interface Sci.* 239, 241-253 (2001)

[181] S. R. P. da Rocha, K. L. Harrison, K. P. Johnston. Effect of Surfactants on the Interfacial Tension and Emulsion Formation between Water and Carbon Dioxide, *Langmuir* 15, 419-428 (1999)

[182] G. B. Jacobson, C. T. J. Lee, S. R. P. daRocha, K. P. Johnston. Organic Synthesis in Water/Carbon Dioxide Emulsions, *J. Org. Chem.* 64, 1207-1210 (1999)

[183] K. P. Johnston, D. Cho, S. R. P. DaRocha, P. A. Psathas, W. Ryoo, S. E. Webber, J. Eastoe, A. Dupont, D. C. Steytler. Water in Carbon Dioxide Macroemulsions and Miniemulsions with a Hydrocarbon Surfactant, *Langmuir* 17, 7191-7193 (2001)

[184] J. L. Dickson, P. G. Smith, V. V. Dhanuka, V. Srinivasan, M. T. Stone, P. J. Rossky, J. A. Behles, J. S. Keiper, B. Xu, C. Johnson, J. M. DeSimone, K. P. Johnston. Interfacial Properties of Fluorocarbon and Hydrocarbon Phosphate Surfactants at the Water-CO_2 Interface, *Ind. Eng. Chem. Res.* 44, 1370-1380 (2005)

[185] A. Dupont, J. Eastoe, M. Murray, L. Martin, F. Guittard, E. Taffin de Givenchy, R. K. Heenan. Hybrid Fluorocarbon-Hydrocarbon CO_2-philic Surfactants. 1. Synthesis and Properties of Aqueous Solutions, *Langmuir* 20, 9953-9959 (2004)

[186] A. Dupont, J. Eastoe, L. Martin, D. C. Steytler, R. K. Heenan, F. Guittard, E. Taffin de Givenchy. Hybrid Fluorocarbon-Hydrocarbon CO_2-philic Surfactants. 2. Formation and Properties of Water-in-CO_2 Microemulsions, *Langmuir* 20, 9960-9967 (2004)

[187] M. Sagisaka, T. Fujii, Y. Ozaki, S. Yoda, Y. Takebayashi, Y. Kondo, N. Yoshino, H. Sakai, M. Abe, K. Otake. Interfacial Properties of Branch-Tailed Fluorinated Surfactants Yielding a Water/Supercritical CO_2 Microemulsion, *Langmuir* 20, 2560-2566 (2004)

[188] M. Sagisaka, S. Yoda, Y. Takebayashi, K. Otake, B. Kitiyanan, Y. Kondo, N. Yoshino, K. Takebayashi, H. Sakai, M. Abe. Preparation of a W/scCO_2 Microemulsion using Fluorinated Surfactants, *Langmuir* 19, 220-225 (2003)

[189] J. Eastoe, Z. Bayazit, S. Martel, D. C. Steytler, R. K. Heenan. Droplet Structure in a Water-in-CO_2 Microemulsion, *Langmuir* 12, 1423-1424 (1996)

[190] W. Guo, Zhong Li, B. M. Fung, E. A. O'Rear, J. H. Harwell. Hybrid Surfactants Containing Separate Hydrocarbon and Fluorocarbon Chains, *J. Phys. Chem.* 96, 6738-6742 (1992)

[191] Y. Kondo, N. Yoshino. Hybrid fluorocarbon/hydrocarbon surfactants, *Curr. Opin. Colloid Interface Sci.* 10, 88-93 (2005)

[192] E. J. Beckman, E. G. Ghenciu, N. T. Becker, L. M. Steele. *Extraction of Proteins into Carbon Dioxide*. PCT Int. Appl. WO 9718234 A2 22 May 1997, Application: WO 96-US18168 13 Nov 1996, Priority: US 95-558068 13 Nov 1995

[193] P. Gavezotti (Ausimont Italy), personal communication, e-mail 21st January 2001

[194] M. P. Heitz, C. Carlier, J. deGrazia, K. L. Harrison, K. P. Johnston, T. W. Randolph, F. V. Bright. Water Core within Perfluoropolyether-Based Microemulsions Formed in Supercritical Carbon Dioxide, *J. Phys. Chem. B* 101, 6707-6714 (1997)

[195] M. Ji, X. Chen, C. M. Wai, J. L. Fulton. Synthesizing and dispersing silver nanoparticles in a water-in-supercritical carbon dioxide microemulsion, *J. Am. Chem. Soc.* 121, 2631-2632 (1999)

[196] H. Ohde, X. Ye, C. M. Wai, J. M. Rodriguez. Synthesizing silver halide nanoparticles in supercritical carbon dioxide utilizing a water-in-CO_2 microemulsion, *Chem. Commun.*, 2353-2354 (2000)

[197] C. T. J. Lee, P. A. Psathas, K. J. Ziegler, K. P. Johnston, H. J. Dai, H. D. Cochran, Y. B. Melnichenko, G. D. Wignall. Formation of Water-in-Carbon Dioxide Microemulsions with a Cationic Surfactant: A Small-Angle Neutron Scattering Study, *J. Phys. Chem. B* 104, 11094-11102 (2000)

[198] D. E. Fremgen, E. S. Smotkin, R. E. Gerald, II, R. J. Klingler, J. W. Rathke. Microemulsions of water in supercritical carbon dioxide: an in-situ NMR investigation of micelle formation and structure, *J. Supercrit. Fluids* 19, 287-298 (2001)

[199] R. G. Zielinski, S. R. Kline, E. W. Kaler, N. Rosov. A Small-Angle Neutron Scattering Study of Water in Carbon Dioxide Microemulsions, *Langmuir* 13, 3934-3937 (1997)

[200] T. Nagai, K. Fujii, K. Otake, M. Abe. Water in supercritical CO_2 microemulsion formation by fluorinated surfactants, *Chem. Lett.* 32, 384-385 (2003)

[201] C. Blattner, J. Bittner, G. Schmeer, W. Kunz. Electrical conductivity of reverse micelles in supercritical carbon dioxide, *Phys. Chem. Chem. Phys.* 4, 1921-1927 (2002)

[202] F. Loeker, P. C. Marr, S. M. Howdle. FTIR analysis of water in supercritical carbon dioxide microemulsions using monofunctional perfluoropolyether surfactants, *Colloids Surf., A* 214, 143-150 (2003)

[203] C. T. Lee, K. P. Johnston, H. J. Dai, H. D. Cochran, Y. B. Melnichenko, G. D. Wignall. Droplet Interactions in Water-in-Carbon Dioxide Microemulsions Near the Critical Point: A Small-Angle Neutron Scattering Study, *J. Phys. Chem. B* 105, 3540-3548 (2001)

[204] C. T. Lee, P. Bhargava, K. P. Johnston. Percolation in Concentrated Water-in-Carbon Dioxide Microemulsions, *J. Phys. Chem. B* 104, 4448-4456 (2000)

[205] M. Laguës. Electrical conductivity of microemulsions: a case of stirred percolation, *J. Phys. (Paris) Lett.* 40, L331-L333 (1979)

[206] G. S. Grest, I. Webman, S. A. Safran, A. L. R. Bug. Dynamic Percolation in Microemulsions, *Phys. Rev. A* 33, 2842-2845 (1986)

[207] A. Molski, E. Dutkiewicz. Electrical conductivity and percolation in water-in-oil microemulsions, *Pol. J. Chem.* 70, 959-971 (1996)

[208] H.-F. Eicke, M. Borkovec, B. Das-Gupta. Conductivity of Water-in-Oil Microemulsions: A Quantitative Charge Fluctuation Model, *J. Phys. Chem.* 93, 314-317 (1989)

[209] N. Kallay, A. Chittofrati. Conductivity of microemulsions: refinement of charge fluctuation model, *J. Phys. Chem.* 94, 4755-4756 (1990)

[210] N. Kallay, M. Tomic, A. Chittofrati. Conductivity of water-in-oil microemulsions: comparison of the Boltzmann statistics and the charge fluctuation model, *Colloid Polym. Sci.* 270, 194-6 (1992)

[211] D. G. Hall. Conductivity of microemulsions: an improved charge fluctuation model, *J. Phys. Chem.* 94, 429-430 (1990)

[212] E. D. Niemeyer, F. W. Bright. The pH within PFPE Reverse Micelles Formed in Supercritical CO_2, *J. Phys. Chem. B* 102, 1474-1478 (1998)

[213] K. P. Johnston, T. Randolph, F. Bright, S. Howdle. Toxicology of a PFPE surfactant, *Science* 272, 1726 (1996)

[214] N. Kometani, Y. Toyoda, K. Asami,Y. Yonezawa. An Application of the Water/Supercritical CO_2 Microemulsion to a Novel "Microreactor", *Chem. Lett.*, 682-683 (2000)

[215] M. Z. Yates, D. L. Apodaca, M. L. Campbell, E. R. Birnbaum, T. M. McCleskey. Metal extractions using water in carbon dioxide microemulsions, *Chem. Commun.*, 25-26 (2001)

[216] K. Sawada, J. H. Jun, M. Ueda. Phase behavior of the perfluoropolyether microemulsion in supercritical CO_2 and their use for the solubilization of ionic dyes, *Dyes and Pigments* 60, 197-203 (2004)

[217] G. B. Jacobson, C. T. Lee, K. P. Johnston. Organic Synthesis in Water/Carbon Dioxide Microemulsions, *J. Org. Chem.* 64, 1201-1206 (1999)

[218] K. P. Johnston, C. T. Lee, G. Li, P. Psathas, J. D. Holmes, G. B. Jacobson, M. Z. Yates. Reactions and synthesis in microemulsions and emulsions in carbon dioxide, *Surfactant Sci. Ser.* 100, 349-358 (2001)

[219] C. T. Lee, W. Ryoo, P. G. Smith, J. Arellano, D. R. Mitchell, R. J. Lagow, S. E. Webber, K. P. Johnston. Carbon Dioxide-in-Water Microemulsions, *J. Am. Chem. Soc.* 125, 3181-3189 (2003)

[220] J. Eastoe, A. Paul, A. Downer, D. C. Steytler, E. Rumsey. Effects of Fluorocarbon Surfactant Chain Structure on Stability of Water-in-Carbon Dioxide Microemulsions. Links between Aqueous Surface Tension and Microemulsion Stability, *Langmuir* 18, 3014-3017 (2002)

[221] G. G. Yee, J. L. Fulton, R. D. Smith. Aggregation of polyethylene glycol dodecyl ethers in supercritical carbon dioxide and ethane, *Langmuir* 8, 377-384 (1992)

[222] J. L. Fulton, R. D. Smith. Reverse micelle and microemulsion phases in supercritical fluids, *J. Phys. Chem.* 92, 2903-2907 (1988)

[223] R. D. Smith, C. R. Yonker, J. L. Fulton, J. M. Tingey. Organized molecular assemblies in supercritical fluids; metal ion chelates and reverse micelles, *J. Supercrit. Fluids* 1, 7-14 (1988)

[224] J. M. Tingey, J. L. Fulton und R. D. Smith. Interdroplet attractive forces in AOT water-in-oil microemulsions formed in subcritical and supercritical solvents, *J. Phys. Chem.* 94, 1997-2004 (1990)

[225] T. Ihara, N. Suzuki, T. Maeda, K. Sagaram, T. Hobo. Extraction of Water-Soluble Vitamins from Pharmaceutical Preparations Using AOT (Sodium Di-2-ethylhexyl Sulfosuccinate)/Pentane Reversed Micelles, *Chem. Pharm. Bull.* 43, 626-630 (1995)

[226] T. T. Franco, A. Marty, J. S. Condoret. Protein solubilization in reverse micelles using supercritical CO_2, *Ciênc. Tecnol. Aliment.* 14, 17-28 (1994)

[227] K. Jackson, J. L. Fulton. Microemulsions in Supercritical Hydrochlorofluorocarbons, *Langmuir* 12, 5289-5295 (1996)

[228] B. H. Hutton, J. M. Perera, F. Grieser, G. W. Stevens. Investigation of AOT reverse microemulsions in supercritical carbon dioxide, *Colloids Surf., A* 146, 227-241 (1999)

[229] B. H. Hutton, J. M. Perera, F. Grieser, G. W. Stevens. AOT reverse microemulsions in $scCO_2$ – a further investigation, *Colloids Surf., A* 189, 177-181 (2001)

[230] J. Liu, Y. Ikushima, Z. Shervani. Investigation on the solubilization of organic dyes and micro-polarity in AOT water-in-CO_2 microemulsions with fluorinated co-surfactant by using UV-Vis spectroscopy, *J. Supercrit. Fluids* 32, 97-103 (2004)

[231] J. Eastoe, B. M. H. Cazelles, D. C. Steytler, J. D. Holmes, A. R. Pitt, T. J. Wear, R. K. Heenan. Water-in-CO_2 Microemulsions Studied by Small-Angle Neutron Scattering, *Langmuir* 13, 6980-6984 (1997)

[232] A. Downer, J. Eastoe, A. R. Pitt, E. A. Simister, J. Penfold. Effects of Hydrophobic Chain Structure on Adsorption of Fluorocarbon Surfactants with either CF_3- or H-CF_2- Terminal Groups, *Langmuir* 15, 7591-7599 (1999)

[233] J. Eastoe, A. M. Downer, A. Paul, D. C. Steytler, E. Rumsey. Adsorption of fluoro surfactants at air-water and water-carbon dioxide interfaces, *Prog. Colloid Polym. Sci.* 115, 214-221 (2000)

[234] J. Eastoe, A. Downer, A. Paul, D. C. Steytler, E. Rumsey, J. Penfold, R. K. Heenan. Fluoro-surfactants at air/water and water/CO_2 interfaces, *Phys. Chem. Chem. Phys.* 2, 5235-5242 (2000)

[235] Z. Liu, C. Erkey. Water in Carbon Dioxide Microemulsions with Fluorinated Analogues of AOT, *Langmuir* 17, 274-277 (2001)

[236] X. Dong, C. Erkey, H. Dai, H. Li, H. D. Cochran, J. S. Lin. Phase Behavior and Micelle Size of an Aqueous Microdispersion in Supercritical CO_2 with a Novel Surfactant, *Ind. Eng. Chem. Res.* 41, 1038-1042 (2002)

[237] J. Park, C. H. Lee, K. Yoo, J. S. Lim. The effect of adding organic solvents on the phase behavior in water/surfactants/$scCO_2$ microemulsion in supercritical state, *Key Eng. Mater.* 277-279, 886-892 (2005)

[238] M. Sagisaka, S. Yoda, Y. Takebayashi, K. Otake, Y. Kondo, N. Yoshino, H. Sakai, M. Abe. Effects of CO_2-philic Tail Structure on Phase Behavior of Fluorinated Aerosol-OT Analogue Surfactant/Water/Supercritical CO_2 Systems, *Langmuir* 19, 8161-8167 (2003)

[239] J. Eastoe, A. Paul, S. Nave, D. C. Steytler, B. H. Robinson, E. Rumsey, M. Thorpe, R. K. Heenan. Micellization of Hydrocarbon Surfactants in Supercritical Carbon Dioxide, *J. Am. Chem. Soc.* 123, 988-989 (2001)

[240] D. C. Steytler, E. Rumsey, M. Thorpe, J. Eastoe, A. Paul, R. K. Heenan. Phosphate Surfactants for Water-in-CO_2 Microemulsions, *Langmuir* 17, 7948-7950 (2001)

[241] J. S. Keiper, R. Simhan, J. M. DeSimone, G. D. Wignall, Y. B. Melnichenko, H. Frielinghaus. New Phosphate Fluorosurfactants for Carbon Dioxide, *J. Amer. Chem. Soc.* 124, 1834-1835 (2002)

[242] J. S. Keiper, J. A. Behles, T. L. Bucholz, R. Simhan, J. M. DeSimone, G. W.Lynn, G. D. Wignall, Y. B. Melnichenko, H. Frielinghaus. Self-Assembly of Phosphate Fluorosurfactants in Carbon Dioxide, *Langmuir* 20, 1065-1072 (2004)

[243] B. Xu, G. W. Lynn, J. Guo, Y. B. Melnichenko, G. D. Wignall, J. B. McClain, J. M. DeSimone, C. S. Johnson. NMR and SANS Studies of Aggregation and Microemulsion Formation by Phosphorus Fluorosurfactants in Liquid and Supercritical Carbon Dioxide, *J. Phys. Chem. B* 109, 10261-10269 (2005)

[244] J. Liu, B. Han, G. Li, X. Zhang, J. He, Z. Liu. Investigation of nonionic surfactant Dynol-604 based reverse microemulsions formed in supercritical carbon dioxide, *Langmuir* 17, 8040-8043 (2001)

[245] J. C. Liu, J. L. Zhang, B. X. Han, G. Z. Li, G. Y. Yang. Study on the phase behavior of supercritical CO_2/Dynol-604/water system and solubilization of methyl orange in the microemulsions, *Chin. Chem. Lett.* 13, 87-90 (2002)

[246] J. Liu, J. Zhang, T. Mu, B. Han, G. Li, J. Wang, B. Dong. An investigation of non-fluorous surfactant Dynol-604 based water-in-CO_2 reverse micelles by small angle X-ray scattering, *J. Supercrit. Fluids* 26, 275-280 (2003)

[247] J. Liu, B. Han, J. Zhang, G. Li, X. Zhang, J. Wang, B. Dong. Formation of water-in-CO_2 microemulsions with non-fluorous surfactant Ls-54 and solubilization of biomacromolecules, *Chem. Eur. J.* 8, 1356-1360 (2002)

[248] J. Liu, B. Han, J. Zhang, T. Mu, G. Li, W. Wu, G. Yang. Effect of cosolvent on the phase behavior of non-fluorous Ls-54 surfactant in supercritical CO_2, *Fluid Phase Equilib.* 211, 265-271 (2003)

[249] M. A. Matthews, J. M. Becnel. Diffusion Coefficients of Methyl Orange in Dense Carbon Dioxide with the Micelle-Forming Surfactant Dehypon Ls-54, *J. Chem. Eng. Data* 48, 1413-1417 (2003)

[250] J. Liu, B. Han, Z. Wang, J. Zhang, G. Li und G. Yang. Solubility of Ls-36 and Ls-45 Surfactants in Supercritical CO_2 and Loading Water in the CO_2/Water/Surfactant Systems, *Langmuir* 18, 3086-3089 (2002)

[251] K. Sawada, M. Oshima, M. Sugimito, M. Ueda. Microemulsions in supercritical CO_2 utilizing polyethylene glycol dialkylglycerol ethers and their use for the solubilization of hydrophiles, *Dyes and Pigments* 65, 67-74 (2004)

[252] K. Drauz, H. Waldmann (Eds.). *Enzyme Catalysis in Organic Synthesis. A Comprehensive Handbook*, Vol. I, 2nd Edition, Wiley-VCH, Weinheim (2002)

[253] D. Voeth, J. G. Voeth. *Biochemie*, VCH, Weinheim (1992)

[254] D. A. Hammond, M. Karel, A. M. Klibanov, V. J. Krukonis. Enzymic reactions in supercritical gases, *Appl. Biochem. Biotechnol.* 11, 393-400 (1985)

[255] K. Nakamura, Y. M. Chi, Y. Yamada, T. Yano. Lipase activity and stability in supercritical carbon dioxide, *Chem. Eng. Commun.* 45, 207-212 (1986)

[256] Y. M. Chi, K. Nakamura, T. Yano. Enzymic interesterification in supercritical carbon dioxide, *Agric. Biol. Chem.* 52, 1541-1550 (1988)

[257] T. W. Randolph, H. W. Blanch, J. M. Prausnitz. Enzyme-catalyzed oxidation of cholesterol in supercritical carbon dioxide, *AIChE J.* 34, 1354-1360 (1988)

[258] P. Pasta, G. Mazzola, G. Carrea, S. Riva. Subtilisin-catalyzed transesterification in supercritical carbon dioxide, *Biotechnol. Lett.* 11, 643-648 (1989)

[259] A. Marty, D. Combes, J. S. Condoret. Fatty acid esterification in supercritical carbon dioxide, *Progress Biotechnol.* 8, 425-432 (1992)

[260] T. Dumont, D. Barth, C. Corbier, G. Branlant, M. Perrut. Enzymic reaction kinetic: comparison in an organic solvent and in supercritical carbon dioxide, *Biotechnol. Bioeng.* 40, 329-333 (1992)

[261] Y. Ikushima, N. Saito, T. Yokoyama, K. Hatakeda, S. Ito, M. Arai, H. W. Blanch. Solvent effects on an enzymic ester synthesis in supercritical carbon dioxide, *Chem. Lett.*, 109-112 (1993)

[262] M. Rantakylä, O. Aaltonen. Enantioselective esterification of ibuprofen in supercritical carbon dioxide by immobilized lipase, *Biotechnol. Lett.* 16, 825-830 (1994)

[263] C. Tsitsimpikou, H. Stamatis, V. Sereti, H. Daflos, F. N. Kolisis. Acylation of glucose catalyzed by lipases in supercritical carbon dioxide, *J. Chem. Technol. Biotechnol.* 71, 309-314 (1998)

[264] S.-H. Yoon, H. Nakaya, O. Ito, O. Miyawaki, K.-H. Park, K. Nakamura. Effects of substrate solubility in interesterification with triolein by immobilized lipase in supercritical carbon dioxide, *Biosci. Biotechnol. Biochem.* 62, 170-172 (1998)

[265] T. Matsuda, T. Harada, K. Nakamura. Alcohol dehydrogenase is active in supercritical carbon dioxide, *Chem. Comm.*, 1367-1368 (2000)

[266] S. Srivastava, G. Madras, J. Modak. Esterification of myristic acid in supercritical carbon dioxide, *J. Supercrit. Fluids* 27, 55-64 (2003)

[267] S. Srivastava, J. Modak, G. Madras. Enzymatic Synthesis of Flavors in Supercritical Carbon Dioxide, *Ind. Eng. Chem. Res.* 41, 1940-1945 (2002)

[268] E. Bourquelot, M. Bridel. Action of Emulsin on Gentiopicrin in Alcohol, *J. Pharm. Chim.* 4, 385-390 (1912)

[269] B. C. Buckland, P. Dunnill, M. D. Lilly. Enzymic transformation of water-insoluble reactants in nonaqueous solvents. Conversion of cholesterol to cholest-4-ene-3-one by a Nocardia species, *Biotechnol. Bioeng.* 17, 815-826 (1975)

[270] A. M. Klibanov, G. P. Samokhin, K. Martinek, I. V. Berezin. A new approach to preparative enzymic synthesis, *Biotechnol. Bioeng.* 19, 1351-1361 (1977)

[271] Nakanishi K, Matsuno R. Kinetics of enzymatic synthesis of peptides in aqueous/organic biphasic systems. Thermolysin-catalyzed synthesis of N-(benzyloxycarbonyl)-L-phenylalanyl-L-phenylalanine methyl ester, *Eur. J. Biochem.* 161, 533-540 (1986)

[272] A. M. Klibanov. Enzymes that work in organic solvents, *Chem. Tech.* 16, 354-359 (1986)

[273] C. S. Chen, C. J. Sih. Enantioselective biocatalysis in organic solvents. Lipase catalyzed reactions, *Angew. Chem.* 101, 711-724 (1989)

[274] A. M. Klibanov. Asymmetric transformations catalyzed by enzymes in organic solvents, *Acc. Chem. Res.* 23, 114-120 (1990)

[275] G. Carrea, G. Ottolina, S. Riva, F. Secundo. Effect of reaction conditions on the activity and enantioselectivity of lipases in organic solvents, *Prog. Biotechnol.* 8, 111-119 (1992)

[276] T. Hartmann, E. Schwabe, T. Scheper, D. Combes. *Enzymatic reactions in supercritical carbon dioxide*, in: R. N. Patel (Ed.). *Stereoselective Biocatalysis*, pp. 799-838, Marcel Dekker, New York (2000)

[277] R. Battino (Volume Ed.). *IUPAC Solubility Data Series*, Vol. 7, Pergamon Press, Oxford (1981)

[278] B. Borgström, H. C. Brockmann (Eds.). *Lipases*, Elsevier, Amsterdam (1984)

[279] R. Arreguín-Espinosa, B. Arreguín, C. González. Purification and properties of a lipase from *Cephaloleia presignis* (Coleoptera, Chrysomelidae), *Biotechnol. Appl. Biochem.* 31, 239-244 (2000)

[280] M. Tservistas. *Unteruchungen zum Einsatz von überkritischem Kohlendioxid als Medium für biokatalysierte Reaktionen*, Dissertation, Universität Hannover (1997)

[281] R. D. Schmid, R. Verger. Lipases: interfacial enzymes with attractive applications, *Angew. Chem. Int. Ed.* 37, 1609-1633 (1998)

[282] R. J. Kazlauskas. Elucidating structure-mechanism relationships in lipases: prospects for predicting and engineering catalytic properties, *Trends Biotechnol.* 12, 464-472 (1994)

[283] G. H. Peters, D. M. F. van Aalten, A. Svendsen, R. Bywater. Essential dynamics of lipase binding sites: the effect of inhibitors of different chain length, *Prot. Eng.* 10, 149-158 (1997)

[284] A. M. Brzozowski, H. Savage, C. S. Verma, J. P. Turkenburg, D. M. Lawson, A. Svendsen, S. Patkar. Structural Origins of the Interfacial Activation in *Thermomyces (Humicola) lanuginosa* Lipase, *Biochemistry* 39, 15071-15082 (2000)

[285] L. Brady, A. M. Brzozowski, Z. S. Derewenda, E. Dodson, G. Dodson, S. Tolley, J. P. Turkenburg, L. Christiansen, B. Huge-Jensen, et al. A serine protease triad forms the catalytic center of a triacylglycerol lipase, *Nature* 343, 767-770 (1990)

[286] J. D. Schrag, Y. Li, S. Wu, M. Cygler. Ser-His-Glu triad forms the catalytic site of the lipase from *Geotrichum candidum*, *Nature* 351, 761-764 (1991)

[287] A. M. Brzozowski, U. Derewenda, Z. S. Derewenda, G. G. Dodson, D. M. Lawson, J. P. Turkenburg, F. Bjorkling, B. Huge-Jensen, S. A. Patkar, L. Thim. A model for interfacial activation in lipases from the structure of a fungal lipase-inhibitor complex, *Nature* 351, 491-494 (1991)

[288] H. van Tilbeurgh, M. P. Egloff, C. Martinez, N. Rugani, R. Verger, C. Cambillau. Interfacial activation of the lipase-procolipase complex by mixed micelles revealed by x-ray crystallography, *Nature* 362, 814-820 (1993)

[289] P. Grochulski, Y. Li, J. D. Schrag, F. Bouthillier, P. Smith, D. Harrison, B. Rubin, M. Cygler. Insights into interfacial activation from an open structure of *Candida rugosa* lipase, *J. Biol. Chem.* 268, 12843-12847 (1993)

[290] P. Grochulski, Y. Li, J. D. Schrag, M. Cygler. Two conformational states of *Candida rugosa* lipase, *Protein Sci.* 3, 82-91 (1994)

[291] K. Nakamura. Biochemical reactions in supercritical fluids, *Trends Biotechnol.* 8, 288-292 (1990)

[292] B. G. Davis, V. Boyer. Biocatalysis and enzymes in organic synthesis, *Nat. Prod. Rep.* 18, 618-640 (2001)

[293] K.-E. Jaeger, T. Eggert. Lipases for biotechnology, *Curr. Opin. Biotechnol.* 13, 390-397 (2002)

[294] M. T. Reetz. Lipases as practical biocatalysts, *Curr. Opin. Chem. Biol.* 6, 145-150 (2002)

[295] W. W. Cleland. The kinetics of enzyme-catalyzed reactions with two or more substrates or products. I. Nomenclature and rate equations, *Biochim. Biophys. Acta* 67, 104-137 (1963)

[296] W. W. Cleland. The kinetics of enzyme-catalyzed reactions with two or more substrates or products. II. Inhibition – nomenclature and theory, *Biochim. Biophys. Acta* 67, 173-187 (1963)

[297] I. H. Segel. *Enzyme Kinetics – Behavior and Analysis of Rapid Equilibrium and Steady-State Enzyme Systems*, 2nd Edition, Wiley, New York (1993)

[298] H. Bisswanger. *Enzymkinetik – Theorie und Methoden*, 2nd Edition, VCH, Weinheim (1994)

[299] P. C. Engel (Ed.). *Enzymology Labfax*, BIOS Scientific Publishers, Oxford (1996)

[300] C. W. Dessauer, A. G. Gilman. Purification and characterization of a soluble form of mammalian adenylyl cyclase, *J. Biol. Chem.* 28, 16967-16974 (1996)

[301] P. Sturm. *Transformator-Brücke und Platin-Normalwiderstand zur Temperaturkalibrierung*, Diplomarbeit, Universität Regensburg (1996)

[302] Data sheet D6.157D: *Druckmeßumformer für Hydraulik und Pneumatik ED 517*, Haenni Instruments AG, Jegenstorf, Switzerland (April 1999)

[303] Data sheet: *Digitalanzeiger Digital 280*, Philips Prozeß- und Maschinenautomation GmbH, Kassel, Germany (February 1997)

[304] R. Wachter. *Experimentelle Untersuchungen zur Bestimmung der Struktur nichtwässriger Elektrolytlösungen aus der Temperaturabhängigkeit ihrer elektrischen Leitfähigkeit*, Habilitation, Universität Regensburg (1973)

[305] R. A. Robinson, R. H. Stokes. *Electrolyte Solutions*, 2nd Edition, Butterworths, London (1970)

[306] G. Jones und S. M. Christian. The measurement of the Conductance of Electrolyte. VI. Galvanic Polarization by Alternating Current, *J. Am. Chem. Soc.* 57, 272-280 (1935)

[307] T. B. Hoover. Conductance of Potassium Chloride in highly purified N-Methylpropionamide from 20 to 40 °C, *J. Phys. Chem.* 68, 876-879 (1964)

[308] J. C. Nichol, R. M. Fuoss. A New Cell Design for Precision Conductimetry, *J. Phys. Chem.* 58, 696-699 (1954)

[309] N. Yoshino, N. Komine, J. Suzuki, Y. Arma, H. Hirai. Synthesis of Anionic Surfactants Having Two Polyfluoroalkyl Chains and Their Flocculation Ability for Dispersed Magnetic Particles in Water, *Bull. Chem. Soc. Jpn.* 64, 3262-3266 (1991)

[310] G. S. Gol'din, K. O. Averbakh, L. A. Nekrasova, A. V. Kisin. Synthesis of Alkali-Metal Salts of Bis(fluoroalkyl)sulfosuccinates, *J. Gen. Chem. USSR (Engl. Transl.)* 47, 995-997 (1977)

[311] G. S. Gol'din, K. O. Averbakh, L. A. Nekrasova. Organofluorine Derivatives of Salts of Sulfocarboxylate Esters, *J. Appl. Chem. USSR (Engl. Transl.)* 57, 1463-1467 (1985)

[312] M. Drifford, L. Belloni, M. Dubois. Light Scattering on Concentrated Micellar Systems: Influence of Monomers, *J. Colloid Interface Sci.* 118, 50-67 (1987)

[313] A. Chittofrati, D. Lenti, A. Sanguineti, M. Visca, C. M. C. Gambi, D. Senatra, Z. Zhou. Perfluoropolyether microemulsions, *Prog. Colloid Polym. Sci.* 79, 218-225 (1989)

[314] M. Brun, A. Lallemand, J.-F. Quinson, C. Eyraud. A new method for the simultaneous determination of the size and the shape of pores: the thermoporometry, *Thermochim. Acta* 21, 59-88 (1977)

[315] J. N. Hay, P. R. Laity. Observations of water migration during thermoporometry studies of cellulose films, *Polymer* 41, 6171-6180 (2000)

[316] D. C. Steytler, P. S. Moulson, J. Reynolds. Biotransformations in near-critical carbon dioxide, *Enzyme Microb. Technol.* 13, 221-226 (1991)

[317] H. Nakaya, O. Miyawaki, K. Nakamura. Transesterification between triolein and stearic acid catalyzed by lipase in CO_2 at various pressures, *Biotechnol. Tech.* 12, 881-884 (1998)

[318] D. A. Miller, H. W. Blanch, J. M. Prausnitz. Enzymic interesterification of triglycerides in supercritical carbon dioxide, *Ann. N.Y. Acad. Sci.* 613, 534-537 (1990)

[319] D. A. Miller, H. W. Blanch, J. M. Prausnitz. Enzyme-catalyzed interesterification of triglycerides in supercritical carbon dioxide, *Ind. Eng. Chem. Res.* 30, 939-946 (1991)

[320] M. H. Vermuë, J. Tramper, J. P. J. De Jong, W. H. M. Oostrom. Enzymic transesterification in near-critical carbon dioxide: effect of pressure, Hildebrand solubility parameter and water content, *Enzyme Microb. Technol.* 14, 649-655 (1992)

[321] J. C. Erickson, P. Schyns, C. L. Cooney. Effect of pressure on an enzymic reaction in a supercritical fluid, *AIChE J.* 36, 299-301 (1990)

[322] Y. Ikushima, N. Saito, M. Arai. Promotion of lipase-catalyzed esterification of N-valeric acid and citronellol in supercritical carbon dioxide in the near-critical region, *J. Chem. Eng. Jpn.* 29, 551-553 (1996)

[323] H. Stamatis, A. Xenakis, U. Menge, F. N. Kolisis. Kinetic study of lipase catalyzed esterification reactions in water-in-oil microemulsions, *Biotechnol. Bioeng.* 42, 931-937 (1993)

[324] W. Chulalaksananukul, J. S. Condoret, D. Combes. Geranyl acetate synthesis by lipase-catalyzed transesterification in supercritical carbon dioxide, *Enzyme Microb. Technol.* 15, 691-698 (1993)

[325] W. Chulalaksananukul, J. S. Condoret, D. Combes. Kinetics of geranyl acetate synthesis by lipase-catalyzed transesterification in n-hexane, *Enzyme Microb. Technol.* 14, 293-298 (1992)

[326] W. Chulalaksananukul, J. S. Condoret, P. Delorme, R. M. Willemot. Kinetic study of esterification by immobilized lipase in n-hexane, *FEBS Lett.* 276, 181-184 (1990)

[327] A. Marty, W. Chulalaksananukul, R. M. Willemot, J. S. Condoret. Kinetics of lipase-catalyzed esterification in supercritical carbon dioxide, *Biotechnol. Bioeng.* 39, 273-280 (1992)

[328] H. Stamatis, A. Xenakis, M. Provelegiou, F. N. Kolisis. Esterification reactions catalyzed by lipases in microemulsions: the role of enzyme localization in relation to its selectivity, *Biotechnol. Bioeng.* 42, 103-110 (1993)

[329] N. N. Gandhi, S. B. Sawant, J. B. Joshi. Specificity of a lipase in ester synthesis: effect of alcohol, *Biotechnol. Progr.* 11, 282-287 (1995)

[330] M. S. Shintre, R. S. Ghadge, S. B. Sawant. Kinetics of esterification of lauric acid with fatty alcohols by lipase: effect of fatty alcohol, *J. Chem. Technol. Biotechnol.* 77, 1114-1121 (2002)

[331] J. L. Ford, K. Mitchell. Thermal Analysis of gels and matrix tablets containing cellulose ethers, *Thermochim. Acta* 248, 329-345 (1995)

[332] Y. Taniguchi, S. Horigome. The States of Water in Cellulose Acetate Membranes, *J. Appl. Polym. Sci.* 19, 2743-2748 (1975)

[333] G. Hedström, S. Backlund, F. Eriksson. Influence of Diffusion on the Kinetics of an Enzyme-Catalyzed Reaction in Gelatin-Based Gels, *J. Colloid Interface Sci.* 239, 190-195 (2001)

[334] J. Barauskas, T. Landh. Phase Behavior of the Phytantriol/Water System, *Langmuir* 19, 9562-9565 (2003)

[335] Technical information: *Phytantriol*, BASF AG – Fine Chemicals Division, Ludwigshafen, Germany (January 2003)

[336] E. Wagner. Panthenol and phytanetriol in cosmetics, *Parfuem. Kosmet.* 75, 260-267 (1994)

[337] G. Erlemann, R. Merkle. Panthenol, phytantriol, vitamin E, and vitamin A in cosmetics, *Seifen, Öle, Fette, Wachse* 117, 379-384 (1991)

[338] K. Lunkenheimer, S. Schrödle, W. Kunz. Dowanol DPnB in water as an example of a solvo-surfactant system: Adsorption and foam properties, *Prog. Colloid Polym. Sci.* 126, 14-20 (2004)

[339] P. Bauduin, A. Renoncourt, A. Kopf, D. Touraud, W. Kunz. Unified Concept of Solubilization in Water by Hydrotropes and Cosolvents, *Langmuir* 21, 6769-6775 (2005)

[340] Y. Gao, W. Wu, B. Han, G. Li, J. Chen, W. Hou. Water-in-CO_2 microemulsions with a simple fluorosurfactant, *Fluid Phase Equilib.* 226, 301-305 (2004)

[341] J. Eastoe, A. Dupont, D. C. Steytler, M. Thorpe, A. Gurgle, R. K. Heenan. Micellization of economically viable surfactants in CO_2, *J. Colloid Interface Sci.* 258, 367-373 (2003)

[342] M. T. Stone, P. G. Smith, S. R. P. da Rocha, P. J. Rossky, K. P. Johnston. Low interfacial free volume of Stubby surfactants stabilizes water-in-carbon dioxide microemulsions, *J. Phys. Chem. B* 108, 1962-1966 (2004)

[343] W. Ryoo, S. E. Webber, K. P. Johnston. Water-in-Carbon Dioxide Microemulsions with Methylated Branched Hydrocarbon Surfactants, *Ind. Eng. Chem. Res.* 42, 6348-6358 (2003)

[344] M. T. Stone, S. R. P. Da Rocha, P. J. Rossky, K. P. Johnston. Molecular Differences between Hydrocarbon and Fluorocarbon Surfactants at the CO_2/Water Interface, *J. Phys. Chem. B* 107, 10185-10192 (2003)

[345] S. R. P. da Rocha, K. P. Johnston. Interfacial Thermodynamics of Surfactants at the CO_2-Water Interface, *Langmuir* 16, 3690-3695 (2000)

[346] Programme „AutoCAD“, Version 13, Autodesk Inc. (1982-1996)

[347] R. D. B. Frasier, E. Suzuki. Resolution of Overlapping Absorption Bands by Least Square Procedures, *Anal. Chem.* 38, 1770-1773 (1966)

[348] R. D. B. Frasier, E. Suzuki. Resolution of Overlapping Bands: Functions for Simulating Band Shapes, *Anal. Chem.* 41, 37-39 (1969)

[349] G. W. H. Höhne, H. K. Cammenga, W. Eysel, E. Gmelin, W. Hemminger. The temperature calibration of scanning calorimeters, *Thermochim. Acta* 160, 1-12 (1990)

[350] H. K. Cammenga, W. Eysel, E. Gmelin, W. Hemminger, G. W. H. Höhne, S. M. Sarge. The temperature calibration of scanning calorimeters. Part 2. Calibration substances, *Thermochim. Acta* 219, 333-342 (1993)

[351] S. M. Sarge, E. Gmelin, G. W. H. Höhne, H. K. Cammenga, W. Hemminger, W. Eysel. The caloric calibration of scanning calorimeters, *Thermochim. Acta* 247, 129-168 (1994)

[352] S. M. Sarge, W. Hemminger, E. Gmelin, G. W. H. Höhne, H. K. Cammenga, W. Eysel. Metrologically based procedures for the temperature, heat and heat flow rate calibration of DSC, *J. Therm. Anal.* 49, 1125-1134 (1997)

[353] E. Gmelin, S. M. Sarge. Temperature, heat and heat flow rate calibration of differential scanning calorimeters, *Thermochim. Acta* 347, 9-13 (2000)

[354] C. Eyraud, J. F. Quinson, M. Brun. Role of thermoporometry in the study of porous solids, *Stud. Surf. Sci. Catal.* 39, 295-305 (1987)

[355] A. Hernandez, J. I. Calvo, P. Pradanos, L. Palacio. A multidisciplinary approach towards pore size distributions of microporous and mesoporous membranes, *Surfactant Science Series* 79, 39-90 (1999)

[356] S. Nakao. Determination of pore size and pore size distribution. 3. Filtration membranes, *J. Membrane Sci.* 96, 131-165 (1994)

[357] C. Zhao, X. Zhou, Y. Yue. Determination of pore size and pore size distribution on the surface of hollow-fiber filtration membranes: a review of methods, *Desalination* 129, 107-123 (2000)